



University of  
**Salford**  
MANCHESTER

**The Role of the Human Endonuclease VIII-Like 1 and 3  
In the Repair of DNA Replication Blocking Lesions.**

PhD Thesis  
2018

Peter Ryan Martin

School of Environment and Life Sciences,  
University of Salford

Submitted in Partial Fulfilment of the Requirements of the Degree of Doctor of Philosophy,  
October 2018

<b>Contents.</b>	
<b>Abstract.</b>	<b>vi</b>
<b>Abbreviations.</b>	<b>vii</b>
<b>List of Figures.</b>	<b>xix</b>
<b>List of Tables.</b>	<b>xxviii</b>
<b>Acknowledgements</b>	<b>xxx</b>
<b>1. Introduction.</b>	<b>1</b>
<b>1.1. Cancer.</b>	<b>2</b>
<b>1.2. DNA damage.</b>	<b>5</b>
<b>1.2.1. Oxidative DNA damage</b>	<b>5</b>
<b>1.2.2. Alkylation of DNA.</b>	<b>10</b>
<b>1.2.3. Crosslinking of DNA.</b>	<b>12</b>
<b>1.3. DNA damage response.</b>	<b>17</b>
<b>1.4. DNA replication stress response (RSR).</b>	<b>18</b>
<b>1.5. DNA damage tolerance pathways.</b>	<b>20</b>
<b>1.6. Fanconi anemia pathway.</b>	<b>22</b>
<b>1.7. Nucleotide excision repair.</b>	<b>25</b>
<b>1.7.1. Global Genome Nucleotide Excision Repair.</b>	<b>26</b>
<b>1.7.2. Transcription coupled repair (TC-NER).</b>	<b>27</b>
<b>1.8. Repair of DNA Interstrand crosslinks.</b>	<b>30</b>
<b>1.9. Base excision repair.</b>	<b>35</b>
<b>1.9.1. Short-patch BER.</b>	<b>36</b>
<b>1.9.2. Long-patch BER.</b>	<b>38</b>
<b>1.10. DNA glycosylases.</b>	<b>40</b>
<b>1.11. Prokaryotic DNA glycosylases.</b>	<b>41</b>
<b>1.11.1. Formamidopyrimidine DNA glycosylase (Fpg).</b>	<b>42</b>
<b>1.11.2. Endonuclease VIII (Nei).</b>	<b>42</b>
<b>1.12. Non-Oxidised base eukaryotic DNA glycosylases.</b>	<b>43</b>
<b>1.12.1. Uracil DNA glycosylases.</b>	<b>43</b>
<b>1.12.2. Thymine DNA glycosylase (TDG) and methyl-CpG-binding domain4, DNA glycosylase (MBD4).</b>	<b>44</b>
<b>1.12.3. Alkyladenine DNA glycosylase (AAG)</b>	<b>44</b>
<b>1.13. Oxidised base DNA glycosylases.</b>	<b>46</b>
<b>1.13.1. 8-Oxoguanine DNA glycosylase (OGG1).</b>	<b>46</b>
<b>1.13.2. MutY DNA glycosylase (MUTYH).</b>	<b>46</b>
<b>1.13.3. Nth-like DNA glycosylase 1 (NTH1).</b>	<b>47</b>

1.13.4.	Endonuclease VIII-like 1 (NEIL1).	48
1.13.5.	Endonuclease VIII-like 2 (NEIL2)	51
1.13.6.	Endonuclease VIII-like 3 (NEIL3).	52
<b>1.14.</b>	<b>Ubiquitin proteasome system (UPS).</b>	<b>57</b>
1.14.1.	E3 ubiquitin ligases.....	60
1.14.2.	Ubiquitin proteasome system and cancer.....	61
1.14.3.	Ubiquitin regulation of the Base Excision Repair pathway. ....	63
1.14.4.	Tripartite motif-containing proteins. ....	68
1.14.5.	Tripartite motif-containing protein 26. ....	69
<b>1.15.</b>	<b>Use of bacterial hosts for protein expression.</b> .....	<b>72</b>
1.15.1.	The pET expression system.....	72
1.15.2.	Construction and use of a bicistronic pET vector for hNEIL3 recombinant protein expression.....	73
<b>1.16.</b>	<b>Hypothesis.</b> ....	<b>77</b>
<b>2.</b>	<b>Methods.</b> .....	<b>78</b>
2.1.	Transformation of bacterial cloning and expression hosts.....	79
2.2.	Recombinant protein expression of hNEIL1, hNEIL3 and TRIM26. ....	80
2.3.	Bacterial cell lysis. ....	81
2.4.	HisTrap HP column affinity purification. ....	81
2.5.	SDS-PAGE gel preparation.....	82
2.6.	SDS-PAGE.....	84
2.7.	Western-blot transfer. ....	84
2.8.	Immuno-blot.....	85
2.9.	Generation of model replication fork structured oligonucleotide substrates. ....	87
2.10.	Radioactive labelling of DNA oligonucleotide substrates. ....	89
2.11.	Annealing of DNA oligonucleotide substrates.....	89
2.12.	Psoralen induced DNA interstrand crosslinked oligonucleotide generation.....	89
2.13.	Denaturing PAGE.....	90
2.14.	Non-denaturing PAGE. ....	91
2.15.	Single stranded mono-adducted oligonucleotide generation.....	92
2.16.	Oligonucleotide purification from 20% denaturing PAGE.....	93
2.17.	Three-stranded and Four-stranded DNA ICL construction.....	93
2.18.	DNA glycosylase cleavage assay.....	94
2.19.	Kinetic analysis of hNEIL1 and hNEIL3 recombinant proteins.....	95
2.20.	Generation of hNEIL3 <sup>Cat-K81A</sup> catalytically inactive recombinant protein bacterial expression vector. ....	96

2.21.	Recombinant hNEIL3 <sup>Cat-K81A</sup> expression and protein purification.	98
2.22.	Protein-DNA covalent complex formation, 'Schiff base' affinity assay.	99
2.23.	Characterisation of E3 ubiquitin ligase from HeLa cells and <i>in vitro</i> .	99
2.23.1.	<i>In vitro</i> ubiquitination assay.	100
2.24.	Mammalian cell line culture.	101
2.24.1.	Thawing cells.	101
2.24.2.	Splitting cells.	101
2.24.3.	Freezing cells and long-term storage.	102
2.25.	Tanaka protein extraction.	102
2.26.	Bradford assay.	103
2.27.	RNA interference.	104
2.28.	Transient overexpression of NEIL1, NEIL3 and NTH1.	105
2.29.	Clonogenic survival assay.	105
2.30.	CRISPR/Cas9 mediated gene knockout.	107
	<b>Results &amp; Discussion.</b>	<b>111</b>
<b>3.</b>	<b>Characterisation of the hNEIL1 and hNEIL3 DNA glycosylases in the repair of oxidative DNA damage in association with DNA replication.</b>	<b>112</b>
3.1.	Results: Characterisation of the hNEIL1 and hNEIL3 DNA glycosylases in the repair of oxidative DNA damage in association with DNA replication	113
3.1.1.	Recombinant hNEIL1 purification from <i>E. coli</i> using the pET30a-hNEIL1 bacterial expression vector.	113
3.1.2.	hNEIL1 and hNEIL3 <sup>FL</sup> recombinant protein activity analysis on oxidative DNA lesions containing ss- and ds- oligonucleotide DNA.	115
3.1.3.	hNEIL1 and hNEIL3 <sup>FL</sup> recombinant protein activity analysis on oxidative DNA lesion containing model DNA replication fork oligonucleotide DNA.	116
3.2.	Discussion: Characterisation of the hNEIL1 and hNEIL3 DNA glycosylases in the repair of oxidative DNA damage in association with DNA replication.	121
<b>4.</b>	<b>Characterisation of the hNEIL1 and hNEIL3 DNA glycosylases in the repair of psoralen interstrand DNA crosslinks.</b>	<b>125</b>
4.1.	Results: Characterisation of the hNEIL1 and hNEIL3 DNA glycosylases in the repair of psoralen interstrand DNA crosslinks.	126
4.1.1.	Generation of ICL oligonucleotide DNA substrates.	126
4.1.2.	hNEIL3 protein concentration titration for activity on three-stranded ICL oligonucleotides.	132
4.1.3.	hNEIL3, Nei and hNEIL1 protein concentration titration for activity on Sp1 substrates.	135
4.1.4.	hNEIL3 unhooking activity of a single-stranded HMT generated MA.	137

4.1.5.	hNEIL1, hNEIL3 and Nei unhooking activity of a three-stranded HMT generated ICL oligonucleotide substrate.....	138
4.1.6.	hNEIL3 and Nei unhooking activity of four-stranded HMT generated ICL oligonucleotide substrate.....	142
4.1.7.	hNEIL1, hNEIL3 and Nei unhooking activity of a long three-stranded HMT generated ICL oligonucleotide substrate.....	146
4.1.8.	hNEIL1, hNEIL3 and Nei protein unhooking activity of an 8-MOP generated three-stranded ICL oligonucleotide substrate.....	148
4.1.9.	hNEIL1 and hNEIL3 protein kinetics on ss and ds Sp1 substrate.....	150
4.1.10.	hNEIL1 and hNEIL3 <sup>Cat</sup> protein kinetics on three-stranded ICL compared to ss and ds Sp substrates.....	153
4.1.11.	Generation and confirmation of catalytically inactive mutant hNEIL3 <sup>Cat</sup> .....	156
4.1.12.	hNEIL3 <sup>Cat-K81A</sup> recombinant protein ÄKTA FPLC purification.....	157
4.1.13.	hNEIL3 <sup>Cat-K81A</sup> protein catalytic knockout of DNA glycosylase activity on ss- and ds- Sp1 DNA. 160	160
4.1.14.	hNEIL3 <sup>Cat-K81A</sup> catalytic knockout of unhooking activity on HMT generated three-stranded ICL DNA oligonucleotide.....	162
4.1.15.	hNEIL3 <sup>Cat-K81A</sup> catalytic knockout of unhooking activity on HMT generated four-stranded ICL DNA oligonucleotide.....	164
4.1.16.	hNEIL3 <sup>Cat</sup> and hNEIL1 recombinant protein, protein-DNA substrate covalent complex generation with ss and ds Sp1.....	166
4.1.17.	hNEIL3 <sup>Cat</sup> , hNEIL3 <sup>Trun</sup> , hNEIL3 <sup>FL</sup> , Nei, hNEIL1 and hNEIL3 <sup>Cat-K81A</sup> protein-DNA substrate covalent complex generation with a three stranded HMT ICL.....	168
4.2.	<b>Discussion: Characterisation of the hNEIL1 and hNEIL3 DNA glycosylases in the repair of psoralen interstrand DNA crosslinks.....</b>	<b>170</b>
5.	<b>Characterisation of post-translational modification of hNEIL3 by the ubiquitin proteasome system.....</b>	<b>179</b>
5.1.	<b>Results: Characterisation of post-translational modification of hNEIL3 by the ubiquitin proteasome system.....</b>	<b>180</b>
5.1.1.	Recombinant hNEIL3 <sup>FL</sup> purification from <i>E. coli</i> for <i>in vitro</i> ubiquitination assays. ....	180
5.1.2.	Phosphocellulose purified HeLa WCE fraction <i>in vitro</i> ubiquitination of recombinant hNEIL3 <sup>FL</sup> . 182	182
5.1.3.	HiLoad Mono Q Sepharose Ion exchange fraction <i>in vitro</i> ubiquitination of recombinant hNEIL3 <sup>FL</sup> . 183	183
5.1.4.	Superdex 200 HR 10/30 gel filtration fraction <i>in vitro</i> ubiquitination of recombinant hNEIL3 <sup>FL</sup> . 185	185
5.1.5.	Mono Q 5-50 GL Ion exchange fraction <i>in vitro</i> ubiquitination of recombinant hNEIL3 <sup>FL</sup> . 187	187
5.1.6.	Identification and purification of recombinant the TRIM26 E3 ubiquitin ligase. ....	189
5.1.7.	<i>In vitro</i> ubiquitination of hNEIL3 by TRIM26 E3 ubiquitin ligase.....	191

5.1.8.	Analysis of hNEIL1 and hNEIL3 protein levels post H <sub>2</sub> O <sub>2</sub> and TRIM26 siRNA .....	192
5.1.9.	Analysis of hNEIL3 protein levels in response to cisplatin and TRIM26 siRNA treatment. 194	
5.1.10.	Cisplatin clonogenic analysis of the effect of TRIM26 RNAi or overexpression of hNEIL1/hNEIL3 on U2OS cell survival. ....	195
5.1.11.	CRISPR/Cas9 mediated knockout of endogenous hNEIL3. ....	197
5.2.	<b>Discussion: Characterisation of post-translational modification of hNEIL3 by the ubiquitin proteasome system.</b> .....	200
6.	<b>Discussion.</b> .....	204
7.	<b>Conclusion and Future Perspectives.</b> .....	210
	<b>References.</b> .....	212
	<b>Appendices.</b> .....	243
	<b>Scientific Research Articles.</b> .....	253

## Abstract.

The endonuclease VIII family of DNA glycosylases initiate repair of oxidative DNA base damage through BER and have been shown to resolve DNA inter-strand crosslinks (ICLs), arising from exogenous agents. Human NEIL1 (hNEIL1) activity on psoralen generated mono-adducts (MAs) and three-stranded DNA ICLs was previously described and recently NEIL3 from *Xenopus laevis* was reported to repair psoralen generated MAs and apurinic/apyrimidinic site DNA ICLs. Here, complementary roles of hNEIL1 and hNEIL3 in the removal of two oxidized pyrimidine bases were identified within a model DNA replication fork structure *in vitro*. Further investigation revealed a novel activity of truncated and full-length recombinant hNEIL3 proteins *in vitro* on single-stranded psoralen MAs and three-stranded and four-stranded psoralen ICL DNA substrates, highly toxic replication stalling lesions. For the first time it was shown that NEIL1/3 possess activity on four-stranded DNA ICLs. With the hNEIL3 catalytic knockout mutation K81A, elimination of activity on three- and four-stranded DNA ICLs was confirmed. hNEIL1 was recently shown to be ubiquitinated by the E3 ubiquitin-ligase, tripartite motif-containing protein 26 (TRIM26). Here, TRIM26 was identified as the major ubiquitin ligase for hNEIL3 through HeLa cell fractionation and *in vitro* ubiquitination assays. TRIM26 RNAi in U2OS cancer cells increased steady state levels of hNEIL1/3 and resulted in resistance to the ICL inducing agent cisplatin, determined through clonogenic survival assays. Transient overexpression of hNEIL1/3 complemented the observed phenotype. Finally, a model is proposed for incision-independent ICL repair in mammalian cells. FANCM - facilitated replication traverse of an ICL is envisaged, followed by NEIL1/NEIL3 initiated repair of ICL structures, independent of the induction of double-strand DNA breaks. This pathway is proposed to be modulated by TRIM26, providing resistance to ICL-inducing agents in cancer cells which display ubiquitin proteasome dysfunction.

## Abbreviations.

-	DNA crosslink
●	hydrogen bond complementation
1meA	N1-methyladenine
3'	three prime
3meA	3-methyladenine
3meC	3-methylcytosine
5'	five prime
5-OHC	5-hydroxycytosine
5-OHU	5-hydroxyuracil
7meG	N <sup>7</sup> -methyl-guanine
8-MOP	8, methoxypsoralen
8-OxoG	8-oxoguanine
A	adenine
AAG	alkyl-Adenine-DNA glycosylase
ALDH2	aldehyde dehydrogenase 2
ALDH5	aldehyde dehydrogenase 5
ALKBH2	DNA oxidative demethylase 2
ALKBH3	DNA oxidative demethylase 3
AMP	adenosine monophosphate
AP site	apurinic/ apyrimidinic site
APC	anaphase-promoting complex/cyclosome
APE1	apurinic/apyrimidinic endonuclease I
APOBEC3	DNA dC->dU-editing enzyme
APS	ammonium persulfate
ARF	tumour suppressor ARF
ATM	ataxia telangiectasia mutated kinase
ATP	adenosine triphosphate
ATR	ATM and Rad3-related kinase

ATRIP	ATR-interacting protein
BARD1	BRCA1-associated RING domain protein 1
BCNU	1,3-bis(2-chloroethyl)-1-nitrosourea
Bel-7402	human hepatocellular carcinoma Bel-7402
BER	base excision repair
bp	base pair(s)
BRCA1	breast Cancer Associated protein 1
BSA	bovine serum albumin
C	cytosine
C4-AP	C4'-oxidised abasic site
CARP1	cell division cycle and apoptosis regulator protein 1
CARP2	cell division cycle and apoptosis regulator protein 1
Cas9	CRISPR associated protein 9
CC	coiled-coil
CD38	cluster of differentiation 38
Cdc6	cell division cycle 6
cDNA	complementary DNA
Cdt1	cell division cycle 10-dependent transcript 1
CETN2	centrin 2
CFSS	common fragile sites
CHIP	carboxy terminus of Hsp70-interacting protein
Chk1	checkpoint kinase 1
Chk2	checkpoint kinase 2
CMG	Cdc45-Mcm2-7-GINS complex
CNE2	human nasopharyngeal carcinoma cell line 2
COP1	constitutive photomorphogenesis protein 1
CPD	cyclobutene-pyrimidine dimer
CRISPR	clustered regularly interspaced palindromic repeats
CRL	cullin 4A-regulator of cullins 1 E3 ubiquitin ligase

CSA	Cockayne syndrome protein A
CSB	Cockayne syndrome protein B
CUL1	cullin-1
CUL4	cullin-4
CUL4A	cullin-4A
DDB1	DNA damage binding protein 1
DDB2	DNA damage binding protein 2
DDR	DNA damage response
DDT	DNA damage tolerance
DMEM	Dulbecco's modified Eagle medium
DNA	deoxyribose nucleic acid
DNAPKcs	DNA dependent protein kinase, catalytic subunit
DPBS	Dulbecco's phosphate buffered saline
dRP	deoxyribose phosphate
ds	double-stranded
DSB	double-strand Break
E4F1	E4F transcription factor 1
<i>EcoMap</i>	<i>E. coli</i> methionine amino peptidase
EDTA	ethylenediaminetetraacetic acid
EME1	crossover junction endonuclease EME1
ERCC1	excision repair cross complementing protein 1 endonuclease
ERFSs	early-replicating fragile sites
ES	embryonic stem cell
EXO1	exonuclease 1
FA	Fanconi anemia
FAAP100	Fanconi anemia associated protein of 100 kDa
FAAP20	Fanconi anemia associated protein of 20 kDa
FAAP24	Fanconi anemia associated protein of 24 kDa
FAN1	Fanconi associated nuclease 1

FANCA	Fanconi anemia complementation group A/H
FANCB	Fanconi anemia complementation group B
FANCC	Fanconi anemia complementation group C
FANCD1	Fanconi anemia complementation group D1 (BRCA2)
FANCD2	Fanconi anemia complementation group D2
FANCE	Fanconi anemia complementation group E
FANCF	Fanconi anemia complementation group F
FANCG	Fanconi anemia complementation group G (XRCC4)
FANCH	Fanconi anemia complementation group H/A
FANCI	Fanconi anemia complementation group I
FANCI	Fanconi anemia complementation group J (BRIP1/ BACH1)
FANCL	Fanconi anemia complementation group L/ E3 ubiquitin ligase FANCL(FAAP43)
FANCM	Fanconi anemia complementation group M (KIAA1596/ FAAP250)
FANCN	Fanconi anemia complementation group N/ partner and localizer of BRCA2 (PALB2)
FANCO	Fanconi anemia complementation group O/ RAD51 paralog (RAD51C)
FANCP	Fanconi anemia complementation group P/ SLX-4 structure specific endonuclease subunit (SLX4)
FANCQ	Fanconi anemia complementation group Q/ ERCC excision repair 4, endonuclease catalytic subunit (XPF)
FANCR	Fanconi anemia complementation group R/ RAD51 recombinase (RAD51A/RECA)
FANCS	Fanconi anemia complementation group S/ Breast Cancer Associated protein 1 (BRCA1/RNF53)
FANCT	Fanconi anemia complementation group T/ Ubiquitin conjugating enzyme E2 T (UBE2T)
FANCU	Fanconi anemia complementation group U/ X-Ray repair cross complementing 2 (XRCC2)
FANCV	Fanconi anemia complementation group V/ mitotic arrest deficient 2 like 2 (MAD2L2)
Fapy	formamidopyrimidine

FapyA	4, 6-diamino-5-formamidopyrimidine
FapyG	2, 6-diamino-4-hydroxy-5-formamidopyrimidine
FBXW7	F-box and WD repeat domain containing 7
FEN1	flap endonuclease 1
FOXO1	forkhead box protein O1
Fpg	formamidopyrimidine DNA glycosylase
FPLC	fast protein liquid chromatography
G	guanine
G1 phase	gap 1 phase during cell cycle interphase
G1	gRNA1
G2 phase	gap 2 phase during cell cycle interphase
G2	gRNA2
G2/M phase	gap 2 phase DNA damage checkpoint
GC-MS	gas chromatography-mass spectrometry
GG-NER	global genome nucleotide excision repair
Gh	guanidinohydantoin
GINS	<i>go-ichi-ni-san</i> complex (Sld5-Psf1-Psf2-PS3)
GP78	glycoprotein 78
H2AX	histone 2 A X
H2TH	helix-two-turn-helix domain
HCC	hepatocellular carcinoma
HCT116	human colorectal carcinoma epithelial cells
HeLa	Henrietta Lacks derived cervical adenocarcinoma
HepG2	human hepatocellular carcinoma
HhH	helix-hairpin-helix motif
HIF	hypoxia-inducible factors
HIF $\alpha$	hypoxia-inducible factor alpha
HIV	human immunodeficiency virus
HMGN1	high mobility group nucleosome-binding domain-containing protein 1

HMT	trimethylpsoralen
hNEIL1	human endonuclease VIII-like-1
hNEIL2	human endonuclease VIII-like-2
hNEIL3	human endonuclease VIII-like-3
HR	homologous Recombination
HSC	haematopoietic stem cells
HU	hydroxyurea
ICL	interstrand DNA crosslinks
ICP0	E3 ubiquitin-protein ligase ICP0
IFN- $\beta$	interferon beta
IL-32	interleukin 32
iPSC	inducible pluripotent stem cells
IPTG	isopropyl- $\beta$ -D-thiogalactopyranoside
IR	ionising radiation
IRF3	nuclear Interferon Regulatory Transcription Factor 3
IRF7	interferon Regulatory Transcription Factor 7
Jmjd3	lysine-specific demethylase 6B
KAI1	metastasis suppressor Kangai-1
kDa	kilodalton
Klf4	krueppel-like factor 4
LCMS	liquid chromatography mass-spectrometry
MA	monoadduct
MAf	furan-ring monoadduct
MAp	pyrone-ring monoadduct
MBD4	methyl-CpG Binding Domain 4, DNA Glycosylase/Mediator Complex Subunit 1 (MED1)
Mcm2-Mcm7	minichromosome maintenance proteins 2-7
MDM2	mouse double minute 2 homolog
MEF	mouse embryonic fibroblast
MGMT	<i>O</i> <sup>6</sup> -methylguanine-DNA methyltransferase

MHF1	histone fold protein complex 1
MHF2	histone fold protein complex 2
MMC	mitomycin C
MMR	mismatch repair
MMS	methyl-methanesulfonate treatment
MRE11	meiotic recombination 11 homolog A
MSL2	male-specific lethal 2-like 1
MULE	Mcl-1 ubiquitin ligase E3
MUS81	crossover junction endonuclease Mus81
MutL $\alpha$	DNA mismatch repair protein MutL
MutS $\alpha$	putative DNA mismatch repair protein, C-terminal
MUTYH	adenine DNA glycosylase homolog
MW	molecular weight
NBS1	nibrin
Nei	endonuclease VIII
NEMO	NF $\kappa$ B essential modulator
NER	nucleotide excision repair
NF $\kappa$ B	nuclear factor kappa-light-chain-enhancer of activated B cells
NF $\kappa$ B2	nuclear Factor Kappa B Subunit 2
NHEJ	non-Homologous End Joining
NPC	nasopharyngeal carcinoma
Nth	endonuclease III
NTH1	endonuclease III homolog
O <sup>6</sup> meG	O6-methylguanine
O/E	overexpression
Oct4	octamer-binding transcription factor 4
OGG1	8-oxoguanine DNA glycosylase
ORC1-6	origin recognition complex
ORF6	open reading frame 6

OTU	ovarian tumour proteases
P	phosphate
p130	130 kDa retinoblastoma-associated protein
p21CIP1	cyclin-dependent kinase inhibitor 1A (P21, Cip1), isoform CRA_a
p27KIP1	cyclin-dependent kinase inhibitor p27
p38	mitogen-activated protein kinase 11
p53	cellular tumour antigen p53
p57	cyclin-dependent kinase inhibitor 1C
PA	phospho $\alpha$ , $\beta$ -unsaturated aldehyde
PARK2	PARKIN E3 ubiquitin ligase
PARP-1	poly(ADP-ribose)polymerase 1
PBS	phosphate-buffered saline
PCNA	proliferating cell nuclear antigen
PCR	polymerase chain reaction
PCV	packed cell volume
PdG	N <sup>2</sup> -propano-2'-deoxyguanosine
PHF20	plant homeodomain finger protein 20
PIP box	PCNA interacting protein box
Pirh2	p53-induced RING-H2 protein
PMSF	phenylmethylsulfonyl fluoride
PNKP	polynucleotide kinase/phosphatase
Pol	polymerase
PPi	pyrophosphate
PTM	post-translational modification
RAD23B	UV excision repair protein radiation sensitive 23B
RAD51	DNA repair protein RAD51 homolog 1
RBBC	RING, B-Box(es), Coiled coil domain E3 ubiquitin ligases
RecQ	ATP-dependent DNA helicase RecQ
Rev1	DNA repair protein REV1

RFC	replication factor C
RIG-1	retinoic acid-inducible gene 1 protein
RING	really interesting new gene
RNA	ribonucleic acid
RNAi	ribonucleic acid interference
ROS	reactive oxygen species
RPA	replication protein A
RSR	replication stress response
SC	scramble control
SCF	Skp1, Cul1/Cdc53, Roc1, and an F-box-containing E3 ubiquitin ligase
SCJ	sister chromatin junction
SDS-PAGE	sodium dodecyl sulfate polyacrylamide gel electrophoresis
shRNAi	short hairpin ribonucleic acid interference
siRNA	short interfering ribonucleic acid
SLX4	structure specific endonuclease subunit
SMUG1	single-strand-selective monofunctional uracil-DNA glycosylase 1
S <sub>N</sub> 1	substitution nucleophilic unimolecular
S <sub>N</sub> 2	substitution nucleophilic bimolecular
SNM1A	DNA cross-link repair 1A protein
SNP	single nucleotide polymorphism
Sox2	Sox transcription factor 2
Sp	spiroiminodihydantoin
S-phase	synthesis phase
SQSTM1	sequestosome 1
ss	single-stranded
SSB	single-strand Break
STAT1	signal Transducer and Activator of Transcription 1
STRAP	serine-threonine kinase receptor-associated protein
T	thymine

TAF7	TATA-Box Binding Protein Associated Factor 7
TAK1	nuclear receptor subfamily 2 group C member 2
TBE	tris-borate EDTA
TBK1	serine/threonine-protein kinase
TC-NER	transcription coupled nucleotide excision repair
TDG	thymine DNA glycosylase
TEMED	tetramethylethylenediamine
TFIID	transcription factor IID
TFIIH	transcription initiation factor II H
Tg	thymine glycol
TG	tris-glycine
TGS	tris-glycine SDS
TGF- $\beta$	transforming growth factor beta
THP-1	human acute monocytic leukemia
TIP60	60 kDa Tat-interactive protein
TLS	trans-lesion synthesis
TopBP1	topoisomerase 2-binding protein 1
TOPORS	topoisomerase I-binding RING finger protein
TRAIP	TRAF-interacting protein
TRF2	telomeric repeat-binding factor 2
TRIM	tripartite motif containing protein
TRIM24	tripartite motif containing protein 24
TRIM25	tripartite motif containing protein 25
TRIM26	tripartite motif containing protein 26
TRIM28	tripartite motif containing protein 28
TRIM29	tripartite motif containing protein 29
TRIM32	tripartite motif containing protein 32
TRIM51	tripartite motif containing protein 51
TRIM5 $\alpha$	tripartite motif containing protein 5 alpha

TS	template switching
U	uracil
U2OS	human Bone Osteosarcoma Epithelial Cells
Ub	ubiquitin
UBA52	ubiquitin A-52 residue ribosomal protein fusion product 1
UBA80	ubiquitin carboxyl extension protein 80
UbB	ubiquitin B
UbC	ubiquitin C
UBE2C	ubiquitin-conjugating enzyme E2 C
UBE2N	ubiquitin-conjugating enzyme E2 N
UBE2S	ubiquitin-conjugating enzyme E2 S
UBE2V1	ubiquitin-conjugating enzyme E2 variant 1
UBR3	ubiquitin-protein ligase E3-alpha-3
UCH	ubiquitin carboxyl-terminal hydrolase isozyme L5
Ug	uracil glycol
UNG	uracil DNA N-glycosylase
UPS	ubiquitin Proteasome System
USP	ubiquitin specific proteases
USP1	ubiquitin-specific-processing protease 1
USP7	ubiquitin-specific-processing protease 7
UV	ultraviolet
UVSSA	UV stimulated scaffold protein A
VHL	von Hippel-Lindau tumour-suppressor protein
Vpr	viral protein R
WCE	whole cell extract
WRN	Werner syndrome RecQ helicase
WT	wild type
WWP1	WW domain-containing protein 1
XAB2	XPA-binding protein 2

XPA	xeroderma pigmentosum complementation group A
XPB	xeroderma pigmentosum complementation group B
XPC	xeroderma pigmentosum complementation group C
XPD	xeroderma pigmentosum complementation group D
XPF	xeroderma pigmentosum complementation group F
XPG	xeroderma pigmentosum complementation group G
XRCC1	X-ray repair cross complementing protein 1
YY1	transcriptional repressor protein ying and yang 1
$\gamma$ -H2AX	gamma Histone 2 A X

## List of Figures.

<b>Figure 1.1: Schematic representation of ROS generation through the consecutive reduction of cellular oxygen and superoxide radical catalysis by superoxide dismutase.</b> .....	6
<b>Figure 1.2: Fenton reaction formula showing the generation of ROS as result of the presence of Iron (Fe).</b> .....	6
<b>Figure 1.3: Schematic representation of the major DNA lesions generated through oxidation of guanine, 8-oxoguanine (8-OxoG) and 2,6-diamino-4-hydroxy-5-formamidopyrimidine (FapyG). Further oxidation of 8-OxoG may lead to the formation of open ring Guanidinohydantoin (Gh) and closed ring Spiroiminodihydantoin (Sp). Positions highlighted in red represent those modified.</b> .....	7
<b>Figure 1.4: Schematic representation of the spontaneous dehydration and deamination of cytosine post-oxidation, leading to the formation of the 5-hydroxyuracil (5-OHU) lesion (Adapted from Thiviyanathan <i>et al.</i>, 2008). Positions highlighted in red represent those modified.</b> .....	8
<b>Figure 1.5: Schematic representation of the generation of Thymine glycol (Tg) through <math>\cdot\text{OH}</math> oxidisation of the 5,6 double bond of thymine followed by <math>\text{O}_2</math> addition and decomposition (Adapted from Cadet and Wagner, 2013). Positions highlighted in red represent those modified.</b> .....	9
<b>Figure 1.6: Skeletal formula of the psoralen interstrand crosslinking agents 8-methoxypsoralen (8-MOP) and trimethylpsoralen (HMT).</b> .....	14
<b>Figure 1.7: Skeletal formula of 8-MOP-thymine mono-adducts. MAp.</b> Pyrone-side 8-MOP-dT mono-adduct and <b>MAf.</b> The furan-side 8-MOP-dT mono-adducts shown in two diastereomeric representations. Red structure indicates the thymine nitrogenous base with green bonds representing those formed after covalent modification by 8-MOP (Adapted from Couvé <i>et al.</i> , 2009). .....	15
<b>Figure 1.8: Skeletal formula of 8-MOP mediated ICL generation with UVA exposure.</b> 8-MOP intercalates between two opposing thymine nucleotides and is activated on exposure to UVA generating a thymine-thymine ICL in a 5'-TpA-3' specific manner.'dR' denotes deoxyribose sugar and phosphodiester backbone of DNA. Red structures indicate thymidine residues, black structure represents 8-MOP and green bonds represent those formed after UVA activation (Adapted from Deans and West, 2011). .....	15
<b>Figure 1.9: Schematic representation of GG-NER and TC-NER pathways.</b> IN GG-NER, XPC in complex with CETN2, RAD23 probe for ss-DNA formed by helical distorting lesions. DDB1 and DDB2 facilitate detection through XPC interaction. In TC-NER RNA pol II stalls and CSB and CSA proteins are recruited and backtracks the RNA pol II along the DNA. The TFIIH complex is then recruited and the lesion is verified through XPD, XPA and XPB. RPA coats the non-damaged ss-DNA. ERCC1-XPB and XPG sequentially incised the DNA releasing the damaged DNA. PCNA recruits DNA polymerases to conduct gap filling synthesis and the nick is sealed by DNA ligase I or III (Adapted from Marteijn <i>et al.</i> , 2014). .....	29
<b>Figure 1.10: Schematic model of Fanconi anemia initiated replication associated ICL repair.</b> The CMG complex stalls and is dissociated by BRCA1/BARD1 and the strand is extended towards the ICL. The FA pathway is then initiated through FANCM recruitment of the FANC core complex. Subsequently the FANCI/D2 heterodimer is recruited and monoubiquitinated by FANCT and FANCL. The ICL is incised near an ICL by Mus81/EME1 and XPF/ERCC1, respectively, flipping out the ICL. TLS proceeds generating a three-stranded structure. NER is proposed to remove the ICL remnant followed by homologous recombination to yield two homologous DNA duplex.....	33
<b>Figure 1.11: Schematic representation of the short-patch BER pathway.</b> N-glycosydic bond is hydrolysed by DNA glycosylase activity generating an AP-site. The phosphodiester backbone is then processed through APE1 cleavage of an AP site or associated lyase activity of the DNA glycosylase, to generate a ss-nick. End processing by APE1 or PNKP for then proceeds yielding a 3'-OH group. Pol $\beta$	

may remove the 5'-dRP yielding a 5'-Phosphate group (P), Pol  $\beta$  then conducts gap filling synthesis. The ss-nick is then sealed by (Lig III) in complex with scaffold protein XRCC1. ....37

**Figure 1.12: Schematic representation for long-patch BER pathway.** 5'-dRP becomes modified after APE1 cleavage, preventing removal by Pol  $\beta$ . As result specialised DNA polymerases  $\delta$  or  $\epsilon$  undertake strand displacement, replacing >1 nucleotide generating a flap structure, a substrate for FEN1. The flap is excised, and the ss-DNA nick is sealed by Lig I and restores the duplex.....39

**Figure 1.13: Multiple sequence alignment of the amino acid sequence of *E. coli* Nei, *E. coli* Fpg, hNEIL1, hNEIL2 and hNEIL3.** CLUSTAL O (1.2.4) multiple sequence alignment was used to generate alignment and amino acid sequence conservation was generated with Jalview (2.10.5). Conservation histogram displays the conservation of amino acid domains with a value 0-9 (less conserved to most conserved), where “-” denotes no conservation, “+” denotes conservation of amino acid residue properties and “\*” denotes absolute conservation. Columns displaying no alignment have been removed. ....41

**Figure 1.14: Conserved domain analysis of the human endonuclease VIII like 1 (hNEIL1) DNA glycosylase.** Fpg/Nei superfamily domain, helix-two-turn helix (H2TH) domain and the NEIL1 DNA binding domain. ....48

**Figure 1.15: Conserved domain analysis of the human endonuclease VIII like 2 (hNEIL2) DNA glycosylase.** Fpg/Nei superfamily domain and helix-two-turn helix (H2TH) domain. ....51

**Figure 1.16: Conserved domain analysis of the human endonuclease VIII like 3 (hNEIL3) DNA glycosylase.** Fpg/Nei superfamily domain, helix-two-turn helix (H2TH) domain, zinc finger RanB domain and zinc finger-GRF domain (Zf-GRF). ....54

**Figure 1.17: Schematic representation of the ubiquitin proteasome system.** “Ub” denotes ubiquitin, “E1” denotes E1 ubiquitin activating enzyme, “E2” denotes E2 ubiquitin conjugating enzyme, “E3” denotes E3 ubiquitin ligase, “ATP” denotes adenosine triphosphate, “AMP” denotes adenosine monophosphate and “PPi” denotes pyrophosphate. ....58

**Figure 1.18: Plasmid vector map of the pETDuet1 expression vector developed for dual expression of two genes.** Transcription vector map with sequence landmarks, including: T7 promoters, T7 terminator, 6xHistidine, multiple cloning sites (MCS-1/2), Ampicillin resistance gene (AmpR), Ribosomal binding site (RBS), repressor of primer (ROP), LacI gene (lacI), double-strand replication of origin (ori) and single-stranded replication of origin (F1 ori). ....73

**Figure 1.19: Linear vector maps of the modified pET vectors used in the construction of the pETDuet2-*EcoMap*-ORF6 expression vector backbone.** A: The pET30b intermediate vector ORF6 region, overlapping leader sequence for improved transcription of desired cDNA of interest. B: The bicistronic pETDuet2-*EcoMap*-ORF6-construct for mouse NEIL3 and human glycosylase domain NEIL3 (taken from Liu *et al.*, 2012). ....74

**Figure 1.20: Diagrammatic representation of the hNEIL3 conserved domains encoded by the cDNA cloned into the pETDuet2-*EcoMap*-ORF6 bicistronic expression vector.** A. hNEIL3<sup>Cat</sup> 843 bp cDNA truncation encoding 281 amino acids B. hNEIL3<sup>Trun</sup> 1044 bp truncation encoding 348 amino acids and C. hNEIL3<sup>FL</sup> 1818bp full length cDNA sequence and encoding 605 amino acids. ....76

**Figure 2.1: Western blot transfer sandwich assembly** (Figure taken from Mini Blot Module instruction manual, ThermoFisher). ....85

**Figure 2.2: Schematic representation of three-stranded and four-stranded DNA ICL oligonucleotide substrate generation.** “\*” denotes the position of  $\gamma$  <sup>32</sup>P labelling. ....94

**Figure 2.3: The pCas-Guide vector map.** The pCas-Guide facilitated the transient mammalian expression of wild type Cas9 protein and transcription of target gRNA sequences in complex with gRNA scaffold complex. pCas-Guide vector map shows G1 and G2 gRNA sequences used for targeting exon 1 of the NEIL3 gene sequence and scramble control (SC) gRNA sequence for negative control cell line generation (Adapted from the Origene CRISPR/Cas9 Genome Editing instruction manual). ....108

**Figure 2.4: The pUC-Donor cassette map.** pUC-Donor facilitated the transient expression of puromycin antibiotic resistance gene and provision of the homology directed repair (HDR) cassette for integration at G1, G2 or SC gRNA sequence site. pUC-Donor vector map shows left homologous arm (LHA), green fluorescent protein gene (GFP), Cre/Lox recombinase sequences (Loxp), phosphoglycerate kinase (PGK) promoter, puromycin antibiotic resistance gene (PURO) and right homologous arm (RHA) Adapted from the Origene CRISPR/Cas9 Genome Editing instruction manual).

.....108

**Figure 3.1 HisTrap-HP FPLC purification of hNEIL1.** A. Chromatogram analysis of protein fractions generated by HisTrap chromatography of lysates from *E. coli* overexpressing hNEIL1. B. 10% SDS-PAGE analysis. C. Anti-His western blot analysis. "M" All Blue Prestained Protein Standards (BioRad).....114

**Figure 3.2: Denaturing PAGE analysis of oligonucleotide substrates incubated with hNEIL1 (A, C) or hNEIL3 (B, D).** A. Analysis of 228 nM hNEIL1 incubated with 5 nM ss-DNA oligonucleotide substrates B. Analysis of 150 nM hNEIL3<sup>FL</sup> incubated with 5 nM ss-DNA oligonucleotide substrates. C. Analysis of 228 nM hNEIL1 incubated with 5 nM ds-DNA oligonucleotide substrates. D. Analysis of 300 nM hNEIL3<sup>FL</sup> incubated with 5 nM ds-DNA oligonucleotide substrates. "19<sup>PA</sup>" and "19<sup>P</sup>" denote 19 mer cleavage fragments with a 3'-terminal PA or P, respectively. ....116

**Figure 3.3: Denaturing PAGE analysis of fork structured oligonucleotides incubated with hNEIL1.** A. 10% denaturing PAGE analysis of 228 nM hNEIL1 incubated with 5 nM 5-OHU containing oligonucleotide substrates B. 10% denaturing PAGE analysis of 228 nM hNEIL1 incubated with 5 nM 8-OxoG containing oligonucleotide substrates. C. 10% denaturing PAGE analysis of 228 nM hNEIL1 incubated with 5 nM Tg containing oligonucleotide substrates. D. Quantification of 5-OHU, 8-OxoG and Tg oligonucleotide substrate cleavage by hNEIL1. Ctrl sample in the absence of recombinant hNEIL1. Bacterial *Nei* and *Nth* provide reference for associated  $\beta,\delta$ -elimination and  $\beta$ -elimination, respectively. Representative images of three experiments. ....118

**Figure 3.4: Denaturing PAGE analysis of fork structured oligonucleotides incubated with hNEIL3<sup>FL</sup>.** A. 10% denaturing PAGE analysis of 150 nM hNEIL3<sup>FL</sup> incubated with 5 nM 5-OHU containing oligonucleotide substrates B. 10% denaturing PAGE analysis of 150 nM hNEIL3<sup>FL</sup> incubated with 5 nM 8-OxoG containing oligonucleotide substrates. C. 10% denaturing PAGE analysis of 150 nM hNEIL3<sup>FL</sup> incubated with 5 nM Tg containing oligonucleotide substrates. D. Quantification of 5-OHU, 8-OxoG and Tg oligonucleotide substrate cleavage percentages. Ctrl sample in the absence of recombinant hNEIL3<sup>FL</sup>. Bacterial *Nei* and *Nth* provide reference for associated  $\beta,\delta$ -elimination and  $\beta$ -elimination, respectively (Mustafa Albelazi, University of Salford). ....120

**Figure 4.1: Denaturing PAGE analysis of ICL construct preparation.** (X) Denotes ICL duplex substrate product band. "\*" Denotes 5' <sup>32</sup>P-labelled oligonucleotide strand, "•" Duplex DNA formed by annealing, "-" psoralen/UVA treated annealed duplex DNA oligonucleotide, "+" Mixture of ss-DNA oligonucleotides, "/" psoralen/UVA treated ss-DNA oligonucleotides. ....127

**Figure 4.2: Denaturing PAGE analysis of ICL construct gel excision.** (Lanes 1-2) Before excision of ICL DNA D21\* - C47 and D21 - C47\* HMT ICL oligonucleotides. (Lanes 3-4) After excision of D21\* - C47 and D21 - C47\* ICL oligonucleotides. (Lanes 5-6) Before and after excision of the C47\* - D101 ICL oligonucleotide. Upper bands represent covalently bound ICL DNA, whilst lower bands represent non-crosslinked DNA. "\*" Denotes 5' <sup>32</sup>P labelled oligonucleotide DNA oligonucleotide "-" psoralen(HMT)/UVA ICL duplex. ....128

**Figure 4.3: Non-denaturing PAGE analysis of psoralen/UVA oligonucleotide DNA structures.** Oligonucleotide construct key included below the gel image. "\*" Denotes 5' <sup>32</sup>P labelled oligonucleotide DNA oligonucleotide, "•" hydrogen bond DNA complementation, "-" psoralen/UVA treated and ICL bound DNA. ....130

**Figure 4.4: Denaturing PAGE analysis of psoralen/UVA treated, duplex, three and four-stranded oligonucleotide structures.** Psoralen ICL lesion remain stable after gel purification. DNA substrates

were analysed by denaturing PAGE. (X). Denotes DNA oligonucleotide containing psoralen ICL. "\*" Denotes 5' <sup>32</sup>P labelled oligonucleotide DNA oligonucleotide, "•" hydrogen bond DNA complementation, "-" psoralen/UVA treated and ICL bound DNA. ....131

**Figure 4.5: Denaturing PAGE analysis of XL47 • 47 - 21\* DNA oligonucleotides incubated with hNEIL3 proteins.** hNEIL3 proteins unhook psoralen ICLs in a three-stranded DNA context with a monofunctional profile. hNEIL3<sup>Cat</sup>, hNEIL3<sup>Trun</sup>, hNEIL3<sup>FL</sup> and *Nei* protein activity on ~10 nM XL47 • 47 - 21\*mer generated three-stranded DNA ICL. A. (lanes 1-15) Reactions were without piperidine treatment. B. Reactions were with light piperidine treatment. B. Ctrl sample is in the absence of recombinant protein. *Nei* as control for previously characterised psoralen ICL unhooking activity. "X"denotes substrate, A. "21-MA" denotes 21 mer fragment containing psoralen-derived MA, A. "21-mer" B."47-mer" denote cleavage fragments containing an AP (Lanes 2-13), A. "8<sup>PA</sup>", denotes 8 mer fragments containing a 3'-terminal PA. ....133

**Figure 4.6: Quantification of the percentage cleavage of XL47 • 47 - 21\* three-stranded DNA ICL substrate by hNEIL3<sup>Cat</sup>, hNEIL3<sup>Trun</sup> and hNEIL3<sup>FL</sup>.** "\*" Denotes 5' <sup>32</sup>P labelled oligonucleotide DNA oligonucleotide, "•" hydrogen bond DNA complementation, "-" psoralen/UVA treated and ICL bound DNA. ....134

**Figure 4.7: Denaturing PAGE analysis of Sp1 containing DNA oligonucleotides incubated with hNEIL3<sup>Cat</sup>, hNEIL3<sup>Trun</sup>, hNEIL3<sup>FL</sup>, hNEIL1 and *Nei*.** A. hNEIL3<sup>Cat</sup>, hNEIL3<sup>Trun</sup> and hNEIL3<sup>FL</sup> protein activity upon 10 nM ss Sp1 substrate. B. *Nei* and hNEIL1 activity upon 10 nM ds Sp1 substrate. "17 mer" denotes substrate, A-B. "8<sup>PA</sup>" and "8<sup>P</sup>" denotes 8 mer fragments containing a 3'-terminal PA and P, respectively. C. Quantification of hNEIL3<sup>Cat</sup>, hNEIL3<sup>Trun</sup> and hNEIL3<sup>FL</sup> generated cleavage product percentages after enzymatic cleavage assay on 10 nM ss Sp1 substrate. D. Quantification of *Nei* and hNEIL1 generated cleavage product percentages after enzymatic cleavage assay on 10 nM ds Sp1 substrate.....136

**Figure 4.8: Denaturing PAGE analysis of ~ 10 nM (X): XL21\* - 1 ss MA substrate incubated with hNEIL3<sup>Cat</sup>, hNEIL3<sup>Trun</sup>, hNEIL3<sup>FL</sup>, hNEIL1 and *Nei*.** Samples were incubated for 1 h at 37°C with 500 nM of protein. For positive control 20 nM of bacterial *Nei* was used and 500 nM hNEIL1. (Lanes 1-8) Reactions were without piperidine treatment. "Ctrl" sample in the absence of recombinant protein. (Lanes 9-12) Reactions with light piperidine treatment. "X" denotes substrate, A. "21-MA" denotes 21 mer fragment containing a psoralen-derived MA, "21-mer" denote cleavage fragments containing an AP (Lanes 2-4), "8<sup>PA</sup>" denote 8 mer fragments containing a 3'-terminal PA respectively. ....137

**Figure 4.9: Denaturing PAGE analysis: A. ~10 nM (X): XL47 • 47 - 21\* B. ~10 nM (X) XL47 • 47\* - 21 HMT generated three-stranded DNA ICL incubated with of hNEIL3<sup>Cat</sup>, hNEIL3<sup>Trun</sup>, hNEIL3<sup>FL</sup>, hNEIL1 and *Nei* protein.** Samples were incubated for 1 h at 37°C with 500 nM of protein. For positive control 50 nM of hNEIL1 was used. (Lanes 1-7) Reactions without piperidine treatment. (Lanes 7-12) Reactions with light piperidine treatment. (Lane 7) 21\* mer ds-MA substrate digested with *Nei* cleavage, product control. (Lane 8) 47\* mer ds-MA substrate digested with *Nei*, cleavage product control. (Lane 6) A. 21 C21\* MA B.47 • 47\* ss oligonucleotide size marker. (Lane 10) D47, 47 mer ss oligonucleotide size marker. (Lane 12) A. 21\* B. 47\* mer oligonucleotides. (Lane 13-15) A. 21 U • A duplex B. 47 U • A duplex with UDG/Hot Piperidine treatment, UDG/Nfo and UDG/light Piperidine, respectively. Substrate and cleavage products sizes are indicated to the right of the gel. "X"denotes substrate, A. "21-MA" denotes 21 mer fragment containing a psoralen-derived MA, A. "21-mer" B."47-mer" denote cleavage fragments containing an AP (Lanes 2-4), A. "8<sup>PA</sup>", "8<sup>OH</sup>" and "8<sup>P</sup>" denote 8 mer B. 23<sup>PA</sup>", "23<sup>OH</sup>" and "23<sup>P</sup>" denote 23 mer, fragments containing a 3'-terminal PA, OH and P, respectively. ....140

**Figure 4.10: Schematic representation of the mechanistic biochemical action of *Nei*, hNEIL1 and hNEIL3 DNA glycosylases on three-stranded psoralen ICL oligonucleotide substrates.** A. Mechanism of action of the *Nei*, hNEIL1 and hNEIL3 recombinant DNA glycosylases on three-stranded psoralen ICL oligonucleotides. B. Skeletal formula of an unhooked ss-21\* mer HMT MA with thymine from opposite

complementary DNA strand, produced by Nei, hNEIL1 and hNEIL3 facilitated DNA glycosylases excision. C. Skeletal formula of proposed thymine-HMT-thymine excision product generated post hNEIL3 facilitated unhooking and subsequent downstream processing of ds-MA product by hNEIL1.

.....141  
**Figure 4.11: Denaturing PAGE analysis of hNEIL3<sup>Cat</sup>, hNEIL3<sup>Trun</sup>, hNEIL3<sup>FL</sup>, hNEIL1 and Nei protein activity on:** A. ~10 nM (X): A. XL47 • 47 - 21\* • 21. B. ~10 nM (X): XL47 • 47\* - 21 • 21 HMT generated three-stranded DNA ICL. Samples were incubated for 1 h at 37°C with 500 nM of protein. For positive control 20 nM of bacterial Nei was used and 500 nM hNEIL1. (Lanes 1-7) Reactions without Piperidine treatment. (Lanes 7-12) Reactions with light piperidine treatment (Lane 7) 21\* mer ds-MA substrate digested with Nei cleavage, product control. (Lane 8) 47\* mer ds-MA substrate digested with Nei, cleavage product control. (Lane 6) A. 21 C21\* MA B.47 • 47\* ss oligonucleotide size marker. (Lane 10) D47, 47 mer ss oligonucleotide size marker. (Lane 12) A. 21\* B. 47\* mer oligonucleotides. (Lane 13-15) A. 21 U • A duplex B. 47 U • A duplex treated with UDG/Hot Piperidine, UDG/Nfo and UDG/light Piperidine, respectively. Substrate and cleavage products sizes are indicated to the right of the gel. "X" denotes substrate, A. "21-MA" denotes 21 mer fragment containing a psoralen-derived MA, A. "21-mer" B."47-mer" denote cleavage fragments containing an AP (Lanes 2-4), A. "8<sup>PA</sup>", "8<sup>OH</sup>" and "8<sup>P</sup>" denote 8 mer B. 23<sup>PA</sup>", "23<sup>OH</sup>" and "23<sup>P</sup>" denote 23 mer, fragments containing a 3'-terminal PA, OH and P, respectively.....144

**Figure 4.12: Schematic representation of the mechanistic biochemical action of Nei, hNEIL1 and hNEIL3 DNA glycosylases on four-stranded psoralen ICL oligonucleotide substrates.** A. Mechanism of action of the Nei, hNEIL1 and hNEIL3 recombinant DNA glycosylases on three-stranded psoralen ICL oligonucleotides. B. Skeletal formula of an unhooked ss-21\* mer HMT MA with thymine from opposite complementary DNA strand, produced by Nei, hNEIL1 and hNEIL3 facilitated DNA glycosylases excision. C. Skeletal formula of proposed thymine-HMT-thymine excision product generated post hNEIL3 facilitated unhooking and subsequent downstream processing of ds-MA product by hNEIL1.

.....145  
**Figure 4.13: Denaturing PAGE analysis hNEIL3<sup>Cat</sup>, hNEIL3<sup>Trun</sup>, hNEIL3<sup>FL</sup>, hNEIL1 and Nei proteins on ~10 nM (X): XL101 • 101 – 47\* HMT generated three-stranded DNA ICL.** Samples were incubated for 1 h at 37°C with 500 nM of protein. For positive control 20 nM of bacterial Nei was used and 500 nM hNEIL1. (Lanes 1-10) Reactions without piperidine treatment. (Lanes 11-14) Reactions with light piperidine treatment (Lane 7) 21\* mer ds-MA substrate digested with Nei cleavage, product control. (Lane 8) 47\* mer ds-MA substrate digested with Nei, cleavage product control. (Lane 9) C21, 21 mer ss oligonucleotide size marker. (Lane 10) D47, 47 mer ss oligonucleotide size marker. "X" denotes substrate, A. "47-MA" denotes 47 mer fragment containing a psoralen-derived MA,"47-mer" denote cleavage fragments containing an AP (Lanes 2-4). "23<sup>PA</sup>" and "23<sup>P</sup>" denote 23 mer, fragments containing a 3'-terminal PA and P, respectively. ....147

**Figure 4.14: Denaturing PAGE analysis of hNEIL3<sup>Cat</sup>, hNEIL3<sup>Trun</sup>, hNEIL3<sup>FL</sup>, hNEIL1 and Nei protein on ~10 nM (X): XL47 • 47 – 21\* 8-MOP generated three-stranded DNA ICL.** Samples were incubated for 1 h at 37°C with 500 nM of protein. For positive control 20 nM of bacterial Nei was used and 500 nM hNEIL1. (Lanes 1-10) Reactions without piperidine treatment. (Lanes 11-14) Reactions with light piperidine treatment (Lane 7) 21\* mer ds-MA substrate digested with Nei cleavage, product control. (Lane 8) 47\* mer ds-MA substrate digested with Nei, cleavage product control. (Lane 9) C21, 21 mer ss oligonucleotide size marker. (Lane 10) D47, 47 mer ss oligonucleotide size marker. "X" denotes substrate, "21-MA" denotes 21 mer fragment containing a psoralen-derived MA, "21-mer" denote cleavage fragments containing an AP (Lanes 2-4), "8<sup>PA</sup>" and "8<sup>P</sup>" denote 8 mer fragments containing a 3'-terminal PA and P, respectively. ....149

**Figure 4.15: Time dependent cleavage of ss-DNA containing Sp, by hNEIL3<sup>Cat</sup>, hNEIL3<sup>Trun</sup>, hNEIL3<sup>FL</sup>.** A. Denaturing PAGE analysis of 50 nM hNEIL3<sup>Cat</sup>, 50 nM hNEIL3<sup>Trun</sup> and 100 nM hNEIL3<sup>FL</sup> recombinant

protein activity on 20 nM of ss Sp1 DNA. Cleavage observed on generation of an 8 mer product. “0\*” Reaction was without recombinant protein. “X” denotes substrate, “8<sup>PA</sup>” denotes an 8 mer fragments containing a 3’-terminal PA. B. Quantification of generated cleavage product percentages after enzymatic cleavage assay. Reaction products were treated with light piperidine.....150

**Figure 4.16: Time dependent cleavage of ss-DNA and ds-DNA containing the Sp lesion by hNEIL1 and hNEIL3<sup>Cat</sup>.** A-B. Denaturing PAGE analysis of 20 nM hNEIL1 and 50 nM recombinant protein activity on 20 nM of ss Sp1 DNA. C. Denaturing PAGE analysis of 20 nM hNEIL1 and 50 nM recombinant protein activity on 20 nM of ds Sp1 DNA. Reactions containing NEIL1 were not treated with piperidine. Reactions containing recombinant hNEIL3<sup>Cat</sup> underwent light piperidine treatment. “0\*” Reactions were without recombinant protein. “X”denotes substrate, “8 PA” 3’-terminal PA. “X”denotes substrate, “8<sup>PA</sup>” and “8<sup>P</sup>” denote 8 mer fragments containing a 3’-terminal PA and P, respectively. D-E. Quantification of generated cleavage product percentages after enzymatic cleavage assay. ....152

**Figure 4.17: Time dependent cleavage of psoralen (HMT)/ UVA treated XL47 • 47 – 21\* three-stranded ICL DNA substrate by hNEIL1 and hNEIL3<sup>Cat</sup>.** A. Denaturing PAGE analysis of 20 nM hNEIL1 and 50 nM hNEIL3<sup>Cat</sup> recombinant protein activity on ~10 nM (X): XL47 • 47 – 21\* three-stranded DNA ICL substrate. Reaction samples were without Piperidine treatment. “0\*” Reactions without recombinant protein. “21-MA” denotes 21 mer fragment containing a psoralen-derived MA, A. “21-mer” denotes AP-site containing unhooked fragment. B. Quantification of hNEIL3<sup>Cat</sup> and hNEIL1 generated cleavage product percentages after enzymatic cleavage of XL47 • 47 – 21\*. C Quantification of hNEIL3<sup>Cat</sup> and hNEIL1 generated cleavage product percentages after enzymatic cleavage of ss and ds-Sp1 oligonucleotide substrate. ....155

**Figure 4.18: Sanger sequencing chromatogram analysis of pETDUET2-EcoMap- ORF6-hNEIL3<sup>Cat-K81A</sup> and the corresponding wild type hNEIL3<sup>Cat</sup> nucleotide sequence region, 230-268.** Targeted nucleotides at position 241 and 242, highlighted in red. Targeted mutations AAG-GCG encode for amino acid residue 81, lysine to alanine mutation, for expression and purification of the catalytically inactive hNEIL3<sup>Cat-K81A</sup> recombinant protein. ....156

**Figure 4.19: HisTrap HP FPLC Purification of hNEIL3<sup>Cat-K81A</sup> from E. coli.** A. Chromatogram analysis of protein fractions generated from E.coli lysates overexpressing hNEIL1. B. SDS-PAGE analysis and Instant Blue protein staining. C. Anti-His western blot analysis of hNEIL3<sup>Cat-K81A</sup> FPLC purification fractions. (M) Page ruler prestained protein ladder (ThermoFisher). ....158

**Figure 4.20: Confirmation of purification of hNEIL3<sup>Cat-K81A</sup> protein.** A. Proteomic analysis by LC-MS, peptide sequences detected in hNEIL3<sup>Cat-K81A</sup> purification product which match target amino acid sequence highlighted in red. MS/MS Ion search of matched proteins detected with highest mascot score hNEIL3<sup>Cat</sup> and hNEIL3 in each sample (full lists displayed in Appendix Table 3). B. SDS-PAGE analysis of final recombinant hNEIL3 protein products stained with instant-blue. “M” Page ruler prestained protein ladder (ThermoFisher).....159

**Figure 4.21: Denaturing PAGE analysis of hNEIL3<sup>Cat</sup>, hNEIL3<sup>Trun</sup>, hNEIL3<sup>FL</sup>, hNEIL1, Nei and hNEIL3<sup>Cat-K81A</sup> protein activity on 10 nM ss Sp1 DNA oligonucleotide.** Samples were incubated for 1 h at 37°C with 500 nM of protein. For positive control 20 nM of bacterial Nei was used and 500 nM of hNEIL1 was used. (Lanes 1-7) Reactions were without piperidine treatment. (Lanes 8-15) Reactions were with light piperidine treatment. “Ctrl” samples in the absence of recombinant protein. “8<sup>PA</sup>” and “8<sup>P</sup>” denote 8 mer fragments containing 3’-terminal PA and P, respectively. ....160

**Figure 4.22: Denaturing PAGE analysis of hNEIL3<sup>Cat</sup>, hNEIL3<sup>Trun</sup>, hNEIL3<sup>FL</sup>, hNEIL1, Nei and hNEIL3<sup>Cat-K81A</sup> protein activity on 10 nM (X): ds Sp1 substrate.** Samples were incubated for 1 h at 37°C with 500 nM of protein. For positive control 20 nM of bacterial Nei was used and 500 nM of hNEIL1 was used. (Lanes 1-7). Reactions without piperidine treatment. (Lanes 8-15) Reactions were with light piperidine treatment. “Ctrl” samples in the absence of recombinant protein. “17 mer” denotes substrate, “8<sup>PA</sup>” and “8<sup>P</sup>” denote 8 mer fragments containing a 3’-terminal PA and P, respectively.....161

**Figure 4.23: Denaturing PAGE analysis of hNEIL3<sup>Cat</sup> and hNEIL3<sup>Cat-K81A</sup> protein activity on ~10 nM (X): XL47 • 47 – 21\* HMT generated three-stranded DNA ICL.** Samples were incubated for 1 h at 37°C. For hNEIL3<sup>Cat</sup>, 500 nM of protein was used. For the hNEIL3<sup>Cat-K81A</sup>, 300 nM, 500 nM or 1000 nM of protein was used. For positive control 20 nM of bacterial Nei was used. (Lanes 1-6) Reactions were without piperidine treatment. (Lanes 7-12) Reactions were with light piperidine treatment. “Ctrl” samples in the absence of recombinant protein. “X” denotes substrate, “21-MA” denotes 21 mer fragment containing psoralen-derived MA, “21-mer” denote cleavage fragments containing an AP site (Lane 2), “8<sup>PA</sup>” denote 8 mer fragments containing a 3'-terminal PA.....163

**Figure 4.24: Denaturing PAGE analysis of hNEIL3<sup>Cat</sup> and hNEIL3<sup>Cat-K81A</sup> protein activity on ~10 nM (X): XL47 • 47 – 21\* • 21 HMT generated three-stranded DNA ICL.** Samples were incubated for 1 h at 37°C. For hNEIL3<sup>Cat</sup>, 500 nM of protein was used. For the hNEIL3<sup>Cat-K81A</sup>, 300 nM, 500 nM or 1000 nM of protein was used. For positive control 20 nM of bacterial Nei was used. (Lanes 1-6) Reactions were without piperidine treatment. (Lanes 7-12) Reactions were with light piperidine treatment. “Ctrl” samples in the absence of recombinant protein. “X” denotes substrate, “21-MA” denotes 21 mer fragment containing psoralen-derived MA, “21-mer” denote cleavage fragments containing an AP site (Lane 2), “8<sup>PA</sup>” denote 8 mer fragments containing a 3'-terminal PA.....165

**Figure 4.25: SDS-PAGE analysis of NaBH<sub>4</sub> trapping complexes of hNEIL3<sup>Cat</sup> and hNEIL1 protein formation with 10 nM ss and ds Sp1 DNA lesions.** Reactions were without Piperidine treatment. “Ctrl” samples were without recombinant protein. “DNA-Protein complex” denotes recombinant protein bound by NaBH<sub>4</sub> facilitated reduction of protein amino acid residue to cleavage site on the DNA substrate. “Free substrate” denotes unbound DNA.....167

**Figure 4.26: SDS-PAGE analysis of NaBH<sub>4</sub> of hNEIL3<sup>Cat</sup>, hNEIL3<sup>Trun</sup>, hNEIL3<sup>FL</sup>, Nei, hNEIL1 and hNEIL3<sup>Cat-K81A</sup> formation with ~10 nM 21\*x47-47 HMT generated three-stranded ICL DNA substrate.** 500 nM of recombinant hNEIL1, hNEIL3 and 20 nM of Nei recombinant protein was used. “Ctrl” samples were without recombinant protein. “DNA-Protein complex” denotes recombinant protein bound by NaBH<sub>4</sub> facilitated reduction of protein amino acid residue to cleavage site on the DNA substrate. “Free substrate” denotes unbound DNA.....169

**Figure 4.27: Schematic representation of the mechanisms of action of Nei-like DNA glycosylases on ICLs.** A. Mechanisms of action of Nei-like DNA glycosylases on three-stranded DNA structure containing single psoralen-derived ICL. B. Mechanisms of action of Nei-like DNA glycosylases on four-stranded DNA structure containing single psoralen-derived ICL. C. Skeletal formula of 21 mer fragment containing single thymidine crosslinked to free thymine base by HMT (DNA(T)-HMT-T), an excision product generated by Nei-like DNA glycosylases catalysed repair of ICL in three-stranded DNA structure. D. Skeletal formula of thymine-HMT-thymine cross-link (T-HMT-T), an excision product generated by Nei-like DNA glycosylases catalysed repair of ICL in three- and four-stranded DNA structure. ....172

**Figure 4.28: Schematic representation of the proposed model of three- and four-stranded ICL DNA generation and subsequent resolution by hNEIL1 and hNEIL3 proteins.** 1. Leading strand replication machinery stall, 2. Recruitment of FANCM translocase, 3. Continuation of replication fork and strand synthesis, 4. Lagging strand replication machinery stall and recruitment of FANCM translocase, 5. Continuation of replication fork and strand synthesis.....175

**Figure 5.1: HisTrap-HP FPLC purification of recombinant hNEIL3<sup>FL</sup> from Rosetta 2 (DE3) E. coli expression hosts.** A. Chromatogram analysis of protein fractions generated by HisTrap chromatography of lysates from *E. coli* overexpressing hNEIL3<sup>FL</sup>. B. SDS-PAGE and Instant Blue protein staining. C. Anti-His, D. anti-NEIL3 immunoblot analysis. “M” All Blue Prestained Protein Standard (BioRad). ....181

**Figure 5.2: Immunoblot analysis of hNEIL3<sup>FL</sup> incubated with phosphocellulose FPLC purification fractions of HeLa whole cell extracts.** Analysis of reconstituted *in vitro* ubiquitination reactions of

PC150 and PC1000 fractions from laboratory stocks in the presence of 600 ng recombinant hNEIL3<sup>FL</sup> (Williams and Parsons, 2017) A. anti-His immunoblot B. anti-NEIL3 immunoblot. “M” All Blue Prestained Protein Standards (BioRad).....182

**Figure 5.3: Ubiquitination analysis of HiLoad Mono Q Sepharose column FPLC purification fractions of PC150 elution of HeLa WCE.** A. Chromatogram analysis of previously purified HiLoad Mono Q Sepharose fractions (Williams and Parsons, 2018). *In vitro* ubiquitination reaction of 600 ng recombinant hNEIL3<sup>FL</sup> in the presence of HiLoad Mono Q Sepharose fractionated PC150 laboratory stocks. B. Anti-NEIL3 immunoblot imaged at low scan intensity (5.0), C. anti-NEIL3 immunoblot imaged at high scan intensity (6.5) using the Licor Odyssey InfraRed scanner. “M” All Blue Prestained Protein Standards (BioRad). Arrows identify lanes displaying major ubiquitination activity.....184

**Figure 5.4: Ubiquitination analysis of Superdex 200 HR 10/30 FPLC purification fractions.** A. Chromatogram analysis of previously purified HiLoad Mono Q Sepharose fractions (Williams and Parsons, 2018). *In vitro* ubiquitination reaction in the presence of 600 ng recombinant hNEIL3<sup>FL</sup> and Superdex 200 HR 10/30 gel filtration fractions from laboratory stocks analysed by B. Anti-NEIL3 immunoblot imaged at low scan intensity (5.0), C. anti-NEIL3 immunoblot image at high scan intensity (6.5), using the Licor Odyssey InfraRed scanner. “M” All Blue Prestained Protein Standards (BioRad). .....186

**Figure 5.5: Ubiquitination analysis of Mono Q 5/50 GL purification fractions.** A. Chromatogram analysis of previously purified HiLoad Mono Q 5/50 GL fractions (Williams and Parsons, 2018). *In vitro* ubiquitination reactions in the presence of 600 ng recombinant hNEIL3<sup>FL</sup> and Mono Q 5/50 GL ion exchange fractions from laboratory stocks were analysed by B. Anti-His immunoblot and C. Anti-NEIL3 immunoblot “M” All Blue Prestained Protein Standards (BioRad). .....188

**Figure 5.6: HisTrap-HP FPLC purification of the recombinant TRIM26 from Rosetta 2 (DE3) E. coli expression hosts.** A. Chromatogram analysis of protein fractions generated by HisTrap chromatography of lysates from *E.coli* overexpressing TRIM26. B. 8% SDS-PAGE and Instant Blue protein staining. C. Anti-His immunoblot analysis. “M” All Blue Prestained Protein Standards (BioRad). .....190

**Figure 5.7: Immunoblot analysis of ubiquitination of hNEIL3<sup>FL</sup> in the presence of recombinant TRIM26.** Anti-NEIL3 immunoblot analysis of *in vitro* ubiquitination reactions with increasing concentrations of recombinant TRIM26 in the presence of 600 ng recombinant hNEIL3<sup>FL</sup>. A. anti-NEIL3 immunoblot imaged at low scan intensity (5.0), B. anti-NEIL3 imaged at high scan intensity (6.5) using the Licor Odyssey InfraRed scanner.....191

**Figure 5.8: Anti-NEIL1 immunoblot analysis of U2OS cells treated with TRIM26 siRNA and harvested 0-4 h after treatment with 150µM H<sub>2</sub>O<sub>2</sub>.** A. NEIL1/Actin ratios were quantified from results of two independent experiments displayed. B-C Anti-NEIL1 immunoblot of U2OS cell extract lysates treated with 33 pmol NT or TRIM26 siRNA for 48 h and treated with 150 µM H<sub>2</sub>O<sub>2</sub> for 15 min. “C” in the without of H<sub>2</sub>O<sub>2</sub> treatment. Error bars display standard error.....192

**Figure 5.9: Anti-NEIL3 immunoblot analysis of U2OS cells treated with TRIM26 siRNA and harvested 0-4 h after treatment with 150µM H<sub>2</sub>O<sub>2</sub>** A. Quantification of NEIL3: Actin ratios from results of two independent experiments displayed. B-C Anti-NEIL3 immunoblot of U2OS cell extract lysates treated with 33 pmol NT or TRIM26 siRNA for 48 h and treated with 150 µM H<sub>2</sub>O<sub>2</sub> for 15 min. “C” in the without of H<sub>2</sub>O<sub>2</sub> treatment. T-tests between NT and TRIM26 siRNA at: 0 h *p*= 0.000149923, 0.5 h *p*= 0.0463634, 1 h *p*= 0.0213931, 4 h *p*=0.412032. Error bars display standard error. ....193

**Figure 5.10: Anti-NEIL3 immunoblot dose response analysis of U2OS whole cell extracts treated with TRIM26 siRNA and cisplatin treatment.** A. Quantification of NEIL3/Actin from results of two independent experiments displayed. B-C Anti-NEIL3 immunoblot of U2OS cell extract lysates treated with 33 pmol NT or TRIM26 siRNA for 48 h and treated with 0-10 µM cisplatin for 24 h. “C” without cisplatin treatment.....194

**Figure 5.11: Clonogenic survival assay analysis: cisplatin dose response of U2OS cells pre-treated with NT siRNA, TRIM26 siRNA, NEIL1 or NEIL3.** A. Representative clonogenic plate images. B. Anti-FLAG and anti-actin Immunoblot analysis of overexpression of NEIL1. C. Anti-NEIL3 and anti-actin immunoblot analysis of NEIL3 overexpression, NEIL3/actin ratios displayed below each sample lane. (D-G) Mean surviving fraction is shown with standard errors from the results of three independent experiments.  $P < 2.2 \times 10^{-16}$  (NT siRNA vs TRIM26 siRNA),  $P < 2.2 \times 10^{-16}$  (NT siRNA vs NEIL1 OE) and  $P < 2.2 \times 10^{-16}$  (NT siRNA vs NEIL3 OE) as analysed by the CFAssay for R package.....196

**Figure 5.12: Anti-NEIL3 immunoblot analysis of puromycin resistant U2OS cells.** "G1" denotes whole cell extracts from U2OS cells treated with gRNA sequence 1. "G2" denotes whole cell extracts from U2OS cells treated with gRNA sequence 2. "G2\*" Denotes gRNA 2 containing plasmid treated U2OS clonal populations which were upscaled for screening in a second round of screening.....198

**Figure 5.13: Immunoblot analysis of the U2OS cell G2 30 clone.** "WT" denotes whole cell extracts from wild type and non-treated U2OS cells. "G2" denotes whole cell extracts from U2OS cells treated with gRNA sequence 2. ....199

## List of Tables.

<b>Table 1.1: ICL agent class, DNA sequence context of ICLs and relative level of DNA distortion.</b> (Adapted from Dronkert and Kanaar, 2001). .....	14
<b>Table 1.2: The Mammalian DNA glycosylases, their cellular location and their enzyme functionality.</b> Monofunctional DNA glycosylases demonstrate DNA glycosylase activity only producing an AP-site. Bifunctional DNA glycosylases possess DNA glycosylase activity and an associated lyase which conducts $\beta$ -elimination or $\beta,\delta$ -elimination of an AP-site. DNA glycosylases listed as Monofunctional/Bifunctional display bifunctionality in a substrate specific manner. (Adapted from Krokan and Bjørås (2013)). .....	40
<b>Table 2.1: SDS-PAGE gel mixtures for preparation of 8% SDS-PAGE gels.</b> The volumes indicated are for the production of two SDS-PAGE gels. The separating gel was prepared and cast in advance of the stacking gel. Once stacking gel was poured a 10-well 15-well 1.5 mm width comb was inserted to facilitate well generation.....	83
<b>Table 2.2: SDS-PAGE gel mixtures for preparation of 10% SDS-PAGE gels.</b> The volumes indicated are for the production of two SDS-PAGE gels. The separating gel was prepared and cast in advance of the stacking gel. Once stacking gel was poured a 10-well 15-well 1.5 mm width comb was inserted to facilitate well generation.....	83
<b>Table 2.3: Primary-antibodies used in this study for probing of specific proteins.</b> Host-organism, clonality and dilution ratio displayed.....	86
<b>Table 2.4: Secondary-antibodies used in this study for probing of primary-antibodies.</b> Host-organism, clonality and dilution ratio displayed.....	86
<b>Table 2.5: DNA Oligonucleotide sequences and model DNA replication fork oligonucleotide structures used in BER assays.</b> 'X' denotes the position of the 5-OHU, 8-OxoG and Tg oxidative DNA lesions. DNA substrates are 39 mer in length, DNA glycosylase mediated cleavage yields a 19 mer cleavage product.....	88
<b>Table 2.6: Denaturing PAGE gel mixture for preparation of a 20% denaturing PAGE.</b> The volumes indicated are for the production of one denaturing page gel.....	91
<b>Table 2.7: Non-denaturing PAGE gel mixture for preparation of a 5% denaturing PAGE.</b> The volumes indicated are for the production of one denaturing page gel.....	92
<b>Table 2.8: Mutagenic primers used for site-directed mutagenesis, converting A-G at nucleotide position 241 and A-C at nucleotide position 242 of hNEIL3 cDNA.</b> Primers are underlined, and targeted bases are underlined, italicised and highlighted in yellow. ....	97
<b>Table 2.9: Thermocycling conditions used for site-directed mutagenesis and synthetic vector generation via PCR. ....</b>	98
<b>Table 2.10: Ubiquitin cascade recombinant protein master mix.</b> Wild type Ubiquitin (Boston biochemicals, Cambridge, USA), GST-E1 activating enzyme, E2 conjugating enzymes (UbcH3-UbcH10). .....	100
<b>Table 2.11: Splitting regime of adherent cells based on target vessel for continuous culture. ....</b>	102
<b>Table 2.12: Short interfering ribonucleic acid sequences used for non-targeting RNAi as control and TRIM26 RNAi. ....</b>	104
<b>Table 2.13: Transient mammalian expression vectors.</b> Name of the mammalian expression vector, the encoded DNA glycosylase and C-terminal fusion tag are displayed.....	105
<b>Table 2.14: Clonogenic seeding densities for each RNAi or overexpression treatment and relevant cisplatin concentration.</b> Numbers denote the two seeding densities seeded into 6 well plates after treatments for outgrowth of colony forming units. ....	106

**Table 3.1: Mock DNA replication fork oligonucleotide DNA structure.** Oligonucleotides 39 mer in length with either 5-OHU, 8-OxoG or Tg at 20 mer, DNA glycosylase cleavage products generate a 19 mer cleavage product. ....117

## Acknowledgements

Firstly, I would like to thank Dr. Rhoderick H. Elder for giving me the chance to work on this project. I would also like to thank him for providing multiple opportunities for collaboration and professional development during my PhD study and inspiring me to continue working in academic research in the field of DNA repair. Finally, I would like to thank him for his support and friendship over the last three years.

I also wish to thank the University of Salford for the award of the Pathway to Excellence studentship that funded my PhD.

I would like to also thank Dr. Jason Parsons, for hosting me in his laboratory at the University of Liverpool and providing resources during our collaboration between 2015 and 2018. I was welcomed into his laboratory as a member of his group and was supported, to achieve my scientific research goals over this period. The advice and mentorship catalysed my professional development.

Additionally, I would like to thank Dr. Murat Saparbaev for hosting me in his laboratory at the Gustave Roussy Institute, Paris and also providing resources during our collaboration between 2015 and 2017. In his laboratory I was able to develop my scientific research skills exponentially, while being welcomed into an extremely friendly working environment, where I spent some of the most enjoyable moments of my PhD. I also wish to thank Dr. Alexander Ishchenko and Dr. Regina Groisman for their advice and scientific discussions during this period at the Gustave Roussy Institute.

Throughout my PhD study I have worked closely with multiple people and acquired friendships I aim to maintain for life. I would like to especially thank Dr. Soran Mohammed who provided me with exceptional advice, motivation and constructive criticism in regards to scientific research. I also thank him for his friendship over the course of my PhD. I would also like to thank Mustafa Albelazi who has been a close friend throughout my PhD. Our research findings have enhanced one another's hypotheses and our long discussions have enabled the critical evaluation of our shared research interest in the investigation of hNEIL3. Without his preliminary work, my research findings would not have been possible. Additionally, he has always kept a positive attitude towards our shared research topic enabling me to see light of the research challenges faced.

I would also like to thank Dr. Patrick Killoran, Dr. Andrew McGown, Dr Ryan Joynson and Dr. Emyr Bakker who have provided excellent humour, advice and friendship over the years.

I would like to thank Dr. Natalie Barnes, Dr. Firozeh Ashtiani, Dr. Emyr Bakker, Arvind Swamy, Jonathan Hughes, Dr. Katie Nickson, Dr. Rachel Carter, Eleanor Madders, Naren Govindarajah, Vicky Fretwell, Rachel Clifford, Sarah Williams, Caroline Zutterling, Gabriella Zharkovic, Graham Burberry, Stephen Austin, Iwakun, Oluwasegun Abraham for their collaboration, friendship, advice, good humour and good company.

I thank my mother and father for supporting me both financially and emotionally during this period. Without their support I would not have had the opportunity to undertake PhD study and see it through to completion. They are both my greatest sources of inspiration and motivation to achieve my aspirations in life.

I especially thank my girlfriend Rose Parkes for her support, understanding and the sacrifices she has made for me to follow my ambitions.

**Declaration**

The work described in this thesis was carried out at the University of Salford, The Institute Gustave Roussy and the University of Liverpool between October 2015 and October 2018. No part of this thesis has previously been submitted or a degree of any other qualification within the University of Salford or any other Institution.

## 1. Introduction.

With an estimated 30,000 deoxyribose nucleic acid (DNA) damaging events per cell, per day, DNA repair is an essential line of defence against mutation and cytotoxicity (Wallace *et al.*, 2012). Without efficient DNA repair, DNA damage significantly contributes to mutagenesis and carcinogenesis (Maynard *et al.*, 2009; Wallace *et al.*, 2012; Kelley *et al.*, 2014). In eukaryotes the DNA glycosylases 8-Oxoguanine DNA glycosylase (OGG1), MutY homolog (MUTYH), endonuclease III homolog (NTH1), endonuclease VIII-like 1 (NEIL1), 2 (NEIL2) and 3 (NEIL3) are responsible for initiating base excision repair (BER) in the removal and repair of oxidative DNA damage (Krokan and Bjørås, 2013). However, the NEIL3 protein remains relatively uncharacterised (Liu *et al.*, 2013a). That said, an emerging role in the resolution of DNA interstrand crosslinks by NEIL1 and NEIL3 is becoming apparent (Couvé-Privat *et al.*, 2007; Couvé *et al.*, 2009; Semlow *et al.*, 2016; Yang *et al.*, 2017). Thus, the repair of these diverse DNA lesions, implicates the human NEIL proteins in the maintenance of faithful DNA replication, highlighting their relevance as potential targets for therapeutic treatment of malignant tumours.

NEIL3 has been shown to be overexpressed in proliferating cells such as in the testes, thyroid and malignant tumours (Kauffmann *et al.*, 2008; Liu *et al.*, 2013a; Shinmura *et al.*, 2016). In healthy cells NEIL1 and NEIL3 are tightly regulated during the synthesis phase (S-phase), through to the gap 2 phase DNA damage checkpoint (G2/M phase) of the cell cycle (Hazra and Mitra, 2006; Neurauter, 2012; Liu *et al.*, 2013a). Initial biochemical studies on the core glycosylase domain of human endonuclease VIII-like-3 (hNEIL3) have shown affinity for single stranded (ss) DNA substrates (Liu *et al.*, 2013b). NEIL1 knockout mice displayed no significant accumulation of oxidative lesions, suggesting the presence of backup DNA repair systems present within the cell which may also resolve lesions excised by NEIL1 (Parsons and Elder, 2003). Interestingly, overexpression of NEIL1 in Fanconi anemia (FA) deficient cells partially rescued sensitivity to the interstrand DNA crosslinking (ICL) inducing agents mitomycin C (MMC) and 8-methoxyporalen (8-MOP; Macé-Aimé *et al.*, 2010). NEIL3 knockout mouse embryonic fibroblast (MEF) cells display sensitivity to cisplatin (Rolseth *et al.*, 2013). Furthermore, preliminary work has revealed hNEIL3 ribonucleic acid interference (RNAi)

knockdown leads to sensitivity to oxaliplatin in HCT116 cells (Taylor *et al.*, 2015). However, the biochemical mechanism of hNEIL3 in ICL repair remains to be understood. The focus of the work presented here was to provide further understanding of the biochemical mechanism of human endonuclease VIII-like-1 (hNEIL1) and hNEIL3 in the maintenance of the DNA replication fork and removal of replication blocking lesions. To investigate this, biochemical analysis of recombinant hNEIL1 and hNEIL3 proteins was undertaken in the presence of model DNA replication fork oligonucleotide structured substrates containing oxidative lesions and psoralen monoadducts, three- and four- stranded structured ICL containing oligonucleotide substrates.

In addition, an emerging view is that the BER pathway is modulated through the ubiquitin proteasome system (UPS; Edmonds and Parsons, 2016; Carter and Parsons, 2016). Thus, the identification and investigation of a novel NEIL3 interacting E3 ubiquitin ligase was undertaken and determined to be the same major E3 ubiquitin ligase previously identified for NTH1 and hNEIL1, *i.e.* tripartite motif containing protein 26 (TRIM26). The effect of TRIM26 modulation on NEIL3 protein levels was determined in human bone osteosarcoma epithelial cells (U2OS). Finally, U2OS survival after TRIM26 RNAi and transient overexpression of hNEIL1 or hNEIL3 in response to cisplatin was determined.

This study, therefore, aims to provide evidence that supports distinct biochemical roles of the hNEIL1 and hNEIL3 DNA glycosylases at the DNA replication fork. Furthermore, to demonstrate the modulation of hNEIL1 and hNEIL3 by the ubiquitin post-translational modification (PTM) in response to the DNA crosslinking agent cisplatin. Consequently, highlighting links between BER and resistance to chemotherapy of cancer by upregulation, or dysfunction, of cellular mechanisms.

### **1.1. Cancer.**

Cancer refers to more than 277 different types of disease which share six common definable hallmarks (Hanahan and Weinberg, 2011; Hassanpour and Dehghani, 2017). These six hallmarks are grouped under the ability of cells to resist cell death, possess the ability to undergo invasion/metastasis, induce angiogenesis, display proliferative immortality, evade growth suppressors and demonstrate sustained proliferative signalling (Hanahan and Weinberg, 2011). The root cause of these phenotypes is genomic instability and subsequent

mutation leading to these malignant phenotypes (Hanahan and Weinberg, 2011; Yao and Dai, 2014).

Sustained proliferative signalling is considered one of the core characteristics of cancer cells, resulting in indefinite proliferation. This is achieved by dysregulation of the cell cycle with the disruption of cell cycle check points through mutation and or loss of function in oncogenes, tumour-suppressors such as cyclin proteins, cyclin dependent kinases, and mitotic checkpoint proteins (Wenzel and Singh, 2018)

Worldwide, cancer is the second leading cause of human mortality, with the overall prevalence of cancer increasing. In 2018, 1,735,350 new cancer cases were observed, with 609,640 expected deaths in the USA alone (Siegel *et al.*, 2018). In the UK in 2015, 359,960 new cases of all cancers were observed with 163,444 deaths due to cancer being observed in 2016; together these findings demonstrate the scale and impact of cancer in Western societies (Cancer Research UK, 2015; 2016).

For Men the highest percentages of cancer present in the prostate, lung and bronchus, colon and rectum, respectively. Whereas for Women, they are estimated to display the highest percentages of cancer in the breast, lung and bronchus, colon and rectum, respectively. (Siegel *et al.*, 2018). Cancer in young adults and children is rare, accounting for 1.5% of all cancers. In the UK, within the 0-14-year-old age group the highest percentage of cancers observed per year are leukaemia, cancers of the central nervous system and lymphomas. While in the 15-24-year-old age group the highest percentage of yearly observed cancers is lymphomas, carcinomas and germ cells (Pesola *et al.*, 2017). It was also estimated that prevalence of cancers in the UK in 0-24-year-old was likely to increase up to 2030 (Pesola *et al.*, 2017). Despite the increase in prevalence of cancers, individuals are now much more likely to survive than ever before. Over a 40-year period, Quaresma *et al.* (2015) found that 50% of individuals diagnosed in 1971-1972 were likely to survive for 1-year post-diagnosis, while between 2005-2006 survival was 50%, 5 years after diagnosis and in 2011 the survival rate of 50% was extended to 10 years post-diagnosis.

Cancer occurs through the spontaneous mutation of genes through damage to DNA, changing their function and regulation of biological processes within the cell. Lawley and Brookes (1960) discovered that carcinogenesis may be a result of damage to the DNA molecule,

demonstrating that mustard gas reacted with DNA, modifying guanine residues *in vitro* and *in vivo*. Brookes and Lawley (1964) then demonstrated that a radioactively labelled tobacco carcinogen (polycyclic-aromatic-hydrocarbon) had the ability to induce tumours in mice and this phenotype correlated with its binding to DNA. It is now known that both environmental risk factors and genetic predisposition play a significant role in the development of cancer. Tobacco smoke, chemical pollutants, UV and ionising radiation (IR) have all been identified as examples of exogenous influences which promote genetic mutation within the cell (Poon *et al.*, 2014; Aizawa *et al.*, 2016). Since the first conclusive evidence that cancer was caused through damage to DNA by Brookes and Lawley in 1964, 120 agents have been identified by the International Agency for Research on Cancer as group 1 carcinogens with “sufficient evidence of carcinogenicity in humans”, 82 group 2A “probably carcinogenic to humans”, 302 group 2B “Possibly carcinogenic to humans” (IARC, 2018).

Acquired drug resistance is one of the primary challenges faced in the treatment of cancer as it abrogates the clinical response of the therapy (Foo and Michor, 2014). Platinums and alkylating agents are molecules used with widespread clinical application for the broad-spectrum treatment of cancer. They represent a class of agents known to induce interstrand DNA crosslinks amongst other forms of DNA damage (Fu *et al.*, 2012; Deans and West, 2011). Cancer often becomes resistant to these agents reducing their efficacy (Shen *et al.*, 2012). One such mechanism of acquired resistance to these agents is the enhancement of the capacity of the cell to remove DNA adducts, through the upregulation of associated DNA repair pathways. It has been shown that a pattern of cross resistance is acquired in response to the use of ICL inducing agents (Torres-Garcia *et al.*, 1989). One such example is the acquired resistance to cisplatin, one type of crosslinking agent, which may additionally facilitate cross resistance to other ICL inducing agents (Taniguchi *et al.*, 2003). This indicates common underlying mechanisms of acquired resistance to this class of genotoxic agents. Thus, the molecular targeting of DNA repair pathways associated with the repair of ICL DNA adducts provides a promising therapeutic strategy (Seetheram *et al.*, 2010; Huang and Li, 2013).

## 1.2. DNA damage.

The genomic stability of a cell is crucial for its survival in the face of endogenous and exogenous genotoxic insult. The cellular response to DNA damage is synchronised with the initiation of DNA repair pathways or apoptosis (cell death). Apoptosis (cell death), is initiated following significant DNA damage, removing cells which may proliferate with further harmful potential (Schärer, 2003). DNA damage can arise from the generation of reactive oxygen species (ROS), IR, ultraviolet (UV) and chemical agents targeting DNA (Ciccia and Elledge, 2010). Such damage leads to modifications of the DNA molecule including, oxidative base damage, single- and double-strand breaks (SSBs and DSBs), alkylation, intra and interstrand DNA crosslinks, all of which have a deleterious effect on the cell (Klaunig *et al.*, 1998).

### 1.2.1. Oxidative DNA damage

Healthy cells balance antioxidant defence mechanisms with ROS levels; if this balance is lost, cellular oxidative stress results. ROS are generated endogenously through leakage of electrons to oxygen in the electron transport chain and through lipid peroxidation (Jena, 2012; Ayala *et al.*, 2014). Alternatively, ROS are generated as a result of oxidative stress from exogenous agents such as tobacco smoke, diesel exhaust particulates found in the air, chemical agents, UV and IR (Krokan and Bjørås, 2013). The generation of ROS can form DNA intrastrand crosslinks, SSBs and DSBs, oxidation of apurinic/apyrimidinic (AP) sites, oxidation of sugar fragments, formation of deamination products and many different oxidised bases (Schärer, 2003; Jiang *et al.*, 2007; van Loon *et al.*, 2010; Jena, 2012).

Oxygen free radicals are generated through the reduction of molecular oxygen and have a short half-life, therefore causing damage locally. ROS are generated during normal cellular metabolism, including the super-oxide radical anion ( $O_2^-$ ), peroxynitrite ( $ONOO^-$ ) and hydroxyl radicals ( $\cdot OH$ ). Hydroxyl radicals are produced through dismutation of  $O_2^-$  to hydrogen peroxide ( $H_2O_2$ ) by superoxide dismutase. Hydrogen peroxide is usually cleansed by glutathione peroxidase and converted into innocuous  $H_2O$  by catalase, but excess  $O_2^-$  allows  $\cdot OH$  production (**Figure 1.1**). Formation of highly reactive hydroxyl radicals is a major contributor to DNA damage (Bandaru *et al.*, 2002; Wallace *et al.*, 2003). Hydroxyl radicals can also be generated through UV-induced photolysis of  $H_2O_2$  and finally through the presence of

transition metals allowing the generation of  $\cdot\text{OH}$  through the Fenton reaction (**Figure 1.2**; Lu *et al.*, 2007; Jena, 2012).

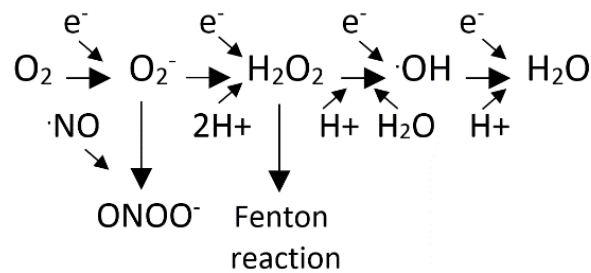


**Figure 1.1:** Schematic representation of ROS generation through the consecutive reduction of cellular oxygen and superoxide radical catalysis by superoxide dismutase.



**Figure 1.2:** Fenton reaction formula showing the generation of ROS as result of the presence of Iron (Fe).

Oxidative lesions are generated at a frequency of 10,000 DNA lesions per cell per day and are responsible for over 100 different types of oxidative molecular modification (Klaunig *et al.*, 2011). Guanine has the lowest redox potential of the four nitrogenous bases and as result is readily oxidised by ROS (Kino *et al.*, 2017). Important examples of oxidative lesions include the mutagenic formamidopyrimidines (Fapy) such as FapyG, generated through ROS attack of C8, opening the 5 carbon ring and resulting in FapyG-A mispairs (**Figure 1.3**; Jena and Mishra, 2013). Additionally, the abundant 8-oxoguanine (8-OxoG) can be generated by addition at C8 and its further oxidation generates the spiroiminodihydantoin (Sp) and guanidinohydantoin (Gh) DNA lesions (**Figure 1.3**; Niles *et al.*, 2004; Jena and Mishra, 2012). 8-OxoG is associated with aging and cancer due to frequent mispairing with adenine by both eukaryotic and prokaryotic DNA polymerases resulting in GC to TA transversion mutations (Klaunig *et al.*, 2011; Krokan and Bjørås, 2013).

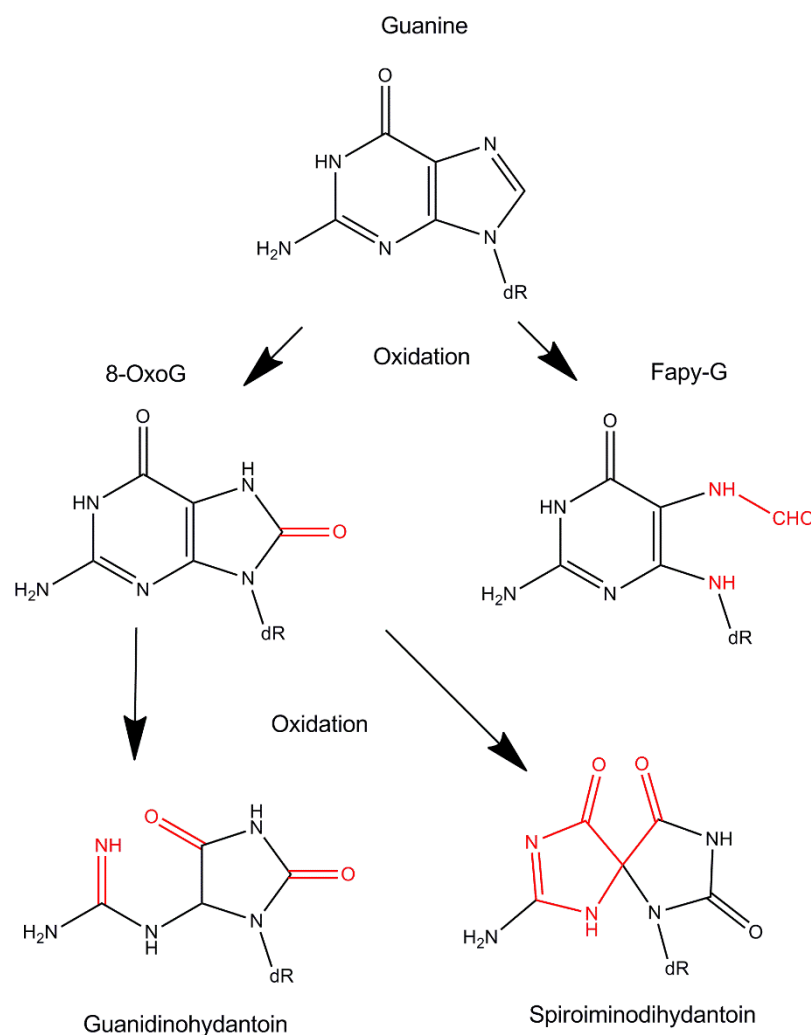


**Figure 1.3:** Schematic representation of the major DNA lesions generated through oxidation of guanine, 8-oxoguanine (8-OxoG) and 2,6-diamino-4-hydroxy-5-formamidopyrimidine (FapyG). Further oxidation of 8-OxoG may lead to the formation of open ring Guanidinohydantoin (Gh) and closed ring Spiroiminodihydantoin (Sp). Positions highlighted in red represent those modified.

Hydroxyl radicals, peroxy radicals and hydroperoxides may interact with cytosine, with the latter accounting for the generation of the stable 5-hydroxyuracil (5-OHU) DNA lesion after rapid decomposition of oxidised cytosine (Cadet and Wagner, 2013). Initially oxidation leads to generation of cytosine-glycol which is highly unstable and can dehydrate, deaminate or both to sequentially generate 5-hydroxycytosine, uracil glycol and 5-OHU, respectively (**Figure 1.4**; Thivyanathan *et al.*, 2008). This spontaneous deamination and incorporation of 5-OHU into DNA may promote mutagenesis if not removed, through mispairing adenine after DNA replication leading to CG-TA transition, that account for the most abundant base substitutions observed in DNA (Thivyanathan *et al.*, 2008).

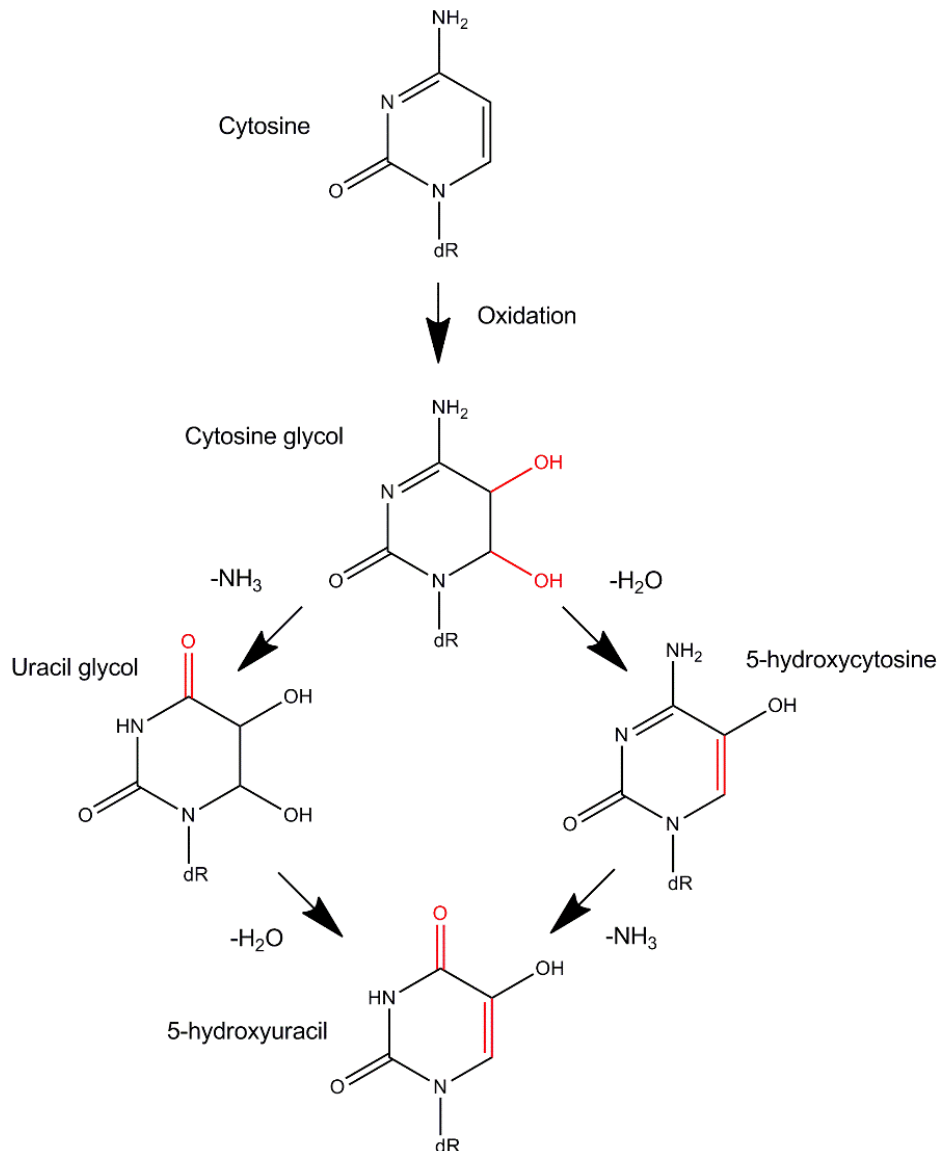


**Figure 1.4: Schematic representation of the spontaneous dehydration and deamination of cytosine post-oxidation, leading to the formation of the 5-hydroxyuracil (5-OHU) lesion (Adapted from Thivyanathan *et al.*, 2008).** Positions highlighted in red represent those modified.

Thymine may be oxidised by  $\cdot\text{OH}$ , with H-atom abstraction from the methyl group and the 5,6-pyrimidine bond (**Figure 1.5**). This in turn results in rapid addition of cellular  $\text{O}_2$  to the radical site to generate an intermediate product which degrades to generate thymine glycol (Tg; **Figure 1.5**). Thymine glycol has been demonstrated to be the most abundant base modification generated as a product of IR and oxidation of thymine (Pouget *et al.*, 2002; Yoon *et al.*, 2010). Thymine glycol stalls DNA replication due to the modification of the 5, 6-double bond of thymine, resulting in the loss of aromatic character and conversion into a planar structure. As a result, the C5 methyl group projects in a perpendicular direction blocking replicative DNA polymerases (Aller *et al.*, 2007; Yoon *et al.*, 2010). If left unrepaired, Tg requires the activation of translesion synthesis (TLS) with the recruitment of low-fidelity TLS

DNA polymerases which can synthesise past a replication blocking lesion with varied efficiency and accuracy, potentially resulting in TA to GC transversions, highlighting the mutagenic potential of Tg (Yoon *et al.*, 2010). Furthermore, the stalling of the replication machinery may activate the DNA damage response and lead to DNA replication stress. This has been demonstrated with the stalling of the FANCD1 helicase in association with replication protein A (RPA) in the presence of Tg (Suhasini *et al.*, 2009).

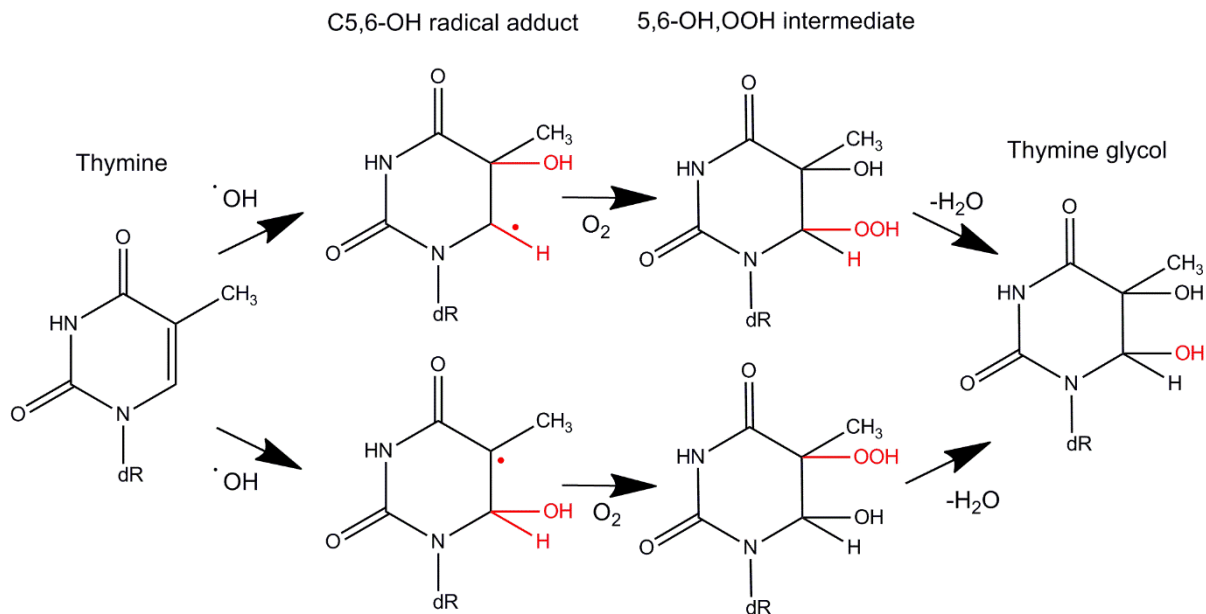


**Figure 1.5: Schematic representation of the generation of Thymine glycol (Tg) through  $\cdot\text{OH}$  oxidation of the 5,6 double bond of thymine followed by  $\text{O}_2$  addition and decomposition (Adapted from Cadet and Wagner, 2013).** Positions highlighted in red represent those modified.

Prokaryotic and eukaryotic cells have evolved complex DNA repair mechanisms to counter potential mutagenic events. The pathway responsible for the removal of oxidised bases is BER, initiated in prokaryotes by the endonuclease VIII (Nei), formamidopyrimidine DNA glycosylase (Fpg), and endonuclease III (Nth) DNA glycosylases, whereas mammalian cells possess the DNA glycosylases 8-oxoguanine DNA glycosylase (OGG1), NTH1 and Nei-like DNA glycosylases (NEIL1, NEIL2 and NEIL3; Prakash *et al.*, 2012; Rolseth *et al.*, 2013).

### 1.2.2. Alkylation of DNA.

Extracyclic oxygen and ring nitrogens in DNA bases are vulnerable to alkylation. Monofunctional or bifunctional alkylating agents can modify the DNA at one or two sites, respectively. Monofunctional alkylating agents such as dacarbazine, procarbazine, temozolomide (TMZ) and streptozotocin result in complex DNA lesions that may distort the DNA helix, potentially blocking transcription and or DNA replication (Fu *et al.*, 2012). Additionally, bifunctional agents such as melphalan, mechloroethamine, cyclophosphamide and bendamustine may form interstrand DNA crosslinks, which are highly toxic due to their ability to also prevent the progression of transcription and DNA replication leading to replication stress and possible DNA replication fork collapse (Fu *et al.*, 2012; Soll *et al.*, 2017). It is thought that ICLs are subsequently processed through nucleotide excision repair (NER) and FA initiated repair pathways (Wang, 2007; Deans and West, 2011).

Alkylating agents can generate different DNA damage based on their mode of interaction with DNA and are sub-categorised based on their mechanism of nucleophilic substitution as substitution nucleophilic unimolecular ( $S_N1$ ) or substitution nucleophilic bimolecular ( $S_N2$ ) alkylating agents.  $S_N1$  agents can target both extracyclic oxygens and ring nitrogens, while  $S_N2$  agents mainly target ring nitrogens. Due to the additional reactivity possessed by  $S_N1$  agents, they include the most commonly used chemotherapeutic alkylating agents such as TMZ and melphalan (Shrivastav *et al.*, 2010; Fu *et al.*, 2012).

The simplest form of alkylation damage is a result of the transfer of a single methyl group to a DNA base. A methyl donor may react extracyclic oxygen or ring nitrogens to generate one of 12 diverse DNA lesions. The prominent lesion generated in this manner is N7-methyl-guanine (7meG), which accounts for ~75% of all methylation damage (Baranek, 1990). 7meG is not a particularly toxic lesion, however it is vulnerable to depurination which leads to the generation of an apurinic/apyrimidinic site (AP site), which is potentially mutagenic and can be a source of spontaneous SSB generation (Soll *et al.*, 2017). Other forms of DNA damage resulting from methyl group transfer may be cytotoxic due to their ability to block replicative DNA polymerases, thus activating a low-fidelity DNA polymerase (pol) to facilitate trans-lesion synthesis (TLS) and implicating these forms of DNA damage as sources of mutagenesis due to the error prone nature of TLS (Fu *et al.*, 2012).

*O*<sup>6</sup>-methylguanine (*O*<sup>6</sup>meG) is another lesion of interest that is both cytotoxic and readily forms mispairing with thymine within the DNA duplex leading to GC to AT transitions. In addition, *O*<sup>6</sup>-ethylguanine is the major lesion generated by ethylating agents and is also a significant contributor to mutagenesis inducing GC to AT transitions (Fu *et al.*, 2012). *O*<sup>6</sup>meG may be directly reversed by *O*<sup>6</sup>-methylguanine DNA methyltransferase (MGMT) which transfers the methyl group to a catalytic cysteine residue (Olsson and Lindahl, 1980). Subsequently, MGMT-*O*<sup>6</sup>meG is targeted for proteasomal degradation through ubiquitination by the Skp1, Cul1/Cdc53, Roc1, and an F-box-containing (SCF) E3 ubiquitin ligase complex (Soll *et al.*, 2016). *O*<sup>6</sup>meG is generated in abundance when DNA is exposed to agents such as TMZ. Resistance to TMZ has been demonstrated by the over expression of MGMT and thus, cancer cells that display inactivated MGMT are more sensitive to TMZ (Christmann *et al.*, 2011). Subsequently, methylation of the promoter of MGMT, often observed in tumours, is a useful biomarker for resistance to TMZ treatment (Esteller *et al.*, 2000; Hegi *et al.*, 2005; Weller *et al.*, 2010). Mismatch repair (MMR) is implicated in the removal of thymine mispaired with *O*<sup>6</sup>meG. MMR competency is essential for *O*<sup>6</sup>meG cytotoxicity and has been proposed to be as result of two models. The first model, “the futile cycle” model, requires recruitment of the putative DNA mismatch repair protein, C-terminal (MutS $\alpha$ ) and DNA mismatch repair protein MutL (MutL $\alpha$ ) complexes facilitating removal and resynthesis of the thymine containing DNA strand. If this process replaces the mispaired thymine multiple times, it is suggested to promote DSB formation with increased levels of sister chromatid exchange implicating homologous recombination (HR), defects in which may lead to apoptosis (Mojaš *et al.*, 2007; Quiros *et al.*, 2010). Alternatively, it has been suggested that MutS $\alpha$  and MutL $\alpha$  may bind and lead to DNA damage response signalling through ataxia telangiectasia mutated kinase and Rad3-related kinase (ATR) and ATR interacting protein (ATRIP) leading to cell cycle arrest and apoptosis (Yoshioka *et al.*, 2006).

N1-methyladenine (1meA) and 3-methylcytosine (3meC) may be generated in single-stranded DNA context, with normal base pairing usually protecting against their formation (Shrivastav *et al.*, 2010). 1meA and 3meC are produced by the S<sub>N</sub>2 alkylating agent methylemethanesulfonate (MMS) and are cytotoxic due to their ability to prevent the progression of DNA replication by blocking replicative DNA polymerases. To deal with this form of DNA damage, human cells respond through DNA oxidative demethylase 2 and 3

(ALKBH2 and ALKBH3) enzymes. These enzymes achieve repair through  $\alpha$ -ketoglutarate- and iron dependent oxidation of the base to release the methyl group in the form of formaldehyde, subsequently regenerating the undamaged base (Duncan *et al.*, 2002).

Additionally, methylation of adenine bases after monofunctional alkylating agent treatment can generate 3-methyladenine (3meA) that is cytotoxic due to its ability to block DNA replication, indicated through activation of cellular tumour antigen p53 (p53), S-phase arrest and chain termination (Engelward *et al.*, 1998; Elder *et al.*, 1998). Alkyl-Adenine-DNA glycosylase (AAG) has been shown to be the major DNA glycosylase responsible for the removal of 3meA, initiating BER, *in vitro* and *in vivo* (Smith and Engelward, 2000).

Taken together, DNA alkylation includes several events that lead to a diverse set of DNA lesions that require multiple DNA repair pathways for their efficient removal, protecting against the possible cytotoxic or mutagenic affects they may impose. These pathways include direct reversal by MGMT, ALKBH2, ALKBH3 BER, NER, FA and MMR (Fu *et al.*, 2012; Soll *et al.*, 2017).

### 1.2.3. Crosslinking of DNA.

Interstrand DNA crosslinks are highly toxic DNA lesions (Muniandy *et al.*, 2010). Interstrand DNA crosslinks block DNA replication, recombination and transcription by preventing strand separation by helicases (McCabe *et al.*, 2009, Deans and West, 2011). In prokaryotic organisms just one lesion may be responsible for cell death, whereas in mammalian cells 20-40 lesions left unrepaired may induce cell death (Lawley and Phillips, 1996). Intrastrand crosslinks may also be formed, crosslinking DNA on the same strand, but are more readily removed through the NER pathway and do not block DNA replication (Huang and Li, 2013).

Crosslinking agents are in widespread use in the chemotherapy of cancer, due to the highly toxic nature of the induced DNA damage (Deans and West, 2011). Exogenous ICL inducing agents introduce genotoxic links within the DNA molecule inducing cellular apoptosis when unrepaired, through the activation of the DNA damage response (DDR) pathway. Interstrand DNA crosslinks can also be generated by endogenous agents, with acetaldehyde, formaldehyde and malondialdehyde being products of alcohol metabolism, histone

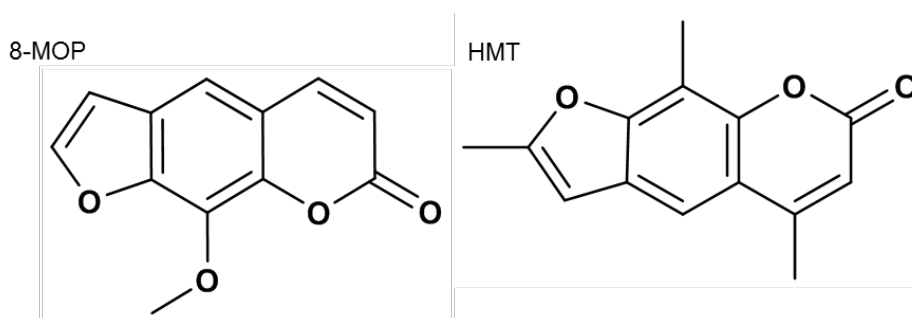
demethylation and lipid peroxidation, respectively (Cho *et al.*, 2006; Marietta *et al.*, 2009; Huang and Li, 2013; Ayala *et al.*, 2014; Wallace *et al.*, 2014).

Examples of ICL inducing agents include oxaliplatin, cisplatin, carboplatin, cyclophosphamide, MMC, melphalan, nitrogen mustard derivatives, nitrosoureas and psoralens amongst others (Dronkert and Kanaar, 2001; Siddik, 2003; Muniandy *et al.*, 2010; Huang and Li, 2013). These molecules contain two reactive groups that react with two nucleotides on opposite strands of a DNA duplex to generate an ICL or a 'bulky' mono-adduct (Couvé-Privat *et al.*, 2007; Couvé *et al.*, 2009). In the case of platinating agents, this is usually at the N2 or N7 position of guanine, resulting in the covalent modification of both DNA strands (Siddik, 2003; Couvé – Privat *et al.*, 2007; Deans and West, 2011; Huang and Li, 2013). The mode of action of crosslinking agents is similar, differing in the DNA sequence specificity and the extent to which they distort DNA, producing bends, kinks and unwinding, inducing a varying proportion of ICLs compared to other lesions such as oxidative damage, alkylation, helical distortions and DNA breaks (**Table 1.1**; Dronkert and Kanaar, 2001; Deans and West, 2011; Slyskova *et al.*, 2018). As an example, cisplatin induces a wide variety of DNA damage, with up to 90% being intrastrand crosslinks and less than 5% ICLs, whilst forming major distortion to the DNA duplex (Dronkert and Kanaar, 2001; Couvé *et al.*, 2009; Deans and West, 2011; Slyskova *et al.*, 2018).

**Table 1.1: ICL agent class, DNA sequence context of ICLs and relative level of DNA distortion.** (Adapted from Dronkert and Kanaar, 2001).

ICL Agent class	DNA sequence context	Percentage of ICLs (%)	Relative DNA distortion levels
Platinum compounds	5'-GC-3' 3'-CG-5'	3-30	Major
Psoralens	5'-TA-3' 3'-AT-5'	30-40	Minor
Mitomycin C	5'-CG-3' 3'-GC-5'	5-13	Minor
Nitrosoureas	5'-G-3' 3'-C-5'	2.5-8	Unknown
Nitrogen mustards	5'-GNC-3' 3'-CNG-5'	1-5	Major

Psoralens are model agents for the study of ICLs due to 5'-TpA-3' site selectivity and ability to generate a high percentage of ICLs and low percentages of other lesions (Dronkert and Kanaar, 2001; Couvé-Privat *et al.*, 2007; Couvé *et al.*, 2009). Psoralens are furanocoumarins, a class of organic compounds generated by a variety of plants, which are used in the treatment of psoriasis, vitiligo and other skin diseases, but are also used for the treatment of T-cell lymphomas (Huang and Li, 2013). Commonly used psoralen agents include 8-MOP and trimethylpsoralen (HMT; Dronkert and Kanaar, 2001; Deans and West, 2011). With 8-MOP generating up to 40% ICLs with the remaining adducts being MAs (Figure 1.6; Dronkert and Kanaar, 2001).

**Figure 1.6: Skeletal formula of the psoralen interstrand crosslinking agents 8-methoxypsoralen (8-MOP) and trimethylpsoralen (HMT).**

When exposed to UVA light at a 310-400 nm wavelength, psoralen intercalated DNA becomes covalently adducted. The UVA absorption of psoralen is higher than DNA and proteins, facilitating crosslinking without additional damage to DNA and proteins (Sastry *et al.*, 1997). Crosslinking is facilitated by initial cycloaddition at the 5,6-double bond of pyrimidines and single molecule addition at the 3,4-double bond of the pyrone ring or the 4,5-double bond of the furan ring of psoralen, activated by a UVA photon. Generating a pyrone-side 8-MOP-dT mono-adduct (MAp) or a furan-side 8-MOP-dT mono-adduct (MAf), the absorption of a second photon then facilitates interstrand crosslinking at the available pyrone or furan double bond, in a 5'-TpA-3' sequence context (**Figure 1.7**; **Figure 1.8**; Sastry *et al.*, 1997; Couvé-Privat *et al.*, 2007).

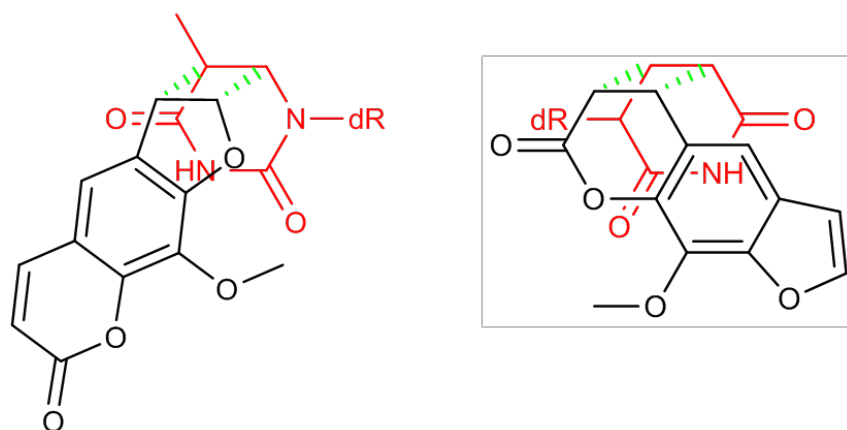


**Figure 1.7: Skeletal formula of 8-MOP-thymine mono-adducts. MAp.** Pyrone-side 8-MOP-dT mono-adduct and **MAf.** The furan-side 8-MOP-dT mono-adducts shown in two diastereomeric representations. Red structure indicates the thymine nitrogenous base with green bonds representing those formed after covalent modification by 8-MOP (Adapted from Couvé *et al.*, 2009).

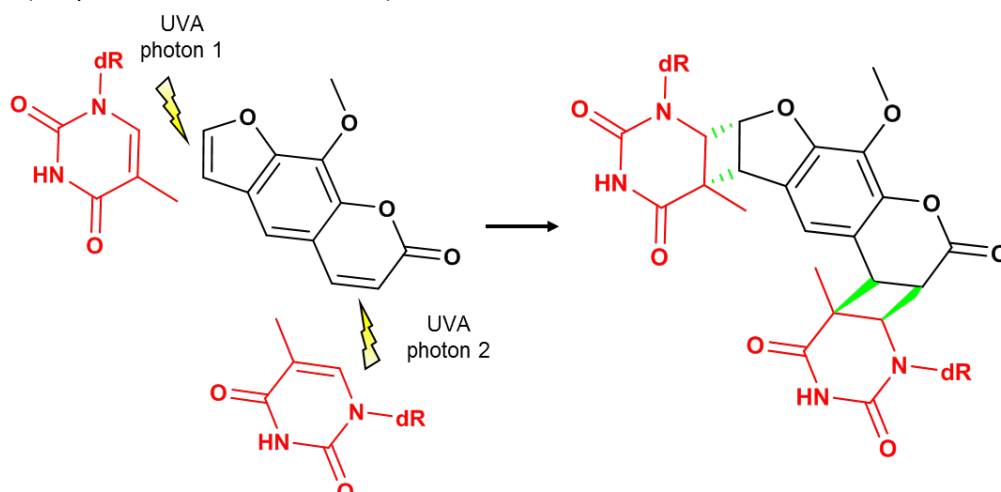


**Figure 1.8: Skeletal formula of 8-MOP mediated ICL generation with UVA exposure.** 8-MOP intercalates between two opposing thymine nucleotides and is activated on exposure to UVA generating a thymine-thymine ICL in a 5'-TpA-3' specific manner. 'dR' denotes deoxyribose sugar and phosphodiester backbone of DNA. Red structures indicate thymidine residues, black structure represents 8-MOP and green bonds represent those formed after UVA activation (Adapted from Deans and West, 2011).

Endogenous sources of ICLs have been identified and provide clues to the evolutionary selective pressure that provided the requirement for the development of ICL repair pathways. Linkage of C4'-oxidised abasic-site (C4-AP) to an adenine or a guanine is one such example (Dutta *et al.*, 2006; Szczepanski *et al.*, 2008; Semlow *et al.*, 2016). The estimated number of AP sites present at steady state levels in a normal tissue are between 50,000-200,000 sites per cell, making it the most common form of DNA lesion after DNA breaks and thus, providing suitable opportunity for spontaneous abasic site ICL generation. Furthermore, it has been shown that AP site ICLs are relatively stable in duplex with a half-life of between 66 h and 85 h at 37°C (Nakamura and Swenberg, 1999; Dutta *et al.*, 2006; Szczepanski *et al.*, 2008; Price *et al.*, 2015). Taken together AP site ICLs may be a physiologically relevant endogenous DNA replication blocking structure.

Other candidates for endogenous sources of ICLs are reactive aldehydes (Voulgaridou *et al.*, 2011). Malondialdehyde, crotonaldehyde and 4-hydroxynonenal are produced through lipid peroxidation and have been shown to form DNA ICLs (Summerfield and Tappel, 1984; Voulgaridou *et al.*, 2011). Specifically, malondialdehyde generates etheno-adducts that may become rearranged to form ICLs. This has been demonstrated *in vivo*, with mice that were fed malondialdehyde displaying an increase in ICLs (Summerfield and Tappel, 1984).

Formaldehyde is another endogenous source of ICLs and may be generated as a product of DNA demethylation by ALKBH2 and 3 or through histone demethylation. Formaldehyde may subsequently form ICLs through the production of a methylene bridge between exocyclic groups of nucleotides (Huang and Hopkins, 1993; Mosammamarast and Shi, 2010; Shen *et al.*, 2014).

Acetaldehyde is another source of endogenous DNA ICLs, being a metabolic intermediate product of carbohydrates and a bi-product of ethanol oxidation (Brooks and Zakhari, 2003). Acetaldehyde and crotonaldehyde generate N<sup>2</sup>-propano-2'-deoxyguanosine (PdG), demonstrated by PdG generation after incubation with two molecules of acetaldehyde with mammalian DNA (Garcia *et al.*, 2011). The PdG lesion may then react with a deoxyguanosine opposite to form a DNA ICL (Cho *et al.*, 2006).

### 1.3. DNA damage response.

The cell responds to DNA damage through the DDR, limiting further damage to the cell through the loss of genome integrity. The response is influenced by the stage of the cell cycle, damage type and load (Liang *et al.*, 2009; O'Connor, 2015).

At the core of the DDR are two protein kinases that work in parallel, the ataxia telangiectasia mutated serine/threonine kinase (ATM) and ATR. ATM and ATR initiate a protein cascade composed of transducers, sensors and effectors (Elledge, 2015). The ATM branch, is responsible for DSB detection, and the ATR branch is associated with SSB detection. ATM and ATR are responsible for activating transduction through checkpoint kinase 1 (Chk1) and 2 (Chk2). Chk1 is activated by ATM and ATR whilst Chk2 is only associated with ATM. Chk1 and Chk2 are recruited by DNA damage specific recognition proteins, meiotic recombination 11 homolog A (MRE11), RAD50, Nibrin (NBS1) in complex, in ATM dependent recruitment to DSBs. Chk1 is recruited by RPA through ATR dependent recruitment to SSBs (Liang *et al.*, 2009). The effectors in the resulting cascade currently include over a thousand proteins that are involved in apoptosis, DNA repair, DNA transcription, cell cycle regulation and DNA replication, including p53 (Liang *et al.*, 2009; Elledge, 2015). The DNA damage response can be initiated in a multiple pathway manner (Chou *et al.*, 2008; O'Connor, 2015).

The DNA damage response is controlled through the PTMs, phosphorylation, ubiquitination, poly(ADP-ribosyl)ation, acetylation and methylation. These modifications relocalise proteins temporally and spatially, altering the interactions within the DDR and the response (Huen and Chen, 2008).

SSBs are repaired through BER, MMR and NER. DSBs are repaired by HR repair and non-homologous end joining (NHEJ; Ciccia and Elledge, 2010; O'Connor, 2015). The loss of proteins involved in these pathways is concomitant with predisposition to oncogenesis, however the maintenance of cancer cell genomic stability by DNA repair enzymes is well established and is consequently targeted therapeutically (O'Connor, 2015).

#### 1.4. DNA replication stress response (RSR).

Human DNA replication is initiated at specific sites within the chromosome, known as origins of replication. Human chromosomes possess thousands of origins of replication, while yeast possess just a few hundred (Sacco *et al.*, 2012). Firstly, origin licensing commences as early as early gap 1 phase during cell cycle interphase (G1 phase) or late G2/M phase of the cell cycle, where the pre-replication complex is assembled. This complex consists of, the minichromosome maintenance proteins 2-7 (Mcm2-Mcm7), the origin recognition complex (ORC1-6) the cell division cycle 6 (Cdc6) and cell division cycle 10-dependent transcript 1 (Cdt1; Gambus *et al.*, 2011; Yamazaki *et al.*, 2013). The Mcm2-7 complex then assemble into two oppositely oriented DNA replication forks with one hexamer of the Mcm2-7 complex at the junction of the fork (Boos *et al.*, 2012). The recruitment of multiple additional proteins then initiates the conversion of the Mcm2-7 complex into the Cdc45-Mcm2-7- *go-ichi-ni-san* complex (GINS (CMG)) complex. The CMG complex facilitates the unwinding of the DNA at the origin of replication, followed by replisome assembly and progression of two replication forks in opposite directions along the chromosomal DNA (Ilves *et al.*, 2010; Tanaka and Araki, 2010).

Efficient and faithful DNA replication is crucial to maintain genome stability to prevent mutagenesis. Cells have evolved mechanisms to inhibit the impact that endogenous and exogenous stress has upon the cell during DNA replication within the S-phase of the cell cycle, to facilitate faithful replication of DNA and transfer to daughter cells on completion of mitosis. These include BER, HR and FA pathways (Wang, 2007, Petermann and Helleday, 2010; Ronson *et al.*, 2018). Replication stress is defined as the stalling or slowing in the progression of the DNA replication fork and does so to enable the restoration of the DNA. Replication stress may originate from many different sources and includes the incorporation of ribonucleotides, secondary DNA structures, early-replicating fragile sites (ERFSs) and common fragile sites (CFSs). However, some of the most common sources of replication stress are DNA lesions that inhibit the progression of the replisome (Zeman and Cimprich, 2013).

Fragile sites are loci within the human genome that appear to be particularly difficult to replicate. ERFs are G/C rich regions of DNA in open chromatin that display early initiation of DNA replication. CFSs have a high number of A/T nucleotides, are susceptible to formation of

secondary structure and appear in compact chromatin, demonstrating late initiation of DNA replication (Mortusewicz *et al.*, 2013; Glover, 2017). CFSs are prone to replication stress induced DSBs, prevention of which is postulated to be specific to the action of structure specific endonucleases Crossover junction endonuclease MUS81 (MUS81)-crossover junction endonuclease EME1 (EME1) and bloom syndrome protein (BLM) helicase removing replication intermediates (Naim *et al.*, 2013). CFSs can range from 1 Mb to 10 Mb in size and consequently the study of CFSs has led to the identification of large genes, some of which have been implicated as tumour suppressors (Mazouzi *et al.*, 2014). For example, PARK2 encodes for the E3 ubiquitin ligase PARKIN and is often deleted in colorectal cancer cells (Poulogiannis *et al.*, 2010).

Single-stranded DNA and SSBs are by association tied to replication stress, being both sources and signs of stress. DNA breaks are generated as intermediates in several DNA repair pathways including BER (Krokan and Bjørås, 2013). Stretches of ss-DNA in the DNA replication fork become coated with the single-stranded DNA binding protein RPA, the persistence of this interaction signals the activation of the replication stress response (RSR; Byun *et al.*, 2005). In turn this structure facilitates the recruitment of multiple replication stress response proteins, crucial components of the DNA damage response pathway (Zou and Elledge, 2005, Nam and Cortez, 2011). The study of ATR function at stalled DNA replication forks has revealed that it actively inhibits cell-cycle progression through phosphorylation of Chk1 (Lopez-Contreras and Fernandez-Capetillo, 2013). Dysregulation of ATR or Chk1 lead to checkpoint defects and chromosomal breakage (Fernandez-Capetillo and Nussenzweig, 2013). In addition, ATR can promote replication restart after successful removal of DNA lesions (Nam and Cortez, 2011).

The replication fork may fail to restart when replication stress persists. It is postulated that absence in ATR signalling pathway components leads to dissociation of the replisome, leading to DNA replication fork collapse (Ragland *et al.*, 2013). Evidence also exists for the formation of DSBs involved in fork collapse. The absence of ATR has been shown to enhance the formation of DSBs associated with DNA replication fork collapse and the activation of ATM signalling, through the phosphorylation of histone 2 A X (H2AX) on serine 139 (Chanoux *et al.*, 2009). It has been shown that single-stranded DNA and unrepaired SSBs present at a persistently stalled DNA replication fork may be prone to passive conversion into a DSB,

possibly through HR based replication restart or aberrant MUS81-EME1 cleavage (Kuzminov, 2001; Pascucci *et al.*, 2005; Hanada *et al.*, 2006; Petermann and Helleday, 2010).

Furthermore, DNA replication fork reversal and remodelling can be initiated at stalled replication forks, with four-way junctions and chicken foot structures being described (Singleton *et al.*, 2001; Quintet *et al.*, 2017). When ATR mediated DNA replication restart fails, fork reversal is observed and can lead to HR based repair of the replication fork and restart of replication (Peterman and Helleday, 2010). Indeed, it has been shown that many DSB repair proteins help regulate the reversal of the replication fork and prevent its aberrant degradation by extended nucleolytic degradation in a non-canonical manner, such as BRCA2 and PARP1 (Mijic *et al.*, 2017; Quintet *et al.*, 2017).

DNA damage promotes DNA replication stress directly, with UV irradiation, cisplatin and aphidicolin being shown to uncouple the CMG helicase complex and inhibit DNA polymerase activity during DNA replication. Furthermore, it was shown that this uncoupling was essential for the Chk1 phosphorylation by ATR (Byun *et al.*, 2005). Replication blocking lesions are a source of DNA replication stress and include ICLs and the oxidative DNA lesion Tg (Aller *et al.*, 2007; Suhasini and Brosh, 2010; Yang *et al.*, 2017). When ICLs are encountered the progressing CMG helicase complex becomes stalled and initiates replication stress and FA pathway-initiated repair (Wang *et al.*, 2007; Yang *et al.*, 2017). In addition, Tg blocks the action of replicative DNA polymerases and leads to the initiation of DNA damage tolerance pathways (DDT) including TLS (Suhasini and Brosh, 2010).

### **1.5. DNA damage tolerance pathways.**

While the replication stress response aims to repair DNA damage responsible for the initiation of the response, it is not always possible. When significant blocks to DNA replication accumulate it may be more appropriate to bypass the replication stalling lesion instead of potential fork collapse (Ghosal and Chen, 2013). In this context the cell has evolved DNA damage tolerance pathways that bypass DNA lesions for the continuation of replication to prevent prolonged DNA replication fork stalling and possible fork collapse. Two DDT pathways have been proposed. These pathways restart the stalled replication fork by initiating synthesis downstream of DNA damage and facilitate repair in a post-replicative

manner. This is facilitated by TLS and template switching (TS) pathways (Ghosal and Chen, 2013; Xin, 2015).

Conserved from prokaryotes through to higher eukaryotes, TLS is an error prone process that involves the replacement of replicative DNA polymerases when encountering a DNA replication blocking lesion. The replicative DNA polymerase is transiently replaced by low-fidelity DNA polymerases (Fuchs and Fujii, 2013; Trakselis *et al.*, 2017). Mammalian cells possess seven characterised low-fidelity DNA polymerases, two A family DNA polymerases (pol  $\theta$  and pol  $\nu$ ), one B-family DNA polymerase (pol  $\zeta$ ) four Y family DNA polymerases (pol  $\eta$ , pol  $\iota$ , pol  $\kappa$ , Rev1) that possess the ability to synthesise past a DNA lesion and are capable of inserting a small number of nucleotides (Sale *et al.*, 2012; Fuchs and Fujii, 2013; Ghosal and Chen, 2013). Each of these error-prone DNA polymerases is recruited in a DNA damage specific manner. Pol  $\zeta$  has been reported to perform DNA synthesis in an error-free manner in the presence of Tg lesions (Johnson *et al.*, 2003). The DNA repair protein REV1 (Rev1) inserts cytosine opposite (cytosine void of OH at the 2' position) opposite guanine, AP sites, 8-OxoG and  $O^6$ meG (Haracska *et al.*, 2002). Together Pol  $\zeta$  and Rev1 are implicated in resistance to DNA damage, with deletion leading to sensitivity to UV, MMS, ICL inducing agents and DSB induction. Polymerase  $\zeta$  and Rev1 were first implicated in the repair of cisplatin and MMC induced DNA damage in a FANCC dependent epistasis and are now associated with canonical FA pathway repair of ICLs (Niedzwiedz *et al.*, 2004; Wang, 2007). However, these DNA polymerases lack any proof-reading capability, which enables them to recognise modified bases but may lead to incorporation of incorrect nucleotides. For this reason, TLS is considered a source of cellular mutagenesis (Ghosal and Chen, 2013).

Template switching is an error-free method of DNA damage tolerance. In this instance the stalled nascent DNA strand temporarily switches to the nascent sister strand. Once gap filling using the sister-DNA strand as a non-damaged template has completed, a sister chromatid junction (SCJ) is formed and then resolved (Xin, 2015).

Both DDT pathways are regulated by the proliferating cell nuclear antigen (PCNA). PCNA is a ring heterotrimer that interacts with replicative DNA polymerases affecting their processivity, after being loaded to primed DNA by the clamp loader replication factor C (RFC; Kannouche *et al.*, 2004). The ubiquitin proteasome system regulates the choice in DDT pathway. Monoubiquitination of PCNA on Lys164 has been confirmed to promote TLS by facilitating

replacement of the replication DNA polymerase by binding the error-prone DNA polymerases pol  $\zeta$  and pol  $\eta$  (Stelter and Ulrich, 2003; Kannouche *et al.*, 2004). Ubiquitination of PCNA has been shown to be essential for the repair of UV-induced DNA damage in yeast. It is thought that ubiquitination strengthens the PCNA interacting protein box (PIP-box) domain interactions with associated DNA polymerases, acting as an anchor. Despite this, several examples of ubiquitin independent TLS are reported and include TLS facilitated by Rev1, pol  $\zeta$  and pol  $\kappa$  (Xin, 2015). Where Rev1 and pol  $\zeta$  play important roles in the repair of ICL lesions and resistance through error-prone synthesis (Zafar and Eoff, 2017). Poly-ubiquitination of PCNA has been indicated to promote TS however, the exact mechanisms in which it achieves this remains unknown (Xin, 2015).

### **1.6. Fanconi anemia pathway.**

The Swedish physician Guido Fanconi first described FA in 1927, nearly a century ago (Lobitz and Velleuer, 2006). Since then, the disease has been shown to be a mainly autosomal recessive disorder with mutations in one or more of the FA gene family that consists of over 21 genes (A-V with two characterised D proteins, D1 and D2; Nalepa and Clapp, 2018). FA patients display a high frequency of congenital, haematological disorders and predisposition to cancer (Kee and D'Andrea, 2012). The X-linked FA complementation group B (FANCB) is the only observed case of FA where dominant-negative mutations lead to a rare sub-type of FA (Ameziane *et al.*, 2015). FA is rare and affects 1 in every 100,000 individuals (Rosenberg, *et al.*, 2011).

Fanconi anemia is characteristically associated with genomic instability, bone marrow failure, haematopoietic stem cell dysfunction, predisposition to cancer and myelodysplastic syndromes (Cheung and Taniguchi, 2017; Nalepa and Clapp, 2018). However, multiple other clinical manifestations have been observed and include osteoporosis (Giri *et al.*, 2007), immune deficiency (Fagerlie and Bagby, 2006), endocrine dysfunction (Giri *et al.*, 2007) and sarcopenia (Neveling *et al.*, 2009).

Due to the associated predisposition to cancer and genomic instability, the FA pathway is largely studied as a model for mechanisms of carcinogenesis (Nalepa and Clapp, 2018). The FA pathway has been primarily characterised, as a DNA damage response pathway associated with the repair of ICLs in a DNA replication associated manner (Duzin and Walter, 2013;

Clauson *et al.*, 2013). This was identified due to the characteristic hypersensitivity to ICL inducing agents that FA dysfunctional cells display. Cells derived from patients that are treated with low doses of the ICL inducing agent MMC also display chromosome breakage. Concomitantly, treatment of patient derived cells with ICL inducing agents and surveillance for chromosomal breakage is a diagnostic tool for the FA disease (Nalepa and Clapp, 2018). In addition, FA dysfunctional cells display an oxidative stress sensitive phenotype with evidence suggesting an associated downregulation of the human oxidative DNA glycosylase NEIL1 (Macé-Aimé *et al.*, 2010).

When ICL damage occurs, DNA replication stalls due to the ICL block, in turn activating the DNA replication stress response, initiated through ATR and subsequent activation of Chk1, stalling cell cycle progression. ATR also phosphorylates multiple FA proteins including the Fanconi anemia complement group (FANC) M protein (Andreassen *et al.*, 2004; Singh *et al.*, 2013). The CMG helicase complex stalls 20-40 bases away from the ICL. Breast cancer associated protein 1 (BRCA1) in association with BRCA1-associated really interesting new gene (RING) domain protein 1 (BARD1) unloads the CMG helicase complex, possibly through associated ubiquitination activity possessed by BRCA1 which may target CMG subunits for removal (Ceccaldi *et al.*, 2016). However, it was shown that CMG unloading defects observed by BRCA1 deficient cells cannot be rescued with the addition of recombinant BRCA1, alluding to the involvement of other proteins (Long *et al.*, 2014). The leading strand is then extended to within ~1 nucleotide of the ICL (Semlow *et al.*, 2016). The ICL is then recognised through FANCM recruitment, with FA associated protein of 24 kDa (FAAP24), histone fold protein complex 1 (MHF1) and histone fold protein 2 (MHF2) in an ATR dependent phosphorylation manner (Ceccaldi *et al.*, 2016). FANCM is a protein highlighted as an ICL sensor and translocase that interacts with PCNA, with the ability to facilitate replication fork remodelling at the site of an ICL leading to the formation of ss-DNA gaps with RPA bound and DNA replication fork reversal (Gari *et al.*, 2008; Huang *et al.*, 2013; Rohleder *et al.*, 2016).

FANCM subsequently functions as a platform for the recruitment of the FANC core complex consisting of FANCA, FANCB, FANCC, FANCE, FANCF, FANCG, FANCL, FANCT, FA associated protein of 100 kDa (FAAP100) and FA associated protein of 20 kDa (FAAP20; Shimamura *et al.*, 2002; Ceccaldi *et al.*, 2016). The FANCI-FANCD2 heterodimer is then recruited by phosphorylation by ATR (Andreassen *et al.*, 2004; Ishiai *et al.*, 2008; Roques *et al.*, 2009).

Subsequently, the core complex activates the FANCI-FANCD2 heterodimer through monoubiquitination, facilitated by the E2 ubiquitin conjugating enzyme FANCT and the RING E3 ubiquitin ligase FANCL, subunits of the FANCD2 core complex. More than 90% of patients who have upstream mutations display abnormalities in this FANCI-FANCD2 monoubiquitination step, highlighting its importance in ICL repair (Shimamura *et al.*, 2002). Consecutively, the structure specific endonucleases MUS81 in complex with crossover junction endonuclease EME1 and excision repair cross complementing protein 1 endonuclease (ERCC1) in complex with xeroderma pigmentosum complementation group F (XPF) are recruited with the scaffold protein structure specific endonuclease subunit (SLX4) and together facilitate ICL incision. The MUS81-EME1 heterodimer is associated with the first incision and its absence has been reported to inhibit the accumulation of DSBs associated with ICL agent treatment (Hanada *et al.*, 2006). ERCC1-XPF endonuclease has been proposed to undertake the second incision as significant sensitivity to ICL agents has been observed upon its depletion (Niedernhofer *et al.*, 2004; Seetheram *et al.*, 2010). At this stage the ICL swings free, generating a DSB within the DNA and a ss-DNA gap directly opposite the ICL (Wang *et al.*, 2007; Martin *et al.*, 2017). Next TLS, facilitated by the low-fidelity DNA polymerases Rev1 and Pol  $\zeta$  seals the ss-DNA-gap (Niedzwiedz *et al.*, 2004; Wang, 2007). NER or BER then complete the removal of the ICL remnant (Wang, 2007; Couvé *et al.*, 2009; Clauson *et al.*, 2013; Martin *et al.*, 2017). The FANCI-FANCD2 heterodimer is then deactivated, facilitated by the Ubiquitin-specific-processing protease 1 (USP1) deubiquitinase enzyme (Nijman *et al.*, 2005). TLS DNA polymerases and HR proteins are then recruited to rescue the stalled replication fork (Wang, 2007; Duxin and Walter, 2015).

More recently reactive aldehyde metabolism has been linked to the FA repair pathway. This was shown through aldehyde dehydrogenase 2 (ALDH2)<sup>-/-</sup> and FANCD2<sup>-/-</sup> double knockout mice which displayed an associated spontaneous development of acute lymphoblastic leukemia and reduction in survival when compared to FANCD2<sup>-/-</sup> or ALDH2<sup>-/-</sup> single gene knockout mice (Langevin *et al.*, 2011; Garaycochea *et al.*, 2012). ALDH2<sup>-/-</sup> and FANCD2<sup>-/-</sup> mice that did not display lethality developed bone marrow dysfunction, displayed a significant reduction in haematopoietic stem cells (HSCs). Additionally, ALDH2<sup>-/-</sup> and FANCD2<sup>-/-</sup> HSCs displayed a significant increase in sensitivity compared to WT, ALDH2<sup>-/-</sup> or FANCD2<sup>-/-</sup> mice derived HPCs to acetaldehyde (Garaycochea *et al.*, 2012). Furthermore, an associated role

of aldehyde dehydrogenase 5 (ALDH5) with FA was also shown, with double FANCD2<sup>-/-</sup> ALDH5<sup>-/-</sup> mice observed to developed hematopoietic stem cell depletion and bone marrow failure earlier than ALDH2<sup>-/-</sup> FANCD2<sup>-/-</sup> mice. FANCD2<sup>-/-</sup> ALDH5<sup>-/-</sup> mice also demonstrated a significant reduction in survival vs FANCD2<sup>-/-</sup> or ALDH5<sup>-/-</sup> single gene knockout mice. Splenic B cells grown in formaldehyde from FANCD2<sup>-/-</sup> ALDH5<sup>-/-</sup> mice also displayed a significant increase in sensitivity compared to splenic B cells derived from WT, FANCD2<sup>-/-</sup>, ALDH5<sup>-/-</sup> or mice (Pontel *et al.*, 2015). It was also shown that chicken lymphoblast (DT40) FANCL knockout cells were hypersensitive to formaldehyde when compared to WT cells (Rosado *et al.*, 2011). Therefore, it was proposed that DNA damage generated by formaldehyde is removed by the FA pathway and formaldehyde is a greater source of endogenous DNA damage compared to acetaldehyde (Rosado *et al.*, 2011; Pontel *et al.*, 2015). Further evidence for the activation of FA pathway in response to reactive aldehydes was previously shown by dose-dependent stimulation of the monoubiquitination of the FANCI-FANCD2 heterodimer in response to acetaldehyde treatment of lymphoblastoid cell lines (Marietta *et al.*, 2009). Taken together these studies provide *in vitro* and *in vivo* evidence indicating that aldehydes are an important source DNA damage associated with the FA pathway, presumably through the generation of ICLs.

AP site ICLs, generated by the linkage of the C4-AP site to an adenine, have also been shown to be repaired by the FA pathway in the absence of the NEIL3 DNA glycosylase in a *X. laevis* egg extract system (Sczepanski *et al.*, 2008; Semlow *et al.*, 2016). Evidence indicates that endogenous ICLs pose a significant threat to genomic instability, requiring the evolution of distinct DNA repair mechanisms, such as the FA pathway, to counter their detrimental effects (Nalepa and Clapp, 2018).

### **1.7. Nucleotide excision repair.**

The nucleotide excision repair pathway is unique in its ability to remove a wide range of helix distorting DNA damage. NER is responsible for repair of DNA lesions that form helical distortions, termed 'bulky' DNA lesions including those induced by UV damage (Kamileri *et al.*, 2012). NER comprises global genome NER (GG-NER) and transcription-coupled NER (TC-NER). In humans it has been shown that defects in NER proteins give rise to the rare genetic disease, xeroderma pigmentosum with a predisposition to skin cancer and other syndromes resulting in photosensitivity such as Cockayne syndrome and trichothiodystrophy (Kraemer

*et al.*, 2007). NER is implicated in ICL repair in quiescent cells, with initial incision followed by TLS and a second round of incision followed by gap filling by DNA polymerases (Wang, 2010; Deans and West, 2011; Hashimoto *et al.*, 2016). Indeed, cells deficient in the Cockayne syndrome protein B (CSB), treated with FANCD2 siRNA, are more sensitive to MMC and cisplatin than FANCD2 siRNA treated CSB complemented fibroblast cells (Enoiu *et al.*, 2012). As indicated earlier in (Section 1.6) NER is also associated with replication dependent ICL repair initiated by the FA pathway followed by the involvement of the ERCC1-XPF nuclease (Wang, 2007; Deans and West, 2011; Clauson *et al.*, 2013).

### 1.7.1. Global Genome Nucleotide Excision Repair.

Proteins involved in GG-NER scan the genome to detect helical distortions, such as those produced by the cyclobutane–pyrimidine dimer (CPD) as result of UV irradiation (Schärer, 2013). The xeroderma pigmentosum, complementation group C (XPC) protein in association with Centrin 2 (CETN2) and UV excision repair protein radiation sensitive 23B (RAD23B), act as the primary DNA sensor. This sensor searches for disrupted DNA in a single-stranded (ss) conformation, caused by DNA mispairing due to the incorporation of bulky DNA damage (Masutani *et al.*, 1994; Schärer, 2013). Investigation, by crystallography of the XPC ortholog in fission yeast, Rad4, revealed that it inserts a C-terminal double  $\beta$ -hairpin in the junction between ss-DNA and double-stranded (ds-DNA; Min and Pavletich, 2007). This is suggested to be a fundamental process that enables broad spectrum recognition of lesions. However, additional recognition factors have been identified and are required for CPD repair. These include DNA damage binding protein 1 (DDB1) and 2 (DDB2), that form a complex with cullin 4A–regulator of cullins 1 E3 ubiquitin ligase (CRL). This complex facilitates DDB2 binding to the DNA lesion which kinks the DNA to facilitate XPC recognition of ss-DNA (Groisman *et al.*, 2003; Scrima *et al.*, 2008).

Xeroderma pigmentosum complementation group C serves as a substrate for the transcription initiation factor II H (TFIIH) complex. TFIIH consists of 10 subunits that may also function in TC-NER (Yokoi *et al.*, 2000; Compe and Egly, 2012). Within this complex Xeroderma pigmentosum complementation group B (XPB) and Xeroderma pigmentosum complementation group D (XPD) serve as helicases that unwind the DNA from the site of the lesion creating an open conformation within the DNA (bubble structure) in opposite

directions (Compe and Egly, 2012). TFIIH scans the DNA for the helix distorting lesion in a 5'-3' direction and if the XPD helicase does not detect a DNA lesion, the process is aborted at this stage (Mathieu *et al.*, 2013). The structure specific endonuclease ERCC1-XPF and xeroderma pigmentosum complementation group G (XPG) are then recruited, cleaving the damaged DNA 5' and 3' a small number of nucleotides from the lesion, respectively (Fagbemi *et al.*, 2011). The accuracy of this incision step requires the presence of RPA and Xeroderma complementation group A (XPA) at the site of the lesion, where XPA acts as a coordinator possessing the ability to interact with most NER proteins, while RPA protects the non-damaged DNA strand (Marteijn *et al.*, 2014). The ERCC1-XPF structure specific endonuclease, initiates incision prior to XPG, creating a ss-DNA-gap, releasing an oligonucleotide containing the 'bulky' DNA damage (Staresinic *et al.*, 2009). DNA polymerases and DNA ligases then fill the gap, such as X-ray repair cross complementing 1 (XRCC1) in complex with Ligase (Lig) III or Pol  $\delta$ , Pol  $\epsilon$ , Pol  $\kappa$  and Lig I, coordinated by PCNA. With XRCC1-Lig III and Pol  $\epsilon$  being most active in non-proliferating cells whilst Pol  $\delta$  and Pol  $\kappa$  have been found to be the main NER DNA polymerases in replicating cells (Moser *et al.*, 2007; Ogi *et al.*, 2010).

### 1.7.2. Transcription coupled repair (TC-NER).

Bulky DNA lesions can hinder the processes of transcription and DNA replication despite GG-NER efficiency. As previously discussed, the stalling of DNA replication activates the DDR through the RSR and in turn activates many different repair pathways to compensate to avoid the detrimental generation of DSBs, such as HR, TLS and FA repair. This said, no dedicated translesion ribonucleic acid (RNA) polymerases have been identified for the continuation of transcription. Thus, the TC-NER sub pathway of NER facilitates the removal of bulky DNA adducts that block transcription, a crucial requirement as it has been reported that lack of repair of these lesions may promote cell death (Ljungman and Zhang, 1996). Furthermore, deficiencies in cockayne proteins lead to hypersensitivity to oxidative DNA damage, suggesting that GG-NER may not efficiently recognise the range of lesions that the TC-NER machinery can. It may also indicate overlapping roles between TC-NER and BER (de Waard *et al.*, 2004; Stevnsner *et al.*, 2008). During transcription, the RNA DNA polymerase becomes stalled when encountering a DNA lesion, recruiting the TC-NER specific proteins cockayne syndrome protein A (CSA) and B (CSB), ubiquitin-specific-processing protease 7 (USP7), XPA-

binding protein 2 (XAB2), UV-stimulated scaffold protein A (UVSSA), high mobility group nucleosome-binding domain-containing protein 1 (HMGN1; Fousteri *et al.*, 2006). Once localised CSA and CSB reverse-translocates RNA DNA polymerase II, allowing TFIIH to bind, recruiting downstream proteins as in GG-NER (Marteijn *et al.*, 2014).

CSB has been shown to interact with PARP1 and it has been shown that poly(ADP-ribosyl)ation of CSB inhibits DNA dependent adenosine triphosphatase activity possessed by CSB (Thorslund *et al.*, 2005). CSB has also been shown to interact with APE1, with evidence suggesting CSB stimulates APE1 incision of AP sites in duplex and in bubble structured DNA (Wong *et al.*, 2007). Furthermore, it was shown that deficiency in CSB leads to the accumulation of 8-OxoG in nuclear and mitochondrial DNA through the downregulation of OGG1, however CSB had no effect on the status of thymine DNA glycosylase (TDG) and uracil DNA glycosylase (UDG) BER proteins (Dianov *et al.*, 1999; Stevnsner *et al.*, 2002).

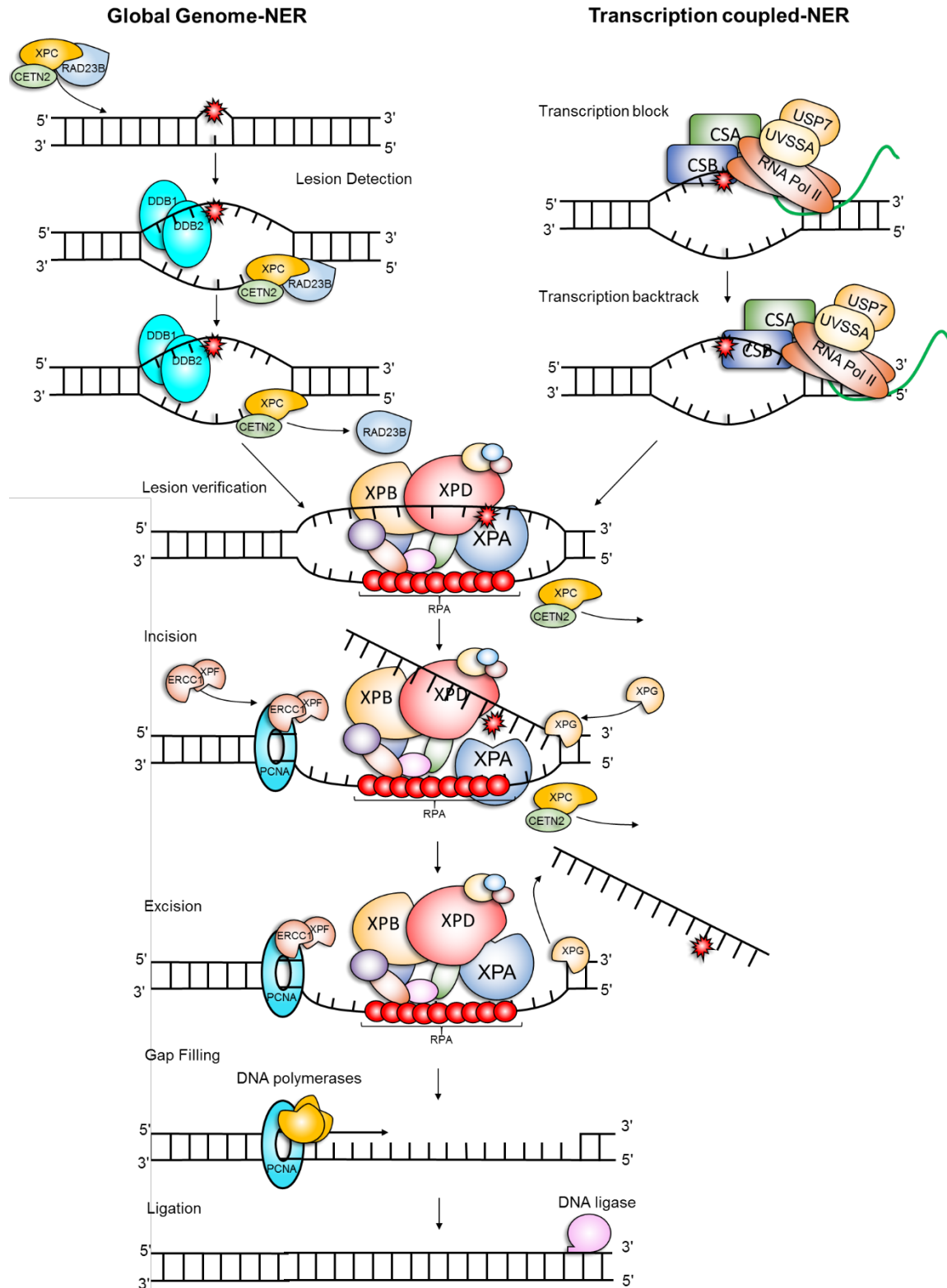


**Figure 1.9: Schematic representation of GG-NER and TC-NER pathways.** IN GG-NER, XPC in complex with CETN2, RAD23 probe for ss-DNA formed by helical distorting lesions. DDB1 and DDB2 facilitate detection through XPC interaction. In TC-NER RNA pol II stalls and CSB and CSA proteins are recruited and backtracks the RNA pol II along the DNA. The TFIIH complex is then recruited and the lesion is verified through XPD, XPA and XPB. RPA coats the non-damaged ss-DNA. ERCC1-XPF and XPG sequentially incised the DNA releasing the damaged DNA. PCNA recruits DNA polymerases to conduct gap filling synthesis and the nick is sealed by DNA ligase I or III (Adapted from Martejijn *et al.*, 2014).

### 1.8. Repair of DNA Interstrand crosslinks.

As previously discussed, repair of ICLs is essential for the avoidance of persistent replication stress and DNA replication fork collapse, to ensure the maintenance of genomic stability. Many different models have been proposed for the repair of an ICL, however there is general agreement that differential processing of an ICL occurs in a cell cycle dependent manner. ICL repair may therefore be conducted in a replication associated manner or a replication independent manner (Wang, 2007; Deans and West, 2011).

The repair of an ICL in quiescent cells in eukaryotic organisms relies on the NER machinery, with the lesion recognised as 'bulky' with distortion to the DNA helix. An initial round of GG-NER or TC-NER flips out the ICL, followed by TLS across the ss-DNA break generated, by pol  $\kappa$ , Pol  $\zeta$  and Rev1 (Sarkar et al., 2006; Wood, 2010; Deans and west, 2011 Williams et al., 2012). The three-stranded intermediate is then subsequently processed by a second incision round followed by gap filling by Pol  $\delta$  in association with PCNA (Wang, 2007; Hashimoto et al., 2016).

Replication associated repair of an ICL is currently suggested to be initiated by the FA pathway and as previously discussed, ICL repair is initiated when the replisome becomes stalled by an ICL, with the CMG helicase complex stalling 20-40 bases from the ICL (Muniandy *et al.*, 2010; Semlow *et al.*, 2016 Yang *et al.*, 2017). The single strand binding protein, RPA binds to ss-DNA initiating ATR signalling (Zou and Elledge, 2003). Single-stranded DNA may be converted to DSBs and in cases of ATR deficiency the DNA replication fork may be destabilised and induce DNA replication fork collapse. Subsequently, DSBs are detected after treatment with DNA replication fork stalling agents, with initiation of ATM and the DDR. The effect of this is stimulated in the presence of ATR defects and has been demonstrated in mammalian cells (Zeman and Cimprich, 2014; Cortez, 2015). When a DNA replication fork collapses, it is suggested DSBs are processed through HR, which can lead to mutagenic chromosomal rearrangement, through sister chromatid exchange (de Silva *et al.*, 2000).

Subsequently the RSR is initiated through ATR and cell cycle arrest proceeds via Chk1 phosphorylation. ATR also phosphorylates FANCM, recruiting it to the stalled DNA replication fork with MHF1, MHF2 and FAAP24 (Singh *et al.*, 2013; Ceccaldi *et al.*, 2016). At this stage the

remodelling of the replication fork may be stimulated, with the formation of ss-DNA gaps (Gari *et al.*, 2008).

The FANCM and FAAP24 proteins then proceed to recruit the FANC core complex followed by FANCD2-FANCI which are then monoubiquitinated by FANCT and FANCL, subunits of the FANC core complex (Kim *et al.*, 2008; Liang *et al.*, 2016). Henrietta Lacks derived cervical adenocarcinoma (HeLa) cells depleted of FANCM, displayed an inhibition of the recruitment of the FA core complex to an ICL and by association, depletion of FAAP24 inhibited FANCM recruitment to chromatin and the downstream FANC core complex recruitment (Kim *et al.*, 2008).

The FANCD2-FANCI complex then associates with the structure specific endonucleases such as MUS81-EME1, ERCC1-XPF, Fanconi associated nuclease 1 (FAN1) under the coordination of the scaffold protein SLX4 (Kim *et al.*, 2011b; Clauson *et al.*, 2013; Kottemann and Smogorzewska, 2013). It has been suggested that cleavage on the 5' side of the ICL occurs, facilitated by the MUS81-EME1 heterodimer followed by the 3' side by ERCC1-XPF (Couvé *et al.*, 2009; Clauson *et al.*, 2013; Douwel *et al.*, 2014; Semlow *et al.*, 2016; Douwel *et al.*, 2017). However, MUS81-EME1 has the same polarity as ERCC1-XPF and thus, may or may not undertake 5' incision. Indeed, ERCC1-XPF has been shown to cleave both 5' and 3' of an ICL *in vitro* (Kuraoka *et al.*, 2000). However, DSB formation at an ICL has been shown to be dependent on MUS81-EME1 thus indicating a role in 5' incision releasing the splayed strand. Therefore, it has been proposed that the ERCC1-XPF and MUS-EME1 nucleases incise different ICL intermediates (Hanada *et al.*, 2006; 2007). Concomitantly, MUS81-EME1 has been shown to play a role in the resolution of Holliday junctions, a result of recombination events at a persistently stalled DNA replication fork (Chen *et al.*, 2001). FAN1 has also been shown to incise within unwound 5'-flap structures and degrade ds-DNA 5'-3' containing an ICL. However, FAN1 cleavage required an ~10 nucleotide region of ds-DNA surrounding an ICL to conduct incision activity *in vitro* (Pizzolato *et al.*, 2015). Additional, evidence for the role of FAN1 in ICL repair comes from its direct interaction with mono-ubiquitinated FANCD2, however enzymatic redundancy is observed as ICL sensitivity/FA is not observed in the absence of FAN1 (Ceccaldi *et al.*, 2016). Subsequently MUS81-EME1 is a prime candidate for 5' ICL incision based on hypersensitivity observed in mouse embryonic stem (ES) cells deficient in MUS81 to ICL inducing agents (Hanada *et al.*, 2006). In addition, the DNA cross-

link repair 1A protein (SNM1A) nuclease, exhibits 5'-3' exonuclease activity from a ss-DNA-nick past an ICL, with its depletion yielding ICL sensitivity and MUS81 dependent replication associated DSBs (Wang *et al.*, 2011). Also, SLX4 is highlighted as an important component of the ICL incision machinery, with evidence demonstrating that it may bind the nucleases MUS81 and XPF, while maintaining interaction with monoubiquitinated FANCD2 (Fekairi *et al.*, 2009). Furthermore, lack of SLX4 results in ICL sensitivity, however mutational analysis of SLX4 revealed that this sensitivity was ERCC1-XPF binding dependent (Yamamoto *et al.*, 2011; Kim *et al.*, 2013). Taken together, SLX4 is likely a scaffold protein important for nuclease choice and recruitment to the site of an ICL. In conclusion, incision steps in ICL repair, have been proposed to involve multiple structure specific nucleases, however the exact mechanisms of this ICL incision are a subject of ongoing study (Ceccaldi *et al.*, 2016).

The incision step, unhooks an ICL, inducing a single ended DSB on the incised strand, but permits TLS by the consecutive action of DNA polymerases such as Pol  $\nu$ , Pol  $\kappa$  or Pol  $\eta$ , extension then by REV1 and pol  $\zeta$ , filling the gap created to generate an intact sister chromatid (Hanada *et al.*, 2006; Ho and Schärer, 2010; Hicks *et al.*, 2010; Ho *et al.*, 2011; Clauson *et al.*, 2013). This generates a three-stranded DNA structure in the form of a crosslink remnant attached to a DNA duplex. The ICL remnant is then proposed to be removed by the NER machinery resulting in a DNA duplex, potentially forming further DSBs (Cipak *et al.*, 2006; Sczepanski *et al.*, 2009; Clauson *et al.*, 2013; Wakasugi *et al.*, 2014). At this stage it is suggested that HR would take place to rescue the DSB (Michl *et al.*, 2016). This proceeds via 5' strand resection in part due to the 5'-3' exonuclease activity of exonuclease 1 (EXO1), which subsequently generates a ss 3' overhang, a structure that promotes both ATR and ATM signalling (Liu and Huang, 2016). Then the ss 3' DNA may invade the homologous sister chromatid duplex, generating a Holliday junction and a D-loop structure (Hinz *et al.*, 2010). The invading 3' strand is then primed for DNA synthesis. The Holliday junctions generated may then be cleaved by endonucleolytic incision, possibly by MUS81-EME1 (Chen *et al.*, 2001; Hinz, 2010; Clauson *et al.*, 2013). The accuracy in this terminal step of conventional ICL repair is vital to avoid gross genomic instability through chromosomal breakage, which in turn may promote tumorigenesis and lethality (Hinz *et al.*, 2010).

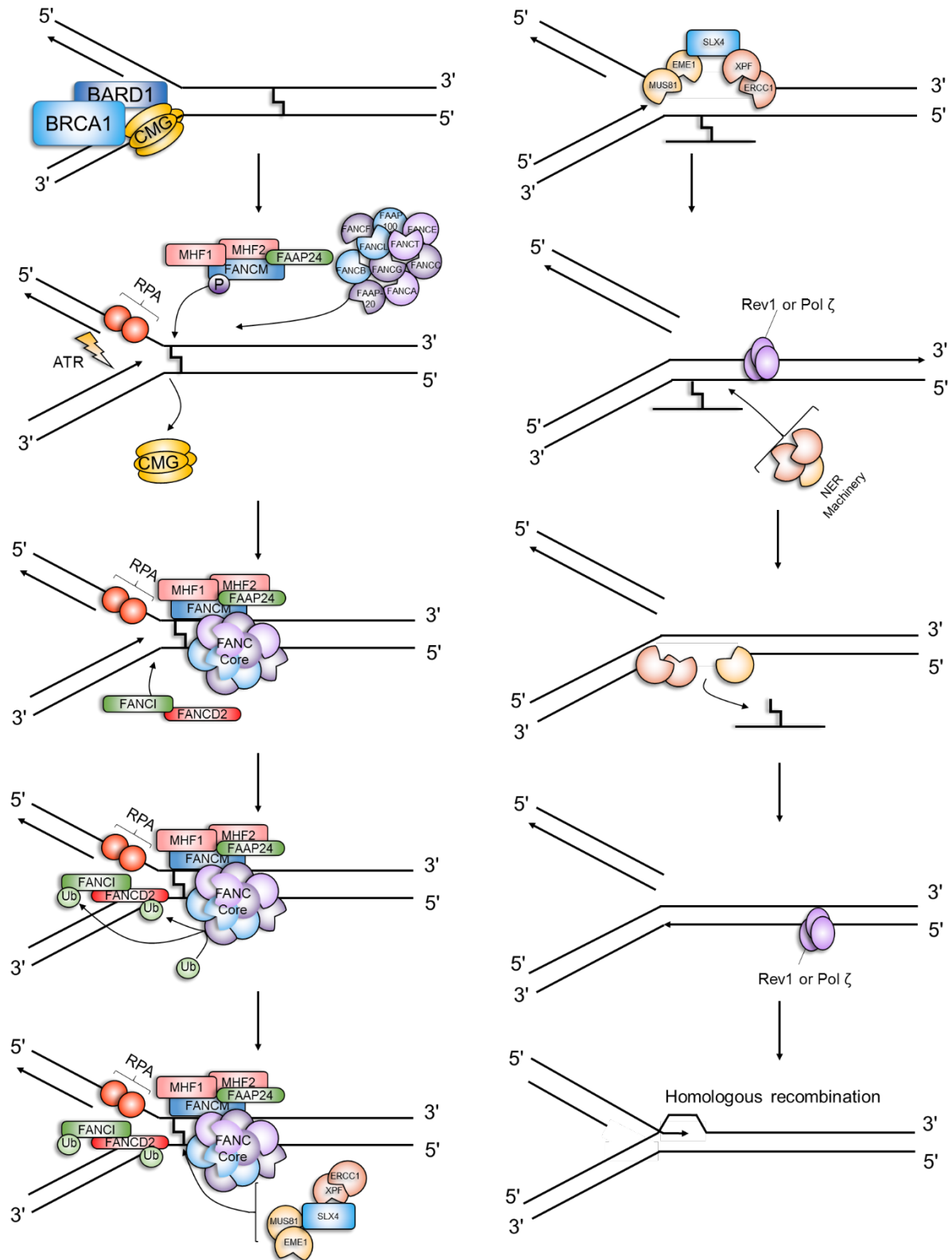


**Figure 1.10: Schematic model of Fanconi anemia initiated replication associated ICL repair.** The CMG complex stalls and is dissociated by BRCA1/BARD1 and the strand is extended towards the ICL. The FA pathway is then initiated through FANCM recruitment of the FANC core complex. Subsequently the FANCI/D2 heterodimer is recruited and monoubiquitinated by FANCT and FANCL. The ICL is incised near an ICL by Mus81/EME1 and XPF/ERCC1, respectively, flipping out the ICL. TLS proceeds generating a three-stranded structure. NER is proposed to remove the ICL remnant followed by homologous recombination to yield two homologous DNA duplex.

Additionally, Saparbaev's group demonstrated that the hNEIL1 DNA glycosylase can excise an ICL in a three-stranded structure and MAs in a DNA duplex context. This unhooking activity generated a ss-DNA-nick flanked by a 5' and a 3' phosphate at the site of the ICL, that is then proposed to be processed by BER (Couvé-Privat *et al.*, 2007; Couvé *et al.*, 2009). This highlighted a role of hNEIL1 in the resolution of a three-stranded ICL structure that represents the intermediate product generated by structure specific endonuclease unhooking of an ICL (Couvé *et al.*, 2009). This was the first time that mechanistic evidence was provided for the role of a DNA glycosylase and BER in ICL repair.

Despite the accepted notion that an ICL is an absolute block to DNA replication, Seidman's group demonstrated that the FANCM-MHF complex possessed an unconventional activity in the presence of a labelled psoralen ICL (Huang *et al.*, 2013). It was shown that the FANCM/MHF complex can promote replication traverse across an ICL in DNA, with DNA combing analysis demonstrating continued DNA replication past ~85% of MA and HMT ICLs after 60 min. This observation was inhibited in FANCM<sup>-/-</sup> cells in an ICL specific manner. Thus, it was suggested that FANCM facilitates the traverse of the replication machinery past an ICL in cells (Huang *et al.*, 2013). It was later shown that this activity was stimulated by interaction with PCNA through the PIP box domain. This interaction increased 10-fold under DNA replication stress induced by hydroxyurea (HU) treatment of HeLa cells (Rohleder *et al.*, 2016).

In addition, Walter's group proposed that dual collision of DNA replication forks with an ICL was required for its subsequent repair. Evidence was provided for this with incubation of *X. laevis* egg extracts with a DNA plasmid containing a cisplatin ICL. It was observed that in the presence of a plasmid structure representing a single replication fork an ICL could not be excised and the CMG helicase did not dissociate (Zhang *et al.*, 2015). This plasmid structure contained a *lacO* array which inhibited fork progression from the opposite direction independent of an ICL for 3 hours. Subsequently it was found that in a plasmid structure that did not contain the *lacO* array DNA repair of a cisplatin ICL proceeded, indicating the requirement of an X-shaped structure mimicking dual replication fork collision (Zhang *et al.*, 2015). Despite these findings the role of repair components, downstream of the incision step of ICL repair, was not addressed. It was also acknowledged that FANCM replication traverse was not observed in their model system (Huang *et al.*, 2013; Zhang *et al.*, 2015).

More recently, Walter's group revealed a novel role of the NEIL3 DNA glycosylase in the repair of AP site ICLs and psoralen ICLs with incubation of plasmids containing AP site, psoralen and cisplatin ICLs with NEIL3 competent and NEIL3<sup>-/-</sup> *X. laevis* egg extracts. It was observed that NEIL3 could resolve an AP-site ICL and a psoralen ICL independent of the FANCD2-FANCI heterodimer. Absence of NEIL3 resulted in the activation of FA initiated repair of AP-site and psoralen ICLs. In addition, psoralen ICL repair did not require the dissociation of the CMG complex. Furthermore, it was shown that the cisplatin ICL was refractory to NEIL3 initiated repair and the FA pathway was the primary pathway responsible for its resolution. Importantly, NEIL3 dependent ICL excision did not generate DSBs and resolution was faster than that typically associated with FA initiated repair (Semlow *et al.*, 2016). This was the first mechanistic evidence in support of the role of NEIL3 in the repair of ICLs. It was proposed NEIL3 dependent excision is the primary pathway for the resolution of AP-site ICLs and psoralen ICLs. The fact that NEIL3 may resolve AP site ICLs is of significance due to the abundance of AP sites in the cell, which present suitable opportunity for spontaneous cross-linking (Nakamura and Swenberg, 1999; Dutta *et al.*, 2006; Szczepanski *et al.*, 2008). Furthermore, the repair of AP sites is essential in mammals, with embryonic lethality observed in APE1<sup>-/-</sup> mice (Izumi *et al.*, 2005). It may be speculated that AP-site ICL excision by the NEIL3 DNA glycosylase may be an essential function that defines it from its homologs NEIL1 and NEIL2, while redundancy is observed with the FA pathway (Semlow *et al.*, 2016). However, the data presented by Semlow *et al.* (2016) also demonstrated that cisplatin ICLs were refractory to NEIL3 excision despite the sensitivity of NEIL3<sup>-/-</sup> MEFs to cisplatin previously observed (Rolseth *et al.*, 2013).

### 1.9. Base excision repair.

The BER pathway is the primary repair pathway initiated in response to single DNA base damage and SSBs. The discovery of BER was marked by the identification of the uracil-DNA glycosylase (UNG) by Tomas Lindahl (1974). Lindahl set out to discover the enzyme responsible for deaminating cytosine and instead identified the enzyme which cleaved the N-glycosidic bond between uracil and the deoxyribose sugar, thus generating an AP site. Furthermore, Lindahl suggested that this site was further processed by exonuclease, DNA polymerase and DNA ligase activity, resulting in the removal and repair of DNA damage

(Lindahl, 1990). His further discoveries and propositions provided the foundations for the current understanding of BER (Krokan and Bjørås, 2013).

BER functions to remove and replace chemically modified, non-helix distorting nitrogenous bases in a series of sequential steps, conducted through the recruitment of the DNA glycosylase, AP-endonuclease, DNA polymerase and DNA ligase enzymes (Liu *et al.*, 2013a; Krokan and Bjørås, 2013).

Base excision repair occurs in both the nucleus and the mitochondria, recruiting genetically distant isoforms of proteins (Mandal *et al.*, 2011; Prakash and Doublé, 2015). The first step of BER is facilitated by DNA glycosylases, which cleave the N-glycosidic bond, through hydrolysis, between the damaged nucleotide base and the deoxyribose sugar. Hydrolysis conducted by a monofunctional DNA glycosylase forms an AP site which is further processed by APE1, Pol  $\beta$  and the XRCC1-Ligase III complex. In general, DNA glycosylases are independently active upon DNA substrates, allowing activity *in vitro* and *in vivo* to be studied (Krokan and Bjørås, 2013; Wallace, 2014).

### 1.9.1. Short-patch BER.

In short-patch BER, a mono-functional DNA glycosylase catalyses the hydrolysis of the N-glycosidic bond producing an AP site, which may be processed by the apurinic/aprimidinic endonuclease I (APE1), cleaving the phosphodiester backbone resulting in a 5'-deoxyribose phosphate (5'-dRP) moiety and a 3' hydroxyl (3'-OH) moiety (Balakrishnan and Bambara, 2013). A bifunctional DNA glycosylase may cleave the phosphodiester backbone in addition to DNA glycosylase activity through associated AP lyase activity. This lyase activity may proceed via  $\beta$ -elimination or  $\beta,\delta$ -elimination.  $\beta$ -elimination of the phosphodiester backbone generates a 3'-phosphor- $\alpha$ ,  $\beta$ -unsaturated aldehyde (PA) and a 5'-phosphate (P). The 3' end at the site of the ss-nick produced after  $\beta$ -elimination is then processed by the 3'-phosphodiesterase activity of APE1 to yield a 3'-OH (Hegde *et al.*, 2008). A bifunctional enzyme with associated AP-lyase activity that conducts  $\beta,\delta$ -elimination of the phosphodiester backbone generates a 3'-P and a 5'-P. However, the 3' end generated by  $\beta,\delta$ -elimination requires the 3'-phosphatase activity of poly-nucleotide kinase (PNKP) to generate a 3'-OH (Hegde *et al.*, 2008; Kim and Wilson, 2012). The 5'-dRP, generated by APE1 cleavage of an AP site subsequently employs the associated lyase activity of Pol  $\beta$  to eliminate the sugar to

generate a 5'-P (Balakrishnan and Bambara, 2013). Pol  $\beta$  may then conduct gap filling synthesis through DNA polymerase activity, inserting the missing nucleotide between the 3'-OH and the 5'-P. The nick is subsequently sealed by DNA ligase III in complex with the scaffold protein XRCC1 restoring the DNA duplex and preventing potential mutagenesis associated with DNA base modification (**Figure 1.11**; Wallace *et al.*, 2012).

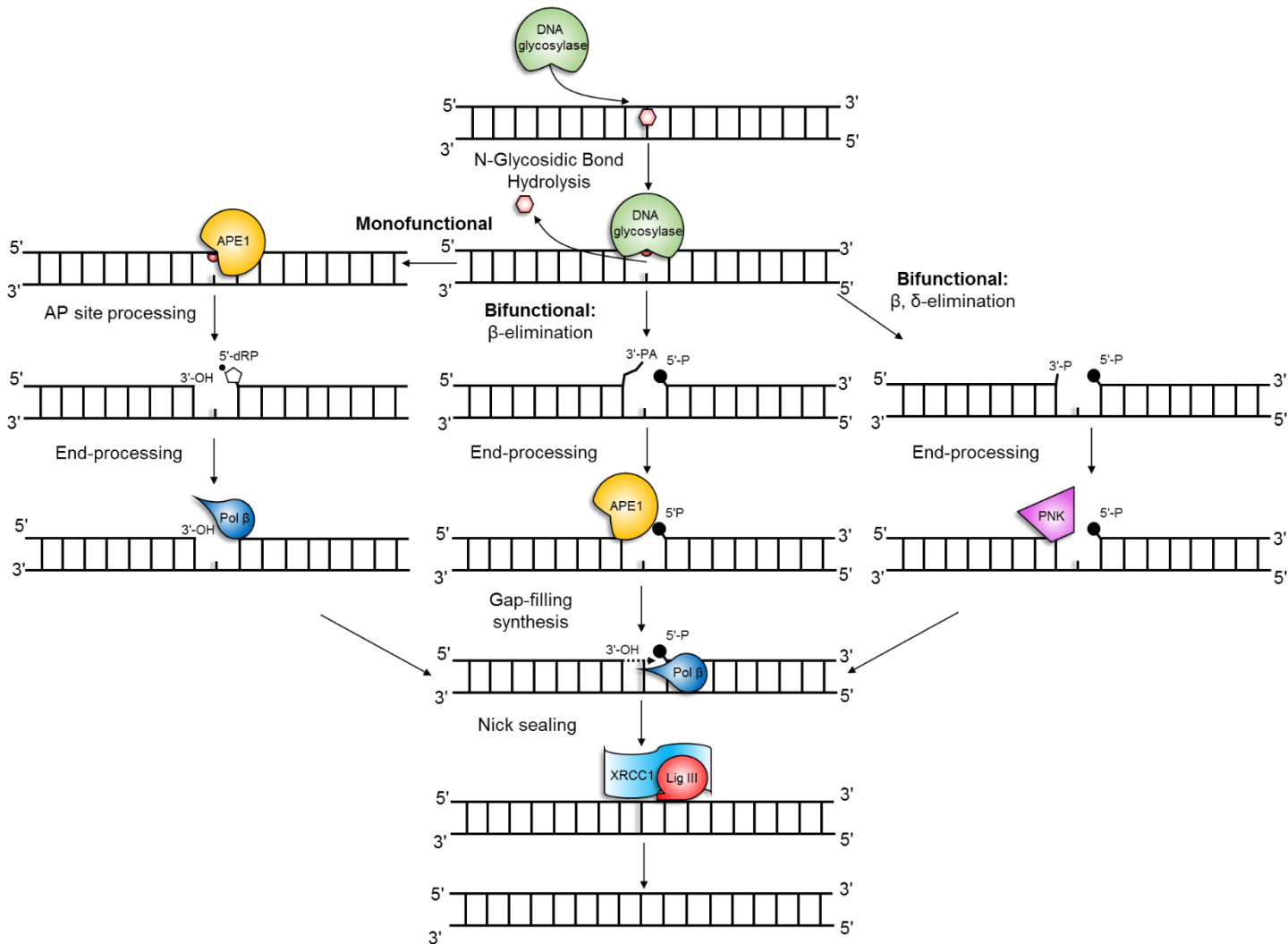


**Figure 1.11: Schematic representation of the short-patch BER pathway.** N-glycosidic bond is hydrolysed by DNA glycosylase activity generating an AP-site. The phosphodiester backbone is then processed through APE1 cleavage of an AP site or associated lyase activity of the DNA glycosylase, to generate a ss-nick. End processing by APE1 or PNKP for then proceeds yielding a 3'-OH group. Pol  $\beta$  may remove the 5'-dRP yielding a 5'-Phosphate group (P), Pol  $\beta$  then conducts gap filling synthesis. The ss-nick is then sealed by (Lig III) in complex with scaffold protein XRCC1.

### 1.9.2. Long-patch BER.

Long-patch BER is a sub-pathway of BER and is suggested to be activated when a cleaved AP site is further oxidised or reduced to generate a 5'-blocking lesion, suggested to be refractory to the lyase activity of pol  $\beta$  (Wallace *et al.*, 2012). Thus, gap filling proceeds through the DNA polymerase activity of pol  $\delta$  or  $\epsilon$  which continues to synthesise new DNA, between 2 and 6 nucleotides, thus shifting DNA downstream of the damage site in a process called strand displacement (Kim and Wilson 2012; Balakrishnan and Bambara, 2013). This results in a flap DNA structure which is a substrate for removal by the flap endonuclease 1 (FEN1), which is stimulated by PCNA creating a nick which is sealed by DNA ligase I restoring the DNA duplex (**Figure 1.12**; Kim and Wilson, 2012; Wallace, 2014).

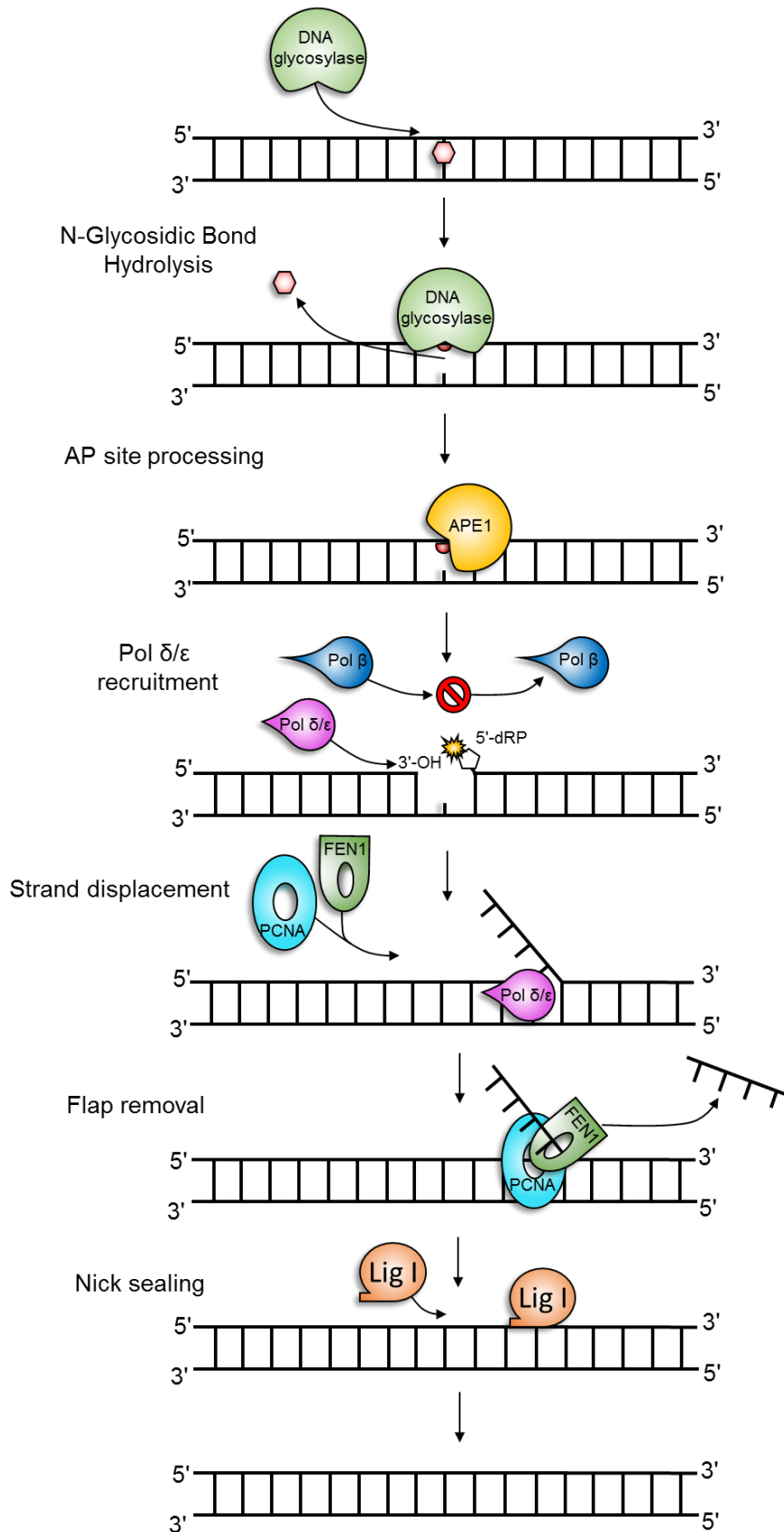


**Figure 1.12: Schematic representation for long-patch BER pathway.** 5'-dRP becomes modified after APE1 cleavage, preventing removal by Pol  $\beta$ . As result specialised DNA polymerases  $\delta$  or  $\epsilon$  undertake strand displacement, replacing >1 nucleotide generating a flap structure, a substrate for FEN1. The flap is excised, and the ss-DNA nick is sealed by Lig I and restores the duplex.

### 1.10. DNA glycosylases.

To date, eleven distinct DNA glycosylases have been described in *Homo sapiens*: UDG, single-strand-selective monofunctional Uracil-DNA Glycosylase 1 (SMUG1), TDG, methyl-CpG Binding Domain 4, DNA Glycosylase (MBD4), AAG, OGG1, MUTYH, NTH1, NEIL1, NEIL2 and NEIL3 (Krokan and Bjørås, 2013; Wallace, 2014). In general, these proteins locate and remove chemically modified DNA bases through hydrolysis of the N-glycosidic bond and initiate BER (**Table 1.2**; Krokan and Bjørås, 2013).

In mammals, four DNA glycosylases are responsible for the removal of mispaired thymine and uracil, six are involved in the removal of oxidative base damage and one for the removal of certain alkylated bases and lipid peroxidation derived ethenoadducts (**Table 1.2**; Krokan and Bjørås, 2013 Wallace 2014). The DNA glycosylases are divided into four structural groups the UNG sub-family (UNG, SMUG1 and TDG), the Helix-hairpin-Helix structural family (HhH; OGG1, NTH1, adenine DNA glycosylase homolog (MUTYH) and methyl-CpG Binding Domain 4, DNA Glycosylase/Mediator Complex Subunit 1 (MBD4)), the Helix-two-Turn-Helix structural family (H2tH; NEIL1, NEIL2 and NEIL3) and a unique structural family containing AAG (Wallace, 2014).

**Table 1.2: The Mammalian DNA glycosylases, their cellular location and their enzyme functionality.** Monofunctional DNA glycosylases demonstrate DNA glycosylase activity only producing an AP-site. Bifunctional DNA glycosylases possess DNA glycosylase activity and an associated lyase which conducts  $\beta$ -elimination or  $\beta,\delta$ -elimination of an AP-site. DNA glycosylases listed as Monofunctional/Bifunctional display bifunctionality in a substrate specific manner. (Adapted from Krokan and Bjørås (2013)).

Enzyme	Subcellular localisation	Monofunctional or Bifunctional DNA glycosylase
UNG2	Nucleus	Monofunctional
UNG1	Mitochondria	Monofunctional
SMUG1	Nucleus	Monofunctional
TDG	Nucleus	Monofunctional
MBD4/MED1	Nucleus	Monofunctional
AAG	Nucleus	Monofunctional
OGG1	Nucleus	Monofunctional/ Bifunctional
MUTYH	Nucleus	Monofunctional
NTH1	Nucleus/Mitochondria	Bifunctional
NEIL1	Nucleus	Bifunctional
NEIL2	Nucleus	Bifunctional
NEIL3	Nucleus	Monofunctional/ Bifunctional

### 1.11. Prokaryotic DNA glycosylases.

BER is a highly conserved DNA repair pathway, present in prokaryotic and eukaryotic organisms (Wallace *et al.*, 2012; Krokan and Bjørås, 2013). Distinct DNA glycosylases have been identified and subsequently characterised from prokaryotic organisms (Prakash *et al.*, 2012). The homology shared between prokaryotic and eukaryotic DNA glycosylases has been crucial in driving hypotheses for the characterisation of DNA glycosylases found in higher organisms. An example of this is the homology shared between Fpg, Nei and their human homologs hNEIL1, human endonuclease VIII-like-2 (hNEIL2) and hNEIL3 DNA glycosylases (Figure 1.13). The biochemical characterisation of Fpg and Nei *in vitro* and *in vivo* have provided important insights into the evolutionary conserved function of the NEIL DNA glycosylases in humans.

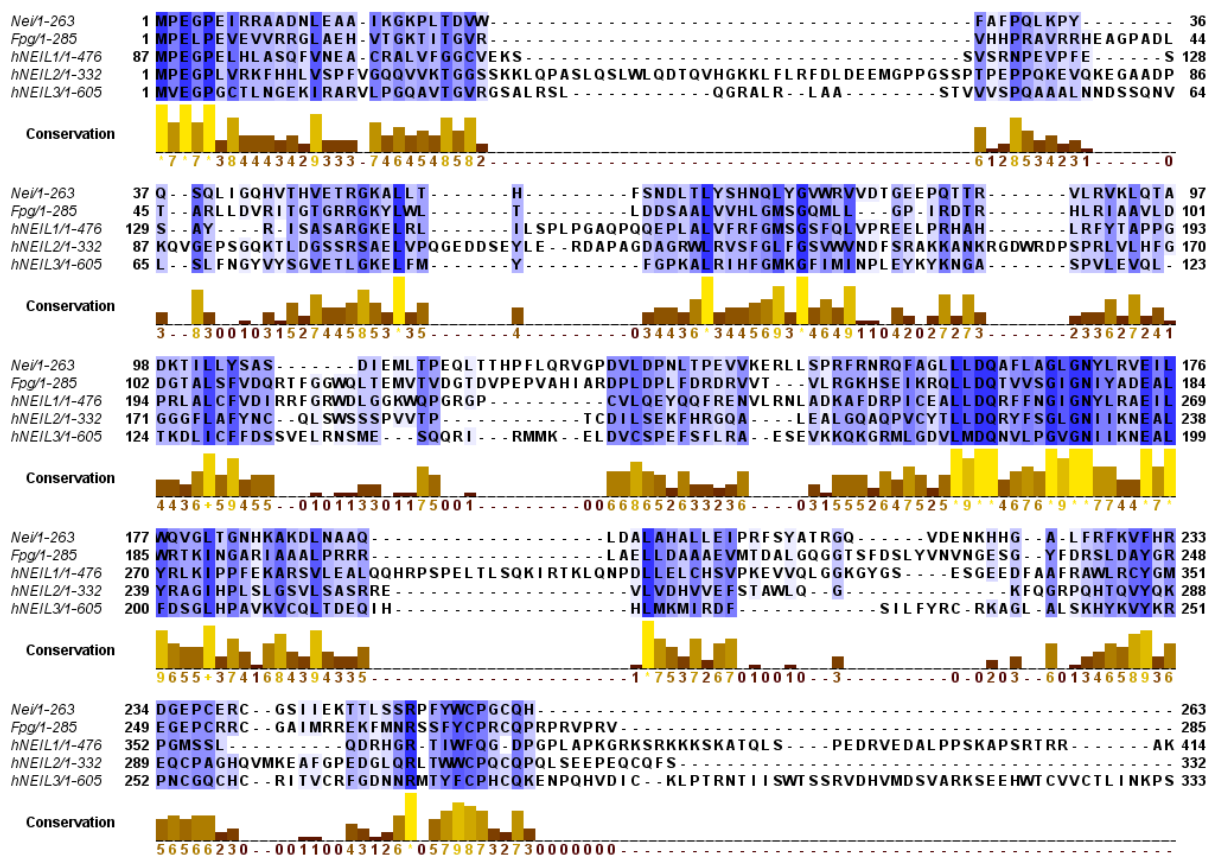


**Figure 1.13: Multiple sequence alignment of the amino acid sequence of *E. coli* Nei, *E. coli* Fpg, hNEIL1, hNEIL2 and hNEIL3.** CLUSTAL O (1.2.4) multiple sequence alignment was used to generate alignment and amino acid sequence conservation was generated with Jalview (2.10.5). Conservation histogram displays the conservation of amino acid domains with a value 0-9 (less conserved to most conserved), where “-” denotes no conservation, “+” denotes conservation of amino acid residue properties and “\*” denotes absolute conservation. Columns displaying no alignment have been removed.

### 1.11.1. Formamidopyrimidine DNA glycosylase (Fpg).

Formamidopyrimidine DNA glycosylase (Fpg) is a 30.2 kDa protein consisting of 269 amino acids in *E. coli*, initially discovered by Tomas Lindahl's laboratory, when studying the removal of methylFapyG from alkylated DNA (Chetsanga and Lindahl, 1979). Fpg is a bifunctional DNA glycosylase, that cleaves on the 3' side of an AP site followed by the 5' side, via  $\beta,\delta$ -elimination (Bhagwat and Gerlt, 1996). Investigation revealed that Fpg was responsible for the excision of 4,6-diamino-5-formamidopyrimidine (FapyA), 2,6-diamino-4-hydroxy-5-formamidopyrimidine (FapyG) and 8-OxoG, determined by gas chromatography-mass spectrometry (GC-MS) analysis of cleavage activity of DNA (Boiteux *et al.*, 1992). However, Fpg was also revealed to process uracil glycol (Ug; Prakash *et al.*, 2012). Determination of protein kinetics revealed similar affinity for FapyA, FapyG and 8-OxoG (Karakaya, *et al.*, 1997). Due to the affinity displayed by Fpg for 8-OxoG and the high frequency of adenine mispairing after DNA replication associated with 8-OxoG, it was suggested that the removal of 8-OxoG was the most biologically relevant substrate for Fpg. Subsequently the 'GO' model was proposed, which suggested that if 8-OxoG is not removed by Fpg and DNA replication proceeds without repair, the complementary bacterial DNA glycosylase, adenine DNA glycosylase (MutY), removes mispaired adenine. Furthermore, 8-dihydroguanine-triphosphatase (MutT) can convert 8-OxoG triphosphates present in the dNTP pool to 8-OxoG monophosphate preventing their incorporation into DNA (Maki and Sekiguchi, 1992; Michaels and Miller, 1992; Michaels, *et al.*, 1992). More recently it was shown that Fpg removes Sp, a further oxidation product of 8-OxoG from ds-DNA with greater processivity than 8-OxoG (Luo *et al.*, 2000; Guo *et al.*, 2010). Fpg was also shown to possess the ability to unhook psoralen ds-MAs and three-stranded ICL structures through DNA glycosylase activity and  $\beta,\delta$ -elimination (Couv -Privat *et al.*, 2007; Couv  *et al.*, 2009).

### 1.11.2. Endonuclease VIII (Nei).

Originally discovered by Wallace's group, the 29.8 kDa endonuclease VIII (Nei) is a DNA glycosylase principally associated with the removal of oxidized pyrimidines from DNA (Prakash *et al.*, 2012). The Nei protein possesses sequence homology with Fpg but is distinct to Nth that also removes oxidized pyrimidines in DNA from prokaryotic cells. Nei has been reported to remove a variety of oxidised pyrimidines, including the replication blocking lesion

Tg, dihydrothymine, Ug, dihydrouracil, 5-OHU and 5-hydroxycytosine (5-OHC) while also cleaving DNA containing an AP-site. Thus, has overlapping substrate specificity with endonuclease III (Nth; Melamede *et al.*, 1994). Indeed, Nei and Nth double mutants are observed to be prone to mutation and are sensitized to ROS induced DNA damage by H<sub>2</sub>O<sub>2</sub> and ionising radiation, while single Nei mutants present no observable phenotype (Jiang *et al.*, 1997a). Nei processes oxidative lesions through DNA glycosylase activity and  $\beta,\delta$ -elimination of the phosphodiester backbone (Jiang *et al.*, 1997b). Interestingly, the double Nth and Nei double mutants display accumulation of only C-T transition. This may suggest that cytosine lesions are the most biologically relevant substrates for Nei, as 5-OHU and Ug mispairs with adenine leading to C-T transitions (Purmal *et al.*, 1998). Furthermore, the addition of a Nei mutation, to an Fpg and MutY double mutant resulted in a three-fold increase in spontaneous mutations that were found to be G-T transversions (Blaisdell *et al.*, 1999). This indicated that Nei serves as a backup for Fpg for the removal of 8-OxoG a lesion that if left unrepaired would lead to adenine mispairing. Subsequently biochemical analysis revealed that at relatively high concentrations Nei could excise 8-OxoG paired with cytosine, adenine or guanine (Hazra *et al.*, 2000). Nei was also shown to possess the ability to unhook psoralen ds-MAs and three-stranded ICL structures through DNA glycosylase activity and associated  $\beta,\delta$ -elimination, to a greater extent than Fpg (Couvé-Privat *et al.*, 2007; Couvé *et al.*, 2009).

## **1.12. Non-Oxidised base eukaryotic DNA glycosylases.**

### **1.12.1. Uracil DNA glycosylases.**

The first of the DNA glycosylases to be discovered was the Uracil DNA glycosylase (UNG), responsible for the cleavage of the N-glycosidic bond of uracil from the misincorporation of deoxyuridine monophosphate (Krokan *et al.*, 1997). Also, cytosine deamination is estimated to generate 100-500 residues of uracil in the mammalian genome every day (Lindahl, 1993). The DNA glycosylase encoded for by the SMUG1 gene has a more invasive structural affinity than other members of the UDG superfamily but has overlapping substrate specificity. SMUG1 cleaves the N-glycosidic bond between the deaminated cytosine product uracil mispaired with guanine bases. The UNG family possess only DNA glycosylase activity and are therefore monofunctional (Krokan & Bjørås, 2015).

### 1.12.2. Thymine DNA glycosylase (TDG) and methyl-CpG-binding domain4, DNA glycosylase (MBD4).

Mismatch specific DNA glycosylases have been identified and characterised. In humans these include TDG and MBD4. Thymine DNA glycosylase can effectively remove thymine mispaired with guanine and can also efficiently remove uracil mispaired with guanine (Krokan *et al.*, 1997). The other human mismatch DNA glycosylase, MBD4, contains domains that remove thymine and uracil mispaired with guanine in hemimethylated and methylated CpG islands. MBD4 has also been shown to play a role in demethylation removing thymine as result of activation-induced cytidine deaminase conversion of 5-methyl-cytosine to uracil, ultimately leading to the misincorporation of thymine (Wallace *et al.*, 2012).

### 1.12.3. Alkyladenine DNA glycosylase (AAG)

Alkyladenine DNA glycosylase is a monofunctional DNA glycosylase with no prokaryotic homologs, which recognises alkylated purines (7meG, 3meA), deaminated adenine (hypoxanthine) and the oxidative lesion 8-OxoG (Bessho *et al.*, 1993; Wallace *et al.*, 2012; Krokan & Bjørås, 2013). Although, 7meG and 3meA are likely to be the primary biological substrates of AAG, 1,N<sup>6</sup>-ethenoadenine, which is a product of the environmental carcinogens ethyl carbamate and vinyl chloride, is processed with a greater efficiency than 3meA by AAG (Saparbaev *et al.*, 1995; Hang *et al.*, 1997). AAG is structurally unique and possesses a positive DNA binding groove within a single domain (Prakash & Doublé, 2015).

Over expression of AAG has been shown to result in the accumulation of AP sites that are a substrate for APE1 (Wallace *et al.*, 2012). However, AAG<sup>-/-</sup> mice accumulate 7meG when treated with the alkylating agent N-methyl-N-nitrosourea (Smith and Engelward, 2000). In addition, a significant increase in AT-TA and GC-TA mutations at the hypoxanthine guanine phosphoribosyl transferase gene, is observed post methyl-methanesulfonate (MMS) treatment in splenic T lymphocytes (Elder *et al.*, 1998). It was suggested that this increase in mutagenesis was due to the persistence of 3meA and 3 or 7meG induced mispairing in the absence of AAG (Elder *et al.*, 1998). Furthermore, previous investigation determined AAG<sup>-/-</sup> embryonic fibroblasts display sensitivity to MMC and 1,3-bis(2-chloroethyl)-1-nitrosourea (BCNU) with additional study identifying AAG<sup>-/-</sup> MEFs were also sensitive to MeOSO<sub>2</sub>(CH<sub>2</sub>)<sub>2</sub>-lexitropsin an agent that induces 3MeA and 1, N<sup>6</sup>-ethenoadenine lesions (Engelward *et al.*,

1996; Engelward *et al.*, 1997). As result AAG is highlighted as the only DNA glycosylase responsible for the excision of alkylated DNA (Krokan and Bjørås, 2013).

However, AAG<sup>-/-</sup> MEFs display residual 3meA repair capabilities, indicating that additional methods of DNA repair for 3meA exist within the cell (Smith and Engelward, 2000). Additionally, it was revealed that no significant displayed phenotype was observed in AAG<sup>-/-</sup> mice, which remained fertile and their MEF cells displayed similar response to treatment when compared to wild type (WT) cells in response to BCNU, mitozolamide and TMZ. However, in support of previous studies sensitivity was observed in response to MMC and was proposed to be a result of the lack of 3meA repair (Elder *et al.*, 1998). This may suggest that alternate DNA repair mechanisms act as a backup to AAG.

Nonetheless, the balance of AAG in mouse cells has been demonstrated to be important (Fu *et al.*, 2012). It was revealed that, AAG<sup>-/-</sup> whole mice display no change in sensitivity, are resistant to retinal degeneration, resistant to cerebellar degeneration, display resistant bone marrow cells, have increased mutagenesis in the spleen and are more likely to develop colon tumours in response to alkylating agents. Interestingly, transgenic AAG whole mice are sensitive, have increased cellular sensitivity in brain, spleen, thymus, pancreas and bone marrow cells while displaying increased retinal degeneration in response to alkylating agents (Fu *et al.*, 2012).

It is proposed that AAG overexpression leads to an increase in the accumulation of AP sites, which in turn are vulnerable to SSB formation and cellular apoptosis. This is demonstrated by alkylating agent treatment of AAG<sup>-/-</sup> mice cells displaying resistance and AAG<sup>Tgen</sup> mice cells are hypersensitive to MMS treatment (Meira *et al.*, 2009; Margulies *et al.*, 2017).

Interestingly, AAG has also been shown to confer cellular resistance to the class of ICL inducing agents, psoralen (Maor-Shoshani *et al.*, 2008). It was revealed that AAG<sup>-/-</sup> mouse embryonic stem cells displayed increased sensitivity to HMT/UVA treatment than that observed in response to MMS treatment when compared to WT cells, in addition displaying increased  $\gamma$ -H2AX foci, a marker of DSB induction. Furthermore, it was demonstrated that AAG<sup>-/-</sup> mouse embryonic stem cells were also sensitised to the ICL inducing agents MMC and BCNU. However, AAG failed to bind and cleave MMC ICLs, monoadducts produced by 8-MOP, HMT or N2-guanine monoadduct *in vitro* (Maor-Shoshani *et al.*, 2008). Subsequently it has

been proposed that AAG may have non-canonical roles in the repair of ICLs produced by bifunctional alkylating agents such as BCNU and nitrogen mustards (Yang *et al.*, 2017).

### **1.13. Oxidised base DNA glycosylases.**

In eukaryotic organisms the DNA glycosylases OGG1, MUTYH, NTH1, NEIL1, 2 and 3 are responsible for initiating BER in response to oxidative DNA damage. They are highlighted as of particular importance due to the high frequency of oxidative lesions formed in the cell (Klaunig *et al.*, 2011; Krokan and Bjørås, 2013).

#### **1.13.1. 8-Oxoguanine DNA glycosylase (OGG1).**

Guanine has the lowest redox potential of the four nitrogenous DNA bases and is frequently oxidised to 8-OxoG, leading to GC-TA transversions, due to the formation of 8-OxoG:A mispairs during DNA replication (Wallace *et al.*, 2012). In prokaryotes both Fpg and MutY act to reduce transversion mutations, in eukaryotic cells OGG1 removes 8-OxoG and MUTYH removes mispaired adenine (Boiteux and Radicella, 2000). OGG1 is a member of the Helix-hairpin-helix motif (HhH) structural family of bifunctional DNA glycosylases, possessing  $\beta$ -elimination AP-lyase activity (Lu *et al.*, 1997; Wallace *et al.*, 2012). OGG1 has also been successfully characterised and crystallised bound to the 8-OxoG lesion (Wallace *et al.*, 2012). Additionally, the amino acid mutation of serine to cysteine at amino acid position 326 of OGG1 is observed in approximately 32% of humans, predisposing them to lung, nasopharyngeal, oesophageal, prostate and oropharyngeal cancer (Weiss *et al.*, 2005; Wallace *et al.*, 2012).

#### **1.13.2. MutY DNA glycosylase (MUTYH).**

The mono-functional DNA glycosylase, MUTYH, is a 60 kDa protein and is a homolog of the bacterial MutY protein. MUTYH removes mispaired adenines base paired to 8-OxoG, 5-OHU, 2-Hydroxyadenine and FapyG (Markkanen *et al.*, 2013; Wallace, 2014). Mutations within the MUTYH protein have been associated with the colorectal cancer syndrome MUTYH-associated polyposis (MAP; Cheadle and Sampson, 2007; Palles *et al.*, 2013). This may be in part due to the protective role in which MUTYH plays in the repair of mispaired adenine with

the 8-OxoG lesion. It was shown that MUTYH RNAi sensitised HeLa cells to H<sub>2</sub>O<sub>2</sub>, affected the cell morphology, increased the 8-OxoG foci, altered cell cycle progression and reduced cell cycle signalling by phosphorylation of Chk1 (Hwang *et al.*, 2014). In contrast overexpression of MUTYH in mismatch repair deficient human Dukes' type C, colorectal adenocarcinoma (HCT15) cells resulted in resistance to H<sub>2</sub>O<sub>2</sub> induced apoptosis and an increase in phosphorylated Chk1 levels. Taken together MUTYH deficiency may lead to an increase in mutagenesis associated with 8-OxoG and also disruption of cell cycle signalling through phosphorylation of Chk1 (Hwang *et al.*, 2014)

### 1.13.3. Nth-like DNA glycosylase 1 (NTH1).

Nth-like DNA glycosylase 1 (NTH1) is a mammalian HhH DNA glycosylase, a homolog of the bacterial Nth protein and is constitutively expressed throughout the cell cycle (Ikeda *et al.*, 1998; Galick *et al.*, 2013). NTH1 is a bifunctional DNA glycosylase, with associated  $\beta$ -elimination AP-lyase activity and is found in both the nucleus and mitochondria of the cell (Ikeda *et al.*, 1998; Galick *et al.*, 2013). NTH1 has been shown to excise the oxidised bases 5-hydroxycytosine (5-OHC), 5-hydroxyuracil (5-OHU), Tg and 5-formamidopyrimidine (Fapy) (Ikeda *et al.*, 1998; Prakash and Doubl  , 2015). It has been shown that NTH1 has overlapping substrate specificity with NEIL1, NEIL2 and NEIL3 releasing open ring purines and oxidised pyrimidines (Krokeide *et al.*, 2013; Krokan and Bj  r  s, 2013). NTH1 knockout mice displayed no observable phenotype. However, mice with a double-knockout of NTH1 and NEIL1 were predisposed to lung and liver tumours (Krokan and Bj  r  s, 2013; Kuiper and Hoogerbrugge, 2015). Recently, steady state levels of the NTH1 protein in human colorectal carcinoma epithelial cells (HCT116) and U2OS cells were shown to be regulated by the UPS through the E3 ubiquitin ligase tripartite motif containing protein 26 (TRIM26), previously shown to regulate hNEIL1. Downregulation of TRIM26 by RNAi increased cellular resistance to H<sub>2</sub>O<sub>2</sub> as did transient overexpression of the NTH1 protein (Williams and Parsons, 2018).

#### 1.13.4. Endonuclease VIII-like 1 (NEIL1).

The NEIL1 DNA glycosylase is a 44 kDa, bifunctional DNA glycosylase conducting  $\beta,\delta$ -elimination of the phosphodiester backbone and part of the Helix-two-turn-helix domain (H2TH) structural family. The activity of NEIL1 is highest during DNA replication, based upon observed interactions with DNA replication proteins and higher expression during the S-phase of the cell cycle (Hazra *et al.*, 2002a; Hazra and Mitra, 2006; Hegde *et al.*, 2013). NEIL1 is a functional hybrid of the bacterial homologs Fpg and Nei, but a closer nucleotide sequence match with Nei, than Fpg (**Figure 1.14**; Hazra *et al.*, 2002b; Hazra and Mitra, 2006).

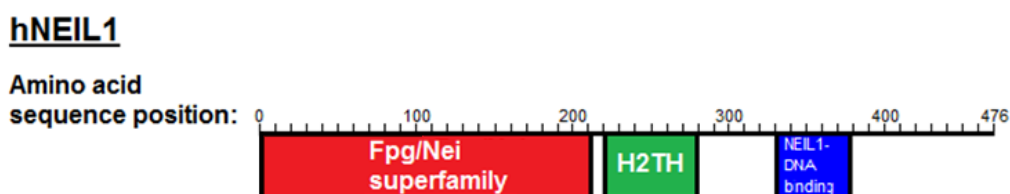


**Figure 1.14: Conserved domain analysis of the human endonuclease VIII like 1 (hNEIL1) DNA glycosylase.** Fpg/Nei superfamily domain, helix-two-turn helix (H2TH) domain and the NEIL1 DNA binding domain.

Substrates for NEIL1 include the oxidised pyrimidines 5-OHU and Tg but it is also active on meFapyG but shows highest activity on Sp and Gh DNA lesions (Bandaru *et al.*, 2002; Hazra *et al.*, 2002a Dou *et al.*, 2003; Krishnamurthy *et al.*, 2008; Rosenquist *et al.*, 2003; Krokeide *et al.*, 2013). NEIL1 recognises ss-DNA, ds-DNA and bubble structured DNA, unlike OGG1 and NTH1, which require double-stranded DNA substrates (Dou *et al.*, 2003; Hazra and Mitra, 2006). Furthermore, hNEIL1 can excise Gh and Sp in G-quadruplex structures and displays a preference for Gh in a telomeric sequence context. G-quadruplex structures may form in guanine rich telomeric TTAGGG<sub>n</sub> repeat sequences and are generated when four guanines are Hoogsteen base paired, which form layers sandwiching a monovalent cation such as K<sup>+</sup> or Na<sup>+</sup> (Williamson, *et al.*, 1989; Smith and Feigon, 1992; Zhou *et al.*, 2013).

Evidence suggests that NEIL1 has a putative associated role within the maintenance of DNA replication and was recently enriched on nascent DNA by immunoprecipitation on nascent DNA (IPOND) in the absence of oxidative stress and was suggested to be indicative of a post-replicative repair function (Bjørås *et al.*, 2017). However, Das *et al.* (2007) provided the

foundations for an emerging model of function of the NEIL1 DNA glycosylase in association with DNA replication. Their experiments demonstrated that the Werner syndrome RecQ helicase (WRN), a helicase associated with DNA replication fork remodelling and promotion of DNA end joining in response to cisplatin treatment, stimulated NEIL1 DNA glycosylase activity in the presence of a 5-OHU lesion substrate. Interestingly, WRN deficient cells accumulate 8-OxoG, FapyG and Fapy A lesions. In addition, this interaction was enhanced with observed colocalisation of NEIL1 and WRN in the nucleus of HCT116 cells after oxidative stress, induced by glucose oxidase treatment (Das *et al.*, 2007). It was subsequently shown that the WRN helicase was the only ATP-dependent DNA helicase (RecQ) that stimulated NEIL1 activity (Popuri *et al.*, 2010). Further investigation of NEIL1 demonstrated direct interaction with RPA and PCNA that inhibited activity in an open DNA replication primer template structure (Theriot *et al.*, 2010). However, RPA was shown to moderately stimulate NEIL1 excision activity in duplex DNA when compared to an RPA interacting domain (aa 312-349) mutant. The inhibition of activity was then demonstrated to be relieved in the presence of PCNA in ds-DNA context. Taken together this interaction with RPA and PCNA displayed modulation of NEIL1 activity at a DNA replication fork (Theriot *et al.*, 2010).

More recently the function of hNEIL1 at the DNA replication fork was elaborated by Hegde *et al.* (2013), who showed using a ss-RPA coated template DNA containing a 5-OHU DNA lesion, that DNA synthesis by Pol  $\delta$  was significantly enhanced by the addition of PCNA but could not proceed past the lesion in the presence of hNEIL1. Furthermore, a lack of excision activity was observed in ss-DNA, thus avoiding replication associated DSB induction. It was subsequently proposed that hNEIL1 acts as a DNA replication machinery 'cowcatcher', in a prereplicative manner, preventing DNA replication fork progression when an oxidised base is encountered. Then the promotion of DNA replication fork regression and chicken foot structure formation, presumably by WRN or other helicases may take place. The subsequent oxidised base, now remodelled into a ds-DNA context, is then processed by NEIL1 and short-patch BER (Hegde *et al.*, 2013). Finally, Hegde *et al.* (2015) demonstrated that hNEIL1 was present in multiprotein complexes, containing replication associated proteins, which could conduct efficient BER *in vitro*. The C-terminal domain of hNEIL1 was shown to interact with the PCNA associated replication clamp loader RFC, DNA polymerase  $\delta$  and DNA ligase I. It was also revealed that this RFC interaction stimulated hNEIL1 activity  $\sim 8$  fold in the presence of 5-OHU in DNA. These

interactions were inhibited in a hNEIL1 N311 deletion mutant lacking the C-terminal domain (Hegde *et al.*, 2015). It has also been shown that the replication associated function of hNEIL1 may affect cellular sensitivity to oxidation; this was demonstrated by generation of mNEIL1 short hairpin ribonucleic acid interference (shRNAi) knockdown MEF cells, which displayed a significant increase in sensitivity to H<sub>2</sub>O<sub>2</sub> during the S-phase of the cell cycle (Yamamoto *et al.*, 2014). These experiments provide biochemical and cellular evidence that NEIL1 is a replication associated DNA glycosylase and is active under replicative stress conditions.

NEIL1 was the first human DNA glycosylase shown to play an active role in the resolution of psoralen MAs in duplex DNA and ICLs in a three-stranded context (Couvé-Privat *et al.*, 2007; Couvé *et al.*, 2009). Furthermore, sensitivity to the ICL inducing agent 8-MOP and UVA on knockout of hNEIL1 and APE1 in HeLa cells was demonstrated (Couvé-Privat *et al.*, 2007; Couvé *et al.*, 2009). Subsequent investigation by Macé-Aimé *et al.* (2010) revealed that FANCA and FANCC deficient cell lines displayed resistance to the ICL inducing agent MMC and 8-MOP when hNEIL1-FLAG was transiently overexpressed and that expression levels of NEIL1 were associated with an intact FA repair pathway. For the first time it was proposed that ICL sensitivity displayed by FA deficient cell lines may be associated with NEIL1 and BER (Macé-Aimé *et al.*, 2010).

The investigation of NEIL1 PTM, identified novel ubiquitination activity and regulation of steady state levels by the E3-ubiquitin ligases TRIM26 and Mcl-1 ubiquitin ligase E3 (MULE), a known interactor of p53 (Lee and Gu, 2010; Dorn *et al.*, 2014; Edmonds *et al.*, 2017). MULE has previously been shown to ubiquitinate topoisomerase 2-binding protein 1 (TopBP1) an activator of ATR kinase and the DNA RSR (Herold *et al.*, 2008) Furthermore, loss of MULE has been shown to increase phosphorylated ATM and p53 in MEFs (Hao *et al.*, 2012). NEIL1 protein was also demonstrated to be induced in response to IR in a MULE-dependent manner, while resistance to IR was displayed on knockdown of TRIM26, determining the regulation of NEIL1 by PTMs (Edmonds *et al.*, 2017).

Current lines of evidence provide insight into the possible roles in which NEIL1 may play in association with the DNA replication fork machinery. It would be tempting to speculate that

NEIL1 recognises DNA lesions at the DNA replication fork in a structure specific manner, recruited as part of the DNA replication stress response.

#### 1.13.5. Endonuclease VIII-like 2 (NEIL2)

The second member of the H2TH family in mammalian cells is NEIL2. NEIL2 has a molecular weight of 37 kDa, possesses the H2TH domain and is bifunctional conducting  $\beta,\delta$ -elimination. NEIL2 has also been proposed to possess a single C-terminal zinc finger domain (**Figure 1.15**: Das *et al.*, 2004; Hazra and Mitra, 2006). Expression, purification and biochemical characterisation of NEIL2 determined it is active upon oxidised pyrimidines in the presence of poly nucleotide kinase phosphatase (PNKP) and NEIL2 cleaves 5-hydroxyuracil in ss, ds or bubble structured DNA (Dou *et al.*, 2003; Hazra and Mitra, 2006). Aged mice depleted of NEIL2 were found to accumulate oxidised bases in transcribed regions of DNA suggesting a role in transcription coupled repair (Chakraborty *et al.*, 2015). NEIL2 is located in the nucleus and the mitochondria and displays activity on 5-OHU, with weak activity upon 5-OHC and Tg lesions (Hazra *et al.*, 2002; Mandal *et al.*, 2011). Additionally, NEIL2 has been shown to be associated with RNA DNA polymerase II, which taken together with structural affinity for oxidative lesions within a bubble structure and a constitutive expression profile, infer a role within transcription coupled BER (Hazra and Mitra, 2006; Wallace, 2014). It has also been shown that NEIL2 is regulated through PTMs, with acetylation leading to NEIL2 inactivation (Bhakat *et al.*, 2004). NEIL2 was also shown to play a role in protection against carcinogens in second-hand smoke, with significant accumulation of mutagenic oxidative lesions on its depletion in human pulmonary fibroblasts (hPF) and human embryonic kidney epithelial cells (HEK 293) cancer cells (Sarker *et al.*, 2014).

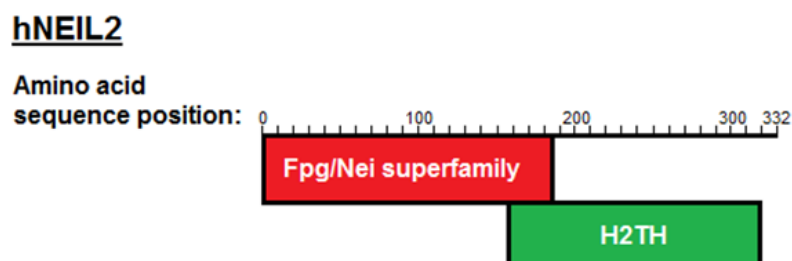


**Figure 1.15: Conserved domain analysis of the human endonuclease VIII like 2 (hNEIL2) DNA glycosylase.** Fpg/Nei superfamily domain and helix-two-turn helix (H2TH) domain.

### 1.13.6. Endonuclease VIII-like 3 (NEIL3).

The NEIL3 DNA glycosylase is the third mammalian homolog of the Nei/Fpg family of bacterial DNA glycosylases and the NEIL3 gene is found at the chromosomal locus 4q34.3 of the human genome, encoding the 67.8 kDa protein NEIL3 (Hillier *et al.*, 2005; Uniprot, 2010). NEIL3 has been shown to be an active DNA glycosylase with a somewhat overlapping substrate specificity to that of NEIL1 (Takao *et al.*, 2009; Wallace *et al.*, 2012).

NEIL3 has an organ specific expression pattern and is found in the brain, the thymus, spleen, bone marrow and testes in mice (Morland *et al.*, 2002; Torisu *et al.*, 2005; Hildrestrand *et al.*, 2009). The protein has been shown to be overexpressed in 13 types of cancer with a positive correlation with somatic mutation load (Kauffmann *et al.*, 2008; Shinmura *et al.*, 2016; de Sousa *et al.*, 2017). However, despite this correlation, triple knockout NEIL1, NEIL2 and NEIL3 mice displayed no increase in the accumulation of spontaneous mutations under normal physiological conditions (Rolseth *et al.*, 2017). It was shown through cell cycle analysis that hNEIL3 expression, at a transcriptional level and protein level, was cell cycle regulated in proliferating cells and induced in early S-phase through to G2/M phase (Neurauter *et al.*, 2012; Zhou *et al.*, 2015; Zhou *et al.*, 2017). More recently it was shown in synchronised HeLa cells that NEIL3 expression peaks 6 hours post release from S-phase (Zhou *et al.*, 2017).

NEIL3 has been shown to have multiple biological protective roles, with aged NEIL3 knockout mice observed to have reduced white blood cell counts, memory deficits, anxious behaviour, reduced neurogenesis, impairment in hippocampal synapses, increased decline in the neuronal nuclei (a marker for mature neurones) and a significantly reduced clinical-phase in a prion disease model (Torisu *et al.*, 2005; Regnell *et al.*, 2012; Jalland *et al.*, 2016). In addition, it has been shown that deficiency of NEIL3 in mice resulted in increased apoptosis of B and T cells highlighting potential evidence for the protective role NEIL3 may provide against autoimmune diseases (Massaad *et al.*, 2016). However, this role may be exploited by human immune deficiency virus (HIV), with RNAi knockdown of hNEIL3 observed to reduce HIV infection, which was rescued with expression of hNEIL3. It was suggested that hNEIL3 plays a role during viral replication or host genome integration (Zhou *et al.*, 2008).

Human NEIL3 possesses a DNA glycosylase domain (1-151 aa), a H2TH domain (61-281 aa), a zf-RanBP domain (317-345 aa) and two zf-GRF domains (505-550 and 552- 596 aa; **Figure 1.16**; Liu *et al.*, 2013a). The conserved N-terminal domain of hNEIL3 has been revealed to facilitate DNA glycosylase activity on a number of oxidised bases in ss-DNA and ds-DNA, with an increase in activity on ss substrates. However, inability to express and purify the full amino acid sequence of hNEIL3 as an active protein has prevented the full biochemical characterisation of hNEIL3 (Krokeide *et al.*, 2009; Liu *et al.*, 2010; Liu *et al.*, 2012; Liu *et al.*, 2013; Krokeide *et al.*, 2013). DNA glycosylase activity has been demonstrated by the glycosylase domain of hNEIL3 with additional weak  $\beta$ -elimination of an AP site containing substrate. However, the highest levels of activity have been observed on Sp and Gh DNA lesion substrates and moderate activity on 5-OHU containing substrates, especially in a ss-DNA context (Takao *et al.*, 2009; Krokeide *et al.*, 2013; Liu *et al.*, 2013a, 2013b). The glycosylase and AP-lyase activities were suggested to be undertaken in a non-concerted manner, with the amino acid mutation of position 2 from valine to proline restoring a concerted bifunctional activity profile. Consequently, it was suggested that in the presence of APE1 in the cell, NEIL3 would be a mainly monofunctional DNA glycosylase (Krokeide *et al.*, 2013). Study of the mouse ortholog of hNEIL3 (mNEIL3) and truncated glycosylase domain hNEIL3 by Liu *et al.*, (2012), revealed activity on Tg, Sp, Gh and AP site in oligonucleotide substrates. It was consistently observed that activity was increased on ss-DNA substrates compared with ds-DNA (Liu *et al.*, 2010; Liu *et al.*, 2012; Liu *et al.*, 2013a, 2013b). Structural characterisation of the glycosylase domain of mNEIL3 provided further evidence for a single-strand affinity, with a lack of a loop that stabilises everted DNA bases and lack of two of the three void-filling residues possessed by NEIL1, that are suggested to stabilise the opposite DNA strand. Also, the possession of an electrostatic environment uncomplimentary to the phosphate backbone of the undamaged strand in duplex DNA, suggested a preference for ss-DNA substrates (Liu *et al.*, 2013b).

## hNEIL3

Amino acid  
sequence position:

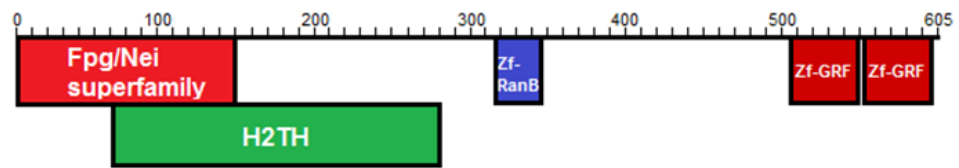


**Figure 1.16: Conserved domain analysis of the human endonuclease VIII like 3 (hNEIL3) DNA glycosylase.** Fpg/Nei superfamily domain, helix-two-turn helix (H2TH) domain, zinc finger RanB domain and zinc finger-GRF domain (Zf-GRF).

Wallace's group have made significant advances in the elucidation of the biochemical role of the hNEIL3 DNA glycosylase as previously discussed. More recently they have described a role for NEIL3 in telomeric sequence maintenance, initially showing substrate preference of mNEIL3 on Tg, Sp and Gh lesions when compared to hNEIL2 and NTH1 DNA glycosylases, in a G-quadruplex structure (Zhou *et al.*, 2013). However, as previously mentioned NEIL1 has been shown to remove Sp, Gh lesions in a G-quadruplex, but not Tg, as efficiently as mNEIL3 (Zhou *et al.*, 2013). More recently, the biological implications of these findings have been described (Zhou *et al.*, 2017). These include a significant mitotic defect after hNEIL3 RNAi in HCT116 cells, with telomeric dysfunction and a significant increase in metaphase arrested cells, leading to apoptosis. In addition, a significant increase in cells displayed anaphase bridging, where APE1 and NEIL3 colocalised. It was also shown that NEIL3 colocalises with telomeric repeat-binding factor 2 (TRF2), a shelterin complex protein which protects telomeres from aberrant processing as DNA breaks by the DDR, in U2OS cells (Zhou *et al.*, 2017). It was subsequently proposed that NEIL3 protects genome stability through repair of oxidative damage in telomeres during the S/G2 phase of the cell cycle, due to maximal NEIL3 levels being observed 6h post release from S-phase in HeLa cells (Zhou *et al.*, 2017). Anaphase bridges are associated with genomic instability and are usually found within vulnerable stretches of DNA such as telomeres. It is suggested anaphase bridges may be products of rapid proliferation and indicative of DNA damage tolerance (Bizard and Hickson, 2018). Together these finding may indicate a role of hNEIL3 in the facilitation of rapid proliferation of cancer cells and removal of DNA damage in preventing formation of chromatin bridge structures (Zhou *et al.*, 2017).

NEIL3 has also been implicated in the repair of ICLs. Semlow *et al.* (2016) used an *X. laevis* NEIL3 knockout cell free egg extract model to show NEIL3 can unhook psoralen ss MA, ICLs and AP site ICLs in an X-shaped structure in an incision-independent manner. They proposed

that NEIL3 was responsible for the removal of ICLs in a structure generated as a product of convergent stalled DNA replication forks. It was also shown that psoralen ICLs were repaired by an incision-dependent repair pathway activated by the FA pathway, when incision-independent repair by NEIL3 was abolished. The study established a role of NEIL3 in ICL repair where redundancy by the FA pathway exists (Couvé-Privat *et al.*, 2007; Couvé *et al.*, 2009). Thus, it was proposed that the X-shaped structure, mimicking convergent DNA replication forks, places the ICL in a ss-DNA context for excision by the NEIL3 DNA glycosylase (Semlow *et al.*, 2016).

Some of the most effective chemotherapeutic agents target the DNA molecule to induce ICLs amongst other DNA damage, initiating cellular apoptosis through the DDR (Patrick and Turchi, 1999; Macé-Aimé *et al.*, 2010). hNEIL3 is proposed to be a resistance factor for this type of chemotherapy as cellular sensitivity after RNAi in colorectal cancer cells and NEIL3 knockout MEF cells was observed in response to oxaliplatin and cisplatin, respectively (Rolseth *et al.*, 2013; Taylor *et al.*, 2015). The targeting of pro-survival proteins has been shown to improve the efficacy of cancer therapy, such as the short interfering ribonucleic acid (siRNA) knockdown of ERCC1 and the use of PARP inhibitors in the clinic (Seetharam *et al.*, 2010; O'Connor, 2015). It has been observed that hNEIL3 co-localises with RPA in the nucleus (Morland *et al.*, 2002). RPA has been shown to have *in vitro* activity, denaturing duplex DNA containing cisplatin ICLs, subsequently generating a ss cisplatin ICL substrate (Patrick and Turchi, 1998; 1999). An RPA associated repair model involving the recruitment of the NER machinery was proposed (Patrick and Turchi, 1998; 1999). Taken together this may suggest overlap between NER and BER pathways, as previously shown in the case of ICL remnant resolution (Patrick and Turchi, 1998; 1999, Morland *et al.*, 2002; Couvé-Privat *et al.*, 2007; Couvé *et al.*, 2009). Recently, it has been shown that in highly radio- and chemo-resistant glioblastoma cells, hNEIL3 shRNAi leads to increased DNA replication associated DSBs and sensitises cells to ATR and synergistic ATR/PARP inhibition. NEIL3 depletion also resulted in increased spontaneous replication stress, impaired DSB repair and reduction in chromatin bound PCNA, DNA repair protein RAD51 homolog 1 (RAD51) and Chk1 thus, indicating an associated loss in DSB repair efficiency on the depletion of hNEIL3 (Klattenhoff *et al.*, 2017).

Therefore, current lines of evidence indicate a significant role of hNEIL3 in facilitating successful DNA replication. Furthermore, considerable redundancy is observed between

NEIL1, NEIL2, NEIL3 and NTH1 for the removal of oxidative DNA lesions (Parsons and Elder, 2003; Couvé-Privat *et al.*, 2007; Couvé *et al.*, 2009; Wallace *et al.*, 2012; Krokeide *et al.*, 2013; Rolseth *et al.*, 2017). In mammals, multiple DNA glycosylases are required for the processing of DNA lesions in distinct DNA structures for the maintenance of genomic stability (Wallace *et al.*, 2012). However, triple knockout of the NEIL DNA glycosylases in mice, displayed no increase in spontaneous mutagenesis, accumulation of oxidative DNA damage and telomere length was not affected under normal physiological conditions, perhaps due to defined redundancy between the NEIL and NTH1 DNA glycosylases. It was therefore proposed that the NEIL DNA glycosylases may have roles beyond that of canonical repair through BER (Rolseth *et al.*, 2017). These roles are suggested to be exploited by cancer cells to promote acquired cellular resistance to therapy.

The next step in understanding the role of hNEIL3 in chemotherapeutic resistance, is to probe the biochemical activity of hNEIL3 *in vitro* on DNA replication blocking lesions such as Tg and psoralen ICL oligonucleotide substrates, as a model for the study of ICL resolution (Couvé-Privat *et al.*, 2007; Couvé *et al.*, 2009). Consequently, this should provide a biochemical mechanism for the observed sensitisation to RSR inhibition and ICL inducing agents after NEIL3 knockdown or knockout (Rolseth *et al.*, 2013; Taylor *et al.*, 2015; Klattenhoff *et al.*, 2017). Elucidation of PTM by the UPS may also provide further additional information on the mechanism of modulation in response to DNA damage in cancer cells, in a similar manner to NEIL1 and NTH1 (Edmonds *et al.*, 2017; Williams and Parsons, 2018). Furthermore, the generation of a hNEIL3<sup>-/-</sup> stable cancer cell line using clustered regularly interspaced palindromic repeats (CRISPR)/ CRISPR associated protein 9 (Cas9) gene editing should provide a model system for the further characterisation of the role of NEIL3 in mechanisms of genomic instability and modulation by PTM systems.

Strict cellular control, lack of a mutagenic phenotype on deficiency of NEIL DNA glycosylases under normal physiological conditions, while sensitising cancer cells to therapy, provides a promising motive for the effective therapeutic targeting of the NEIL3 DNA glycosylase, for the treatment of cancers overexpressing NEIL3 (Morland *et al.*, 2002; Torisu *et al.*, 2005; Hildrestrand *et al.*, 2009; Rolseth *et al.*, 2013; Taylor *et al.*, 2015; Klattenhoff *et al.*, 2017; Rolseth *et al.*, 2017; Zhou *et al.*, 2017).

#### 1.14. Ubiquitin proteasome system (UPS).

Post-translational modification by the highly conserved 76 amino acid protein, ubiquitin, is an important regulatory mechanism, typically associated with the identification of target proteins for degradation by the 26S proteasome (Weissman, 2001; Glickman and Ciechanover, 2002). The 26S proteasome, made up of the 19S and 20S complexes, is an approximately 33 protein subunit complex, containing proteolytic sites which hydrolyse polypeptides to generate short peptides ranging from 2 to 10 residues (Inobe and Matouschek, 2014; Collins and Goldberg, 2017). This irreversible degradation of proteins is regulated by controlled access to these proteolytic sites by the N-termini of 20S  $\alpha$ -subunits and C-termini interaction with 19S subunit complexes, allowing access to the inner chamber of the 20S complex (Collins and Goldberg, 2017). Additionally, ubiquitin has several other important roles, including the modulation of DNA damage repair and DNA replication, innate immune signalling and cell surface endocytosis (Mukhopadhyay and Riezman; 2007; Chen and Sun, 2009; Grabbe *et al.*, 2011). It is estimated that in HeLa cells approximately 1.3% of all cellular protein is ubiquitin (Kulak *et al.*, 2014)

In human cells the ubiquitin protein is encoded by four different genes. These are ubiquitin B (UbB), ubiquitin C (UbC), ubiquitin A-52 residue ribosomal protein fusion product 1 (UBA52) and ubiquitin carboxyl extension protein 80 (UBA80). UbB and UbC are processed by DUB family enzymes to generate ubiquitin (Monia *et al.*, 1989). Cellular ubiquitin can be considered in three distinct states, free ubiquitin, activated ubiquitin that is linked by thioester to ubiquitin conjugating enzymes (E2s) and conjugated ubiquitin that is isopeptide bound to target substrate proteins (Clague *et al.*, 2015).

The process of ubiquitination proceeds by adenosine triphosphate (ATP) hydrolysis and the release of pyrophosphate (PPi), in turn generating an ubiquitinyl adenylate intermediate which subsequently binds to an E1 activating enzyme. Then the E1 activating enzyme forms a thioester bond with ubiquitin and adenosine monophosphate (AMP) is released (**Figure 1.17**; Myung *et al.*, 2001; Parsons and Dianov, 2013). Then, the Ub-thioester is passed to a cysteine residue on an E2 conjugating enzyme (Udeshi *et al.*, 2012). Finally, the E2-Ub forms a complex with an E3 ubiquitin ligase and a protein target, this complex facilitates conjugation of ubiquitin to the protein substrate at a specific lysine residue, by formation of an isopeptide

bond between the ubiquitin C-terminal and a NH<sub>2</sub> group (**Figure 1.17**; Parsons *et al.*, 2008; Jackson and Durocher, 2013). This facilitates single ubiquitin monomer addition, termed mono-ubiquitination and is typically associated with cell signalling (Edmonds and Parsons, 2014). Alternatively, successive processing by E2 unloading and reloading of charged E2-Ub to a target protein, forms progressive homotypic or heterotypic poly-ubiquitin chains at one of seven ubiquitin lysine amino acids (Lys6, Lys11, Lys27, Lys29, Lys33, Lys48, Lys63) or less commonly the N-terminal methionine (Ikeda and Dikic, 2008, Ye and Rape, 2009; Jackson and Durocher, 2013; Inode and Matouschek, 2014). Those protein substrates poly-ubiquitinated with homotypic Lys11, Lys29 and Lys48 ubiquitin chains are typically targeted for degradation by the 26S proteasome, where proteins are broken down into free peptides and ubiquitin (**Figure 1.17**; Parsons *et al.*, 2008; Jackson and Durocher, 2013; Inode and Matouschek, 2014). The 26S proteasome consists of the “lid” and “base” 19s subunits and the 20S core made of four heptameric rings, forming a hollow barrel like structure (Myung *et al.*, 2001). Proteins targeted for degradation are recognised by the ‘lid’ which has an affinity for ubiquitinated protein and the base unfolds and guides these protein substrates into the catalytic inner compartment of the 20S particle. Subsequently, peptide bonds are cleaved through hydrolysis by the multiple proteolytic activities possessed by the 20S core (**Figure 1.17**; Myung *et al.*, 2001; Collins and Goldberg, 2017).

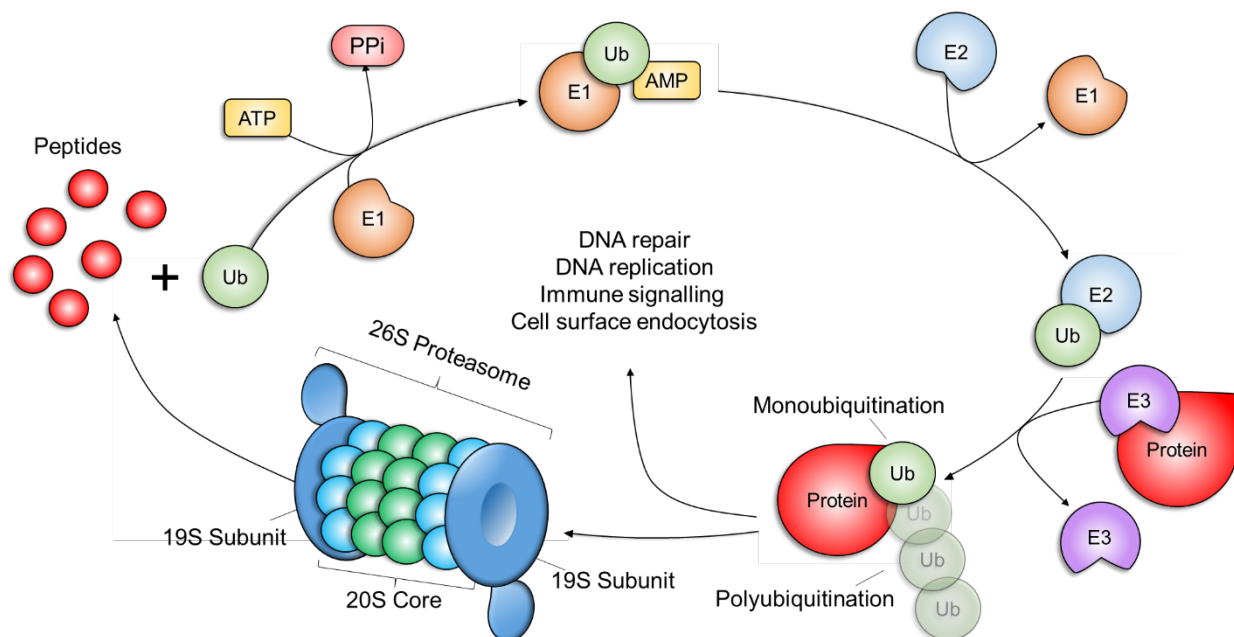


**Figure 1.17: Schematic representation of the ubiquitin proteasome system.** “Ub” denotes ubiquitin, “E1” denotes E1 ubiquitin activating enzyme, “E2” denotes E2 ubiquitin conjugating enzyme, “E3” denotes E3 ubiquitin ligase, “ATP” denotes adenosine triphosphate, “AMP” denotes adenosine monophosphate and “PPi” denotes pyrophosphate.

In human cells the presence of 10 E1 activating enzymes, 40 E2 conjugating enzymes and >600 E3 ubiquitin ligases have been estimated, with a further 90 complementary de-ubiquitinating enzymes (DUBs; Cohen and Tcherpakov, 2010; Sacco *et al.*, 2010). DUBs are subdivided into 5 distinct groups, the ubiquitin C-terminal hydrolases (UCHs), ubiquitin-specific proteases (USPs), Joesephines, JAMM/MPN+ metalloenzymes and ovarian tumour proteases (OTUs; Komander *et al.*, 2009). These DUBs have been shown to work in direct coordination with specific E3 ligases, fine tuning the orchestration of ubiquitin conjugation to target proteins and preventing autoubiquitination by specific E3 ligases which would lead to dysfunction (Wilkinson, 2009).

The UPS plays an important role within the DNA damage response and DNA repair, through regulation of activity, stability and the cellular localisation of numerous proteins. One well characterised example is the polyubiquitination of the tumour suppressor protein p53, by the RING family E3 ubiquitin ligase, mouse double minute 2 (MDM2) which targets Lys370, Lys372, Lys373, Lys381, Lys382, or Lys386 of p53 for proteasomal degradation (Haupt *et al.*, 1997; Rodriguez *et al.*, 2000). This said, multiple other E3 ubiquitin ligases have been identified to monoubiquitinate or polyubiquitinate p53 through Lys48 and Lys63 ubiquitin chains independent of MDM2 (Lee and Gu, 2010). These include, the RING domain E3 ligases: p53-induced RING-H2 protein (Pirh2), E3 ubiquitin-protein ligase ICP0 (ICP0), constitutive photomorphogenesis protein 1 (COP1), Topoisomerase I-binding RING finger protein (TOPORS), carboxy terminus of Hsp70-interacting protein (CHIP), Synoviolin, Cell division cycle and apoptosis regulator protein 1 (CARP1), Cell division cycle and apoptosis regulator protein 2 (CARP2), male-specific lethal 2-like 1 (MSL2), the homologous to the E6AP carboxyl terminus (HECT) domain E3 ligases: MULE, WW domain-containing protein 1 (WWP1) and the non-conventional: UBE2N and E4F transcription factor 1 (E4F1; Lee and Gu, 2010). Highlighting the elegant level of control that the ubiquitin system orchestrates within the cell.

Recently, the RING E3 ubiquitin ligase TRAF-interacting protein (TRAIIP) has been shown to play a role within regulation of DNA damage response factors at stalled-replication forks in a PCNA dependent manner through PIP box domain interaction, co-localising with DSB associated  $\gamma$ -H2AX foci. It was also shown that protein ubiquitination is vital for ss-DNA formation through ATR dependent signalling and RPA loading. It is suggested that DNA replication fork proteins are directly ubiquitinated, highlighting the importance of the

maintenance of protein homeostasis of DNA replication associated proteins by the UPS, in the orchestration of successful DNA replication (Hoffmann *et al.*, 2016).

#### 1.14.1. E3 ubiquitin ligases.

E3 ubiquitin ligases facilitate and complete the conjugation of ubiquitin monomers or polymers to target proteins. As a result, these enzymes control specificity of the ubiquitination reaction and the ubiquitin pathway (Zheng and Shabek, 2017). Two distinct major families of E3 ubiquitin ligases have been identified, they are determined by the presence of either RING domains or HECT domains. The mode of action of conjugating ubiquitin to target proteins differs between RING and HECT E3 ubiquitin ligases (Zheng and Shabek, 2017).

The E6 associated protein (E6-AP) was the first (HECT) E3 ubiquitin ligase which was mechanistically elucidated. It was shown that the HECT domain possesses a cysteine residue that accepts an E2 conjugating enzyme bound to Ub, in turn the HECT domain would facilitate the formation of a thioester linkage to E6-AP, followed by transfer to a lysine residue of the protein substrate targeted (Scheffner *et al.*, 1995).

The RING domain E3 ubiquitin ligases were shown to possess a different method of facilitating ubiquitination, demonstrated through the identification that the SCF ubiquitin ligase sub-unit, Rbx1, RING domain was essential for E3 ligase activity and that its coordination of zinc was a key feature. In addition, the Cul1 protein was identified as an important interactant with Rbx1, for binding and activation of the Cdc34 E2 conjugating enzyme. While HECT domain proteins create a thioester bound intermediate with the E3 ubiquitin ligase, studies revealed the Cul1-Rbx1 complex facilitated direct transfer of Ub between Cdc34 and the protein substrate (Kamura *et al.*, 1999; Ohta *et al.*, 1999; Tan *et al.*, 1999; Seol *et al.*, 1999; Metzger *et al.*, 2014). Polyubiquitination catalysed by RING domain E3s can be highly processive and is facilitated by consecutive transfer of single Ub monomers (Pierce *et al.*, 2009). It has been shown that to extend ubiquitin chains the cooperative action of E2 and E3 ubiquitin enzymes are required and several E3 ubiquitin ligases have been identified to generate Ub chains with the aid of one E2 conjugating enzyme. In contrast, multiple E2 conjugating enzymes may also be engaged by a single E3 ubiquitin ligase to generate Ub chains (Christensen *et al.*, 2007; Stewart *et al.*, 2016).

### 1.14.2. Ubiquitin proteasome system and cancer.

The UPS system maintains homeostasis at a protein level, orchestrating the degradation of damaged, misfolded and surplus proteins for proteasomal degradation (Collins and Goldberg, 2017). In addition, the UPS system modulates protein localisation, the interaction of specific proteins and can initiate cellular signalling pathways. The physiological role of the UPS system extends to inflammatory signalling, autophagy, multi-protein complex assembly and regulation of DNA repair systems (Bhattacharjee and Nandi, 2017; Kattah *et al.*, 2017).

#### 1.14.2.1 E2 conjugating enzymes and cancer.

The E2 conjugating enzyme Ubiquitin-conjugating enzyme E2 C (UBE2C) is overexpressed in many different cancers, including breast, ovary, thymus, uterus, lung and prostate cells (Narayan *et al.*, 2007; Fujita *et al.*, 2009; van Ree *et al.*, 2010; Tzelepi *et al.*, 2012). UBE2C functions together with the anaphase-promoting complex/cyclosome (APC) to facilitate completion of chromosomal segregation and alignment during mitosis. Overexpression has been shown to increase the incorrect segregation of chromosomal DNA and transgenic mice become prone to lung and several other types of cancer (van Ree *et al.*, 2010).

Ubiquitin-conjugating enzyme E2 S (UBE2S) conjugating enzyme was shown to facilitate the polyubiquitination of the von Hippel-Lindau (VHL) protein for proteasomal degradation (Jung *et al.*, 2006). VHL regulates hypoxia inducible factors (HIF) and in turn induces the expression of oncogenic genes (Rankin and Giaccia, 2016). In tumours, HIF $\alpha$  and UBE2S are overexpressed with reduced expression of VHL. VHL stabilises oxygen levels within the cell and overexpression of UBE2S dysregulates its function and leads to an increase in HIF transcription factors and thus an oncogenic phenotype through upregulation of associated oncogenes (Witkiewicz *et al.*, 2015; Beltran *et al.*, 2016).

Ubiquitin-conjugating enzyme E2 N (UBE2N) and its cofactor Ubiquitin-conjugating enzyme E2 variant 1 (UBE2V1) are specific for Lys63 chain building and vital in the inflammatory response through initiation of NF $\kappa$ B (Chen and Chen, 2013). Indeed, UBE2N is overexpressed in pancreatic, breast, prostate, colon, lymphoma and ovarian carcinomas. In breast cancers UBE2N facilitates metastasis to the lung as a secondary site through transforming growth factor beta (TGF- $\beta$ ) activation of mitogen-activated protein kinase 11 (p38) and transforming

growth factor beta-activated kinase 1 (TAK1) which lead to expression of metastasis associated genes. Furthermore, the downregulation of UBE2N by short hairpin RNAi has been shown to suppress metastasis in the same manner (Wu *et al.*, 2014). Thus, highlighting the role of UBE2N and UBE2V1 in inflammatory signalling through TGF- $\beta$  and NF $\kappa$ B in promoting metastasis.

#### 1.14.2.2 E3 ubiquitin ligases and cancer.

E3 ubiquitin ligases and their association with DUB enzymes have been characterised to regulate tumorigenic or tumour-suppression pathways, the most notable example being p53 and its regulation by the MDM2 E3 ubiquitin ligase (Shangary and Wang, 2008; Love *et al.*, 2013). The tumour-suppressor protein p53, which controls cell cycle, apoptotic and DNA repair proteins is regulated by the RING E3 ubiquitin ligase MDM2 in healthy cells (Momand *et al.*, 1992). In many forms of cancer, MDM2 is overexpressed and escalates ubiquitination of p53, leading to degradation by the UPS and inhibition of normal tumour-suppression pathways regulated by p53 (McCann *et al.*, 1995; Haupt *et al.*, 1997).

The SCF protein complex has also been shown to be overexpressed in malignant tumours, with its RING E3 ubiquitin ligase Rbx1 subunit facilitating degradation of cyclin-dependent kinase inhibitors cyclin-dependent kinase inhibitor p27 (p27KIP1), cyclin-dependent kinase inhibitor 1A (P21, Cip1), isoform CRA\_a (p21CIP1), Forkhead box protein O1 (FOXO1; Huang *et al.*, 2005), 130 kDa retinoblastoma-associated protein (p130; Tedesco *et al.*, 2002) and cyclin-dependent kinase inhibitor 1C (p57; Kamura *et al.*, 2003), promoting cellular proliferation. Upstream regulators of SCF have also been shown to function in oncogenesis. For example, the sequestosome 1 (SQSTM1) was proposed to be a biomarker in oesophageal squamous cell carcinoma due to its positive correlation with SCF, a phenotype of increased proliferation and resistance to apoptosis being observed (Shi *et al.*, 2018). Within the SCF complex, the F-box and WD repeat domain containing 7 (FBXW7) subunit also possesses E3 ubiquitin ligase activity. In cancer cells FBXW7 is downregulated and is subsequently correlated with poor prognosis and metastasis (Ibusuki *et al.*, 2011; Yang *et al.*, 2015). It is suggested that downregulation of FBXW7 reduces the degradation of mTOR, a key member of mTORC1 and mTORC2 complexes that are involved in facilitating metastatic potential,

protein synthesis and cell proliferation (Hay and Sonenberg, 2004; Lipton and Sahin, 2014; Yang *et al.*, 2015).

E3 ubiquitin ligases have been shown to promote metastasis. For example, the E3 ubiquitin ligase Glycoprotein 78 (GP78) controls protein levels of the tetraspanin Metastasis suppressor Kangai-1 (KAI1) tumour suppressor through polyubiquitination. Loss of KAI1 is associated with metastasis through inflammatory signalling of NF $\kappa$ B,  $\beta$ -catenin and p53 (Liu and Zhang, 2006). Another example includes the E3 ubiquitin ligase VHL, which ubiquitinates VHF. Degradation through the UPS system maintains homeostasis of HIF in hypoxia conditions, however, the lack of VHL can lead to the adaptation of renal tumours to hypoxic conditions by facilitating their vascularisation (Rankin and Giaccia, 2016).

### 1.14.3. Ubiquitin regulation of the Base Excision Repair pathway.

The expression of BER proteins does not fluctuate dramatically in response to acute exogenous DNA damaging treatment, which suggests minimal capacity of BER in the immediate cellular response to exogenous DNA damage (Parsons and Dianov, 2013). However, the BER pathway has been shown to be regulated through PTMs, with the most common PTM identified as phosphorylation, which is primarily associated with checkpoint pathway signalling through specific kinases (Almeida and Sobol, 2007; Carter and Parsons, 2016). The UPS has since been shown to play key roles in the regulation of BER proteins (Edmonds and Parsons, 2014).

The end processing proteins in BER, PNKP and APE1, have been shown to be regulated through the UPS. PNKP is responsible for the processing of 3'P termini as result of  $\beta$ , $\delta$ -elimination by bifunctional DNA glycosylases and for the repair of SSBs (Weinfeld *et al.*, 2011). It was identified by cellular fractionation that the controlled response of PNKP to DNA damage was through an E3 ubiquitin ligase complex, consisting of the Cullin-4A (CUL4A), DDB1 and the serine-threonine kinase receptor-associated protein (STRAP; Angers *et al.*, 2006; He *et al.*, 2006; Parsons *et al.*, 2012). This complex was found to ubiquitinate PNKP at lysine 414, 417 and 484, while STRAP<sup>-/-</sup> MEF cells displayed increased protein levels of PNKP and an increase in resistance to H<sub>2</sub>O<sub>2</sub> treatment when compared to WT MEF cells (Parsons *et al.*, 2012). PNKP was previously shown to be phosphorylated by ATM in response to IR and subsequently evidence was provided for crosstalk between ATM dependent phosphorylation and CUL4A-

DDB1-STRAP complex dependent ubiquitination of PNKP (Barzilai *et al.*, 2002; Segal-Raz *et al.*, 2011; Zolner *et al.*, 2011). This was demonstrated through the overexpression of a PNKP S114/126E phosphomimetic protein that demonstrated reduced levels of ubiquitination by the CUL4A-DDB1-STRAP complex and was more stable (Parsons *et al.*, 2012).

The major E3 ligase responsible for the regulation of APE1 by polyubiquitination was shown to be Ubiquitin-protein ligase E3-alpha-3 (UBR3; Meisenberg *et al.*, 2012). However, APE1 was previously shown to be polyubiquitinated by the MDM2 E3 ligase at Lys24, Lys25 and Lys27 of APE1 and was suggested to target APE1 for proteasomal degradation as the depletion of MDM2 resulted in an increase in APE1 protein levels (Busso *et al.*, 2009). Interestingly, it was shown that the overexpression of APE1 in UBR3<sup>-/-</sup> mice resulted in genetic instability with an increase in the NHEJ associated 53BP1 and HR associated gamma histone 2 A X ( $\gamma$ -H2AX) foci, indicating increased DSB generation. This was suggested to be a result of the imbalance of SSBs and downstream gap filling and sealing enzymes (Meisenberg *et al.*, 2012).

The downstream gap filling enzyme Pol  $\beta$  has been shown to be ubiquitinated by the E3 ubiquitin ligase CHIP. Overexpression of CHIP resulted in a decrease in Pol  $\beta$  protein levels whereas RNAi lead to an increase in Pol  $\beta$  protein levels. This subsequently demonstrated the role of CHIP in modulating Pol  $\beta$  protein levels within the cell (Parsons *et al.*, 2008). In addition, the MULE E3 ubiquitin ligase was shown to monoubiquitinate Pol  $\beta$ , resulting in relocalisation to the cytoplasm. Furthermore, MULE dependent monoubiquitination of Pol  $\beta$  was required in advance of CHIP dependent polyubiquitination and degradation (Parsons *et al.*, 2009). The knockdown of the MULE inhibiting protein, tumour suppressor ARF (ARF), was shown to increase cellular levels of monoubiquitinated Pol  $\beta$  (Chen *et al.*, 2005; Parsons *et al.*, 2009). It was revealed, that after monoubiquitination and localisation to the cytoplasm, the Pol  $\beta$  specific DUB, USP47, removes ubiquitin from Pol  $\beta$  subsequently reinstating availability for gap filling and associated lyase activity in response to DNA damage. It was shown that USP47 deubiquitinates both mono- and poly-ubiquitinated Pol  $\beta$  and USP47 RNAi, led to a decrease in Pol  $\beta$ . However, the co-knockdown of MULE and USP47 rescued exogenously expressed Pol  $\beta$  protein levels previously reduced by USP47 RNAi (Parsons *et al.*, 2011). Thus, providing evidence that MULE is responsible for the regulation of newly synthesised Pol  $\beta$ . To highlight this interaction as a dynamic response to DNA damage, HeLa cells deficient in USP47 displayed a delay in repair kinetics in response to both MMS and H<sub>2</sub>O<sub>2</sub> treatment and also sensitivity to

H<sub>2</sub>O<sub>2</sub> treatment. Therefore, demonstrating the relevance of USP47 in the modulation of the cellular response to both oxidative and alkylation DNA damage (Parsons *et al.*, 2011).

XRCC1 protein levels influence Ligase III protein levels, as XRCC1 mutant and deficient CHO cells displayed a reduction in Ligase III and Pol  $\beta$ , while presenting a hypersensitive phenotype to the DNA alkylating agents ethyl methanesulfonate (EMS) and MMS (10-fold), moderate sensitivity to H<sub>2</sub>O<sub>2</sub> and camptothecin (2-5 fold), minor sensitivity to IR, UVA, UVC, near visible light, blue, light, heavy metals, ethylnitrosurea (ENU), N-methyl-N'-nitro-N-nitrosoguanidine (MNNG) and MMC (Thompson *et al.*, 1982; Christie *et al.*, 1984; Cantoni *et al.*, 1987; Churchill *et al.*, 1991; Thompson *et al.*, 2000; Parsons *et al.*, 2008). XRCC1 and Ligase III were shown to be polyubiquitinated *in vitro* by the E3 ubiquitin ligase CHIP, additionally knockdown of CHIP resulted in stabilisation of XRCC1 and Ligase III protein levels providing evidence of targeting for proteasomal degradation (Parsons *et al.*, 2008). An additional E3 ubiquitin ligase was implicated in the ubiquitination of XRCC1 but in a poly-(ADP-ribose)ation dependent manner, signalling proteasomal degradation. This E3 ubiquitin ligase was termed Iduna and was found to have a protective role against IR and MNNG treatment. However, additional protein substrates were identified for Iduna and included poly(ADP-ribose)polymerase 1 (PARP-1), Ligase III and Ku70 indicating a more complex interaction within the DNA damage response (Kang *et al.*, 2011). Taken together, CHIP and Iduna mediated ubiquitination of XRCC1-Ligase III are suggested to be important in influencing the cellular response to multiple forms of DNA damage.

NTH1, has been recently shown to be polyubiquitinated by the E3 ubiquitin ligase, TRIM26. It was observed that steady state levels were increased in response to TRIM26 RNAi in both HCT116 and U2OS cells, implicating a role in protein stabilisation. A significant increase in repair kinetics and resistance in response to H<sub>2</sub>O<sub>2</sub> after TRIM26 RNAi was also observed, with the phenotype complemented by transient overexpression of NTH1 (Williams and Parson, 2018).

It was demonstrated that OGG1 DNA glycosylase was ubiquitinated by CHIP after exposure of HeLa cells to mild hyperthermia. This exposure to hyperthermia resulted in the inactivation of OGG1 and its relocalisation from the nuclear to the peri-nuclear regions of the cell. In addition, exposure to mild hyperthermia promoted the degradation of OGG1 and resulted in an impaired cellular proliferation phenotype (Fantini *et al.*, 2013). It was also shown that

hyperthermia reduced the repair kinetics of DNA damage and the cellular survival of HeLa cells treated with the oxidative damaging agent Ro19-8022 (Will *et al.*, 1999; Fantini *et al.*, 2013). It was proposed that ubiquitination of OGG1 by CHIP was in part responsible for the observed chemosensitivity displayed in HeLa cells exposed to hyperthermia, due to an impairment in the removal of OGG1 associated DNA damage (Fantini *et al.*, 2013).

MUTYH has been shown to be ubiquitinated by the E3 ubiquitin ligase MULE an E3 ubiquitin ligase also shown to ubiquitinate p53 in a MDM2 independent manner, as previously discussed (Lee and Gu, 2010; Dorn *et al.*, 2014). In addition, MULE RNAi increased cellular MUTYH protein levels while MULE overexpression decreased protein levels of MUTYH. It was also shown that abolishment of ubiquitin binding through generation of a MUTYH mutant (KK477RR, K495R, KK506RR) increased accumulation of MUTYH on chromatin whereas the WT MUTYH was found to be mainly cytoplasmic (Dorn *et al.*, 2014). It was suggested that MULE plays an important role in regulating the cellular response to oxidative DNA damage through MUTYH as it was previously shown that RNAi of MUTYH in HeLa cells resulted in sensitivity to H<sub>2</sub>O<sub>2</sub> (Hwang *et al.*, 2014; Dorn *et al.*, 2014).

The E3 ubiquitin ligases Cullin-1 (CUL1) and Cullin-4 (CUL4) were identified to ubiquitinate UNG and SMUG1, displaying stimulatory interactions with the accessory viral protein Vpr from HIV. These interactions are proposed to result in a reduction of the number of AP sites generated in reverse transcripts as a result of DNA dC->dU-editing enzyme (APOBEC3) catalysed cytosine deamination and subsequent uracil excision by UNG or SMUG1 (Schröfelbauer *et al.*, 2005). UNG, SMUG1, MBD4 and TDG have also been identified as substrates for ubiquitination in proteomic ubiquitination screens, however the E3 ubiquitin ligases responsible are yet to be determined (Danielsen *et al.*, 2011; Kim *et al.*, 2011a; Wagner *et al.*, 2011; Udeshi *et al.*, 2012; Oshikawa *et al.*, 2012).

The NEIL1 DNA glycosylase has been identified as a substrate for ubiquitination through HeLa cell fast protein liquid chromatography (FPLC) fractionation and liquid chromatography mass-spectrometry (LCMS). It was shown that MULE and TRIM26 are the major E3 ubiquitin ligases which facilitate ubiquitination of hNEIL1, generating polyubiquitin chains at the same amino acid residues (Lys319, 333, 356, 357, 361, 374, 376; Edmonds *et al.*, 2017). Additionally, it was shown that hNEIL1 is induced in response to IR in a MULE dependent manner but TRIM26 siRNA led to IR resistance and increased hNEIL1 steady state protein levels in U2OS cells.

TRIM26 RNAi induced resistance to IR was only partially complemented up to 2 Gray by hNEIL1 over expression, suggesting that the observed increase in steady state levels of hNEIL1 due to TRIM26 RNAi is only partially responsible for the observed IR resistance (Edmonds *et al.*, 2017). Putative sites of ubiquitination have been identified on the hNEIL2 DNA glycosylase, at Lys96, Lys234 and Lys299, however E3 ubiquitin ligases which ubiquitinate hNEIL2 are yet to be characterised (Kim *et al.*, 2011a; Udeshi *et al.*, 2013). The hNEIL3 DNA glycosylase has been identified to possess 28 putative sites of ubiquitination amongst the 49 lysine residues present within the amino acid sequence, through high throughput screens (Kim *et al.*, 2011a; Mertins *et al.*, 2013; Udeshi *et al.*, 2013; Hornbeck *et al.*, 2015). However, to date no E3 ubiquitin ligases have been identified to interact and modulate NEIL3 protein stability, localisation or activity.

It is evident that several E3 ubiquitin ligases have multiple substrates within BER, including CHIP (OGG1, XRCC1, Lig III, Pol  $\beta$ ), MULE (MUTYH, Pol  $\beta$ , NEIL1), Cul1 (UNG, SMUG1), Cul4 (UNG, SMUG1 and PNKP in complex with DDB1 and STRAP), Iduna (XRCC1, Lig III and PARP-1), while only one DUB has been identified for Pol  $\beta$ , which facilitated the further understanding of the dynamic role of the UPS in the regulation of the cellular response to DNA damage through BER (Parsons *et al.*, 2011). It is likely that E3 ubiquitin ligases which have multiple substrates recognise specific structural motifs present within BER proteins, modulating the cellular response to distinct DNA damage through the orchestration of multiple BER proteins. To further the understanding of the role of the UPS in modulating BER, the identification of interacting E3 ubiquitin ligases with TDG, NEIL2 and NEIL3 is required. Furthermore, the structural characterisation of motifs in BER protein substrates that are ubiquitinated by the same E3 ubiquitin ligase, may further the understanding of how dysfunction in the UPS may have knock-on effects on the protective function of multiple BER proteins. Finally, the identification of additional BER protein specific DUBs will further the understanding of the dynamic cellular response to DNA damage.

Evidence begins to suggest the BER pathway is intrinsically involved in the repair of non-conventional DNA lesions such as ICLs (Couvé-Privat *et al.*, 2007; Couvé *et al.*, 2009; Semlow *et al.*, 2016; Martin *et al.*, 2017). Therefore, the elucidation of the role of E3 ubiquitin ligases in modulating the cellular response to ICL inducing agents through BER, may lead to the

identification of novel mechanisms that promote the acquired resistance of cancer cells to ICL inducing agents.

#### **1.14.4. Tripartite motif-containing proteins.**

In humans approximately 70 tripartite motif-containing (TRIM) proteins have been identified and are mainly RING E3 ubiquitin ligases, which facilitate the ubiquitination of substrate proteins through the RING zinc finger domain facilitating direct transfer of Ub from an E2 ubiquitin conjugating enzyme to the protein substrate (Metzger *et al.*, 2014; Watanabe and Hatakeyama, 2017). They are also known as RING, B-Box(es), Coiled coil domain E3 ubiquitin ligases (RBBC) proteins due to their characteristic RING, B-box(es) and coiled-coil (CC) domain structure followed by a differentiated C-terminal (Reymond *et al.*, 2001; Torok and Etjkin, 2001). B-box domains are zinc finger domains and have been suggested to enhance RING dependent E3 ubiquitin ligase activity and confer E3 ubiquitin ligase activity to TRIM proteins which do not possess a RING domain (Bell *et al.*, 2012). The CC domain has been indicated to promote homo-oligomerisation of TRIM proteins and has been advised as an essential feature that facilitates E3 ubiquitin ligase activity (Napolitano and Meroni, 2012). The substrate specificity and recognition of TRIM proteins is also proposed to be mediated through the hetero-oligomerisation of closely related TRIM proteins, through the interaction of their differentiated C-terminal domains (Napolitano and Meroni, 2012; Esposito *et al.*, 2017).

Many TRIM substrates are associated with immune response signalling, including TRIM25 which ubiquitinates retinoic acid-inducible gene 1 product (RIG-1), a detector of viral infection, leading to the production of type I interferons (Gack *et al.*, 2007). Tripartite motif containing protein 5 alpha (TRIM5 $\alpha$ ) has also been shown to play a role in the inhibition of HIV-1 infection by trimerizing and coating the capsid of a virus, whereas a TRIM5 $\alpha$  CC domain ( $\Delta$ CC GCN4) mutant protein did not inhibit the virus and could not bind to the capsid despite being able to trimerize (Javanbakht *et al.*, 2006).

TRIM proteins have been identified as biomarkers of carcinogenesis with TRIM24, 28, 29, 32 and 51 being shown to interact with the tumour suppressor protein p53, their dysfunction suggested to lead to an alteration in p53 protein levels disrupting its tumour-suppressive function (Yang *et al.*, 2007; Allton *et al.*, 2009; Kanno *et al.*, 2014; Borlepawar *et al.*, 2017). More recently, TRIM32 has also been shown to be a positive regulator of cell proliferation in

gastric cancer *in vivo*, through its enhancement of the  $\beta$ -catenin protein signalling pathway promoting metastatic potential (Wang *et al.*, 2018). In general, dysfunction of TRIM E3 ubiquitin ligases have been associated with cancer through differential cellular function including transcriptional regulation, cell proliferation, immune response signalling, apoptosis and metastasis (Hatakeyama, 2017).

Interestingly, TRIM proteins have been identified to regulate DNA repair, their dysfunction proposed to promote genomic instability and resistance to therapeutic intervention of malignant tumours (Hatakeyama, 2011). TRIM29 is one such example and revealed to be a histone binding protein which facilitated the incorporation of DSB repair proteins, BASC, cohesion, DNA dependent protein kinase, catalytic subunit (DNAPKcs) and 60 kDa Tat-interactive protein (TIP60; Masuda *et al.*, 2015). It was also shown that TRIM29 was phosphorylated by ATM in response to ionising radiation supporting its role in DSB repair modulation (Wang *et al.*, 2014). As previously discussed, TRIM26 has been highlighted as an important modulator of the NEIL1 and NTH1 DNA glycosylases and its downregulations infers resistance of cancer cells to IR and the ROS inducing agent H<sub>2</sub>O<sub>2</sub>, respectively (Edmonds *et al.*, 2017; Williams and Parsons, 2017).

#### **1.14.5. Tripartite motif-containing protein 26.**

The Tripartite motif-containing protein 26 is a 62.2 kDa E3 ubiquitin ligase of the TRIM subfamily C-IV-1 protein (Edmonds *et al.*, 2017; Watanabe and Hatakeyama, 2017; Williams and Parsons, 2018). TRIM26 consists of a N-terminal RING finger domain, a B-box 2 domain, a CC domain and two C-terminal PRY domains (Watanabe and Hatakeyama, 2017).

Human and mouse somatic cells can be reprogrammed to a pluripotent embryonic stem cell –like state and this facilitates the generation of inducible pluripotent stem cells (iPSCs). This process is achieved with the use of four transcription factors Sox transcription factor 2 (Sox2), octamer-binding transcription factor 4 (Oct4), Krueppel-like factor 4 (Klf4) and MYC (Takahashi and Yamanaka, 2006; Takahashi *et al.*, 2007 Yu *et al.*, 2007). Plant homeodomain finger protein 20 (PHF20) transcription factor was shown to regulate p53 in response to UV induced DNA damage (Li *et al.*, 2013). It was identified that lysine-specific demethylase 6B (Jmjd3) is a negative regulator of reprogramming, partially through its recruitment of TRIM26 for Lys48 polyubiquitination and degradation of PHF20 that results in a reduction of Oct4 and

thus reducing reprogramming efficiency (Zhao *et al.*, 2013). TRIM26 silencing resulted in an increase in PHF20 and Oct4 and subsequently resulted in an increase in the efficiency of iPSC reprogramming. It was also observed that in *Jmjd3*<sup>-/-</sup> MEF cells, PHF20 protein levels were significantly increased. *Jmjd3*<sup>-/-</sup> MEF cells displayed reduced senescence, apoptosis and increases cell proliferation which may be suggested to be due to disrupted *Jmjd3*-TRIM26 interaction (Zhao *et al.*, 2013). These findings may implicate TRIM26 in inhibition of pluripotency which may have important implications for pluripotent models of study including pluripotent cancer stem cells.

TRIM26 has been implicated in the regulation of the cellular immune response. Ran *et al.* (2016) demonstrated that TRIM26 regulated the immune response to RNA virus infection. It was shown by coimmunoprecipitation that TRIM26 interacted with Serine/threonine-protein kinase (TBK1) and nuclear factor kappa-light-chain-enhancer of activated B cells (NF $\kappa$ B) essential modulator (NEMO). In the absence of viral infection TRIM26 was associated with TBK1 and then NEMO post infection. It was also shown that TRIM26 enhanced interferon beta (IFN- $\beta$ ) protein levels in response to viral infection, which was ablated when mutating a conserved Cys (C31S) within the RING domain (Ran *et al.*, 2016). Due to previous findings that NEMO can bind polyubiquitin chains, it was proposed that autoubiquitinated TRIM26 in complex with TBK-1 is recruited to facilitate TBK1-NEMO interaction in response to RNA virus infection (Husnjak and Dikic, 2012; Wang *et al.* 2015b). However, counter to these findings of positive regulation of IFN- $\beta$ , Wang *et al.* (2015b) demonstrated that TBK1 negatively regulates IFN- $\beta$  production in TRIM26 transgenic mice. They suggested that this was through polyubiquitination and degradation of nuclear Interferon Regulatory Transcription Factor 3 (IRF3) and the interaction serves as an innate protective mechanism against autoimmune disease (Wang *et al.*, 2015b). Ran *et al.* (2016) suggested that this discrepancy was due to either the use of different model systems used in their investigations (HeLa, human acute monocytic leukemia (THP-1) and MEFs vs mouse peritoneal macrophages), or that high levels of TRIM26 affects the substrate specificity of TRIM26. Regardless, TRIM26 seems to have a role in an innate immune response modulating IFN- $\beta$ .

In support of a role in the immune response and providing link to a role in cancer, Lyu *et al.* (2018) revealed that TRIM26 downregulation and the single nucleotide polymorphism rs117565607\_A were strongly associated with nasopharyngeal carcinoma (NPC) through the

inhibition of transcription factor transcriptional repressor protein ying and yang 1 (YY1) binding. Their investigation determined that low TRIM26 NPC samples displayed association with immune response genes. Validation was undertaken by TRIM26 RNAi in the human nasopharyngeal carcinoma cell line 2 (CNE2), NPC cell line and normal peripheral blood mononuclear cell lines. This resulted in consistent observation of the downregulation of nuclear factor kappa B subunit 2 (NF $\kappa$ B2), Interleukin 32 (IL-32), interferon regulatory transcription factor 7 (IRF7), cluster of differentiation 38 (CD38), and signal transducer and activator of transcription 1 (STAT1). This data suggested that TRIM26 downregulation through YY1 transcriptional processes results in a repressed immune response, increasing NPC risk (Lyu *et al.*, 2018).

Importantly, TRIM26 has been previously shown to be associated with transcriptional regulation through ubiquitination of the general transcription factor TFIID (TFIID) sub-unit, transcription initiation factor TFIID subunit 7 (TAF7) in mouse epithelial cells. It was revealed that TGF- $\beta$  mediated proliferative arrest, induced the transcription of TRIM26 and subsequently TAF7 degradation. Furthermore, sustained TGF- $\beta$  exposure led to inhibition of TRIM26 induction via MYC through TRIM26 gene promoter binding. Thus, indicating that TRIM26, is a negative regulator of cellular proliferation through degradation of TAF7 with induction of TGF- $\beta$  regulated cell cycle arrest and apoptosis. However, with MYC overexpression observed in many cancers, it was suggested that MYC may facilitate malignant evasion of this TRIM26 antiproliferative mechanisms through TAF7 degradation (Nakagawa *et al.*, 2017).

Previously, TRIM26 has been identified as a possible tumour suppressor in hepatocellular carcinomas, with significant correlation identified between low TRIM26 levels and poor prognosis in patients. In agreement with Nakagawa *et al.* (2017) it was also demonstrated that TRIM26 RNAi in hepatocellular carcinoma (HCC) cell lines HepG2 and Bel-7402 enhanced cancer cell migration, invasion and proliferation. It was also identified that TRIM26 levels are reduced in cholangiocellular carcinoma which display increased resistance to radiotherapy and chemotherapy, eluding to the role of TRIM26 dysfunction in cancer therapeutic resistance (Wang *et al.*, 2015a).

In support of the possible role in which TRIM26 plays as a tumour suppressor and as previously discussed, TRIM26 RNAi has been demonstrated to provide significant resistance to IR and oxidative stress inducing agent H<sub>2</sub>O<sub>2</sub> in U2OS and HCT116 cells, respectively. (Edmonds *et al.*, 2017; Williams and Parsons, 2018). Taken together it may be proposed that TRIM26 dysfunction may be a common feature of cancer. Parsons' group recently identified that one possible mechanism of resistance to radiotherapy and chemotherapy may be TRIM26 regulation of BER DNA repair proteins. NEIL1 and NTH1 were recently identified as substrates for TRIM26 ubiquitination and TRIM26 RNAi increased protein steady state levels of NEIL1 and NTH1 (Edmonds *et al.*, 2017; Williams and Parsons, 2018).

### **1.15. Use of bacterial hosts for protein expression.**

Bacterial expression vectors can facilitate the production of recombinant proteins for *in vitro* biochemical analysis (Brown, 2010). An example of a traditional vector is the bacterial DNA plasmid, independent of host chromosomal DNA and utilised for gene expression through plasmid design, plasmid DNA purification, restriction digestion, ligation and transformation (Brown, 2010). *E. coli* remains the most commonly used host system for recombinant plasmid DNA models of expression (Anderson and Krummen, 2002).

#### **1.15.1. The pET expression system.**

The pET vector system permits the inducible control of protein expression, in *E. coli*. This plasmid construct has transcription driven by T7 bacteriophage RNA DNA polymerase and T7 promoter recognition, allowing a two-part gene expression (Novagen, 2005; Kesik-Brodacka *et al.*, 2012).

Rosetta (DE3) expression hosts for pET expression vectors possess a chromosomal copy of T7 RNA DNA polymerase and 'rare' tRNA genes translated from a chloramphenicol-resistant pRARE plasmid. These tRNA codons are AGG, AGA, AUA, CUA, CCC, GGA and the additional CGG codon in Rosetta 2 (DE3) hosts, supplementing the tRNA pool, for improved translation of heterologous genes. This is particularly useful if codon bias proves restrictive in protein expression (Novagen, 2004; Gou *et al.*, 2009).

T7 RNA DNA polymerase is expressed in the presence of IPTG, due to upstream inducible transcription by the *lacUV5* promoter, providing a pool of T7 RNA DNA polymerase and

permitting T7 RNA DNA polymerase binding on the pET vector activating the T7 promoter, then transcription and translation of the encoded complementary DNA (cDNA; **Figure 1.18**; Novagen, 2005). This system is reported to yield target protein expression levels as high as 50% of all the bacterial cellular proteins, producing a larger total target protein than alternative systems (Jevsevar *et al.*, 2005; Novagen, 2005; Tegel *et al.*, 2011).

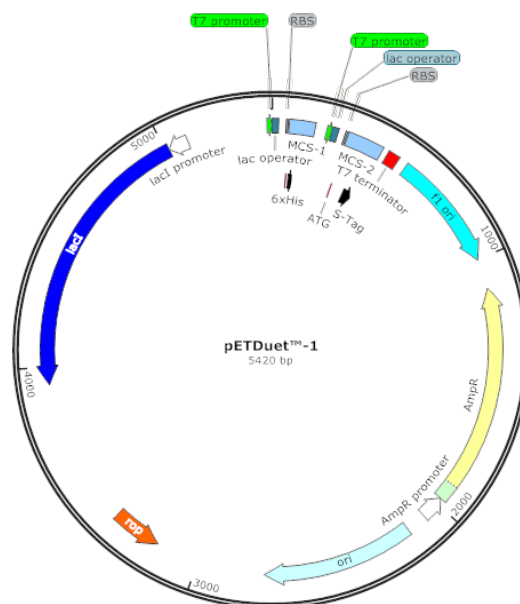


**Figure 1.18: Plasmid vector map of the pETDuet1 expression vector developed for dual expression of two genes.** Transcription vector map with sequence landmarks, including: T7 promoters, T7 terminator, 6xHistidine, multiple cloning sites (MCS-1/2), Ampicillin resistance gene (AmpR), Ribosomal binding site (RBS), repressor of primer (ROP), LacI gene (lacI), double-strand replication of origin (ori) and single-stranded replication of origin (F1 ori).

The pET vector system offers the addition of fusion tags for protein detection via western blot and purification via affinity purification. The pET vector has been exploited to express and purify active NEIL proteins (Bandaru *et al.*, 2002; Liu *et al.*, 2012). However, hNEIL3 has proved difficult to express as an active full-length protein and warranted the modification of the pET-based vectors (Krokeide *et al.*, 2009; Gou *et al.*, 2009; Liu *et al.*, 2012).

### 1.15.2. Construction and use of a bicistronic pET vector for hNEIL3 recombinant protein expression.

Issues preventing active full amino acid sequence hNEIL3 expression were previously identified. The initiator methionine requires removal for translation of active eukaryotic proteins in *E. coli* (Liu *et al.*, 2012). The formation of mRNA secondary structure was also

highlighted to hinder translation initiation (Gou *et al.*, 2009). A bicistronic vector construct was subsequently developed by Gou *et al.* (2009) and Liu *et al.* (2012) using the pETDuet-1 vector backbone (**Figure 1.18**). The construct includes an open reading frame 6 (ORF6), comprised of 15 amino acids from the N-Terminal of the maltose binding protein and a modified *E. coli* methionine amino peptidase (*EcoMap*; Gou *et al.*, 2009; Liu *et al.*, 2012). The ORF6 was found to improve ribosomal binding stability in the transcription initiation region of the hNEIL3 cDNA. This resulted in improved transcription efficiency through the prevention of secondary structure formation (Guo *et al.*, 2009). *EcoMap* facilitated the removal of the translation initiator methionine present at amino acid position 1. This amino-peptidase proved critical for processing, increasing translation of active mouse and hNEIL3 glycosylase domain protein within *E. coli* (Liu *et al.*, 2012). The dual expression of *EcoMap* and the hNEIL3 DNA glycosylase domain within the bicistronic vector (**Figure 1.19 B**) was found to result in 76% successful methionine processing and a yield of 44% active hNEIL3 glycosylase domain protein (Liu *et al.*, 2012). However, the critical role that the NdeI site plays in the bicistronic plasmid construction conflicted with the NdeI restriction site—located within hNEIL3 at nucleotide position 865 (Vincze *et al.*, 2003; Liu *et al.*, 2012).

A.



B.

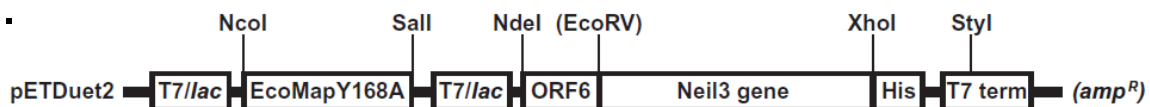


**Figure 1.19: Linear vector maps of the modified pET vectors used in the construction of the pETDuet2-*EcoMap*-ORF6 expression vector backbone.** **A:** The pET30b intermediate vector ORF6 region, overlapping leader sequence for improved transcription of desired cDNA of interest. **B:** The bicistronic pETDuet2-*EcoMap*-ORF6-construct for mouse NEIL3 and human glycosylase domain NEIL3 (taken from Liu *et al.*, 2012).

Using an *in vitro* cell free transcription and translation, inactive full amino acid sequence hNEIL3 was expressed using the TNT® Coupled Reticulocyte Lysate System (Krokeide *et al.*, 2009). The coupled reticulocyte initiates transcription and translation simultaneously, as *E. coli* normally would (Laursen *et al.*, 2005). In a more recent article by Krokeide *et al.* (2013) a method was presented for active hNEIL3 glycosylase domain expression, within BL21-CodonPlus (DE3)-RIL strain *E. coli* hosts that supplement the tRNA pool with rare codons,

similar to Rosetta cells. Partial cleavage of the initiator methionine was observed, in support of its requirement for active protein expression. The method used unusual incubation conditions of 16°C to express active protein (Krokeide *et al.*, 2009; Krokeide *et al.*, 2013).

Previously in our laboratory the cDNA for the full length human NEIL3 (hNEIL3<sup>FL</sup>) and two cDNA truncations of 843 base pairs (bp; hNEIL3<sup>Cat</sup>) and 1044 bp (hNEIL3<sup>Trun</sup>; **Figure 1.20**) were cloned into the pETDuet2-*EcoMap*-ORF6 expression vector (**Figure 1.19 B**; Mustafa Albelazi, University of Salford; Liu *et al.*, 2012). Using a pET30b vector to construct the ORF6 region in fusion with the hNEIL3 cDNA sequence (**Figure 1.19 A**) similar to that described by Gou *et al.* (2009). This was conducted with the aim to express and purify three versions of the hNEIL3 protein, to biochemically characterise differences in activity due to the encoded conserved protein domains (**Figure 1.20**). Plasmid vector construction was achieved using NdeI and XhoI restriction endonuclease digestion to prepare the pETDuet2-*EcoMap*-ORF6 vector backbone, followed by mung bean nuclease digestion to remove the 5' cohesive end at the NdeI restriction site within the vector, creating a blunt end (Desai and Shankar, 2003; Rittié and Perbal, 2008). Using the pET30b-ORF6-hNEIL3 vector as a template, polymerase chain reaction (PCR) was conducted to amplify ORF6 in fusion with the respective hNEIL3 DNA sequence (**Figure 1.20**). The PCR product was digested with XhoI and ligated into the pETDuet2-*EcoMap*-ORF6 backbone after agarose gel purification. The pETDuet2-*EcoMap*-ORF6-hNEIL3 expression vectors were shown to actively express both *EcoMap* and hNEIL3 simultaneously when induced with IPTG. Subsequently, the three version of the human hNEIL3 protein were previously expressed at 16°C overnight using 1 mM IPTG and purified using a HisTrap HP affinity FPLC column and the ÄKTA prime FPLC system. hNEIL3<sup>FL</sup> required further purification via Mono S 5/50 GL ion exchange FPLC column and the ÄKTA prime FPLC system. Recombinant protein products were confirmed by SDS-PAGE and immunoblot analysis (**Appendix Figure 1**; **Appendix Figure 2**; **Appendix Figure 3**). The final hNEIL3 recombinant protein products were stored at -80°C for use as laboratory stocks.

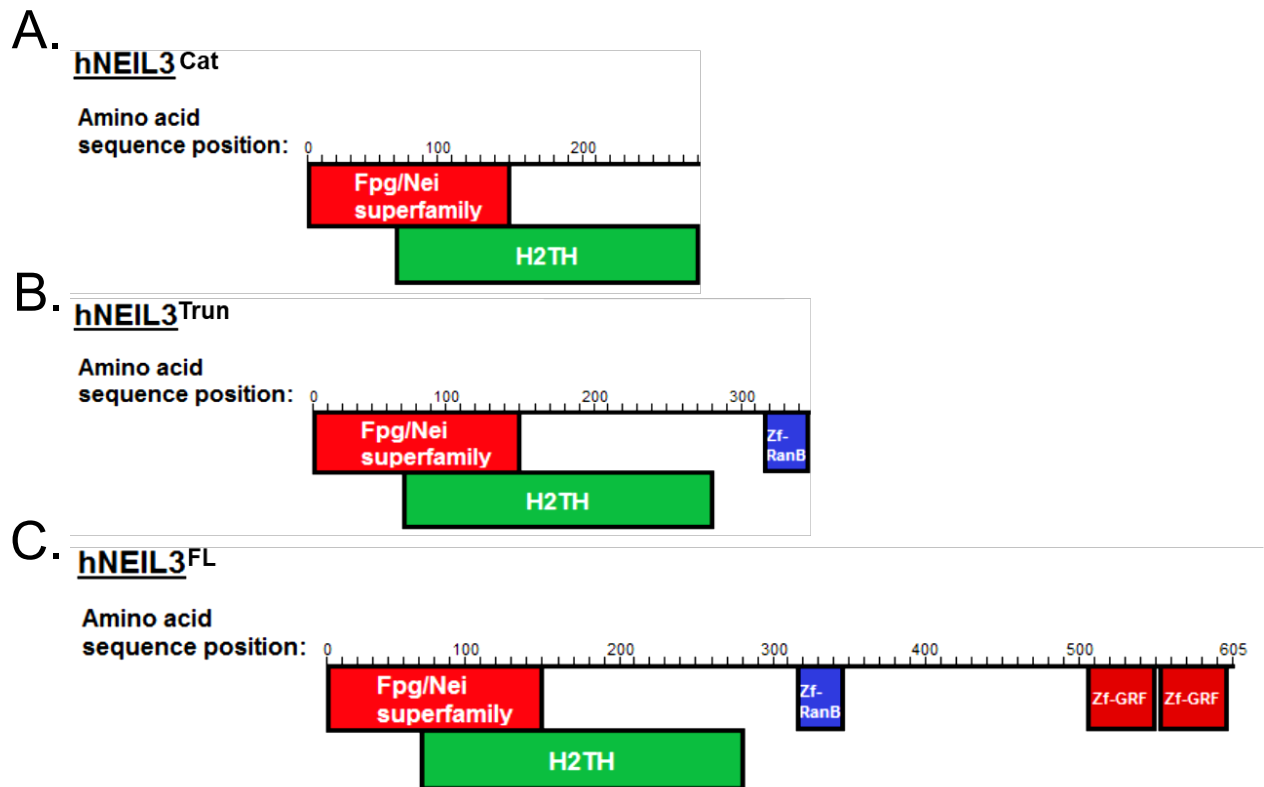


**Figure 1.20: Diagrammatic representation of the hNEIL3 conserved domains encoded by the cDNA cloned into the pETDuet2-*EcoMap*-ORF6 bicistronic expression vector. A. hNEIL3<sup>Cat</sup> 843 bp cDNA truncation encoding 281 amino acids B. hNEIL3<sup>Trun</sup> 1044 bp truncation encoding 348 amino acids and C. hNEIL3<sup>FL</sup> 1818bp full length cDNA sequence and encoding 605 amino acids.**

### 1.16. Hypothesis.

It is hypothesised that the DNA glycosylases hNEIL1 and hNEIL3, or mechanisms that modulate them, play a distinct and fundamental role in replication associated repair of DNA replication blocking lesions. The null hypothesis is that hNEIL1 and hNEIL3, or the mechanisms that modulate them, have no replication associated repair function of replication blocking lesions.

The aims of the presented study are as follows:

1. Determine the alternate activity profiles of recombinant hNEIL1 and hNEIL3 on ss-, ds- and model DNA replication fork structured oligonucleotides substrates possessing oxidative DNA lesions.
2. To use psoralen/UVA treatment to generate MA, three-stranded and four-stranded ICL DNA substrates for the biochemical characterisation of replication blocking interstrand crosslink unhooking by hNEIL1 and hNEIL3.
3. Successfully generate an expression vector, express and purify from *E. coli* a catalytically inactive truncated hNEIL3<sup>Cat</sup> protein for use as control.
4. Characterise hNEIL1, hNEIL3 and catalytically inactive truncated hNEIL3 recombinant protein activity on psoralen/UVA generated DNA oligonucleotides.
5. Conduct *in vitro* ubiquitination assays using previously generated HeLa cell extracts to identify post-translational modification of recombinant hNEIL3<sup>FL</sup>.
6. Use *E. coli* to express and purify an identified E3 ubiquitin ligase to validate specificity of its function in post-translational modification of hNEIL3<sup>FL</sup>.
7. Knockdown an identified E3 ubiquitin ligase in U2OS cells using RNAi, to assess the role it may play in cisplatin resistance and modulation of the hNEIL3 DNA glycosylase.
8. Transiently overexpress NEIL1 and NEIL3 in U2OS cells to assess the role, if any, in cisplatin resistance.
9. Generate a stable U2OS hNEIL3 knockout cell line using CRISPR/Cas9 for use as a model system for the future characterisation of DNA replication associated maintenance.

## 2. Methods.

For the study of the DNA replication associated repair of DNA replication blocking lesions, previously generated active recombinant hNEIL3<sup>FL</sup> protein was used from laboratory stocks (Mustafa Albelazi, University of Salford: **Appendix Figure 2; Appendix Figure 3**) in addition to expressed and purified recombinant hNEIL1 and commercial Nei and Nth (New England Biolabs). These recombinant proteins were used for the biochemical characterisation of DNA glycosylase and associated AP lyase activity to determine distinct preferences for the processing of specific oxidative lesions or structural preferences within a model DNA replication fork oligonucleotide structure. The literature and obtained data prompted the further investigation of hNEIL1 and hNEIL3 unhooking activity in the presence of DNA substrates containing DNA replication blocking psoralen ICLs. Thus, a panel of ss-MA, three- and four-stranded oligonucleotide structures were generated for use as substrates in the comparative biochemical characterisation of hNEIL3<sup>Cat</sup>, hNEIL3<sup>Trun</sup>, hNEIL3<sup>FL</sup> proteins (**Appendix Figure 1; Appendix Figure 2; Appendix Figure 3**), hNEIL1 and Nei psoralen ICL unhooking activity. Site-directed mutagenesis, expression, purification from Rosetta 2 (DE3) *E. coli* expression hosts and confirmation through SDS-PAGE, Immunoblot and liquid chromatography mass spectrometry (LC-MS) proteomic analysis were conducted for the production of a catalytically inactive hNEIL3<sup>Cat-K81A</sup> for use in DNA glycosylase activity control assays. Kinetic analysis was also conducted in a comparative manner between hNEIL1 and hNEIL3<sup>Cat/Trun/FL</sup> proteins on oligonucleotides containing the Sp lesion in ss-DNA and ds-DNA context, then hNEIL1 and hNEIL3<sup>Cat</sup> on three- and four-stranded psoralen ICL oligonucleotide substrates.

The investigation and characterisation of ubiquitin mediated PTM of hNEIL3<sup>FL</sup> through identification of a specific E3 ubiquitin ligase was undertaken, through sequential *in vitro* ubiquitination assays using previously generated FPLC purified HeLa cell fractions, recombinant E1 activating and E2 conjugating enzymes from laboratory stocks. The major E3 ubiquitin ligase activity was determined to be facilitated by TRIM26 and was subsequently expressed and purified by HisTrap FPLC HP column FPLC from Rosetta 2 (DE3) *E. coli* expression hosts. The effect of cellular manipulation by RNAi of TRIM26 on hNEIL1 and hNEIL3 protein levels in the cancer cell line U2OS was investigated through immunoblot in response

to the oxidising agent H<sub>2</sub>O<sub>2</sub> and the ICL inducing agent cisplatin. In addition, the effect of TRIM26 RNAi, hNEIL1 and hNEIL3 overexpression on clonogenic survival of U2OS cells treated with cisplatin was examined. Finally, generation of an U2OS NEIL3<sup>-/-</sup> cell line was undertaken through use of CRISPR/Cas9 and confirmed through anti-NEIL3 immunoblot screening of puromycin resistant U2OS cell extracts.

### 2.1. Transformation of bacterial cloning and expression hosts.

Plasmid DNA constructs were transformed into bacterial hosts for propagation and for recombinant protein expression. Transformation of pETDuet2-*EcoMap*-ORF6-hNEIL3<sup>FL</sup>, pET30a-hNEIL1 and pET28a-TRIM26 into Rosetta 2 (DE3) *E. coli* expression hosts were carried out by the heat shock method, as described in the pET expression system manual, for use in recombinant protein expression (Novagen, 2005). pETDuet2-*EcoMap*-ORF6-hNEIL3<sup>Cat-K81A</sup> was transformed by electroporation into Nova XG cloning host cells and Rosetta 2 (DE3) expression host cells for recombinant protein expression. For electroporation, 20 µl of cell solution was pipetted into an electroporation cuvette, 2 µl of plasmid DNA (1-50 ng/ µl) was added to the cell solution and mixed. Cells were electroporated using the Nucleofector® II (Lonza) and transferred to 200 µl of SOC medium (2% tryptone, 0.5% yeast extract, 10 mM NaCl, 2.5 mM KCl, 10 mM MgCl<sub>2</sub>, 10 mM MgSO<sub>4</sub>, and 20 mM glucose). Cells were then incubated for 60 min at 37°C and 180 rpm for an 1 h outgrowth period. For the propagation of transient mammalian expression vectors pCMV-hNEIL1-Tag3a, pCMV-ac-hNEIL3 and CRISPR/Cas9 plasmid vectors (pCas-Guide-gRNA1/2 and pUC-Donor), cells were transformed via the heat shock method into dh5a chemically competent cells (ThermoFisher). Initially, 1 µl of 1-10 ng/µl of plasmid DNA was mixed with 50 µl of dh5a cells and placed on ice for 30 min. Then, the plasmid cell mix was incubated for 45 s at 42°C. Subsequently, the plasmid cell mix was placed on ice for 2 min, then 950 µl of LB broth was added and then incubated at 37°C for 1 h at 220 rpm. The competent cells were then plated on LB-agar antibiotic selective plates and incubated overnight at 37°C. Single colonies were then selected for upscaling. Colonies were picked with a sterile 1-10 µl pipette tip which was then placed in 4 ml antibiotic selective LB-Broth. The 4 ml culture was then incubated at 37°C at 220 rpm.

For the propagation of plasmid vectors containing the antibiotic resistant gene for ampicillin, 50 µg/ml was used. For kanamycin resistance, 34 µg/ml was used. For recombinant protein

expression 30 µg/ml chloramphenicol was used for selection of the pRARE plasmid contained with Rosetta 2 (DE3) expression hosts.

## 2.2. Recombinant protein expression of hNEIL1, hNEIL3 and TRIM26.

For the expression of recombinant hNEIL1, hNEIL3<sup>FL</sup> and TRIM26 recombinant proteins in *E. coli*, the bacterial expression vectors pET30a-hNEIL1, pETDuet2-*EcoMap*-ORF6-hNEIL3<sup>FL</sup> and pET28a-TRIM26 were transformed via the heat shock method into Rosetta 2 (DE3) expression hosts. For antibiotic selection of expression vectors 50 µg/ml kanamycin antibiotic selection (pET30a-hNEIL1, pET28a-TRIM26) or 100 µg/ml ampicillin (pETDuet2-*EcoMap*-ORF6-hNEIL3<sup>FL</sup>) were used throughout. Cells were selected for on LB-agar plates containing the relevant antibiotic selection, with the addition of 30 µg/ml chloramphenicol and incubated at 37°C overnight. For the expression of each recombinant protein a colony was chosen for culture growth and transferred from LB-agar plates to 4 ml LB broth containing the relevant antibiotics selection. Cultures were incubated overnight at 37°C at 220 rpm. Then 400 µl of bacterial culture was transferred to each of three 40 ml LB broth cultures containing the relevant antibiotic selection, 30 µg/ml chloramphenicol and 0.1% glucose. The culture was then incubated at 37°C at 220 rpm. The culture was monitored for growth with use of a spectrophotometer, where optical density (O.D) was measured at a wavelength of 600 nm and blanked using LB broth. When a 40 ml culture reached an O.D<sub>600</sub> of 0.6-0.8, the total volume of the culture was transferred to 400 ml LB broth containing the relevant antibiotic selection and 0.1% glucose, then incubated at 37°C and 220 rpm. The growth was monitored and at an O.D<sub>600</sub> of 0.6-0.8, the cultures were induced by the addition of 1 mM IPTG. Cultures containing cells possessing the pET30a-hNEIL1 and pETDuet2-*EcoMap*-ORF6-hNEIL3<sup>FL</sup> expression vectors were subsequently incubated at 16°C at 220 rpm for 20 h, whereas those containing the pet28a-TRIM26 expression plasmid were incubated for 3 h at 30°C.

Each culture was then harvested by centrifugation for 10 min at 8000 rpm. Cultures that had been induced for expression of the same recombinant protein were resuspended in 10 ml LB broth and pooled by transferring to a 50 ml tube. Then, the cell suspension was centrifuged at 5000 rpm at 4°C for 20 min. Excess LB broth was discarded and the Rosetta 2 (DE3) cell pellet was stored at -80°C for downstream recombinant protein purification and to aid in cell lysis by the action of freezing and thawing.

### 2.3. Bacterial cell lysis.

For the extraction of bacterial whole cell soluble protein content, previously prepared and induced Rosetta 2 (DE3) expression host cell pellets were thawed to room temperature to commence cell lysis. Bacterial cell pellet was then resuspended in lysis buffer (25 mM Tris-HCl pH 8, 500 mM NaCl, 5% glycerol, 5mM imidazole, 1 µg/ml Leupeptin, chemostatin, pepstatin a, aprotinin and 100 µM phenylmethylsulfonyl fluoride (PMSF)). The bacterial cell suspension was then ultrasonicated at 40% amplitude with 3 x 30 s bursts with 30 s intervals between each burst. The crude cell lysate was then centrifuged at 25,000 rpm for 20 min to facilitate separation of soluble cell lysate and insoluble cell contents. The cell lysate was then sequentially syringe filtered through a 1 µm, 0.44 µm and a 0.22 µm syringe filter, facilitating the removal of high molecular weight cell components. The filtered cell lysate was then stored on ice for immediate purification by FPLC chromatography using the ÄKTA prime FPLC system (GE healthcare).

### 2.4. HisTrap HP column affinity purification.

For the purification of hNEIL1, hNEIL3<sup>FL</sup> and TRIM26 C-terminal 6x Histidine tagged recombinant proteins, purification by use of a 1 ml HisTrap HP column was undertaken. The FPLC buffer pumps A and B were initially washed with dH<sub>2</sub>O using the pump wash basic input to remove the 20% ethanol in which the system is stored in. Subsequently, the 1 ml HisTrap HP column was attached to the FPLC system and washed with 3 column volumes of dH<sub>2</sub>O to remove storage buffer. The pump wash basic protocol was then repeated with the use of buffer A (25 mM Tris-HCl pH 8.0, 500 mM NaCl, 5% glycerol, 5mM imidazole and 100 µM PMSF), followed by washing the HisTrap HP column with 3 column volumes of buffer A. Previously prepared bacterial cell lysate was then transferred to a 50 ml superloop previously rinsed with buffer A. The superloop was then connected to the HisTrap HP column and the Rosetta 2 (DE3) expression host cell lysate was loaded on to the HisTrap HP column at a flow rate of 0.5 ml/min. The flow through was collected simultaneously. After the bacterial cell lysate was loaded on to the column, the superloop was disconnected and the HisTrap HP column was washed with 10 ml buffer A to facilitate the removal of non-specifically bound protein. Then, a 20 ml linear gradient between buffer A and buffer B (25 mM Tris-HCl pH 8.0, 500 mM NaCl, 5% glycerol, 500mM imidazole and 100 µM PMSF) at a flow rate of 0.5 ml/ min

was undertaken, with the system set to elute fractions of 0.5 ml. The FPLC chromatogram was monitored, to determine elution of protein based on UV absorbance at 280 nm.

Fractions which displayed evidence of protein elution based on the FPLC chromatogram were collected and transferred to 1.5 ml microcentrifuge tubes. Five microliters of each fraction were prepared for analysis by mixing with 5  $\mu$ l 3x SDS loading dye (75 mM tris-HCl pH 6.8, 7.5%  $\beta$ - mercaptoethanol, 3% SDS, 30% glycerol, 0.15mg/ml bromophenol blue, 3 mM Ethylenediaminetetraacetic acid (EDTA)) and 5  $\mu$ l dH<sub>2</sub>O. Samples were then incubated for 5 min at 95°C and then analysed by SDS-PAGE.

## 2.5. SDS-PAGE gel preparation.

For the electrophoretic separation of proteins in a sample by electrophoresis sodium dodecyl sulfate polyacrylamide gel electrophoresis (SDS-PAGE) was conducted. SDS gels were produced by initially preparing a separating gel master mix of appropriate volume for the number of gels required (**Table 2.1; Table 2.2**). The separating gel mix was then poured into a gel cassette (Novex) to fill  $\sim$ 3/4 of the cassette volume. Then, the separating gel was overlaid with 1 ml 100% ETOH to remove air bubbles and provide a level edge to the gel. The gel was then incubated for 30 min at room temperature to facilitate gel casting.

The 100% ETOH was then removed and the gel cassette was rinsed with dH<sub>2</sub>O. A 5% stacking gel master mix, of appropriate volume for the required number of gels, was then prepared (**Table 2.1; Table 2.2**) and poured into the inner chamber on top of the separating gel. A well-comb (10/15 wells) was then inserted and the gel was incubated for a further 30 min at room temperature. Once cast, the gel was wrapped in blue paper roll, soaked in dH<sub>2</sub>O, then placed in a sealable plastic bag and stored at 4°C until use.

**Table 2.1: SDS-PAGE gel mixtures for preparation of 8% SDS-PAGE gels.** The volumes indicated are for the production of two SDS-PAGE gels. The separating gel was prepared and cast in advance of the stacking gel. Once stacking gel was poured a 10-well 15-well 1.5 mm width comb was inserted to facilitate well generation.

	<b>5% stacking gel</b>	<b>8% separating gel</b>
<b>Reagent stock</b>	<b>Volume (ml)</b>	<b>Volume (ml)</b>
1M Tris HCl	1.25 (pH 6.8)	7.54 (pH 8.8)
10% SDS	0.1	0.2
0.5 M EDTA	0.040	0.080
Acrylamide (30:0.8)	1.66	5.33
dH <sub>2</sub> O	6.88	6.71
APS	0.100	0.200
TEMED	0.010	0.020
<b>Total volume (ml)</b>	<b>10</b>	<b>20</b>

**Table 2.2: SDS-PAGE gel mixtures for preparation of 10% SDS-PAGE gels.** The volumes indicated are for the production of two SDS-PAGE gels. The separating gel was prepared and cast in advance of the stacking gel. Once stacking gel was poured a 10-well 15-well 1.5 mm width comb was inserted to facilitate well generation.

	<b>5% stacking</b>	<b>10% separating</b>
<b>Reagent stock</b>	<b>Volume (ml)</b>	<b>Volume (ml)</b>
1M Tris HCl	1.25 (pH 6.8)	7.54 (pH 8.8)
10% SDS	0.1	0.2
0.5 M EDTA	0.040	0.080
Acrylamide (30:0.8)	1.66	6.66
dH <sub>2</sub> O	6.88	5.38
APS	0.100	0.200
TEMED	0.010	0.020
<b>Total volume (ml)</b>	<b>10</b>	<b>20</b>

## 2.6. SDS-PAGE.

For the analysis of whole cell extract (WCE) proteins or fractions prepared through FPLC purification, SDS-PAGE analysis was undertaken. An SDS-PAGE gel was prepared in advance and as described in section 2.5. Samples were prepared in 1x SDS loading dye (25 mM Tris-HCl (pH 6.8), 2.5%  $\beta$ -mercaptoethanol, 1% SDS, 10% glycerol, 0.05mg/ml bromophenol blue, 1 mM EDTA) and incubated at 95°C for 5 minutes. A gel stored at 4°C was unwrapped and the well comb was removed. The gel was then rinsed thoroughly with dH<sub>2</sub>O and placed in a SDS-PAGE Mini Gel Tank (ThermoFisher), assembled according to manufacturer's instructions. The inner and outer chamber were then filled with 1 x Tris-glycine SDS (TGS; 25 mM Tris-HCl pH 8.3, 192 mM glycine, 0.1% SDS). Samples were then loaded into the SDS-PAGE gel wells, starting at the second well, followed by loading 2  $\mu$ l of All Blue Prestained Protein Standard (BioRad) or 3  $\mu$ l PageRuler Prestained protein Ladder (ThermoFisher), in the first well of the gel. This was to prevent diffusion of the protein marker stain into the gel prior to electrophoresis. The Mini Gel Tank lid was attached, then connected to a powerpack and electrophoresis was commenced at 125 V for 120 min.

## 2.7. Western-blot transfer.

After electrophoretic separation of protein samples by SDS-PAGE as described in 2.6, transfer of proteins to Immobilon<sup>®</sup>-FL polyvinylidene difluoride (PVDF) membrane (Merk) was conducted, in preparation for immunoblotting. The SDS-PAGE Mini Gel Tank (ThermoFisher) and gel were rinsed thoroughly in dH<sub>2</sub>O. The Immobilon<sup>®</sup>-FL PVDF membrane was activated by rinsing in 100% methanol for 15 s, then cold dH<sub>2</sub>O for 1 min and finally >1 min in cold transfer buffer (20% Methanol, 1x TG (25 mM Tris-HCl pH 8.3, 192 mM glycine). Two transfer sponges and two pieces of filter paper, were soaked in the transfer buffer for >1 min. The SDS-PAGE gel was then removed from the cassette and briefly rinsed in transfer buffer. The western blot transfer sandwich was then prepared in a Mini Blot Module (ThermoFisher; **Figure 2.1**). During assembly excess air was removed from the sponges and the area of contact between the filter paper, gel and PVDF membrane stack, using a western blot roller. The blot module was then closed, transferred to the Mini Gel Tank and the inner chamber of the Mini Blot Module was filled with cold transfer buffer. The outer chamber of the Mini Gel Tank was

filled with cold dH<sub>2</sub>O, the lid then closed, then attached to a powerpack and transfer was conducted by supplying 20 V for 60 min.

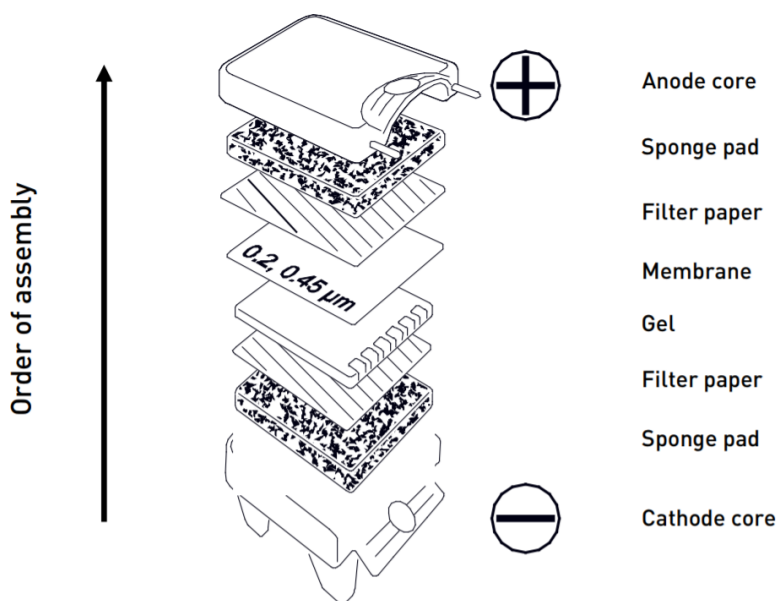


**Figure 2.1: Western blot transfer sandwich assembly** (Figure taken from Mini Blot Module instruction manual, ThermoFisher).

## 2.8. Immuno-blot.

For the probing of specific proteins present in a sample, immunoblot analysis was conducted. After western blot transfer, the Mini Blot module was unassembled and the PVDF membrane was transferred to a western blot incubation box (Licor) and rinsed for 5 min in 1 x phosphate-buffered saline (PBS) to remove acrylamide residue. Then the PBS was discarded and 8 ml of Odyssey blocking buffer:PBS (Licor) was applied and incubated at room temperature for >1 h with rocking at 26 rpm. The blocking buffer was then discarded and 8 ml of Odyssey blocking buffer:PBS (Licor) diluted in 1x PBS at a 1:1 ratio and containing 0.1% Tween-20 with the relevant dilution of primary antibody, was then applied to the membrane and incubated overnight at 4°C with rocking at 26 rpm (**Table 2.3**). The membrane was rinsed three times for 5 min each with 10 ml 1x PBS, 0.1% TWEEN-20 and then 8 ml Odyssey blocking buffer:PBS, diluted in 1x PBS at a 1:1 ratio, containing 0.1% Tween-20 and the relevant dilution of secondary antibody was applied to the membrane and incubated at room temperature for 1 h with rocking at 26 rpm (**Table 2.4**). The membrane was then rinsed three times for 5 min each with 10 ml 1x PBS, 0.1% TWEEN-20, followed by one 5 min wash with 1x PBS. The

membrane was then imaged and quantified using the Licor Odyssey Infrared scanner system and analysis tool.

For analysis of recombinant hNEIL3<sup>Cat-K81A</sup>, immunoblot analysis was conducted using iBlot 2 Nitrocellulose Regular Stacks (ThermoFisher), with the membrane substituted for methanol activated PVDF membrane, for protein transfer using the iBlot 2 dry blotting system (ThermoFisher). PVDF membrane was incubated overnight at 4°C in primary rabbit polyclonal anti-NEIL3 (Proteintech) antibody and 1-2 hours at room temperature with secondary donkey IgG anti-rabbit antibody (Sigma), respectively. Chemiluminescence was induced with SuperSignal West Pico stable peroxide solution and SuperSignal West Pico Luminol enhancer Solution (ThermoFisher scientific). The membrane was imaged using the Amersham Imager 600 (GE healthcare).

**Table 2.3: Primary-antibodies used in this study for probing of specific proteins.** Host-organism, clonality and dilution ratio displayed.

Primary antibody	Host-Organism	Clonality	Dilution ratio
Anti-HisTag (Abcam)	Mouse	Mono-clonal	1:1000
Anti-NEIL1 (Thomas Rosenquist)	Rabbit	Poly-clonal	1:500
Anti-NEIL3 (ProteinTech)	Rabbit	Poly-clonal	1:5000
Anti-actin (Abcam)	Mouse	Mono-clonal	1:20000

**Table 2.4: Secondary-antibodies used in this study for probing of primary-antibodies.** Host-organism, clonality and dilution ratio displayed.

Primary antibody	Host-Organism	Target Isotype	Dilution ratio
Alexa Fluor 680 Anti-Mouse (Invitrogen)	Goat	IgG	1:10000
IR Dye 800 Anti-Mouse (Li-Cor)	Goat	IgG	1:10000
Alexa Fluor 680 Anti-Rabbit (Invitrogen)	Goat	IgG	1:10000
IR Dye 800 Anti-Rabbit (Li-Cor)	Goat	IgG	1:10000
Horseradish Peroxidase Whole Antibody Anti-Rabbit (Amersham)	Donkey	IgG	1:5000

### 2.9. Generation of model replication fork structured oligonucleotide substrates.

For use in DNA glycosylase activity assays, ss-, ds- and DNA replication fork structured oligonucleotide DNA substrates were prepared. For the preparation of a ss oligonucleotide DNA substrate 1  $\mu$ l of 10  $\mu$ M 5'-fluorescently labelled oligonucleotide, 8  $\mu$ l 5 M NaCl and 191  $\mu$ l TE buffer were mixed. For the generation of ds and model DNA replication fork structured oligonucleotide substrates 1  $\mu$ l of 10  $\mu$ M 5'-fluorescently labelled oligonucleotide, 1.5  $\mu$ l of unlabelled complementary oligonucleotide, 8  $\mu$ l 5 M NaCl and 189.5  $\mu$ l TE buffer were mixed. DNA oligonucleotide mixtures containing labelled and complementary oligonucleotides were incubated at 95°C for 3 min in a heat block, then the heat block was turned off and allowed to cool slowly to room temperature, facilitating annealing of complementary oligonucleotides. The 5'-fluorescently labelled oligonucleotide contained one of three modified bases, either a 5-OHU, 8-OxoG or a Tg lesion. Excision of the modified base by DNA glycosylase activity followed by associated AP lyase activity would be visualised by electrophoretic separation and imaging. The 5'-fluorescent tag for the 5-OHU containing oligonucleotide was Alexa Fluor 680. The 5'-fluorescent tag for the 8-OxoG and Tg containing oligonucleotide was IR Dye 700. The complementarity of the complement oligonucleotide sequence was altered to facilitate the generation of uncomplemented regions of DNA to produce a model DNA replication fork structured oligonucleotide substrate after annealing. These substrates were termed '-4', 'Fork' and '+4', where the name denoted the position of the 5-OHU, 8-OxoG or Tg lesion relative to the fork junction (**Table 2.5**).

**Table 2.5: DNA Oligonucleotide sequences and model DNA replication fork oligonucleotide structures used in BER assays.** 'X' denotes the position of the 5-OHU, 8-OxoG and Tg oxidative DNA lesions. DNA substrates are 39 mer in length, DNA glycosylase mediated cleavage yields a 19 mer cleavage product.

Oligonucleotide name	Oligonucleotide sequence	Oligonucleotide structure
-4	<p><b>Fluorescently labelled DNA oligonucleotide sequence:</b> 5'-ATCTACCGAGTCCGTC CGA<b>X</b>CACGCTTATTGG CTACCGA-3'</p> <p><b>Complementary DNA oligonucleotide sequence:</b> 5'-GAATGCATTCCGCCAT CGATATCGACGGACTC GGTAGAT-3'</p>	
Fork	<p><b>Fluorescently labelled DNA oligonucleotide sequence:</b> 5'-ATCTACCGAGTCCGTC CGA<b>X</b>CACGCTTATTGG CTACCGA-3'</p> <p><b>Complementary DNA oligonucleotide sequence:</b> 5'-GAATGCATTCCGCCAT CGAGTCGGACGGACT CGGTAGAT-3'</p>	
+4	<p><b>Fluorescently labelled DNA oligonucleotide sequence:</b> 5'-ATCTACCGAGTCCGTC CGA<b>X</b>CACGCTTATTGG CTACCGA-3'</p> <p><b>Complementary DNA oligonucleotide sequence:</b> 5'-GAATGCATTCCGCCAC GTGGTCGGACGGACTC GGTAGAT-3'</p>	

### 2.10. Radioactive labelling of DNA oligonucleotide substrates.

For use in enzymatic assays, oligonucleotides were radioactively labelled with the phosphorus isotope  $^{32}\text{P}$ . A reaction mixture of 1  $\mu\text{M}$  of oligonucleotide was incubated at 37°C for 40 min in 1x polynucleotide kinase buffer (PNKP buffer A (ThermoFisher)), 10 units of polynucleotide kinase (PNKP; ThermoFisher), 1  $\mu\text{l}$   $\gamma$   $^{32}\text{P}$  ATP and sterile  $\text{dH}_2\text{O}$  to the final reaction volume of 30  $\mu\text{l}$  was prepared. The reaction was then desalted by preparing a spin column from a 0.5 ml microcentrifuge tube pierced with a sterile needle and placed in a 2 ml microcentrifuge tube, 400  $\mu\text{l}$  of G25 sedaphex dissolved in  $\text{dH}_2\text{O}$  was then added to the 0.5 ml tube and the column was centrifuged for 2 min at 4000 rpm. The 2 ml microcentrifuge tube containing the flow through was discarded. The spin column was then transferred to a 1.5 ml microcentrifuge tube, then the labelled oligonucleotide sample was loaded on the spin column and centrifuged for 3 min at 4000 rpm, to facilitate the removal of excess  $\gamma$   $^{32}\text{P}$  ATP. The labelled oligonucleotide in the flow through was then stored at -20°C under appropriate radioactive protection conditions.

### 2.11. Annealing of DNA oligonucleotide substrates.

Complementary synthetic oligonucleotide substrates were selected based upon the DNA lesions they would harbour once annealed (**Appendix Table 1**). Annealing of oligonucleotides was achieved with the addition of complement non-labelled oligonucleotides at a molar ratio of 1:1.2 of 5'  $\gamma$   $^{32}\text{P}$  labelled to complement oligonucleotide, in 20 mM KCl and 10 mM HEPES-KOH pH 7.6. Samples were then incubated at 95°C for 5 minutes to facilitate denaturing and gradient cooled at -0.5°C/30 s for up to 160 cycles in a thermocycler, unless otherwise stated. Products were stored at -20°C, until required for use in enzymatic assays.

### 2.12. Psoralen induced DNA interstrand crosslinked oligonucleotide generation.

Annealed complementary DNA oligonucleotides containing a single 5'-TpA-3' site were incubated at room temperature in the dark with 500 nM HMT or 8-MOP dissolved in ~100% chloroform. Reaction mixtures were then transferred to a small petridish lined with Parafilm and irradiated at 365 nm and 240  $\text{kJ}/\text{m}^2$  for 30 min (HMT) or 60 min (8-MOP) on ice. After

irradiation the final volume was adjusted to 100  $\mu$ l with dH<sub>2</sub>O. Samples were then collected and stored at -20°C under radioactivity safe conditions until required for use in enzymatic assays or further construct preparation and analysis.

### **2.13. Denaturing PAGE.**

To analyse DNA oligonucleotide substrate cleavage resulting from the DNA glycosylase and AP lyase activity of recombinant proteins or ICL generation and separation under denaturing conditions, denaturing PAGE was carried out.

For 10% denaturing PAGE analysis, denaturing PAGE gel mixture (16.8 g of Urea, 10 ml of 40% Bis-Tris acrylamide, 8 ml of 5 x tris-borate EDTA (TBE) buffer (450 mM Tris-borate pH 8.3, 10 mM EDTA) and made to a final volume of 40 ml with dH<sub>2</sub>O) was prepared and incubated at 37°C for 30 min. Then two glass plates were assembled with two 1.5 mm gel casting spacers and placed in the casting position in a SE400 electrophoresis unit (Hoefer). At this stage, 250  $\mu$ l of 10% APS was added to the denaturing PAGE mixture and vortexed, followed by the addition of 20  $\mu$ l tetramethylethylenediamine (TEMED) and then mixed using a vortex.

The 10% denaturing PAGE mixture was then poured between the glass plates and a 10-well 1.5 mm well comb was placed between the plates. The gel was left to cast at room temperature for 45 min. Then, the gel comb was removed, and the wells were rinsed with dH<sub>2</sub>O. The gel was then pre-ran for 30 min at 300 V in 1x TBE. Samples containing fluorescently labelled oligonucleotides were prepared by the addition of 5  $\mu$ l 99% formamide/1% bromophenol blue and incubated at 95°C for 5 min. Samples were then loaded and separated by electrophoresis for 1 h 45 min at 300 V. The gel was then removed and imaged using the Odyssey infrared scanner (Licor).

For 20% denaturing PAGE the PROTEAN II xi (BioRad) PAGE glass plate sandwich was assembled using a 20 cm x 20 cm inner and 22.3 cm x 20 cm outer glass plates, two 1.5 mm gel spacers and two sandwich clamps (BioRad). The glass plate sandwich was laid flat on a level surface with the aid of a spirit level. The 20% denaturing PAGE gel mix was prepared in a 50 ml tube (**Table 2.6**).

**Table 2.6: Denaturing PAGE gel mixture for preparation of a 20% denaturing PAGE.** The volumes indicated are for the production of one denaturing page gel.

	<b>20% denaturing PAGE gel</b>
<b>Reagent stock</b>	<b>Volume (ml)</b>
~21.17% Bis-Tris acrylamide/7.5 M Urea mix	28.5
10x Tris Borate EDTA (TBE)	1.5
20% Ammonium persulfate (APS)	0.15
TEMED	0.015
<b>Total volume (ml)</b>	<b>30.165</b>

The solution was vortexed to mix and slowly pipetted between the glass sandwich plates, preventing formation of air bubbles by tapping the glass plates. A 20 well 1.5 mm comb was then inserted at the top of the glass plate sandwich and incubated at room temperature between 45 min to 1 h, to facilitate casting. The well comb was then removed, and the wells washed using sterile dH<sub>2</sub>O. The wells were then dried by swinging the sandwich in a downward motion to expel excess dH<sub>2</sub>O. The cassette was then attached to the Protean II xi electrophoresis tank cooling core, connected to a water bath at 42°C, with a buffer dam attached and was then placed into the inner chamber of the tank containing 0.5x TBE buffer. The inner chamber between the gel sandwich cooling core and buffer dam was filled with 0.5x TBE buffer. Electrophoresis was then conducted at 600 V for 1 h, to homogenise the urea in the gel. Samples were then loaded, and electrophoretic separation was commenced at 600 V for 2 h.

After, the gel was removed from the tank and the outer glass plate was removed. The denaturing PAGE was wrapped in cellophane and subsequently exposed to a phospho-screen and imaged using the Typhoon FLA 9500 scanner (GE healthcare).

#### **2.14. Non-denaturing PAGE.**

To analyse DNA constructs under native conditions, a 5% non-denaturing PAGE was carried out. The glass plate sandwich was assembled as described in Section 2.13. The 5% non-denaturing gel solution was prepared in a 50 ml tube (**Table 2.7**).

**Table 2.7: Non-denaturing PAGE gel mixture for preparation of a 5% denaturing PAGE.** The volumes indicated are for the production of one denaturing page gel.

	<b>5% non-denaturing PAGE gel</b>
<b>Reagent stock</b>	<b>Volume (ml)</b>
40% Bis-Tris Acrylamide	6
10 x Tris-glycine (TG)	3
20% Ammonium persulfate (APS)	0.15
TEMED	0.014
dH <sub>2</sub> O	20.85
<b>Total volume (ml)</b>	<b>30.014</b>

The solution was vortexed and pipetted between the inner and outer glass plates, preventing formation of air bubbles by tapping the glass plates. A 20 well 1.5 mm comb was then inserted at the top of the glass plates and was incubated at room temperature for between 1-2 h, to facilitate casting. The well comb was then removed, and the wells were rinsed using sterile dH<sub>2</sub>O. The wells were then dried by swinging the cassette in a downward motion to expel excess dH<sub>2</sub>O. The cassette was then inserted into a PROTEAN II xi electrophoresis tank at 4°C, and the inner chamber was filled with 1x Tris-glycine (TG). Gel electrophoresis was ran for 2 h at 80 V, to remove excess ammonia persulfate ions and unpolymerised acrylamide in the gel. Samples were prepared with 6 µl 80% glycerol, 1x DNA gel loading dye (ThermoFisher) and varying volume of DNA oligonucleotide constructs that were adjusted to an equivalent radioactivity count using a Geiger-Muller counter. Electrophoresis was commenced at 80V, samples were then loaded and separated for a further 12 h.

After, the gel sandwich was taken out of the tank and one of the glass plates was removed. The non-denaturing PAGE was wrapped in cellophane, then exposed to a phospho-screen and imaged using the Typhoon 9500 scanner.

### **2.15. Single stranded mono-adducted oligonucleotide generation.**

The oligonucleotides R18 and D21 (**Appendix Table 1**) were annealed and crosslinked as previously described in Sections 2.11 and 2.12 . The product was then digested with 10 units of RNase A (ThermoFisher) in 1 x RNase A reaction buffer (ThermoFisher) at 37°C for 20 h. The subsequent product was then purified from denaturing PAGE.

### 2.16. Oligonucleotide purification from 20% denaturing PAGE.

For the purification of ICL duplex DNA oligonucleotides, 105.3 pmol was separated by 10% denaturing PAGE. After, the gel was exposed to an X-ray film (Fujifilm) for 10 min in the dark. The film was then developed using an X-Ray developer. Bands corresponding to ICLs were then cut out from the film to generate a template. The template film and sterile scalpels were used to excise polyacrylamide strips containing the ICL DNA bands. The polyacrylamide gel strips were incubated in a 2 ml microcentrifuge tube in 170  $\mu$ l of dH<sub>2</sub>O overnight at 37°C and 600 rpm. Then, 1400  $\mu$ l of 2% LiClO<sub>4</sub> was added to the 170  $\mu$ l of dH<sub>2</sub>O in a separate 2 ml microcentrifuge tube. The samples were then incubated at -20°C overnight. Then the samples were centrifuged at 20000  $xg$  for 10 min. The supernatant was removed and 200  $\mu$ l of 100% ETOH was added to each sample and centrifuged for 5 min at 20000  $xg$ . The supernatant was removed and 200  $\mu$ l of 70% ETOH was added to each sample and centrifuged for a further 5 min at 20000  $xg$ . Then the supernatant was discarded and the samples were incubated for ~1 h at room temperature to facilitate evaporation of excess ETOH, leaving behind the DNA precipitate. The DNA ICL precipitate was then re-suspended in 50  $\mu$ l of dH<sub>2</sub>O, mixed and incubated at -20°C under appropriate radioactivity safe conditions. A Geiger-Muller counter was used to record radioactivity before and after purification for the calculation of the approximate concentration of duplex DNA ICL oligonucleotide purified. Purified samples were subsequently used for further DNA ICL structure construction.

### 2.17. Three-stranded and Four-stranded DNA ICL construction.

After the purification of the duplex DNA ICL oligonucleotide from 10% denaturing PAGE, complementary non-labelled DNA to the larger oligonucleotide strand in the ICL substrate, was added at an approximate molar ratio of 1:1.2 of ICL to complement oligonucleotide. The reaction mix was incubated at 95°C for 5 min and gradient cooled at -0.5°C/30 s for up to 160 cycles using a thermocycler. This facilitated the annealing of the complementary strand to the ICL construct, effectively flipping out the ICL at the side of the smaller oligonucleotide, creating a three-stranded ICL structure mimicking the repair intermediate generated during FA pathway initiated repair of an ICL (**Figure 1.10**; **Figure 2.2**). For the generation of four-stranded DNA ICL oligonucleotide substrates, an oligonucleotide complementary to the small oligonucleotide strand, 'flipped out', was added at an approximate molar ratio of 1:1.2 of

three-stranded ICL oligonucleotide to complementary oligonucleotide (**Figure 2.2**). The reaction mix was then incubated at 65°C for 5 minutes and gradient cooled for 80 cycles.

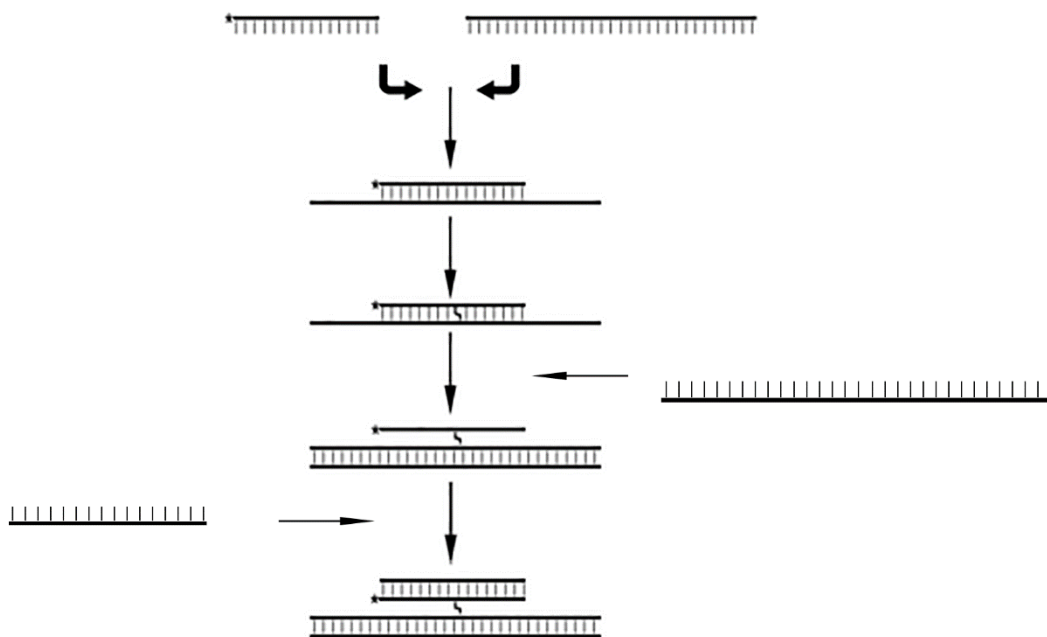


**Figure 2.2: Schematic representation of three-stranded and four-stranded DNA ICL oligonucleotide substrate generation.** '\*' denotes the position of  $\gamma$   $^{32}\text{P}$  labelling.

Confirmation of three-stranded and four-stranded DNA ICL substrates was carried out by 10% denaturing page and 5% non-denaturing PAGE analysis. The gel was exposed to a phosphoscreen overnight and imaged using the Typhoon FLA 9500 scanner. Oligonucleotide structures were stored at -20°C under radioactivity safe conditions.

### 2.18. DNA glycosylase cleavage assay.

To analyse enzymatic activity of hNEIL3<sup>Cat</sup>, hNEIL3<sup>Trun</sup>, hNEIL3<sup>FL</sup>, hNEIL1 and Nei, cleavage assays were undertaken. DNA glycosylases were diluted to working concentration in RDWB buffer (25 mM HEPES pH 7.9, 100 mM KCl, 12 mM MgCl<sub>2</sub>, 1 mM EDTA, 17% glycerol and 2 mM DTT) and were incubated with 5 nM of 5'fluorescently labelled oligonucleotide DNA substrate for 1 h at 30 °C in the reaction mixture 40 mM HEPES pH 7.8, 5 mM MgCl<sub>2</sub>, 0.1 mM EDTA, 0.5 mM DTT, 2 mM ATP, 0.1 mg/ml BSA in a final volume of 10  $\mu\text{l}$ . Reactions were stopped with the addition of 100% formamide/bromophenol blue and analysed by 10% denaturing-PAGE and subsequently imaged using the Odyssey infrared imaging system (Licor).

Previously prepared oligonucleotides labelled with  $^{32}\text{P}$ , containing ICL DNA lesions, were incubated with reaction specific concentrations of enzyme, diluted in RDWB buffer and 1x reaction buffer (25 mM HEPES-KOH- KOH pH 7.6, 100 mM KCl, 1 mM EDTA, 1 mM DTT and 100  $\mu\text{g}/\text{ml}$  bovine serum albumin (BSA)) for 30-60 min at 37°C. Reactions were stopped either by the addition of 0.2% SDS and 4 mM EDTA or were incubated for a further 30 min at 37°C in the presence of 10% piperidine, to cleave AP sites through  $\beta$ -elimination (light piperidine treatment; Couvé-Privat *et al.*, 2007; Couvé *et al.*, 2009). The reaction was then stopped with the addition of 20 mM EDTA and neutralised with 40 mM HCl. For size marker controls 10 nM D21-U and C47-U oligonucleotides were incubated with 10 nM UDG from laboratory stocks for 10 min at 37°C. The product was then incubated with 10% piperidine for 30 min at 37°C and then 20 mM EDTA was added and the reaction was neutralised with 40 mM HCl to generate an 8/23<sup>PA</sup>mer cleavage product processed through  $\beta$ -elimination. Alternatively, the UDG incubation product was incubated with 10% piperidine and incubated at 95°C for 5 min to facilitate the generation of an 8/23<sup>P</sup>mer cleavage product processed through  $\beta,\delta$ -elimination (hot piperidine treatment). Finally, UDG incubation product was alternatively incubated with 20 nM of recombinant Nfo from laboratory stocks at 37°C for 15 min, to generate an 8/23<sup>OH</sup>mer cleavage product. This facilitated the generation of a panel of size marker controls for comparison with hNEIL1, hNEIL3 and Nei cleavage products.

Samples were then desalted using a spin column prepared by piercing a 0.5 ml tube with a syringe needle, then placed in a 2 ml tube. Then, 400  $\mu\text{l}$  of G25 sedaphex dissolved in 7.5 M urea/ bromophenol blue was added and the tube centrifuged for 2 min at 4000 rpm, the flow through was subsequently discarded. The spin column was then transferred to a 1.5 ml tube and the enzymatic assay product was loaded on the column and centrifuged for 3 min at 4000 rpm. The product was then analysed by 10% denaturing PAGE.

### **2.19. Kinetic analysis of hNEIL1 and hNEIL3 recombinant proteins.**

To study the kinetics of hNEIL3 and hNEIL1 dependent DNA lesion substrate cleavage, comparative time course assays were undertaken in the presence of 10 nM of the DNA substrate Sp1 in ss-DNA and ds-DNA context. Then, in the presence of  $\sim 10$  nM of XL47 • 47 - 21\* and XL47 • 47 - 21\* • 21 ICL DNA substrates using hNEIL3<sup>Cat</sup> and hNEIL1. Enzyme concentrations were titrated and analysed with the use of ImageGuage V4.0 (Fujifilm) to

select an appropriate enzyme concentration over a range of 5-500 nM, within the linear range of the retrieved data.

Subsequently, reactions were carried out as described in section 2.18, however time course and DNA glycosylase concentrations were adjusted based on the DNA glycosylases and the oligonucleotide substrate used. Reaction samples were stopped as described in section 2.18 and analysed by 20% denaturing PAGE as described in Section 2.13. Typhoon 9500 scanner images were then analysed with use of ImageGuage V4.0 (Fujifilm), comparing cleavage product values minus the relative background value, to the total sample value minus relative background value, converted to a final percentage.

## **2.20. Generation of hNEIL3<sup>Cat-K81A</sup> catalytically inactive recombinant protein bacterial expression vector.**

The expression vector pETDuet2-*EcoMap*-ORF6-hNEIL3<sup>Cat</sup> was targeted for site-directed mutagenesis to generate the pETDuet2-*EcoMap*-ORF6-hNEIL3<sup>Cat-K81A</sup> expression vector to express the catalytically inactive glycosylase domain of hNEIL3.

The identified nucleotides targeted for site-directed mutagenesis were at nucleotide positions 241 of the hNEIL3<sup>Cat</sup> cDNA, to convert adenine to a guanine and at nucleotide position 242 of the hNEIL3<sup>Cat</sup> cDNA to convert adenine to cytosine. At the amino acid level this would encode a substitution of lysine 81 to alanine, previously described by Krokeide *et al.* (2013) to remove the DNA glycosylase and AP lyase activity of hNEIL3.

The following mutagenic primers were designed using the online Agilent technologies primer design tool (<http://www.genomics.agilent.com/primerDesignProgram.jsp>) and are displayed in **Table 2.8**.

**Table 2.8: Mutagenic primers used for site-directed mutagenesis, converting A-G at nucleotide position 241 and A-C at nucleotide position 242 of hNEIL3 cDNA.** Primers are underlined, and targeted bases are underlined, italicised and highlighted in yellow.

Primer name	Primer-Template Duplex
a241g_a242c Forward	5' - <u>tggcgtggaaactttggggg</u> <u>cgagctctttatgtacttt</u> - 3'     gtcaccgcacctttgaaacccc <u>tt</u> cctcgagaaatacatgaaacct
a241g_a242c Reverse	cagtggcgtggaaactttgggg <u>aa</u> ggagctctttatgtactttgga     3' - <u>accgcacctttgaaacccc</u> <u>gcctcgagaaatacatgaaa</u> - 5'

Mutagenesis was carried out by preparing a stock master mixture of 1x Pfu Ultra high-fidelity reaction buffer (Agilent technologies), 25 ng of template plasmid DNA (pETDuet2-*EcoMap*-ORF6-hNEIL3<sup>Cat</sup>), 6 μM of a241g\_a242c forward primer, 6 μM of a241g\_a242c reverse primer and 0.6 mM dNTP mix. Then, a working reaction mixture was prepared containing 6.73 μl of the master mixture, 0.1 mM of dNTP mix, 1.75 units of Pfu Ultra DNA polymerase and made to a final volume of 20 μl with dH<sub>2</sub>O. Thermocycling conditions (**Table 2.9**) were carried out to facilitate site directed mutagenesis and amplification of a pETDuet2-*EcoMap*-ORF6-hNEIL3<sup>Cat-K81A</sup> synthetic vector. The reaction product was then digested by preparing a reaction mixture containing 16 μl PCR product, 1x Cutsmart buffer (New England Biolabs) and 5 units of DpnI restriction endonuclease (New England Biolabs), subsequently incubated for 1 h 20 mins at 37°C, then 20 min at 80°C. This resulted in the digestion of the template plasmid DNA and inactivation of DpnI restriction endonuclease. Then, 2 μl of digested product was transformed via the electroporation method in to Nova XG cells, previously described in section 2.1 and upscaled for growth in LB broth containing 100 μg/ml ampicillin. Plasmid DNA was then purified via the Nucleospin Plasmid miniprep kit (Macherey-Nagel) following manufacturer instructions and sequenced using the GATC *SUPREME*run sequencing kit (GATC Biotech). Mutagenesis was confirmed by sequencing chromatogram analysis.

**Table 2.9: Thermocycling conditions used for site-directed mutagenesis and synthetic vector generation via PCR.**

Step	Temperature (°C)	Time (s)	Cycles
<b>Initial denaturation</b>	98	120	1
<b>Denaturation</b>	98	20	21
<b>Annealing</b>	58.5	30	
<b>Extension</b>	72	240	
<b>Final Extension</b>	72	600	1

### 2.21. Recombinant hNEIL3<sup>Cat-K81A</sup> expression and protein purification.

After confirmation of the construction of the expression vector pETDuet2-*EcoMap*-ORF6-hNEIL3<sup>Cat-K81A</sup>, Rosetta 2 (DE3) expression hosts were transformed by the electroporation method as previously described in section 2.1. Colonies were selected and grown overnight at 37°C with 200 rpm shaking in 4 ml LB broth under 50 µg/ml ampicillin, 34 µg/ml chloramphenicol antibiotic selection. Subsequently, 400 µl of overnight culture was used to inoculate each of three 40 ml LB broth cultures, then grown at 37°C with 200 rpm shaking to an O.D<sub>600</sub> of 0.6-0.8 under 50 µg/ml ampicillin, 34 µg/ml chloramphenicol antibiotic selection. The entirety of the three 40 ml cultures was used to inoculate three 400 ml LB broth cultures under 50 µg/ml ampicillin antibiotic selection, then grown at 37°C with 200 rpm shaking to an O.D<sub>600</sub> of 0.6-0.8. At this stage, cultures were induced with 1 mM IPTG and incubated for 20 h at 16°C.

Cells were then pelleted by centrifugation at 8000 *xg* for 10 minutes and then the excess LB broth was discarded. Then 10 ml of LB broth was used to resuspend the cells from all three cultures, to transfer cells to a 50 ml falcon tube and pellet by centrifugation for 10 min at 8000 *xg*. The excess LB broth was then discarded, and the cell pellet was stored overnight at -80°C, to aid in cell lysis. Thirty millilitres of lysis buffer (25 mM Tris-HCl pH 8.0, 500 mM NaCl, 5% glycerol, 5 mM imidazole, 1 µg/ml leupeptin, 1 µg/ml chemostatin, 1 µg/ml pepstatin, a 1 µg/ml aprotinin, 0.33 mM PMSF) was added to the thawed cell pellet and sonicated for 60 s in bursts of 15 s with 30 s intervals between each burst. The cell lysate was then centrifuged

at 25,000 rpm for 30 min at 4°C to separate insoluble and soluble cell components. FPLC protein purification using a HisTrap HP column and the ÄKTA Prime FPLC was undertaken as described in section 2.2.

Fractions were then analysed by 10% SDS-PAGE and anti-NEIL3 immunoblot (Proteintech). Protein fractions of relative target protein purity were pooled and concentrated to ~0.5 ml using an Amicon Ultra-15 centrifugal filter with a 10 kDa cut off (Merk). The hNEIL3<sup>Cat-K81A</sup> candidate protein band was sent for liquid chromatography mass-spectrometry (LC-MS) analysis, with reference to the hNEIL3<sup>Cat</sup> protein band (Mustafa Albelazi, University of Salford). The Esi-Quad-TOF instrument and MS/MS Ion search were used, with a significance threshold of  $p < 0.0104$  and an Ion score or cut off of 25.

### **2.22. Protein-DNA covalent complex formation, 'Schiff base' affinity assay.**

Reactions were prepared as stated previously in Section 2.18, but with the addition of 50 mM NaBH<sub>4</sub> prior to incubation at 37°C. The reactions were then stopped by the addition of 1x RunBlue LDS Sample Buffer (Expedeon) and 10 mM DTT, then incubated for 10 min at 70°C. Samples were then analysed by electrophoretic separation at 125V for 120 min on a RunBlue SDS precast protein gel (10%). The gel was subsequently exposed to a phospho-screen and imaged using the Typhoon 9500 scanner.

### **2.23. Characterisation of E3 ubiquitin ligase from HeLa cells and *in vitro*.**

For the identification of a hNEIL3<sup>FL</sup> interacting E3 ubiquitin ligase, previously prepared and sequentially purified HeLa cell extracts fractionated by phosphocellulose, HiLoad Mono Q Sepharose Ion exchange, Superdex 200 HR 10/30 size exclusion, 1 ml CHT ceramic hydroxyapatite column and Mono Q 5/50 GL were used (Williams and Parsons, 2018). Laboratory stocks of each fraction were then analysed by *in vitro* ubiquitination assays for the identification of ubiquitination activity.

### 2.23.1. *In vitro* ubiquitination assay.

To identify *in vitro* PTM of recombinant hNEIL3<sup>FL</sup> by ubiquitin, *in vitro* ubiquitination assays were undertaken. The following previously purified recombinant proteins were mixed to form an E1, E2 and ubiquitin protein reaction master mix (**Table 2.10**):

**Table 2.10: Ubiquitin cascade recombinant protein master mix.** Wild type Ubiquitin (Boston biochemicals, Cambridge, USA), GST-E1 activating enzyme, E2 conjugating enzymes (UbcH3-UbcH10).

Recombinant protein	Stock solutions	1 reaction (µl)	10 reactions µl
Ubiquitin (5 µg)	10 mg/ml	0.5	5
E1 (100 ng)	1.9 mg/ml	0.052	0.52
UbcH2 (40 ng)	0.975 mg/ml	0.041	0.41
His-UbcH3 (40 ng)	0.26 mg/ml	0.153	1.53
UbcH5a (40 ng)	0.478mg/ml	0.083	0.83
UbcH5b (40 ng)	0.980 mg/ml	0.041	0.41
UbcH5c (40 ng)	0.380 mg/ml	0.105	1.05
His-UbcH6 (40 ng)	1.02mg/ml	0.039	0.39
UbcH7 (40 ng)	0.710 mg/ml	0.056	0.56
UbcH8 (40 ng)	0.4 mg/ml	0.1	1
His-UbcH10 (40 ng)	0.240 mg/ml	0.166	1.66
dH <sub>2</sub> O		0.314	3.14
<b>Total</b>		1.65	16.5

Individual reaction mixtures were prepared in 50 mM Tris-HCl pH 8.0, 5 mM MgCl<sub>2</sub> 200 µM CaCl<sub>2</sub>, 1 mM DTT, 10 µM MG-132, 4 mM ATP with the addition of 5 µg ubiquitin, 100 ng recombinant E1, 40 ng of each E2, 600 ng of recombinant hNEIL3<sup>FL</sup> and 1-3 µl of fractionated HeLa WCE. Reactions were made to a final volume of 15 µl with dH<sub>2</sub>O.

Reaction mixtures were then incubated for 60 min at 30°C and 800 rpm. The reaction was then stopped with the addition of 7.5 µl of 3x SDS loading dye, followed by 5 min incubation at 95°C. Samples were then analysed by 8/10% SDS-PAGE and anti-NEIL3 immunoblot analysis.

HeLa WCE fractions displaying ubiquitination activity were previously pooled and concentrated with an Amicon Ultra-15 Centrifugal Filter Unit with a 10 K cut off. The final MONO Q 5/50 GL purification fraction identified for E3 ubiquitin ligase activity was then sent for LCMS tandem mass spectrometry analysis by tandem mass spectrometry using a Q Exactive instrument operated in data-dependent positive (electrospray ionization+ [ESI+])

mode as previously described (**Appendix Table 5**; Edmonds *et al.*, 2017; Williams and Parsons, 2018).

## **2.24. Mammalian cell line culture.**

The osteosarcoma cell line U-2 OS (U2OS) was used for the investigation of the cellular role of hNEIL1 and hNEIL3 in resistance to the ICL inducing agent cisplatin and the role of the E3 ubiquitin ligase, TRIM26, in the modulation of hNEIL1 and hNEIL3 protein levels.

### **2.24.1. Thawing cells.**

U2OS cells were thawed by submerging a cryovial containing 1ml Dulbecco's modified eagle medium (DMEM; 10% FBS, 1% penicillin/streptomycin, 2 mM L-glutamine, 1% non-essential amino acids), 10% DMSO, U2OS cell mixture in a water bath at 37°C for <1 min. Then, 1ml of DMEM medium was added to the cryovial and the cell suspension was mixed by pipetting. The cell suspension was then transferred to a 15 ml tube and centrifuged at 1500 rpm for 3 min, the DMEM medium was removed and replaced with 1 ml DMEM. The cell pellet was then resuspended and transferred to a T75 cell culture flask containing 10 ml DMEM medium. The T75 flask was then incubated at 37°C in 5% CO<sub>2</sub>.

### **2.24.2. Splitting cells.**

T75 flasks containing cells were periodically inspected under a light microscope to determine approximate confluence. At 70-90% confluency DMEM medium was removed from a T75 flask containing U2OS cells using an aspirator, then rinsed with 10 ml Dulbecco's phosphate buffered saline (DPBS) and incubated for 5 min in 1 ml 1 x trypsin EDTA (0.12 % trypsin, 0.02% EDTA) at 37°C in 5% CO<sub>2</sub>. The flask was then viewed under a light microscope to determine that all adherent cells had detached. Then, 9 ml of DMEM medium was added to the flask to neutralise the trypsin and mixed by pipetting to aid in the dissociation of individual cells. At this stage, 10 ml DMEM was added to a new T75 flask and a volume of U2OS cell suspension was transferred to the new flask, based on desired split ratio relative to the 10 ml final volume of the cell suspension. This method of splitting was conducted in the same manner with adjusted volumes based on target vessels ( **Table 2.11**).

**Table 2.11: Splitting regime of adherent cells based on target vessel for continuous culture.**

Vessel type	DPBS volume (ml)	1x Trypsin EDTA volume ( $\mu$ l)	Neutralising DMEM medium volume (ml)
T75	10	1000	9
T25	10	1000	9
96-well plate (individual well)	0.100	10	0.09
24-well plate (individual well)	0.500	50	0.45
6-well plate (individual well)	2	100	0.9
35 mm tissue culture dish	2	100	0.9
10 cm tissue culture dish	8	1000	7

### 2.24.3. Freezing cells and long-term storage

For long term storage of U2OS cells at  $-80/195^{\circ}\text{C}$  cells were brought into suspension following normal procedure outlined in section 2.24.2, neutralised with DMEM medium and transferred to a 15 ml tube. The cell suspension was then centrifuged at 1500 rpm for 3 min. The medium was then removed, and the cell pellet was resuspended in 1 ml 90% FBS/10% DMSO. The cell suspension was then transferred to a cryovial and placed in a 'Mr frosty' storage container at room temperature. The 'Mr Frosty' container was then transferred to  $-80^{\circ}\text{C}$  for 24 h. Cryovials were then removed from the 'Mr Frosty' container and logged in the  $-80^{\circ}\text{C}$  storage or transferred and logged for long-term storage at  $-195^{\circ}\text{C}$  in liquid nitrogen.

### 2.25. Tanaka protein extraction.

To prepare whole cell protein extracts for immunoblot analysis, a 35 mm tissue culture dish containing U2OS cells at 70-80% confluency was rinsed with 2 ml PBS. A further 2ml PBS was added and the adherent U2OS cells were scraped and collected in a 15 ml tube. The 15 ml tube was then centrifuged at 1500 rpm at  $4^{\circ}\text{C}$  for 5 minutes and the supernatant was removed, the pellet was then resuspended in 1 ml cold PBS and transferred to a 1.5 ml microcentrifuge tube. Tubes were then frozen for at least 1 hour at  $-80^{\circ}\text{C}$ .

The approximate packed cell volume (PCV) was then measured and resuspended in 1 PCV of Tanaka buffer 1 (10 mM Tris-HCl pH 7.8, 200 mM KCl, 1 µg/ml aprotinin, 1 µg/ml chymostatin, 1 µg/ml pepstatin A, 1 µg/ml leupeptin, 0.25 mM PMSF and 1 mM DTT). The cell suspension was then mixed with 2x PCV of Tanaka buffer 2 (10 mM Tris-HCl pH 7.8, 600 mM KCl, 2 mM EDTA, 40% glycerol, 0.2% NP-40, 1 µg/ml aprotinin, 1 µg/ml chymostatin, 1 µg/ml pepstatin A, 1 µg/ml leupeptin, 0.25 mM PMSF and 1 mM DTT) and the cell suspension was rotated at 4°C for 30 min. The cell lysate suspension was then centrifuged at 40000 rpm for 20 min to pellet insoluble cellular components. The supernatant was transferred to a 1.5 ml microcentrifuge tube and protein concentration was quantified using the Bradford assay (Section 2.26).

### **2.26. Bradford assay.**

To quantify whole cell extract protein concentrations a Bradford protein assay was conducted. In a 1.5 ml microcentrifuge tube, 1 µl of protein sample was mixed in 39 µl dH<sub>2</sub>O and 960 µl of Bradford reagent (BioRad). A blank was prepared and 40 µl dH<sub>2</sub>O with 960 µl Bradford reagent (BioRad). A protein concentration standard curve was then prepared by mixing 40 µl 0.1-1 mg/ml dilutions of BSA with 960 µl Bradford reagent. All samples were then incubated at room temperature in the dark for 5 min then transferred to 1 ml plastic cuvettes. Absorbance was then measured at a wavelength of 595 nm using a spectrophotometer. Initially the apparatus was blanked with the dH<sub>2</sub>O only control followed by measuring the absorbance of the protein standard samples. Protein samples were then measured, re-blanking with the dH<sub>2</sub>O control between each measurement. A standard curve was plotted from A<sub>595</sub> measurements of the BSA dilutions and used to determine the sample protein concentration after multiplying by the dilution factor used. Quantified protein extract samples were then stored at -80°C for use in downstream analysis by immunoblot.

## 2.27. RNA interference.

To facilitate knockdown of endogenous protein for downstream analysis by immunoblot or clonogenic assays, siRNA transfection was conducted. A 35 mm tissue culture dish was seeded with 100,000 U2OS cells and incubated for 24 h at 37°C in 5% CO<sub>2</sub>.

In a 30 ml universal tube, 33 pmol of siRNA was suspended in 125 µl of supplement free DMEM and mixed by pipetting (**Table 2.12**). In a separate 30 ml universal tube, 2 µl of Lipofectamine RNAiMax (ThermoFisher) was suspended in 125 µl of supplement free DMEM and mixed by pipetting. Then, the supplement free DMEM/Lipofectamine RNAiMax mix was transferred to the tube containing suspended siRNA, mixed by pipetting and incubated at room temperature for 5 min.

**Table 2.12: Short interfering ribonucleic acid sequences used for non-targeting RNAi as control and TRIM26 RNAi.**

SiRNA Name	Target gene	RNA sequence
TRIM26 siRNA-1	Tripartite-motif containing protein 26	5'-CCGGAGAAUUCUCAGAUAA-3'
Non-targeting, control siRNA (SR-CL000-005; Eurogentec, Southampton, UK)	N/A	N/A

DMEM medium was then removed from 35 mm dishes containing U2OS cells, then rinsed with DPBS and replaced with 1.750 µl DMEM medium containing supplements. Then, 250 µl siRNA/Lipofectamine RNAiMax/ supplement free DMEM was applied drop wise to the 35 mm tissue culture dish, then distributed evenly by tilting the dish forward/backwards and left/right. Cells were then incubated at 37°C in 5% CO<sub>2</sub> for 48 hours before analysis by Tanaka protein extraction and immunoblot or treatment as part of clonogenic assays.

## 2.28. Transient overexpression of NEIL1, NEIL3 and NTH1.

To facilitate transient protein overexpression (O/E) for downstream analysis by immunoblot or clonogenic assays, the following transient mammalian expression vectors were used (**Table 2.13**)

**Table 2.13: Transient mammalian expression vectors.** Name of the mammalian expression vector, the encoded DNA glycosylase and C-terminal fusion tag are displayed.

Name	Encoded protein	Tag
pCMVTag3a-NEIL1	NEIL1	FLAG
pCMV-ac-NEIL3	NEIL3	N/A
pCMVTag3a-NTH1	NTH1	FLAG

U2OS cells were seeded in 35 mm tissue culture dishes at a seeding density of 100000 cells/dish and incubated at 37°C in 5% CO<sub>2</sub> for 48 h. Then, 80 ng of transient mammalian overexpression vector was suspended in 250 µl of supplement free DMEM medium, per transfection, in a 30 ml universal tube and mixed by pipetting. In a separate 30 ml universal tube, 2 µl Lipofectamine 2000 (ThermoFisher) was mixed in 250 µl supplement free DMEM, per transfection, by pipetting. 250 µl Lipofectamine 2000/supplement free DMEM mixture was then added to the expression vector/supplement free mixture, then mixed by pipetting and incubated for 10 min at room temperature.

Medium was removed from 35 mm tissue dishes containing U2OS cells, which were then rinsed with DPBS. Then, 1500 µl DMEM was added to each dish and 500 µl Lipofectamine 2000/overexpression vector/supplement free DMEM mix was applied dropwise. The complex was distributed evenly across the dish by tilting the dish backward/forward and left/right. Cells were then incubated at 37°C in 5% CO<sub>2</sub> for 48 h.

## 2.29. Clonogenic survival assay.

Cells were seeded 100,000 cells/35 mm tissue culture dish for each treatment condition and cisplatin drug concentration analysed. Cells were transfected after 24 h with NT siRNA or TRIM26 siRNA. After a further 24 h, cells were transfected with the relative DNA glycosylase mammalian transient overexpression plasmid vector. After a further 24 h, cells were treated with cisplatin at the relative treatment dose (0, 2.5, 5, 7.5 and 10 µM) for 24 h. Post drug treatment, drug containing medium was aspirated, cells were rinsed with DPBS and incubated

for 5 min at 37°C in 100 µl trypsin EDTA. Then, 900 µl DMEM was added to each dish to neutralise the trypsin, cells were mixed by pipetting and counted using a haemocytometer. A cell suspension was prepared as a mastermix in 10 ml DMEM to achieve a seeding density of the relevant low seeding density per 6 well plate/ml of DMEM medium (**Table 2.14**). For each treatment (NT siRNA, TRIM26 siRNA, NEIL1 O/E and NEIL3 O/E) and relative drug concentration, 3 wells of a 6 well plate were seeded with the relevant seeding density previously mixed in 1 ml of DMEM medium and the remaining 3 wells of the plate were seeded with the associated higher seeding density, by pipetting 2 ml of the previously mixed cell suspension into the wells. Then 1 ml of DMEM medium was added to the wells containing 1 ml of cell suspension to maintain consistent culture volume. The 6 well plates were then incubated at 37°C and 5% CO<sub>2</sub> to facilitate colony outgrowth.

**Table 2.14: Clonogenic seeding densities for each RNAi or overexpression treatment and relevant cisplatin concentration.** Numbers denote the two seeding densities seeded into 6 well plates after treatments for outgrowth of colony forming units.

Cisplatin concentration (µM)	Number of cells seeded per well				
	0	2.5	5	7.5	10
NT siRNA	1000/2000	2000/4000	4000/8000	8000/16000	16000/32000
TRIM26 siRNA	1000/2000	1000/2000	2000/4000	4000/8000	4000/8000
hNEIL1 O/E	1000/2000	1000/2000	2000/4000	2000/4000	2000/4000
hNEIL3 O/E	1000/2000	1000/2000	2000/4000	2000/4000	2000/4000

Plates were regularly visually analysed under the light microscope to assess colony size. Two factors were considered for colony outgrowth period: the 0 µM cisplatin treated sample of each treatment condition had formed ~50 cells/ defined colony and that colonies did not overlap and remained defined on all plates. When both conditions were met plates were removed from incubation, the medium was removed, and the wells were rinsed with 2 ml DPBS. Plates were placed on a level surface and 1 ml of crystal violet stain was applied to each well and incubated at room temperature for >1h. Then the crystal violet stain was removed, and the plates were rinsed with H<sub>2</sub>O to remove excess staining solution. Plates were then

inverted and allowed to air dry for 24 hours at room temperature to facilitate evaporation of excess H<sub>2</sub>O.

Colonies on each plate were then counted using the Oxford Optronix: GelCount colony counter selecting for stringency in colony size, shape and overlap. Values retrieved were exported to Microsoft excel and normalised to the original seeding density. Values were plotted against concentration for each condition and converted to log scale. Plating efficiency was calculated based on the values retrieved from the control plate, without cisplatin treatment:

$$\frac{n \text{ Colonies}}{\text{Seeding Density}} = \text{Plating efficiency}$$

The mean average plating efficiency was calculated and used to calculate the normalised surviving fractions of each condition:

$$\frac{n \text{ Colonies}}{(\text{Seeding Density} \times \text{Average Plating efficiency})} = \text{Surviving fraction}$$

The mean average surviving fraction was calculated for each condition, with the 0 μM cisplatin treated plate values now normalised to a value of 1.

Finally, the significance between each treatment condition and the NT siRNA control treated samples was determined through the comparison of linear-quadratic cell survival curves. This was conducted using the R (3.3.1) statistical software with the CFA assay package (Brasemann *et al.*, 2015).

### 2.30. CRISPR/Cas9 mediated gene knockout.

To establish a hNEIL3<sup>-/-</sup> U2OS cell lines, the Origene CRISPR/Cas9 gene knockout kit was used. Two circular plasmid vectors were supplied: **pCAS-Guide (Figure 2.3)** vector containing the Cas9 cDNA under a CMV promotor, and one of three guide sequences (gRNA1(G1), gRNA2 (G2), scramble control gRNA (SC)), with ampicillin resistance for propagation in bacterial cloning cells and the **pUC-Donor (Figure 2.4)** vector containing left and right homologous arms, a GFP and puromycin resistance gene cassette under the control of a PGK promotor.

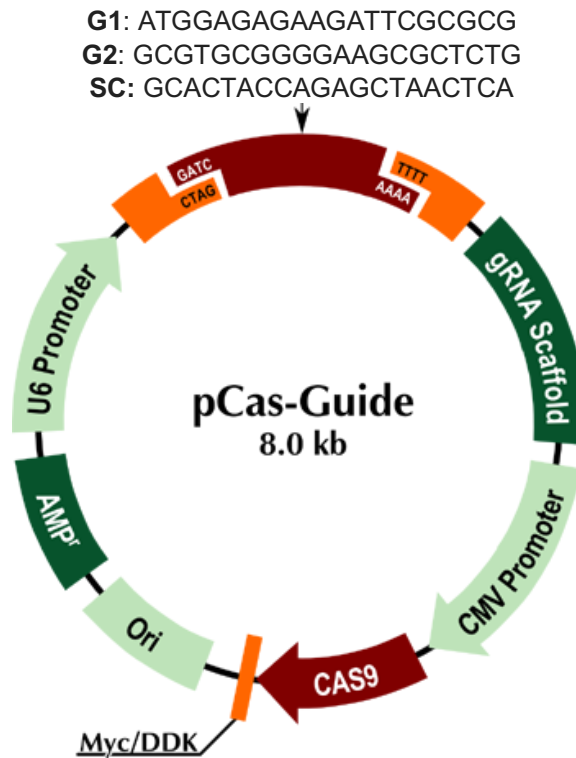


**Figure 2.3: The pCas-Guide vector map.** The pCas-Guide facilitated the transient mammalian expression of wild type Cas9 protein and transcription of target gRNA sequences in complex with gRNA scaffold complex. pCas-Guide vector map shows G1 and G2 gRNA sequences used for targeting exon 1 of the NEIL3 gene sequence and scramble control (SC) gRNA sequence for negative control cell line generation (Adapted from the Origene CRISPR/Cas9 Genome Editing instruction manual).

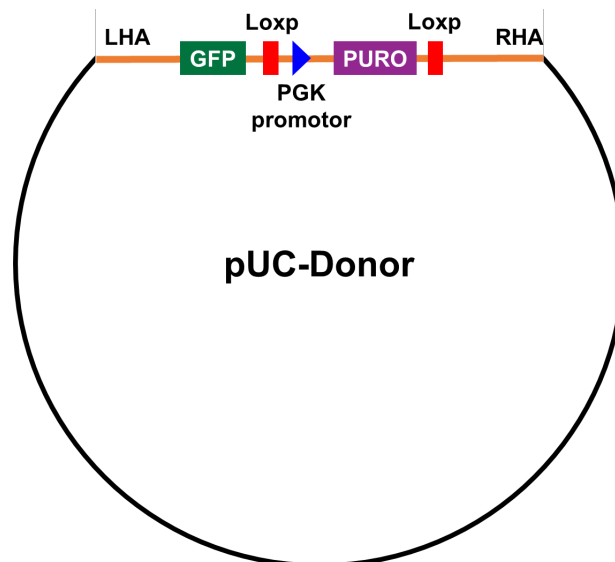


**Figure 2.4: The pUC-Donor cassette map.** pUC-Donor facilitated the transient expression of puromycin antibiotic resistance gene and provision of the homology directed repair (HDR) cassette for integration at G1, G2 or SC gRNA sequence site. pUC-Donor vector map shows left homologous arm (LHA), green fluorescent protein gene (GFP), Cre/Lox recombinase sequences (Loxp), phosphoglycerate kinase (PGK) promotor, puromycin antibiotic resistance gene (PURO) and right homologous arm (RHA) Adapted from the Origene CRISPR/Cas9 Genome Editing instruction manual).

U2OS cells were seeded at 300,000 cells/ 35 mm tissue culture dish 24 hours prior to co-transfection of both pCAS-Guide and pUC-Donor plasmids. 1 µg of G1 (targeting exon 1 of

hNEIL3, G2 exon 1 of hNEIL3) and SC pCAS-Guide vectors were independently suspended in 250  $\mu$ l of supplement free DMEM medium in 30 ml universal tubes and mixed gently by pipetting. Then 1  $\mu$ g of pUC-Donor was suspended in each of the same 30 ml universal tubes. In parallel, 7.5  $\mu$ l of Lipofectamine 2000 was diluted and mixed in 750  $\mu$ l of supplement free DMEM and mixed by gently pipetting. Then, 250  $\mu$ l of Lipofectamine 2000/supplement free DMEM was added to each of the 30 ml universal tubes containing 250  $\mu$ l of 1  $\mu$ g pCAS-Guide/1  $\mu$ g pUC-Donor/supplement free DMEM mix and gently mixed by pipetting. The final mixture was incubated at room temperature for 10 min to facilitate vector/liposome formation. DMEM medium was then removed from 35 mm tissue culture dishes containing U2OS cells, rinsed with 2 ml of DPBS and replaced with 1.5 ml of fresh DMEM (10% FBS, 1% non-essential amino acids, 1% penicillin/streptomycin antibiotic mix and 1% L-glutamine). Then 500  $\mu$ l of the pCAS-Guide/pUC-Donor/Lipofectamine 2000/supplement free DMEM mixtures were added drop-wise to independent 35 mm dishes containing U2OS cells prepared as aforementioned and labelled respectively (G1, G2 and SC). The cells were then incubated at 37°C in 5% CO<sub>2</sub>.

After 48 hrs incubation each of the 35 mm dishes containing co-transfected U2OS cells were split at a 1 in 10 dilution, this was repeated for a further 7 passages every 72 hr. As the pUC-Donor vector contains puromycin resistance under the control of the mammalian promoter PGK, removal of the episomal remnants of the puromycin resistance gene was required. At P8 duplicate dishes were seeded into 10 cm tissue culture dishes and incubated at 37°C in 5% CO<sub>2</sub> to reach 70-80% confluence. One set of which was taken forward for puromycin selection at 1  $\mu$ g/ml for 14 days, with medium/selective agent replaced every 7 days. The duplicate set of 10 cm tissue culture dishes containing transfected U2OS was processed for long term storage as described in section 3.21.3 and stored at -80°C.

G1, G2 and SC U2OS cells incubated in puromycin selective DMEM medium were routinely monitored for colony formation and indication of successful integration of the puromycin resistance gene. Every 96 h medium was removed, cells were rinsed with DPBS and 1  $\mu$ g/ml puromycin selective DMEM medium was replaced. After 14 days, selective medium was removed, cells were rinsed with DPBS and cells were incubated for 5 min in 100  $\mu$ l trypsin EDTA at 37°C. After, 900  $\mu$ l of DMEM was added to each dish individually and suspended cells were transferred to a new 35 mm tissue culture dish.

Once G1, G2 and SC U2OS containing dishes were ~70-80% confluent, medium was removed, cells were rinsed with DPBS and cells were incubated for 5 min in 100  $\mu$ l trypsin EDTA at 37°C and 5% CO<sub>2</sub>. For each of G1, G2 and SC cultures, cells were counted and a dilution of 140 cells/40 ml of DMEM prepared. Using a multichannel pipette 100  $\mu$ l of DMEM/cell mixture was seeded into each well of four 96 well plates. The 96 well plates were then incubated at 37°C and 5% CO<sub>2</sub> for a further 14 days. Each plate was frequently analysed with use of a light microscope and wells containing single colonies were noted.

Medium was removed from colony containing wells, then rinsed with DPBS then incubated at 37°C and 5% CO<sub>2</sub> in 10  $\mu$ l of 1x trypsin EDTA. Then, 90  $\mu$ l of DMEM was added to each colony containing well, gently mixed by pipetting and transferred to one well of a 24 well plate in 500 ml DMEM, to facilitate outgrowth. Once ~80% confluent, medium was removed, cells rinsed with DPBS and incubated in 100  $\mu$ l trypsin EDTA at 37°C and 5% CO<sub>2</sub> for 5 minutes. Then, 900  $\mu$ l of DMEM was added to suspend cells, then split 1 in 2 into separate wells of independent 6- well plates. Once ~50-70% confluent, cells from one of each duplicate clonal well were harvested and WCEs were prepared by the Tanaka method (section 3.26) and analysed for gene knockout by immunoblot analysis.

On confirmation of putative hNEIL3 knockout, medium was removed from the parallel well containing the same clonal population, rinsed with DPBS and incubated in 100  $\mu$ l trypsin EDTA for 5 min at 37°C. Then, 900  $\mu$ l DMEM was added to neutralise the trypsin EDTA, followed by mixing by pipetting. The cell suspension was then split 1 in 2 between a 10 cm tissue culture dish and a T75 flask containing both containing 9 ml DMEM medium. Once ~90% confluent the 10 cm tissue culture dish containing a positive clonal population was re-confirmed by parallel anti-NEIL3 immunoblot analysis while the T75 was processed and stored in liquid nitrogen following standard freezing procedure (section 2.24.3)

## Results & Discussion.

Data presented here provides *in vitro* biochemical evidence for differential and distinct lesion processing activities between recombinant hNEIL1 and hNEIL3 in the presence of oxidative lesions in a model DNA replication fork oligonucleotide substrate structure. In addition, evidence for the *in vitro* biochemical, ss-MA, three-stranded and four-stranded psoralen ICL unhooking activity of Nei, NEIL1 and NEIL3 recombinant proteins is presented. Finally, *in vitro* and cellular analysis provide evidence that hNEIL1, hNEIL3 and TRIM26 are implicated in the cellular response of U2OS cells to the chemotherapeutic agent cisplatin, putatively modulated through the homeostasis of the BER pathway maintained by the ubiquitin proteasome system.

### 3. Characterisation of the hNEIL1 and hNEIL3 DNA glycosylases in the repair of oxidative DNA damage in association with DNA replication.

To investigate the differential biochemical roles hNEIL1 and hNEIL3 play in the repair of oxidative lesions, the previously prepared pET30a-hNEIL1 expression construct was transformed and used to express and purify recombinant C-terminal his tagged hNEIL1. Protein purification products were analysed by SDS-PAGE and western blot. Recombinant hNEIL1 successfully purified at a relatively high purity and previously prepared active hNEIL3<sup>FL</sup> were used for biochemical analysis (Mustafa Albelazi, University of Salford: **Appendix Figure 2; Appendix Figure 3**). Fluorescently labelled ss-DNA, ds-DNA and mock replication fork structured DNA oligonucleotides were used to determine cleavage activity of the oxidative DNA lesions 5-OHU, 8-OxoG and the replication blocking lesion Tg by hNEIL1 and hNEIL3<sup>FL</sup> in varied structural contexts. Comparative analysis determined a structural affinity for DNA replication fork structures and the replication blocking DNA lesion Tg by hNEIL3<sup>FL</sup>.

### 3.1. Results: Characterisation of the hNEIL1 and hNEIL3 DNA glycosylases in the repair of oxidative DNA damage in association with DNA replication

#### 3.1.1. Recombinant hNEIL1 purification from *E. coli* using the pET30a-hNEIL1 bacterial expression vector.

The pET30a-hNEIL1 bacterial expression vector was kindly provided by S. S. Wallace, University of Vermont. The pET30a-hNEIL1 bacterial expression vector was subsequently transformed into Rosetta 2 (DE3) expression hosts, upscaled, induced and purified as described in (Section 2.2). **Figure 3.1 A** displays two major A280 peaks separated by HisTrap HP affinity chromatography. The chromatogram shows the characteristic separation of histidine rich bacterial proteins between fractions 4 and 10, while the second major peak between 11 and 22 is indicative of the successful isolation of recombinant hNEIL1. **Figure 3.1 B** confirms successful isolation of major contaminant proteins from putative recombinant hNEIL1-His at an expected molecular weight of 44.5kDa when compared to the protein size marker (M). **Figure 3.1 C** anti-his western blot analysis confirmed that the putative isolated protein was His-tagged hNEIL1, confirming the expression and HisTrap HP affinity purification of recombinant hNEIL1. Purified fractions 17-21 were subsequently pooled and concentrated using an Amicon Ultra-15 centrifugal-filter unit with a 10 K cut off to yield 1 mg/ml of recombinant hNEIL1.

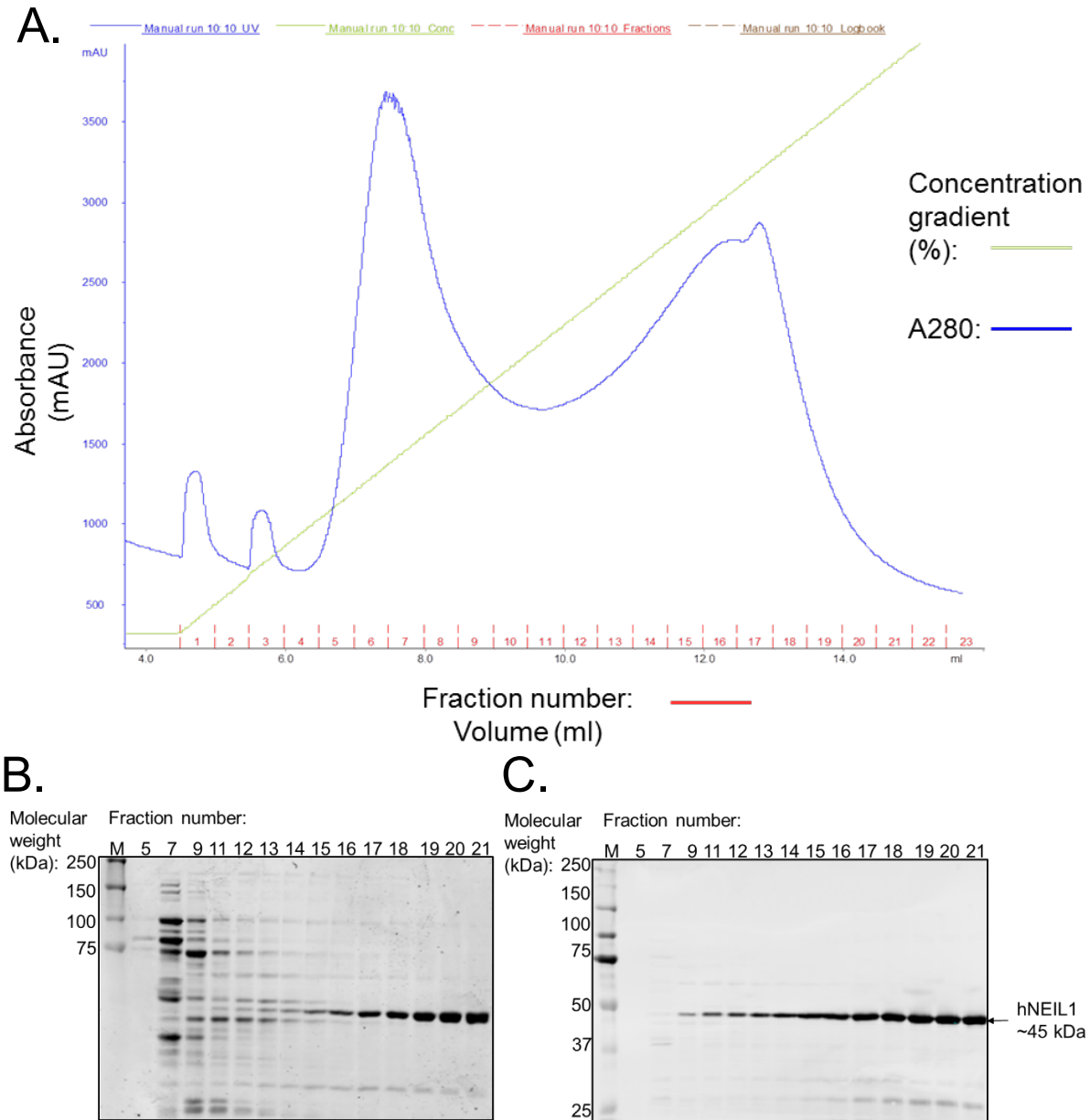


**Figure 3.1 HisTrap-HP FPLC purification of hNEIL1.** A. Chromatogram analysis of protein fractions generated by HisTrap chromatography of lysates from *E. coli* overexpressing hNEIL1. B. 10% SDS-PAGE analysis. C. Anti-His western blot analysis. "M" All Blue Prestained Protein Standards (BioRad).

### 3.1.2. hNEIL1 and hNEIL3<sup>FL</sup> recombinant protein activity analysis on oxidative DNA lesions containing ss- and ds- oligonucleotide DNA.

Confirmation of recombinant hNEIL1 and hNEIL3<sup>FL</sup> protein activity on the DNA lesions 5-OHU, 8-OxoG and Tg were undertaken to determine the DNA glycosylase and AP lyase activity profile. Recombinant proteins were incubated with ss-DNA and ds-DNA oligonucleotides, 39 mer in length as substrates in BER cleavage assays (**Figure 3.2**).

hNEIL1 was observed to cleave 5-OHU and Tg containing oligonucleotides in both ss-DNA and ds-DNA context, producing a 19 mer cleavage product (**Figure 3.2 A; Figure 3.2 C**), indicative of bifunctional AP-lyase activity post-cleavage of the N-glycosidic bond (**Figure 3.2 A**). In ss-DNA context the slower migrating band of the doublet represents a 19-mer product containing a 3'-PUA and the lower representing a 3'-PO<sup>4</sup> group. The major cleavage product observed after NEIL1 incubation with 5-OHU and Tg is the lower of the doublet, representative of  $\beta$ - $\delta$  elimination AP-lyase conducted by NEIL1 in the presence of 5-OHU and Tg in ss-DNA. Analysis of hNEIL1 incubation with ds-DNA generated a 19 mer cleavage product containing a 3'-P and no evidence of a cleavage product containing a 3'-PUA, most likely due to a preference for ds-DNA generating a 3'P residue. hNEIL1 incubated with 8-OxoG in ss-DNA and ds-DNA context, exhibited no evidence of cleavage, indicating that 8-OxoG is a poor substrate *in vitro* for hNEIL1 (**Figure 3.2 A; C**).

Analysis of the incubation of hNEIL3<sup>FL</sup> with ss-DNA and ds-DNA substrates revealed overlapping preference for the 5-OHU and Tg containing substrates as recombinant hNEIL1 (**Figure 3.2 B, D**). When incubated with ss-DNA oligonucleotides containing 5-OHU and Tg lesions, a 19 mer cleavage product doublet can be observed representative of 3'-PUA and 3'-P (**Figure 3.2 B**). Analysis also revealed weak cleavage activity by hNEIL3<sup>FL</sup> on the ss-DNA 8-OxoG DNA substrate. In contrast to hNEIL1, hNEIL3<sup>FL</sup> displays predominant  $\beta$ -elimination and nominal  $\beta$ , $\delta$ -elimination AP-lyase in a ss-DNA context. However, when incubated with ds-DNA oligonucleotides, hNEIL3<sup>FL</sup> displays weak cleavage activity on the 5-OHU and 8-OxoG substrates producing 19 mer cleavage products representative of associated  $\beta$ , $\delta$  elimination of the phosphodiester backbone (**Figure 3.2 B; D**).

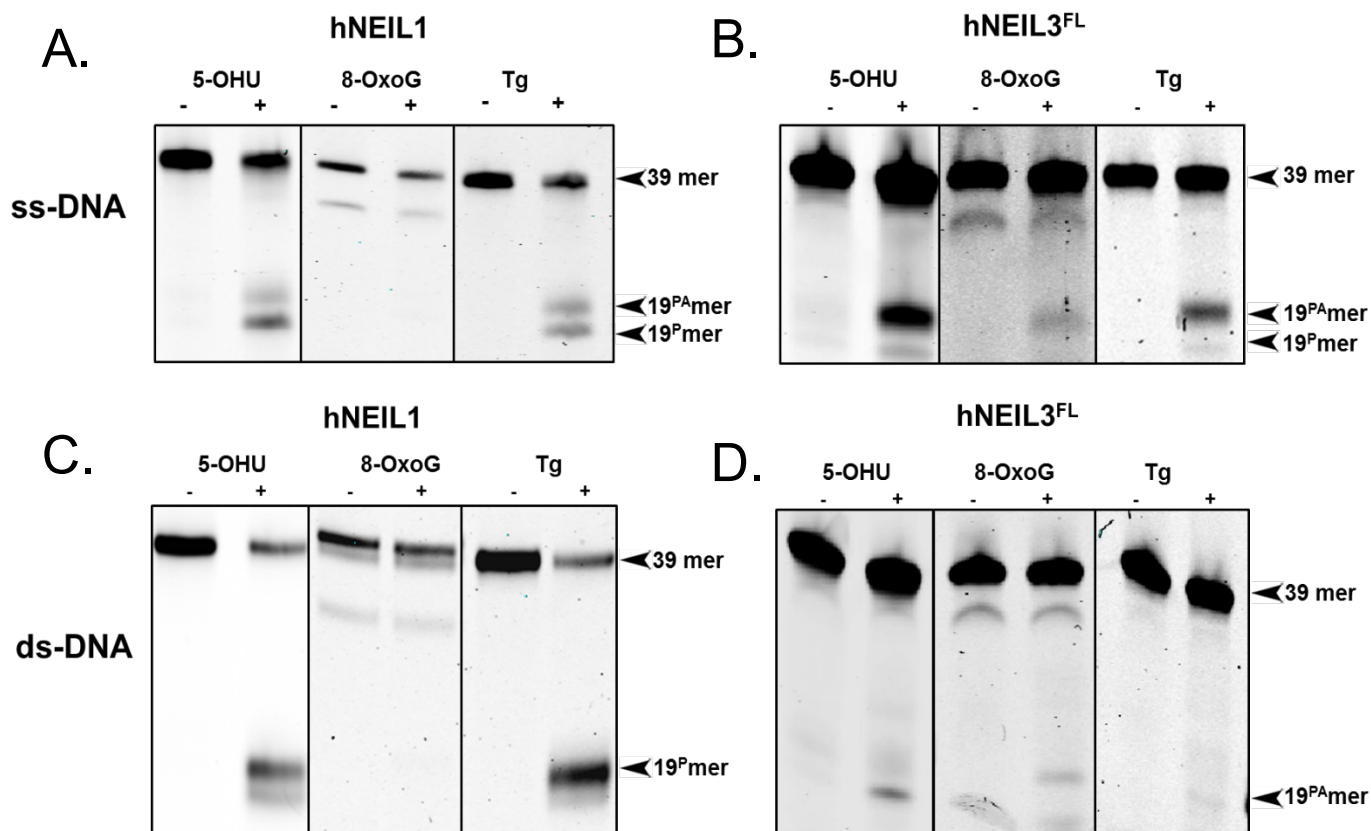
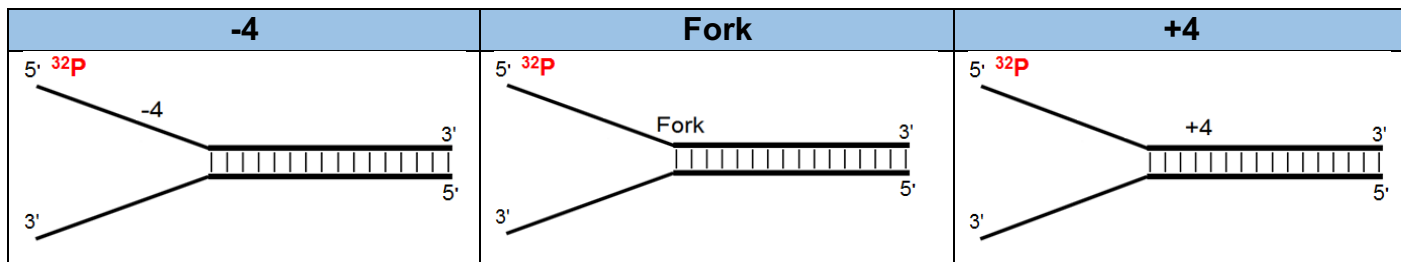


**Figure 3.2: Denaturing PAGE analysis of oligonucleotide substrates incubated with hNEIL1 (A, C) or hNEIL3 (B, D).** A. Analysis of 228 nM hNEIL1 incubated with 5 nM ss-DNA oligonucleotide substrates B. Analysis of 150 nM hNEIL3<sup>FL</sup> incubated with 5 nM ss-DNA oligonucleotide substrates. C. Analysis of 228 nM hNEIL1 incubated with 5 nM ds-DNA oligonucleotide substrates. D. Analysis of 300 nM hNEIL3<sup>FL</sup> incubated with 5 nM ds-DNA oligonucleotide substrates. "19<sup>PA</sup>" and "19<sup>P</sup>" denote 19 mer cleavage fragments with a 3'-terminal PA or P, respectively.

### 3.1.3. hNEIL1 and hNEIL3<sup>FL</sup> recombinant protein activity analysis on oxidative DNA lesion containing model DNA replication fork oligonucleotide DNA.

Current lines of evidence suggest NEIL1 and NEIL3 initiate repair in association with DNA replication. Therefore, the design and generation of a set of three model replication fork structures, based on partially complementary oligonucleotides, to analyse variance in biochemical activity at the DNA replication fork was undertaken (**Table 3.1**). These substrates contained the oxidative lesions 5-OHU, 8-OxoG or Tg at one of three positions: '-4', (four nucleotides from the replication fork junction and within ss-DNA), 'Fork' (at the site of the fork junction and in ds-DNA context) and +4 (a prereplicative position in double-stranded DNA, four nucleotides upstream of the replication fork (**Table 3.1**).

**Table 3.1: Mock DNA replication fork oligonucleotide DNA structure.** Oligonucleotides 39 mer in length with either 5-OHU, 8-OxoG or Tg at 20 mer, DNA glycosylase cleavage products generate a 19 mer cleavage product.



Oligonucleotide cleavage assays with mock DNA replication fork structured DNA oligonucleotides (**Table 3.1**) incubated with recombinant hNEIL1 protein revealed distinct preferences for structural context. Denaturing PAGE analysis of hNEIL1 reaction products with 5-OHU revealed a preference for ds-DNA compared to ss-DNA with 25 percent more cleavage of the ds-DNA substrate (**Figure 3.3 A**). hNEIL1 mediated cleavage was 57% more efficient when incubated with the ds-DNA +4 substrate compared to the ss-DNA -4 substrate, however only 25% more efficient at the fork junction position. While analysis revealed robust cleavage of the ds-DNA substrate, hNEIL1 displayed a preference for fork structured oligonucleotide DNA, with a 17% increase in cleavage of the +4 DNA substrate. Interestingly, hNEIL1 cleaves the 'Fork' substrate with 39% less efficiency compared to that of the +4 structure, while qualitatively presenting a smeared DNA product, representative of the degradation of an AP-site generated after monofunctional DNA glycosylase activity (**Figure 3.3 A**). hNEIL1 demonstrates a consistent  $\beta,\delta$ -elimination AP-lyase activity in the presence of 5-OHU DNA lesions (**Figure 3.3 A**).

Analysis of 8-OxoG substrates incubated with hNEIL1, demonstrated weak activity on ss and ds-DNA substrates (**Figure 3.3 B**). Nominal activity is observed on the fork DNA substrates, with 7% cleavage of the +4 substrate, 3.5% cleavage of the -4 substrate and 2% cleavage of the 'fork' substrate (**Figure 3.3 B**).

Incubation of hNEIL1 with Tg DNA substrates provides the strongest contrast in substrate preference. hNEIL1 cleaves the +4 substrate with 56% more efficiency than -4 substrate and 73% more efficiently than the fork junction substrate. Additionally, similar cleavage activity is observed between the ds-DNA and the +4 substrate (**Figure 3.3 C**). Unique to the Tg substrate hNEIL1 displays evidence of  $\beta$ -elimination in the presence of the ds-DNA and +4 DNA substrate when compared to the cleavage control Nth, previously characterised to conduct

$\beta$ -elimination AP-lyase, whereas hNEIL1 displays evidence of weaker  $\beta,\delta$ -elimination activity at in the presence of ss-DNA and -4 Tg DNA lesion substrates (Figure 3.3 C).

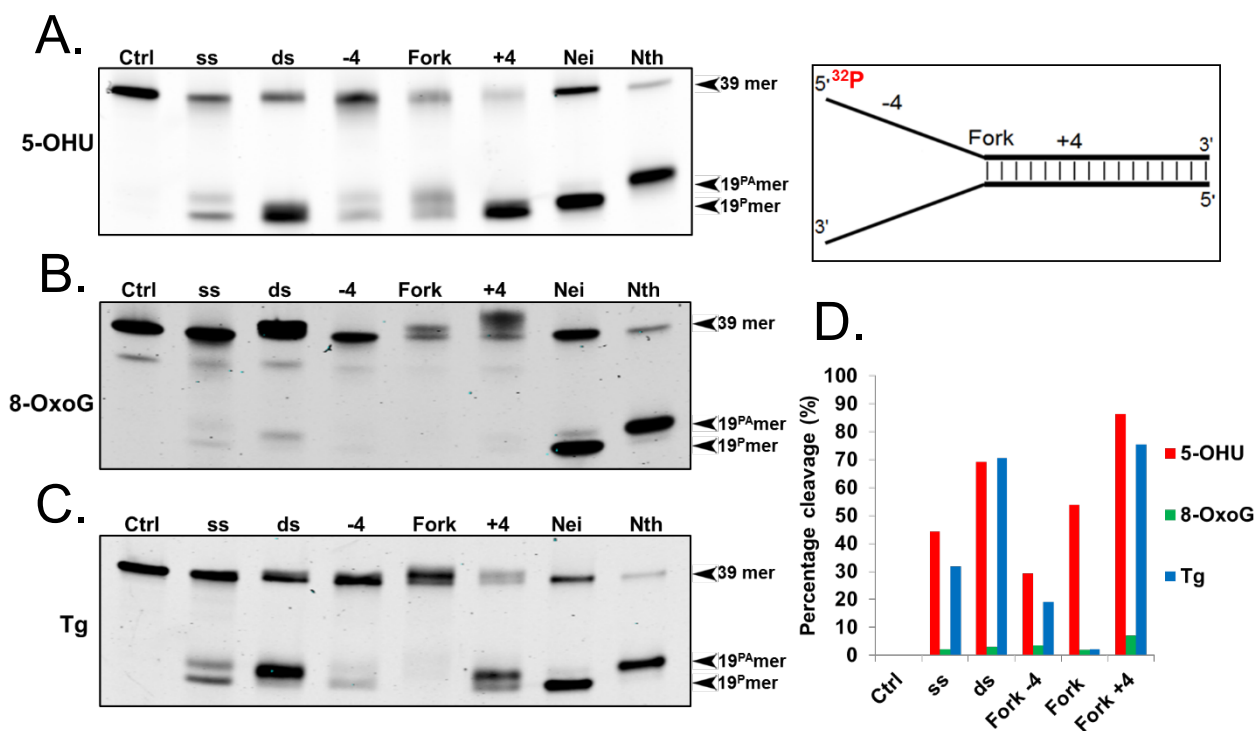


**Figure 3.3: Denaturing PAGE analysis of fork structured oligonucleotides incubated with hNEIL1.** A. 10% denaturing PAGE analysis of 228 nM hNEIL1 incubated with 5 nM 5-OHU containing oligonucleotide substrates. B. 10% denaturing PAGE analysis of 228 nM hNEIL1 incubated with 5 nM 8-OxoG containing oligonucleotide substrates. C. 10% denaturing PAGE analysis of 228 nM hNEIL1 incubated with 5 nM Tg containing oligonucleotide substrates. D. Quantification of 5-OHU, 8-OxoG and Tg oligonucleotide substrate cleavage by hNEIL1. Ctrl sample in the absence of recombinant hNEIL1. Bacterial Nei and Nth provide reference for associated  $\beta,\delta$ -elimination and  $\beta$ -elimination, respectively. Representative images of three experiments.

Oligonucleotide cleavage assays with mock DNA replication fork structured DNA oligonucleotides (Table 3.1) incubated with recombinant hNEIL3<sup>FL</sup> protein, undertaken by Mustafa Albelazi (University of Salford), revealed distinct differences in cleavage activity to that demonstrated by recombinant hNEIL1. Denaturing PAGE analysis of hNEIL3<sup>FL</sup> reaction products with 5-OHU containing oligonucleotide, underlined the overlapping oxidative lesion substrate preference with hNEIL1 (Figure 3.4 A). However, hNEIL3<sup>FL</sup> displayed increased activity on ss-DNA substrates vs ds-DNA. Incubation of hNEIL3<sup>FL</sup> with the -4 DNA substrate displayed an increase in activity when compared to the +4 DNA substrate. hNEIL3<sup>FL</sup> displays a bifunctional DNA glycosylase profile in the presence of 5-OHU containing DNA substrates, with a mainly  $\beta$ -eliminating activity producing 19 mer cleavage products with a 3'PUA (Figure 3.4 A). However, it is observed that hNEIL3<sup>FL</sup> excises the 5-OHU lesion in ds-DNA conformation and the +4 Fork substrate with associated  $\beta,\delta$ -elimination.

Incubation of hNEIL3<sup>FL</sup> with 8-OxoG containing DNA substrates displayed minor activity levels, with cleavage efficiency being at its greatest in the presence of the ds-DNA substrate (**Figure 3.4 B**). Qualitatively, weak bifunctional DNA glycosylase activity is displayed on the ds-DNA substrate, suggesting weak processivity of 8-OxoG in a ds-DNA conformation *in vitro* (**Figure 3.4 B**).

Analysis of cleavage activity of hNEIL3<sup>FL</sup> of Tg containing DNA oligonucleotide substrates exhibited overlapping lesion preference with hNEIL1 (**Figure 3.4 C**). hNEIL3<sup>FL</sup> displays a preference for Tg in a ss-DNA context. An affinity for fork structured DNA is also observed with hNEIL3<sup>FL</sup> processing -4, Fork and +4 oligonucleotide substrates with 12%, 7% and 5% cleavage efficiency, respectively. Unique to the Tg substrate, hNEIL3<sup>FL</sup> displays consistent associated  $\beta$ -elimination.

**Figure 3.3** and **Figure 3.4** underline the structural preference of hNEIL3<sup>FL</sup> for DNA lesions in open replication and fork junction mock DNA replication fork oligonucleotide structure when compared to hNEIL1. In addition, hNEIL3 processes the Tg lesion at all three positions within the mock DNA replication fork with relatively robust activity when compared to standard duplex oligonucleotide DNA (**Figure 3.4 C**). As result, **Figure 3.4 C** provides evidence for hNEIL3<sup>FL</sup> possessing an affinity for the DNA replication blocking lesion Tg at all positions analysed within a DNA replication fork structure, when compared to conventional ds-DNA oligonucleotide substrate (**Figure 3.3 C**).

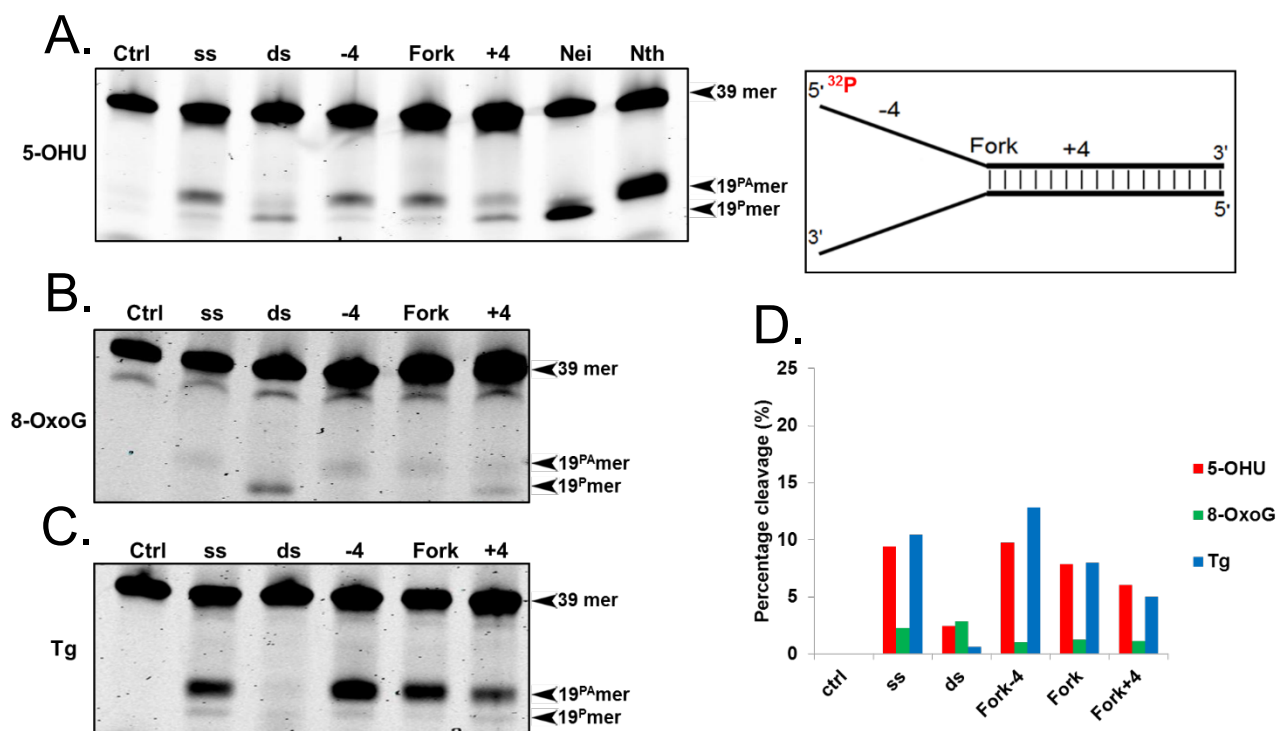


**Figure 3.4: Denaturing PAGE analysis of fork structured oligonucleotides incubated with hNEIL3<sup>FL</sup>.** A. 10% denaturing PAGE analysis of 150 nM hNEIL3<sup>FL</sup> incubated with 5 nM 5-OHU containing oligonucleotide substrates. B. 10% denaturing PAGE analysis of 150 nM hNEIL3<sup>FL</sup> incubated with 5 nM 8-OxoG containing oligonucleotide substrates. C. 10% denaturing PAGE analysis of 150 nM hNEIL3<sup>FL</sup> incubated with 5 nM Tg containing oligonucleotide substrates. D. Quantification of 5-OHU, 8-OxoG and Tg oligonucleotide substrate cleavage percentages. Ctrl sample in the absence of recombinant hNEIL3<sup>FL</sup>. Bacterial *Nei* and *Nth* provide reference for associated  $\beta,\delta$ -elimination and  $\beta$ -elimination, respectively (Mustafa Albelazi, University of Salford).

### 3.2. Discussion: Characterisation of the hNEIL1 and hNEIL3 DNA glycosylases in the repair of oxidative DNA damage in association with DNA replication.

The data presented here demonstrates the different AP-lyase activity of the hNEIL1 and hNEIL3 DNA glycosylases in the presence of the 5-OHU and Tg oxidative lesions in a structure specific manner. hNEIL1 and hNEIL3 display overlapping substrate preference for 5-OHU and Tg but display different processing efficiencies depending on the DNA lesion context. hNEIL1 maintains a preference for lesions in a ds-DNA context while hNEIL3 displays a preference for ss-DNA. However, within a DNA replication fork structured oligonucleotide substrate hNEIL1 displays a preference for the “+4” ds-DNA, in a prereplicative position. hNEIL3 displays a preference for oxidative lesions in a single-stranded “-4” open DNA replication fork context and at the ds-DNA “Fork” junction. Where NEIL1 displays a mainly  $\beta,\delta$ -elimination AP lyase activity NEIL3 displays  $\beta$ -elimination in the single-stranded DNA context lesions substrates including “-4” in the presence of 5-OHU. Conversely In the presence of 5-OHU in ds-DNA context and “+4” the AP lyase activity is observed to switch to  $\beta,\delta$ -elimination AP-lyase. However, in the presence of the DNA replication blocking Tg lesion, distinct differences in processing are observed. hNEIL1 displays a lack of activity at the ds-DNA “Fork” with robust activity at “+4” while NEIL3 displays robust activity on Tg regardless of its position at the DNA replication fork. Furthermore, hNEIL3 exhibits consistent  $\beta$ -elimination AP lyase activity in the presence of Tg at the DNA replication fork. This demonstrates that lesion type and structural context are important for the discriminatory associated lyase activity of hNEIL1 and hNEIL3. Concurrently, this may have important implications in terms of the downstream proteins and their interactors recruited to the DNA replication fork due to differential AP lyase activities of bifunctional DNA glycosylases.

Previous finding by Mitra’s group determined, that hNEIL1 acts as a ‘cowcatcher’ for the replication machinery in the presence of a DNA replication fork (Hegde *et al.*, 2013). It was demonstrated that hNEIL1 functionally interacts with PCNA, RPA, WRN, RFC, Pol  $\delta$  and Lig1. Furthermore, hNEIL1 was purified in multiprotein complexes from mammalian cells, which displayed efficient BER *in vitro* on a 5-OHU lesion and hNEIL1 is proposed to facilitate regression back to a prereplicative ds-DNA structure, in collaboration with the WRN helicase

as part of a 'cowcatcher model' (Das *et al.*, 2007; Theriot *et al.*, 2010; Hegde *et al.*, 2015). The lack of additional cofactors and interacting proteins in our *in vitro* analysis may explain why reduced activity at the -4 and fork junction positioned 5-OHU lesion is observed (**Table 3.1**). However, it is unknown how these interactions may influence the activity of hNEIL1 in the presence of Tg as Hegde *et al.* (2013; 2015) used 5-OHU as a model oxidative lesion. Despite this, it was shown that nascent DNA chain growth was retarded in NEIL1 depleted cells when treated with H<sub>2</sub>O<sub>2</sub>, which is known to induce oxidative DNA damage and Tg lesions (Hegde *et al.*, 2013). Thus, it is highly possible that *in vivo* NEIL1 may efficiently repair 5-OHU and Tg oxidative lesions with the aid of the identified protein partners within multiprotein complexes at the DNA replication fork (Hegde *et al.*, 2015). It is postulated that NEIL1 would bind to ss-DNA and promote DNA replication fork regression to place the DNA lesion in a favourable ds-DNA context, mimicking the "+4" structure examined here (**Table 3.1**; (Hegde *et al.* 2013). In this context the "Fork" junction substrate would not be produced *in vivo*, as DNA replication fork regression would facilitate bypass to generate a ds-DNA structure mimicking the "+4" substrate. Further biochemical analysis is required to elucidate the biochemical activity of hNEIL1 on differentially positioned Tg within a DNA replication fork structure, in the presence of recombinant WRN, PCNA, RFC, Pol  $\delta$ , Lig I and RPA to determine how these interactions may overcome the observed inhibition of DNA glycosylase activity at the DNA replication fork (Das *et al.*, 2007; Theriot *et al.*, 2010; Hegde *et al.*, 2013; Hegde *et al.*, 2015). In contrast, NEIL3<sup>FL</sup> displays robust activity on -4, Fork and +4 regions of DNA containing Tg (**Figure 3.4 C**). In addition, NEIL3 displays consistent associated  $\beta$ -elimination of the phosphodiester backbone, demonstrating that the type of lesion encountered is important for associated AP-lyase activity undertaken by NEIL3. Interestingly, Tg can be removed with relative efficiency when compared to the ds-DNA Tg containing oligonucleotide, where relatively no cleavage is observed, suggesting a preference for the replication fork structure. Furthermore, Where NEIL1 fails to process the lesion at the fork junction, NEIL3 does so with comparable activity to that displayed in the presence of the -4 Tg substrate. This raises the question of how hNEIL3, independent of protein partners, may excise Tg at any of the examined positions within a DNA replication fork examined here. The data presented here suggests that hNEIL3 displays a preference for Tg in a DNA replication fork structure context when compared to linear duplex DNA, advocating an associated role within the maintenance of faithful DNA replication. Despite, hNEIL3 previously being indicated to possess weak, non-concerted,  $\beta$ -

elimination AP-lyase activity and proposed to be a mainly monofunctional DNA glycosylase *in vivo* in the presence of APE1, it is observed that hNEIL3 displays robust associated AP-lyase in the presence of 5-OHU and Tg lesions (Takao *et al.*, 2009; Krokeide *et al.*, 2013). When examining the processing of 5-OHU or Tg at the “-4” or “Fork” DNA replication fork structured substrate, the associated AP lyase activity demonstrated by hNEIL3 has important implications for the potential generation of replication associated DSB generation. Indeed, previous investigation by Klattenhoff *et al.* (2017), demonstrated that hNEIL3 co-localises at DNA replication associated DSBs and its depletion lead to an increase in these DSBs. It may be proposed that hNEIL3 has an important role in the efficient processing of oxidative DNA lesions at the DNA replication fork. The identification of a hNEIL3 BERosome, similar to hNEIL1, may indicate relatively fast repair kinetics of oxidative lesions in a “-4” or “Fork” structural context *in vivo* which may protect against the formation of single ended DSBs (Hegde *et al.*, 2015).

Taken together it is proposed that NEIL3 is the primary DNA glycosylase associated with the removal of the replication blocking Tg lesion at the DNA replication fork, while NEIL1 plays a primary role in pre-replicative repair (Aller *et al.*, 2007; Yoon *et al.*, 2010; Rolseth *et al.*, 2013; Hegde *et al.*, 2013; Hegde *et al.*, 2015). It is proposed that NEIL1 and NEIL3 play distinct roles at the DNA replication fork and therefore redundancy in activity is observed between the constitutively expressed NTH1 and S-phase dependent NEIL1/NEIL3 DNA glycosylases in processing oxidised pyrimidines (Wallace *et al.*, 2012). These findings support previous suggestions made by Rolseth *et al.* (2013), that NEIL3 is involved in the removal of DNA replication blocks within proliferating cells, as they observed that NEIL3<sup>-/-</sup> MEFs display sensitivity to the oxidative agent paraquat and cisplatin. Indeed, it was shown by Bjørås *et al.* (2017) that NEIL1 and NTH1 are detected on nascent DNA, suggested to be outside of the DNA replication fork, while NEIL3 was enriched with the replisome, supporting a role close to or at the DNA replication fork. Taking in to account these findings it is suggested that NEIL1 may indeed be a ‘cowcatcher’-like protein, removing DNA damage in a prereplicative manner, while NEIL3 has a specialised role within the maintenance of open DNA replication forks and NTH1 is a constitutively active DNA glycosylase facilitating repair outside the context of DNA replication (Hegde *et al.*, 2013; 2015; Wallace, 2014). This points to a specialised and redundant set of tools available within the cell for the resolution of oxidised pyrimidines,

where structural context may dictate the DNA glycosylase employed. The essentiality for the repair of oxidised DNA is eluded to by embryonic lethality observed in downstream repair BER proteins Pol  $\beta$ , APE1, XRCC1 and Lig III (Hegde *et al.*, 2012). Therefore, it may be suggested that comprehensive and redundant mechanisms of oxidative DNA repair are required to combat the 10,000 oxidative lesions generated per cell per day and the associated genomic instability through the mispairing of DNA (Klaunig *et al.*, 2011; Hegde *et al.*, 2012). However, these redundant pathways may in turn provide multiple targets for exploitation by cancer for mechanisms of acquired cellular resistance to therapeutic treatment (Rolseth *et al.*, 2013; Yamamoto *et al.*, 2014).

#### **4.Characterisation of the hNEIL1 and hNEIL3 DNA glycosylases in the repair of psoralen interstrand DNA crosslinks.**

To further elucidate the role of hNEIL1 and hNEIL3 in the repair of DNA replication blocking lesions, <sup>32</sup>P labelled synthetic psoralen/UVA generated MA, three-stranded and four-stranded ICL DNA structures were generated and confirmed. Enzymatic activity of hNEIL3<sup>Cat</sup>, hNEIL3<sup>Trun</sup>, hNEIL3<sup>FL</sup>, hNEIL1 and Nei on psoralen/UVA generated ICL structures was assessed. Kinetic analysis of hNEIL3<sup>Cat</sup> and hNEIL1 was conducted on ss-, ds-Sp1, three- and four-stranded psoralen ICL substrates. A catalytically inactive hNEIL3<sup>Cat-K81A</sup> mutant was generated, activity on ss-, ds-Sp1, three- and four-stranded ICL substrates was assessed. Enzyme-DNA covalent complex affinity assays were undertaken with Sp1 substrates, using hNEIL3<sup>Cat</sup> and hNEIL1. An enzyme-DNA covalent complex affinity assay was undertaken with a three-stranded psoralen ICL substrate, using hNEIL3<sup>Cat</sup>, hNEIL3<sup>Trun</sup>, hNEIL3<sup>FL</sup>, Nei, hNEIL1 and hNEIL3<sup>Cat-K81A</sup> recombinant proteins.

#### 4.1. Results: Characterisation of the hNEIL1 and hNEIL3 DNA glycosylases in the repair of psoralen interstrand DNA crosslinks.

##### 4.1.1. Generation of ICL oligonucleotide DNA substrates.

As NEIL3<sup>-/-</sup>MEF cells display sensitivity to the ICL agent cisplatin, ICL lesions block the progression of DNA replication and previous observations display an activity for the removal of the DNA replication blocking lesion Tg (Rolseth *et al.*, 2013; **Figure 3.4**), the hypothesis that hNEIL3 plays a role in the repair of ICL lesions was investigated. Model ICL DNA oligonucleotide substrates were generated with use of psoralen/UVA treatment as described in sections 2.9, 2.11, 2.12, 2.15, 2.16 and 2.17. A shift in the relative size observed after psoralen treatment, was characteristic of ICL formation due to opposing DNA strands remaining covalently bound under denaturing conditions. As shown by **Figure 4.1** the generation of ICL substrates with 18 mer, 21 mer or 47 mer <sup>32</sup>P labelled oligonucleotide DNA, generating 21–47 or 18-21 mer DNA or DNA RNA hybrid duplex was observed post psoralen (HMT)/UVA treatment. However, 100% of component labelled oligonucleotides was not observed to generate a psoralen ICL DNA duplex, warranting gel purification.

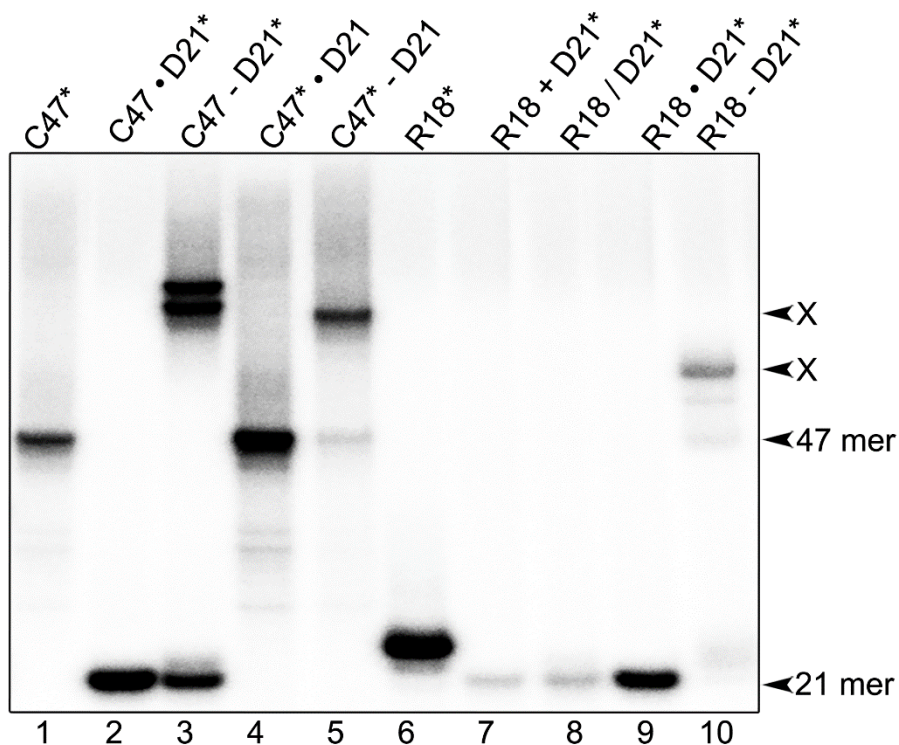


**Figure 4.1: Denaturing PAGE analysis of ICL construct preparation.** (X) Denotes ICL duplex substrate product band. "\*" Denotes 5' <sup>32</sup>P-labelled oligonucleotide strand, "•" Duplex DNA formed by annealing, "-" psoralen/UVA treated annealed duplex DNA oligonucleotide, "+" Mixture of ss-DNA oligonucleotides, "/" psoralen/UVA treated ss-DNA oligonucleotides.

To improve the purity of ICL oligonucleotides prior to construction of three-stranded ICL substrates, labelled duplex ICL oligonucleotides were separated by denaturing PAGE and then gel purified as described in section 2.16. **Figure 4.2** displays the confirmation of the excision of ICL DNA oligonucleotide duplexes composed of 21 mer psoralen crosslinked to 47 mer and 47 mer psoralen crosslinked to 101 mer oligonucleotides, by the excision of the upper band associated with psoralen bound oligonucleotides. **Figure 4.2** lanes 5 and 6 display extensive band smearing above the upper band, which is suggested to be a result of the large size of the construct and retardation entering the polyacrylamide gel during electrophoresis.

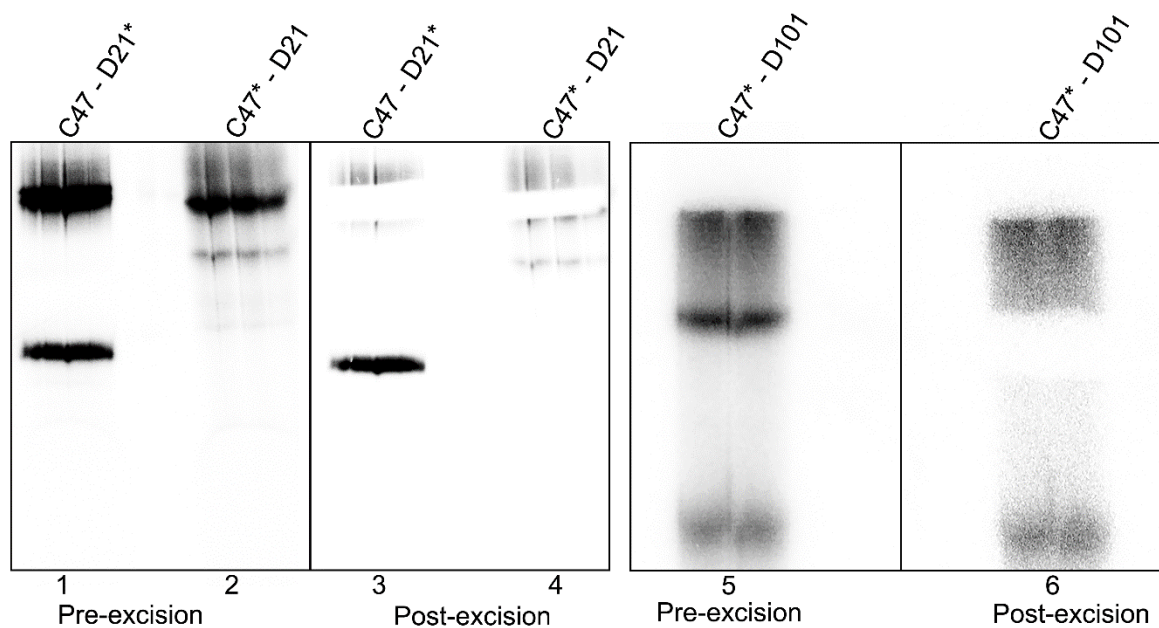


**Figure 4.2: Denaturing PAGE analysis of ICL construct gel excision.** (Lanes 1-2) Before excision of ICL DNA D21\* - C47 and D21 - C47\* HMT ICL oligonucleotides. (Lanes 3-4) After excision of D21\* - C47 and D21 - C47\* ICL oligonucleotides. (Lanes 5-6) Before and after excision of the C47\* - D101 ICL oligonucleotide. Upper bands represent covalently bound ICL DNA, whilst lower bands represent non-crosslinked DNA. "\*" Denotes 5' <sup>32</sup>P labelled oligonucleotide DNA oligonucleotide "-"psoralen(HMT)/UVA ICL duplex.

After purification of psoralen ICL bound duplex oligonucleotides, construction of three-stranded and four-stranded ICL DNA oligonucleotides were performed using 21-47 mer based constructs, whilst three-stranded constructs were generated using 47-101 duplex psoralen ICL constructs.

To confirm three-stranded and four-stranded psoralen ICL oligonucleotide generation under native conditions, non-denaturing PAGE analysis was undertaken (**Figure 4.3**). The generation of an ICL in duplex was marked by a small shift, as the construct migrated slower than the duplex due to incorporation of the psoralen (HMT) molecule. The generation of a three-stranded structure was displayed by a relatively large shift in the position of the band. This was due to slower migration in the gel, representative of an increase in the size of the oligonucleotide construct after a 47/101 mer complementary DNA oligonucleotide was annealed. The generation of a four-stranded structure was marked by a relatively smaller shift in the position of the band, which represented an increase in the size of the construct, due to addition of a 21 mer complementary DNA oligonucleotide.

Migration was relative to constructs of the same size component oligonucleotides. Single stranded labelled oligonucleotides (21\* mer, 47\* mer, 101\* mer) and possible alternate products, based on the incorrect construction of ICLs (21\* - 21 mer, 47\* - 47 mer), were loaded as size markers and control.

**Figure 4.3**, demonstrates successful generation of target constructs with high efficiency as the major product DNA bands generated in each sample migrate at their expected relative position, with nominal additional contaminant DNA bands detected.

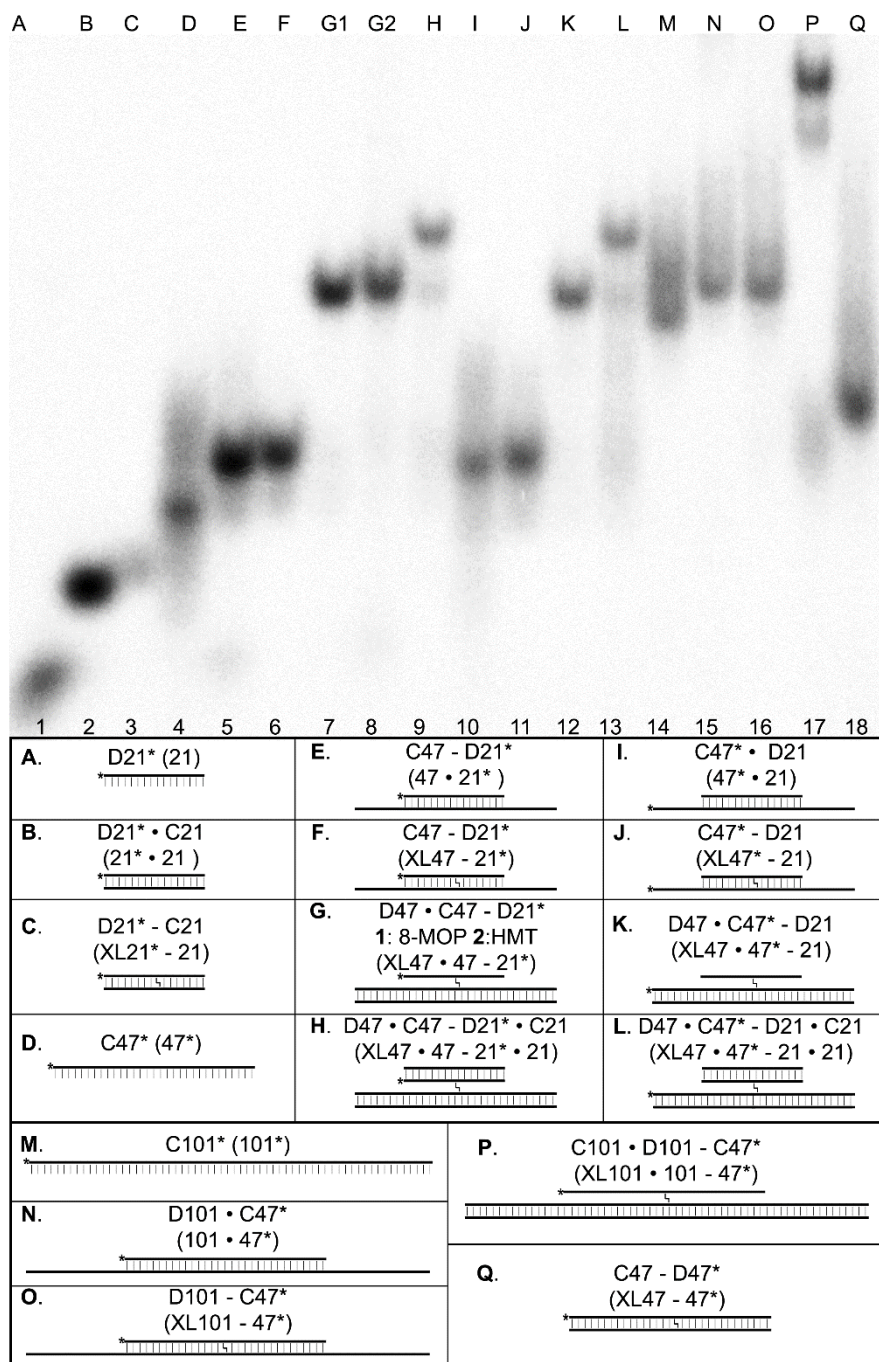


**Figure 4.3: Non-denaturing PAGE analysis of psoralen/UVA oligonucleotide DNA structures.** Oligonucleotide construct key included below the gel image. “\*” Denotes 5' <sup>32</sup>P labelled oligonucleotide DNA oligonucleotide, “•” hydrogen bond DNA complementation, “-” psoralen/UVA treated and ICL bound DNA.

**Figure 4.4** shows that the psoralen generated ICL was maintained after oligonucleotide purification and annealing reactions that generated three-stranded and four-stranded structures. This was shown by a shift and slower migration in the gel in comparison to non-crosslinked duplex oligonucleotide samples. **Figure 4.3** and **Figure 4.4** show the successful generation of three- and four-stranded ICL structures for use in biochemical assays to elucidate unhooking activity of recombinant proteins.

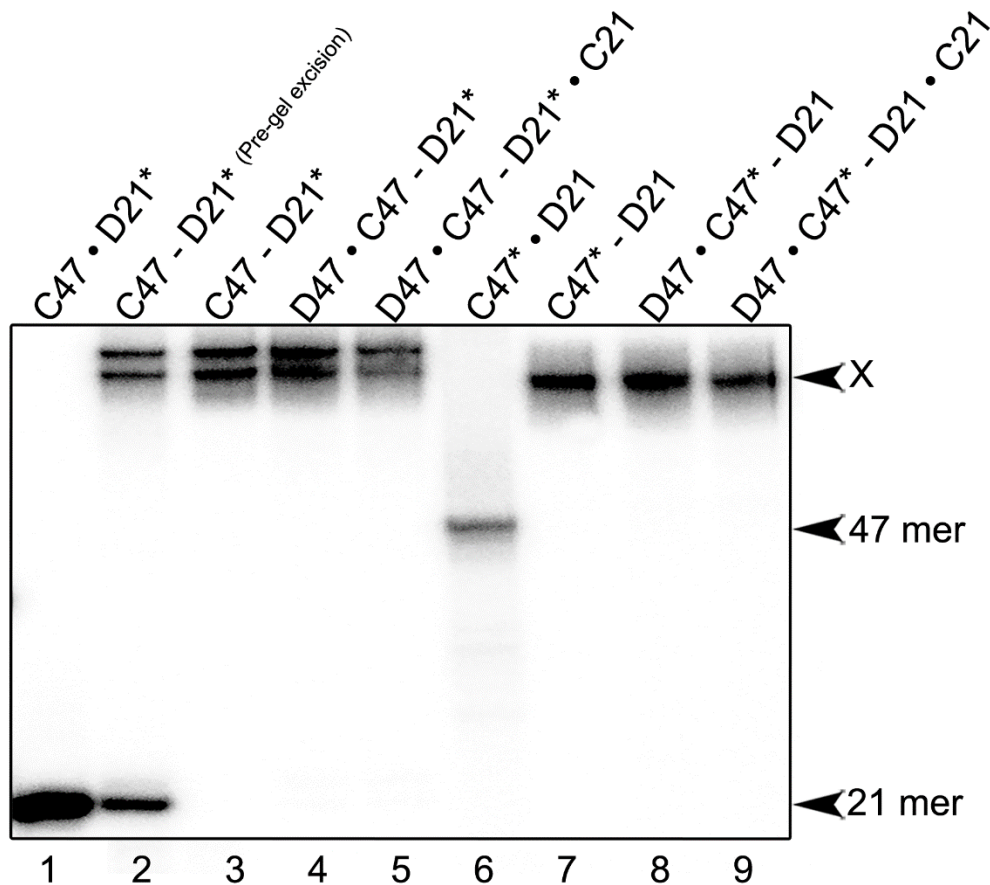


**Figure 4.4: Denaturing PAGE analysis of psoralen/UVA treated, duplex, three and four-stranded oligonucleotide structures.** Psoralen ICL lesion remain stable after gel purification. DNA substrates were analysed by denaturing PAGE. (X). Denotes DNA oligonucleotide containing psoralen ICL. "\*" Denotes 5' <sup>32</sup>P labelled oligonucleotide DNA oligonucleotide, "•" hydrogen bond DNA complementation, "-" psoralen/UVA treated and ICL bound DNA.

#### 4.1.2. hNEIL3 protein concentration titration for activity on three-stranded ICL oligonucleotides.

Due to difficulties in the production of hNEIL3 recombinant proteins, previously prepared hNEIL3<sup>Cat</sup>, hNEIL3<sup>Trun</sup> and hNEIL3<sup>FL</sup> recombinant proteins of high purity from laboratory stocks were used for biochemical characterisation. These proteins were previously analysed through SDS-PAGE, western blot (Mustafa Albelazi, University of Salford: **Appendix Figure 1; Appendix Figure 2; Appendix Figure 3**) and enzymatic activity assays.

As hNEIL1 has been previously confirmed to process three-stranded ICLs (Couvé *et al.*, 2009), enzymatic activity analysis was carried out on alternatively labelled XL47 • 47 – 21 three-stranded ICL substrates, generated as described in 2.17. This was to determine if hNEIL3 was also capable of resolving an ICL adduct in three-stranded context. After generation of three-stranded ICL substrates, activity of hNEIL3<sup>Cat</sup>, hNEIL3<sup>Trun</sup> and hNEIL3<sup>FL</sup> was assessed on the XL47 • 47 - 21\* three-stranded ICL DNA oligonucleotide construct, with and without light piperidine treatment.

As observed in **Figure 4.5**, the addition of increasing concentrations of hNEIL3 recombinant protein resulted in a smeared cleavage product. With use of light piperidine treatment which conducts  $\beta$ -elimination of the phosphodiester backbone, the smeared product became defined as a single band. This is suggested to represent the unhooking of the 21\* mer strand of the three-stranded ICL, generating an AP site on the 21\* mer strand, which degrades under standard reaction conditions to produce a smear. Subsequently, light Piperidine treatment processes the AP-site by  $\beta$ -elimination to generate an 8<sup>PA</sup>mer product. While hNEIL3 was previously characterised to possess an associated weak  $\beta$ -elimination, hNEIL3 recombinant proteins demonstrate a monofunctional profile. This is indicated by unhooking the psoralen ICL, generating an AP site on the 21\* labelled oligonucleotide site of cleavage. Furthermore, without the addition of piperidine, an increase in a cleavage product doublet was observed in the centre of the gel, while in the presence of piperidine the doublet was consistently produced. The lower band of the doublet is proposed to be unhooked 21\* mer strand containing an unprocessed AP site which has not degraded, generated from the unhooking activity discussed above. The upper band of the doublet is suggested to be representative of a second hNEIL3 unhooking activity, which unhooked the ICL from the 47 mer oligonucleotide

side of the ICL, presumably generating an AP site. The 21\*mer strand then retained the ICL adduct resulting in a slower migration in line with the *Nei* control product and thus representative of a ss-MA product. Piperidine is proposed to generate the doublet as product of unhooking at both sides of the ICL construct as observed when conducting hot alkali treatment of ICLs (Couv -Privat *et al.*, 2007).

The data indicates hNEIL3 possesses unhooking activity on both sides of the three-stranded ICL, thus generating an unhooked 21\* mer strand with an AP site and simultaneously an unhooked 21\* mer strand with the ICL retained, which represented a 21\* mer MA migrating in line with the 21-MA product produced by *Nei*. *Nei* was previously characterised to display the later described activity (Couv  *et al.*, 2009). Finally, it is apparent that hNEIL3<sup>Cat</sup> was more active than hNEIL3<sup>Trun</sup> and hNEIL3<sup>FL</sup> recombinant proteins at comparable concentrations, while all recombinant proteins possessed some residual activity on the XL47 • 47 - 21\*substrate. This indicates that the glycosylase domain of recombinant hNEIL3 is responsible for the observed unhooking activity, that the C-terminal domain possesses uncharacterised inhibitory domains or promotes inherent instability and therefore loss of activity at comparable concentrations.

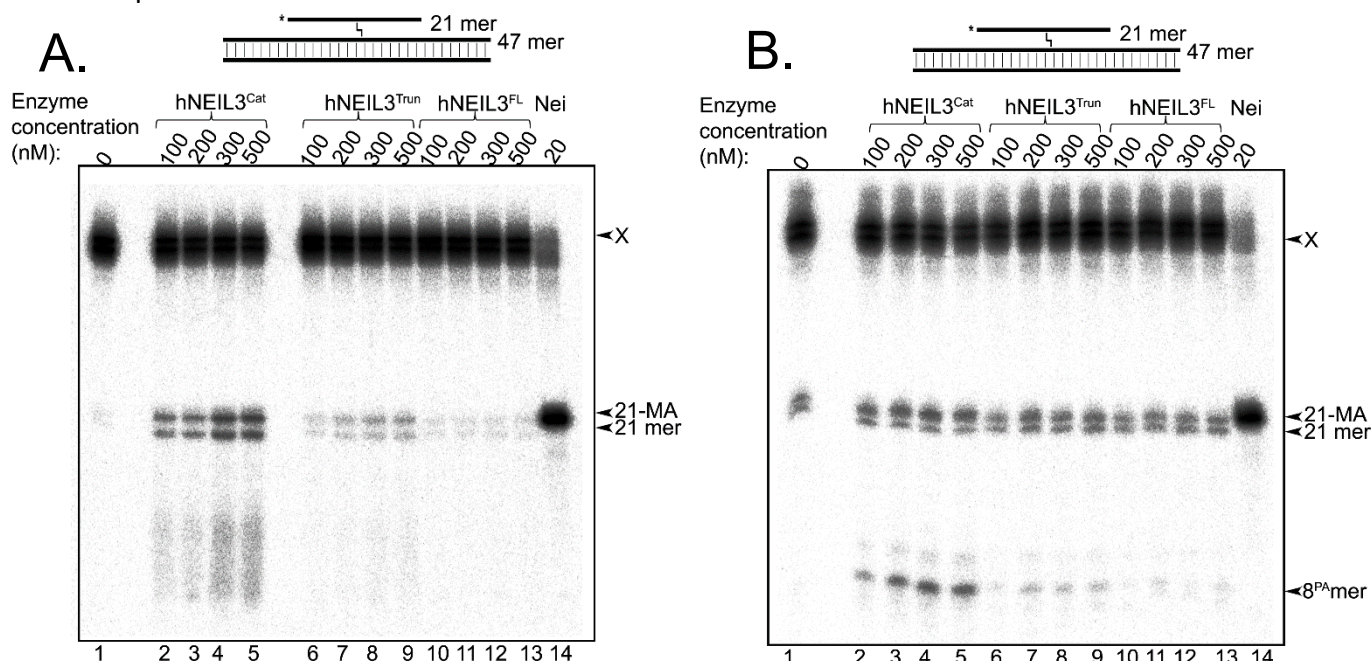


**Figure 4.5: Denaturing PAGE analysis of XL47 • 47 - 21\* DNA oligonucleotides incubated with hNEIL3 proteins.** hNEIL3 proteins unhook psoralen ICLs in a three-stranded DNA context with a monofunctional profile. hNEIL3<sup>Cat</sup>, hNEIL3<sup>Trun</sup>, hNEIL3<sup>FL</sup> and *Nei* protein activity on ~10 nM XL47 • 47 - 21\*mer generated three-stranded DNA ICL. A. (lanes 1-15) Reactions were without piperidine treatment. B. Reactions were with light piperidine treatment. B. Ctrl sample is in the absence of recombinant protein. *Nei* as control for previously characterised psoralen ICL unhooking activity. "X" denotes substrate, A. "21-MA" denotes 21 mer fragment containing psoralen-derived MA, A. "21-mer" B. "47-mer" denote cleavage fragments containing an AP (Lanes 2-13), A. "8<sup>PA</sup>", denotes 8 mer fragments containing a 3'-terminal PA.

**Figure 4.6** displays the percentage cleavage of the XL47 • 47 - 21\* oligonucleotide by recombinant hNEIL3 proteins, determined through use of ImageGuage V4.0 (Fujifilm). It was observed that up to a concentration of 300 nM the increase in cleavage product is relatively linear. Therefore, a concentration within the linear range of the graph was selected for downstream time course analysis for the determination of protein kinetics as the reaction is not saturated by recombinant protein. At 500 nM the cleavage percentage reached a maximal activity plateau for all recombinant proteins analysed and resulted in > 40% cleavage. Consequently, 500 nM of recombinant hNEIL3 proteins was selected for downstream qualitative analysis to achieve comparative maximal cleavage of oligonucleotides substrates for mechanistic elucidation. The observation that cleavage reached a plateau before complete cleavage of the oligonucleotide substrate, indicated that the reaction was limited by an external factor. It may suggest that recombinant hNEIL3 protein requires protein partners or co-factors to increase enzyme processivity.

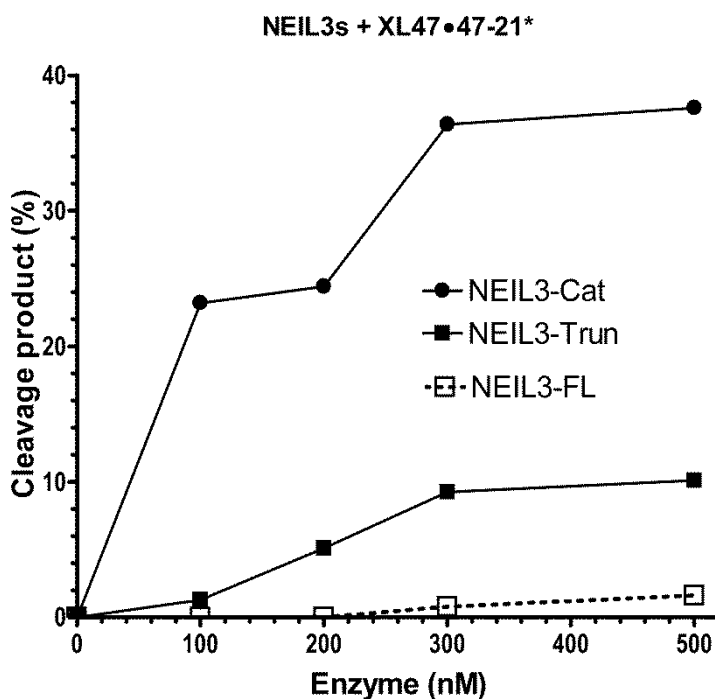


**Figure 4.6:** Quantification of the percentage cleavage of XL47 • 47 - 21\* three-stranded DNA ICL substrate by hNEIL3<sup>Cat</sup>, hNEIL3<sup>Trun</sup> and hNEIL3<sup>FL</sup>. “\*” Denotes 5' 32P labelled oligonucleotide DNA oligonucleotide, “•” hydrogen bond DNA complementation, “-” psoralen/UVA treated and ICL bound DNA.

#### 4.1.3. hNEIL3, Nei and hNEIL1 protein concentration titration for activity on Sp1 substrates.

Nei family protein activity on Sp DNA lesions has been previously established (Krokeide *et al.*, 2013). Therefore, the titration of recombinant hNEIL3 cleavage activity in the presence of Sp containing oligonucleotide substrates was required for the determination of control enzyme kinetics. This in turn would facilitate comparison and characterisation of recombinant hNEIL3 kinetics in the presence of three- and four-stranded psoralen ICL oligonucleotides.

As observed in **Figure 4.7** A and B, cleavage of the ss-Sp1 oligonucleotide substrate by hNEIL3<sup>Cat</sup> was greater than that facilitated by hNEIL3<sup>Trun</sup> and hNEIL3<sup>FL</sup>. However, all hNEIL3 recombinant proteins displayed robust activity when processing the ss-Sp1 oligonucleotide when compared to three-stranded psoralen ICL oligonucleotide (**Figure 4.5**).

As observed in **Figure 4.7** C, linear cleavage activity by hNEIL3<sup>Cat</sup> and hNEIL3<sup>Trun</sup> is observed at concentrations of up to ~100 nM, with hNEIL3<sup>FL</sup> maintaining linear behaviour cleavage up to the maximum concentration of 300 nM. At 100 nM hNEIL3<sup>Cat</sup>, hNEIL3<sup>Trun</sup> and 300 nM hNEIL3<sup>FL</sup> a greater cleavage product percentage was generated compared to the maximal percentage achieved by 500 nM hNEIL3<sup>Cat</sup> in the presence of the three-stranded psoralen ICL oligonucleotide substrate (**Figure 4.6**). This suggests that hNEIL3 recombinant proteins have a preference for Sp substrates rather than three-stranded ICLs, displaying a difference in protein kinetics. In the case of Nei a plateau at 5 nM was produced, whereas this was achieved at 20 nM for hNEIL1 (**Figure 4.7** B; D). Therefore, recombinant hNEIL1 and Nei demonstrate increased activity on ds Sp1 substrates compared hNEIL3 proteins on ss Sp1, saturating at lower concentrations. Alternatively, Nei and NEIL1 proteins may possess increased stability in reaction compared to hNEIL3 proteins which are observed to be unstable (**Appendix Figure 1; Appendix Figure 2; Appendix Figure 3**), accounting for requirement of higher concentrations for comparable cleavage. As demonstrated by all but hNEIL3<sup>FL</sup>, recombinant proteins analysed in **Figure 4.7**, achieve a cleavage percentage plateau before cleaving 100% of the oligonucleotide substrate. This may indicate that the recombinant proteins examined require protein partners or co-factors to improve enzymatic turnover and processivity in the presence of Sp containing lesions.

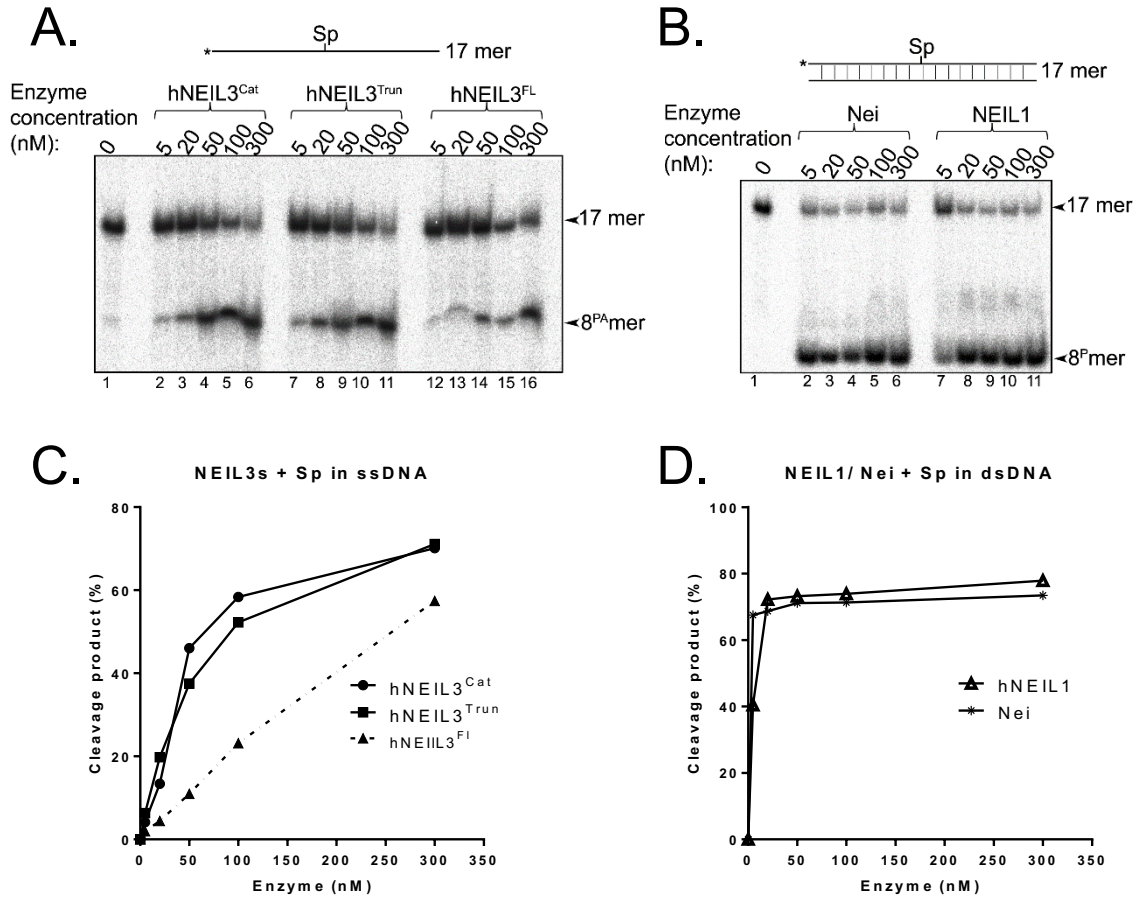


**Figure 4.7: Denaturing PAGE analysis of Sp1 containing DNA oligonucleotides incubated with hNEIL3<sup>Cat</sup>, hNEIL3<sup>Trun</sup>, hNEIL3<sup>FL</sup>, hNEIL1 and Nei.** A. hNEIL3<sup>Cat</sup>, hNEIL3<sup>Trun</sup> and hNEIL3<sup>FL</sup> protein activity upon 10 nM ss Sp1 substrate. B. Nei and hNEIL1 activity upon 10 nM ds Sp1 substrate. "17 mer" denotes substrate, A-B. "8<sup>PA</sup>" and "8<sup>P</sup>" denotes 8 mer fragments containing a 3'-terminal PA and P, respectively. C. Quantification of hNEIL3<sup>Cat</sup>, hNEIL3<sup>Trun</sup> and hNEIL3<sup>FL</sup> generated cleavage product percentages after enzymatic cleavage assay on 10 nM ss Sp1 substrate. D. Quantification of Nei and hNEIL1 generated cleavage product percentages after enzymatic cleavage assay on 10 nM ds Sp1 substrate.

#### 4.1.4. hNEIL3 unhooking activity of a single-stranded HMT generated MA.

As NEIL3 has been observed to display a preference for ss oxidative lesion containing substrates, enzymatic activity analysis was carried out on a ss MA substrate, generated as described in section 2.15. **Figure 4.8** shows active cleavage by hNEIL3 of the XL21\* - 1 substrate, with increased efficiency by hNEIL3<sup>Cat</sup> compared to hNEIL3<sup>Trun</sup> and hNEIL3<sup>FL</sup>. A small cleavage product was observed at ~8 mer as a smear without piperidine treatment, defined after light piperidine treatment. This is representative of the unhooking of the 21\* mer strand at the site of the MA, producing an AP site, which degrades under standard reaction conditions. It is suggested that small oligomers remain present, due to incomplete digestion by RNase A, thus a faint upper and lower band were observed surrounding the major ~8 mer product generated after light piperidine treatment. Nei and hNEIL1 displayed minimal activity on the XL21\* - 1 ss MA substrate. hNEIL3 proteins unhook ss MAs with a monofunctional profile.

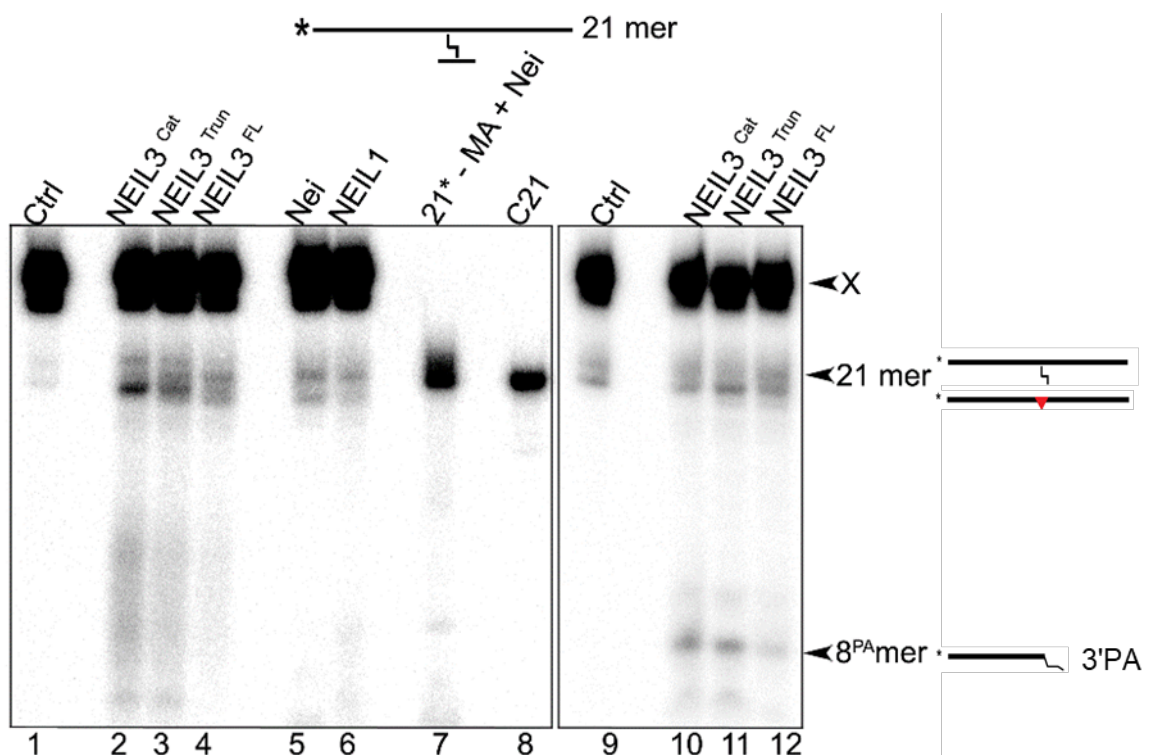


**Figure 4.8:** Denaturing PAGE analysis of ~ 10 nM (X): XL21\* - 1 ss MA substrate incubated with hNEIL3<sup>Cat</sup>, hNEIL3<sup>Trun</sup>, hNEIL3<sup>FL</sup>, hNEIL1 and Nei. Samples were incubated for 1 h at 37°C with 500 nM of protein. For positive control 20 nM of bacterial Nei was used and 500 nM hNEIL1. (Lanes 1-8) Reactions were without piperidine treatment. "Ctrl" sample in the absence of recombinant protein. (Lanes 9-12) Reactions with light piperidine treatment. "X" denotes substrate, A. "21-MA" denotes 21 mer fragment containing a psoralen-derived MA, "21-mer" denote cleavage fragments containing an AP (Lanes 2-4), "8<sup>PA</sup>" denote 8 mer fragments containing a 3'-terminal PA respectively.

#### 4.1.5. hNEIL1, hNEIL3 and Nei unhooking activity of a three-stranded HMT generated ICL oligonucleotide substrate.

To elucidate the mechanism of recombinant hNEIL3 protein resolution of three-stranded psoralen ICL oligonucleotide substrates, qualitative analysis of cleavage activity was undertaken. The use of XL47 • 47 – 21 psoralen ICL oligonucleotide substrate, alternatively  $5^{32}\text{P}$  labelled on either the 21 mer or 47 mer side of the ICL would allow for determination of the cleavage profile presented by recombinant proteins.

**Figure 4.9** A shows cleavage by hNEIL3 of the XL47 • 47 - 21\* substrate, with increased efficiency by hNEIL3<sup>Cat</sup> compared to hNEIL3<sup>Trun</sup> and hNEIL3<sup>FL</sup>. A small cleavage product was observed at ~8 mer as a smear without Piperidine treatment. After light piperidine treatment this smear became defined as an 8<sup>PA</sup> mer in reference to the activity control D21-U+UDG+LP treatment which also yields an 8 mer fragment with a 3' terminal PA. This is representative of unhooking on the 21\* mer strand side of the ICL, producing an AP site, which degrades under standard reaction conditions to yield a smeared pattern. After light Piperidine treatment the AP site becomes further processed by  $\beta$ -elimination, generating an 8 mer 3'-terminal PA. A doublet of cleavage products was also observed in the centre of the gel, the upper of which migrated in line with 21\*-MA substrate and is proposed to be the 21\* mer strand with the ICL remaining attached (ss-MA), unhooked at the 47 mer strand side of the ICL. The lower band represents the 21\* mer strand with an AP site and the ICL unhooked, which migrated in line with D21 size control. Nei and hNEIL1 however resulted in the formation of the upper band of the doublet, representing the 21\* mer strand with the ICL attached, unhooked at the 47 mer strand only and in agreement with previous observations (Couvé *et al.*, 2009).

In reference to D21, C47 and the D21-U+UDG 3' terminal markers, these results suggest that hNEIL3 possesses the same DNA glycosylase unhooking activity as Nei and hNEIL1, however hNEIL3 proteins do not demonstrate incision of the phosphodiester backbone. Additionally, hNEIL3 can unhook an ICL from the 21\* mer strand side of the structure generating an AP site. Finally, hNEIL3 processes the unhooked three-stranded ICL through a mainly monofunctional profile rather than bifunctional as presented by hNEIL1 and Nei. Thus, hNEIL3 mediated cleavage of a three-stranded psoralen ICL is independent of ss-DNA breaks.

**Figure 4.9 B.** shows cleavage by hNEIL3 of the XL47 • 47\* - 21 substrate, with increased efficiency by hNEIL3<sup>Cat</sup> compared to hNEIL3<sup>Trun</sup> and hNEIL3<sup>FL</sup>. A small cleavage product was observed at ~23 mer as a smear without piperidine treatment. After light piperidine treatment this smear became defined as a 23<sup>PA</sup> mer in reference to the activity control C47-U with UDG and light piperidine treatment which also yields a 23 mer fragment with a 3' terminal PA. This is representative of unhooking on the 47\* mer strand side of the ICL, producing an AP site, which degrades under standard reaction conditions to yield a smeared pattern. After light piperidine treatment the AP site becomes further processed by  $\beta$ -elimination generating a 23 mer 3' terminal PA. A cleavage product which migrated in line with both the C47 size marker and the band representing the 47-47\* MA substrate marker was observed. This is proposed to be the 47\* mer strand with the ICL attached (ds-MA), unhooked at the 21 mer strand side and an indistinguishable band representing the 47\* mer strand with an AP site and the ICL unhooked. Nei and hNEIL1 however resulted in the formation of one band, representing the ~23 mer strand after unhooking at the 47 mer strand, creating an AP site, cleaved by the associated  $\beta,\delta$ -elimination AP lyase.

In reference to D21, C47 and the D47-U+UDG 3' terminal markers, these results suggest that hNEIL3 can unhook the same thymine from the 47 mer side of the structure as Nei and hNEIL1. Additionally, hNEIL3 can unhook an ICL from the 21\* mer strand side of the structure generating an AP site. Finally, hNEIL3 processes the unhooked three-stranded ICL through a mainly monofunctional profile rather than bifunctional, as presented by hNEIL1 and Nei. Thus, hNEIL3 mediated cleavage of a three-stranded psoralen ICL is independent of ss-DNA breaks.

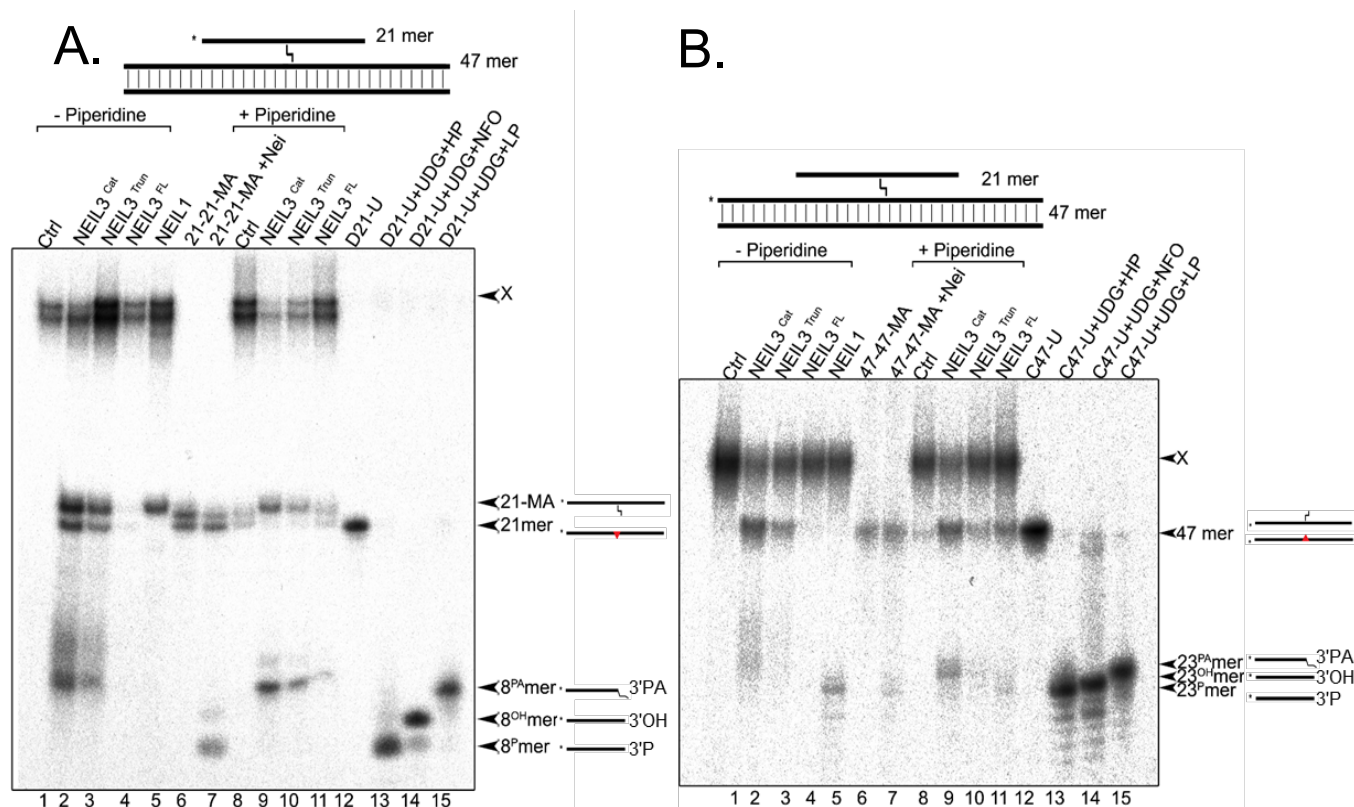


**Figure 4.9: Denaturing PAGE analysis: A. ~10 nM (X): XL47 • 47 - 21\* B. ~10 nM (X) XL47 • 47\* - 21 HMT generated three-stranded DNA ICL incubated with of hNEIL3<sup>Cat</sup>, hNEIL3<sup>Trun</sup>, hNEIL3<sup>FL</sup>, hNEIL1 and Nei protein.** Samples were incubated for 1 h at 37°C with 500 nM of protein. For positive control 50 nM of hNEIL1 was used. (Lanes 1-7) Reactions without piperidine treatment. (Lanes 7-12) Reactions with light piperidine treatment. (Lane 7) 21\* mer ds-MA substrate digested with *Nei* cleavage, product control. (Lane 8) 47\* mer ds-MA substrate digested with *Nei*, cleavage product control. (Lane 6) A. 21 C21\* MA B.47 • 47\* ss oligonucleotide size marker. (Lane 10) D47, 47 mer ss oligonucleotide size marker. (Lane 12) A. 21\* B. 47\* mer oligonucleotides. (Lane 13-15) A. 21 U • A duplex B. 47 U • A duplex with UDG/Hot Piperidine treatment, UDG/Nfo and UDG/light Piperidine, respectively. Substrate and cleavage products sizes are indicated to the right of the gel. "X" denotes substrate, A. "21-MA" denotes 21 mer fragment containing a psoralen-derived MA, A. "21-mer" B."47-mer" denote cleavage fragments containing an AP (Lanes 2-4), A. "8<sup>PA</sup>", "8<sup>OH</sup>" and "8<sup>P</sup>" denote 8 mer B. 23<sup>PA</sup>", "23<sup>OH</sup>" and "23<sup>P</sup>" denote 23 mer, fragments containing a 3'-terminal PA, OH and P, respectively.

Data obtained and displayed in **Figure 4.9** facilitated further mechanistic insight into the biochemical action of hNEIL3 recombinant protein resolution of three-stranded psoralen ICL oligonucleotides. This facilitated the schematic representation of the mechanistic action of recombinant *Nei*, hNEIL1 and hNEIL3 in relation to one another (**Figure 4.10**).

*Nei* and hNEIL proteins unhook the three-stranded psoralen ICL oligonucleotide structure uniquely from the thymidine within the duplex, releasing the ss-MA portion of the structure. In addition, the associated  $\beta,\delta$ -elimination by *Nei* and hNEIL1 induces a ss nick at the AP site within the duplex portion of three-stranded structure after removal of the thymidine. Counter to this hNEIL3 can unhook the psoralen ICL from the thymidine within the ss or duplex portion

of the structure. The activity of hNEIL3 is monofunctional and subsequently results in the generation of AP sites rather than ss-nicks after unhooking of the covalently linked thymidine. In addition, it is proposed that the ds-MA generated as a product of hNEIL3 mediated cleavage, may be processed downstream by the previously characterised activity of hNEIL1 (Couvé-Privat *et al.*, 2007).

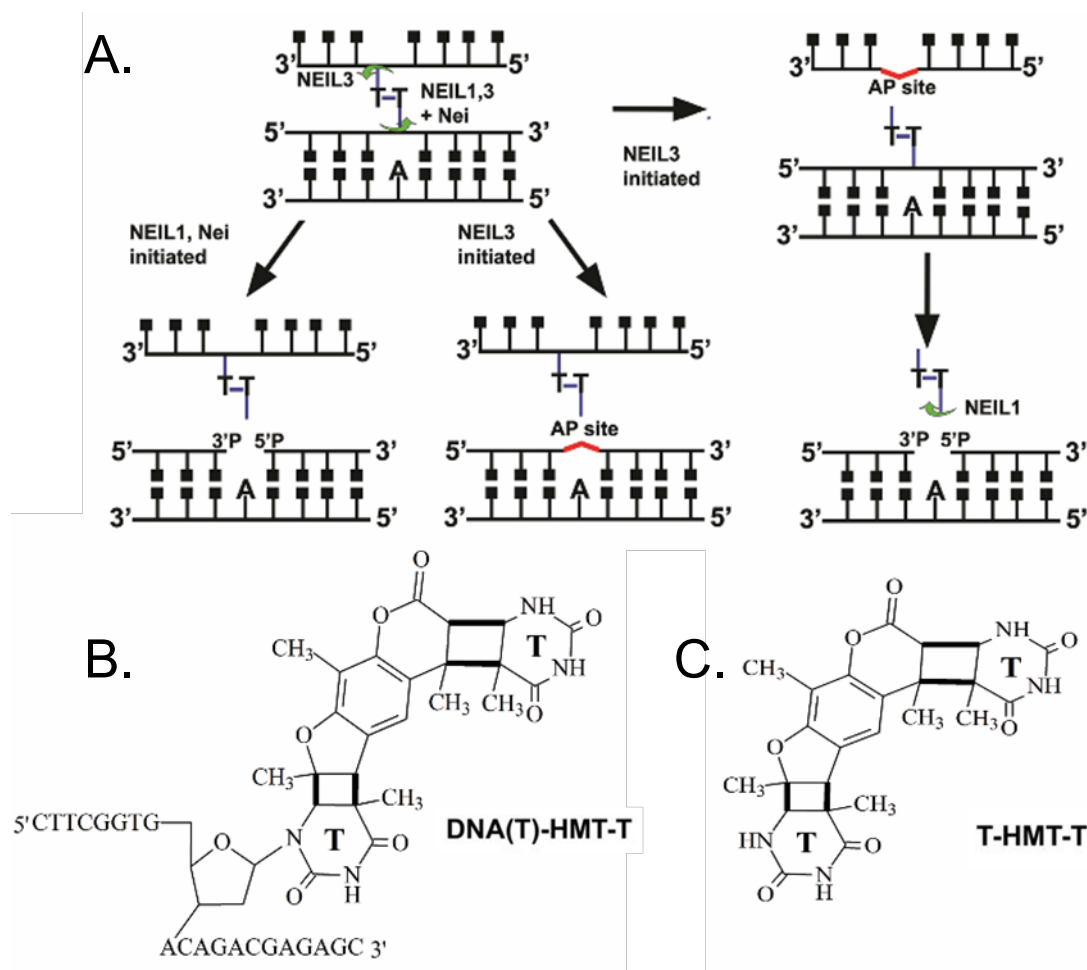


**Figure 4.10: Schematic representation of the mechanistic biochemical action of Nei, hNEIL1 and hNEIL3 DNA glycosylases on three-stranded psoralen ICL oligonucleotide substrates.** A. Mechanism of action of the Nei, hNEIL1 and hNEIL3 recombinant DNA glycosylases on three-stranded psoralen ICL oligonucleotides. B. Skeletal formula of an unhooked ss-21\* mer HMT MA with thymine from opposite complementary DNA strand, produced by Nei, hNEIL1 and hNEIL3 facilitated DNA glycosylases excision. C. Skeletal formula of proposed thymine-HMT-thymine excision product generated post hNEIL3 facilitated unhooking and subsequent downstream processing of ds-MA product by hNEIL1.

#### 4.1.6. hNEIL3 and Nei unhooking activity of four-stranded HMT generated ICL oligonucleotide substrate.

It has previously been shown that TLS DNA polymerases can bypass an ICL lesion with primer extension facilitated by Rev1/Pol $\zeta$ , in addition the FANCM protein has been shown to possess translocase activity, facilitating replication traverse and fork restart (Huang *et al.*, 2013; Budzowska, *et al.*, 2015). This may suggest that continuation of replication past an ICL without the Fanconi anemia mediated incision step may take place *in vivo*. Thus, synthesis on both strands during DNA replication may yield a long four stranded ICL structure. Therefore, enzymatic activity analysis was carried out on alternatively 5<sup>32</sup>P labelled 8-MOP (**Appendix Figure 4**) or HMT XL47 • 47 - 21 • 21 four-stranded ICL DNA oligonucleotides, generated as described in 2.17. This was to determine if hNEIL1 and hNEIL3 were capable of resolving an ICL adduct in four-stranded context.

**Figure 4.11** A shows cleavage by hNEIL3 of the XL47 • 47 - 21\* • 21 substrate, with increased efficiency by hNEIL3<sup>Cat</sup> compared to hNEIL3<sup>Trun</sup> and hNEIL3<sup>FL</sup>. A small cleavage product was observed at ~8 mer as a smear without Piperidine treatment. After light piperidine treatment this smear became defined as an 8<sup>PA</sup>mer in reference to the activity control D21-U with UDG and light piperidine treatment which also yields an 8 mer fragment with a 3' terminal PA. This is representative of unhooking on the 21\* mer strand side of the ICL, producing an AP site, which degrades under standard reaction conditions to yield a smeared pattern. After light piperidine treatment the AP site becomes further processed by  $\beta$ -elimination generating an 8 mer 3'-terminal PA. A doublet of cleavage products was also observed in the centre of the gel, the upper of which migrated in line with the 21\*-MA substrate and is proposed to be the 21\* mer strand with the ICL remaining attached (ss-MA), unhooked at the 47 mer strand side of the ICL. The lower band represents the 21\* mer strand with an AP site and the ICL unhooked, which migrated in line with the D21 size control. Nei however resulted in the formation of an 8<sup>P</sup>mer product with reference to the D21-U+UDG+HP 3' terminal cleavage marker. This is suggested due to initial unhooking of the ICL from either side of the duplex followed by further processing of the ds-MA product formed and or production of a nick through associated  $\beta,\delta$ -elimination of the phosphodiester backbone.

In reference to D21, C47 and the D21-U+UDG 3' terminal markers, these results suggest that hNEIL3 possesses the same initial unhooking activity of Nei. However, hNEIL3 processes the four-stranded ICL through a monofunctional profile rather than  $\beta,\delta$ -elimination as presented by Nei. Thus, hNEIL3 mediated cleavage of a four-stranded psoralen ICL is independent of ss-DNA breaks. **Figure 4.11 B.** shows cleavage by hNEIL3 of the XL47 • 47\* - 21 • 21 substrate, with increased efficiency by hNEIL3<sup>Cat</sup> compared to hNEIL3<sup>Trun</sup> and hNEIL3<sup>FL</sup>. A small cleavage product was observed at ~23 mer as a smear without piperidine treatment. After light piperidine treatment this smear became defined as a 23<sup>PA</sup>mer in reference to the activity control C47-U with UDG and light piperidine treatment which also yields a 23 mer fragment with a 3' terminal PA. This is representative of unhooking on the 47\* mer strand side of the ICL, producing an AP site, which degrades under standard reaction conditions to yield a smeared pattern. After light Piperidine treatment the AP site becomes further processed by  $\beta$ -elimination generating a 23 mer 3' terminal PA. A cleavage product which migrated in line with both the C47 size marker and the band representing the 47-47\* MA substrate marker was observed. This is proposed to be the 47\* mer strand with the ICL attached (ds-MA), unhooked at the 21 mer strand side and an indistinguishable band representing the 47\* mer strand with an AP site and the ICL unhooked. Nei however resulted in the formation of a 23<sup>P</sup>mer product with reference to the D47-U+UDG+HP 3' terminal cleavage marker. This is suggested to be due to initial unhooking of the ICL from the either side of the duplex followed by further processing of the ds-MA product formed and or production of a nick by associated  $\beta,\delta$ -elimination. hNEIL1 displayed inhibited cleavage of the HMT generated four-stranded ICL oligonucleotides. However, robust activity was observed on alternatively labelled (21\*/ 47 \*) 8-MOP generated four-stranded ICL oligonucleotides (**Appendix Figure 4**). hNEIL1 displays unhooking activity by excising the thymine present on the 21 or 47 mer duplex, generating a ss-nick through associated  $\beta,\delta$ -elimination of the phosphodiester backbone.

In reference to D21, C47 and the D47-U+UDG 3' terminal markers, these results suggest that hNEIL3 can unhook the same thymine as Nei and hNEIL1. However, hNEIL3 processes the four-stranded ICL through a mainly monofunctional profile rather than bifunctional as presented by hNEIL1 and Nei. Thus, hNEIL3 mediated cleavage of a four-stranded psoralen ICL is independent of ss-DNA breaks.

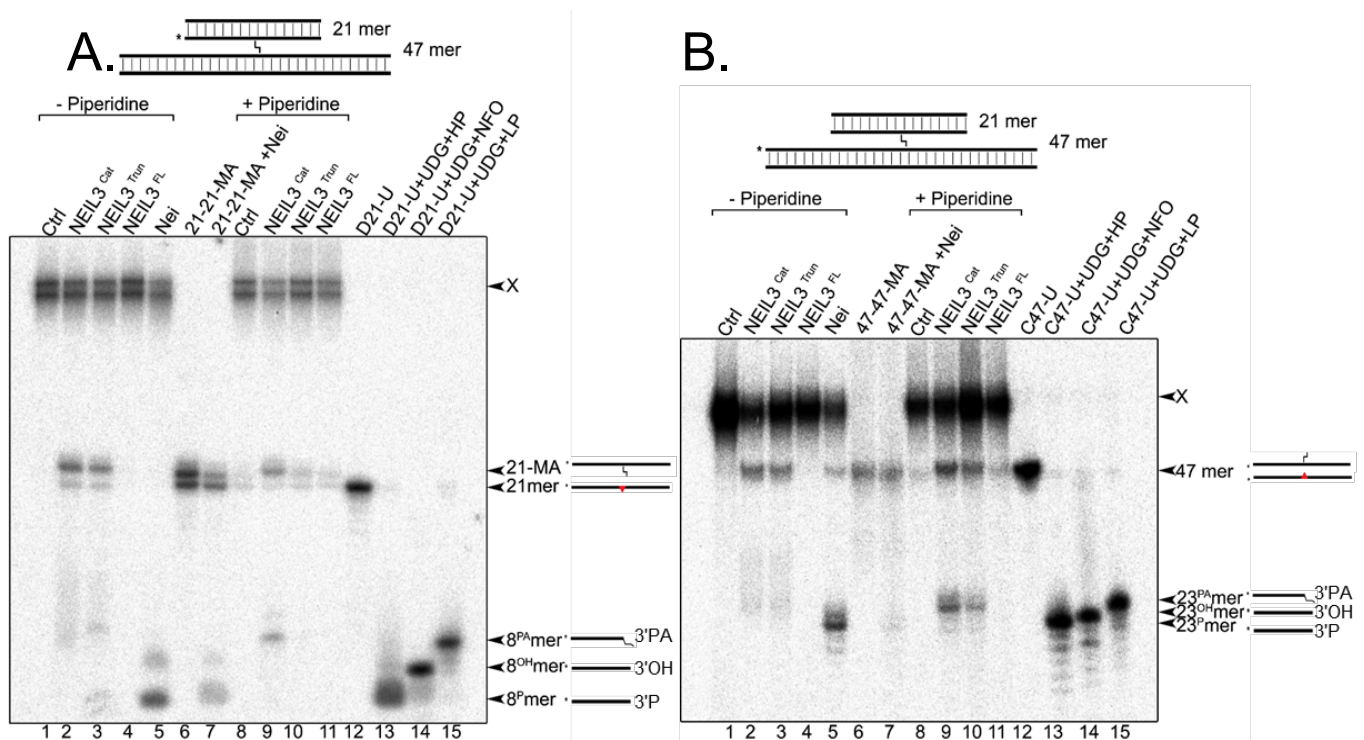


**Figure 4.11: Denaturing PAGE analysis of hNEIL3<sup>Cat</sup>, hNEIL3<sup>Trun</sup>, hNEIL3<sup>FL</sup>, hNEIL1 and Nei protein activity on: A. ~10 nM (X): A. XL47 • 47 - 21\* • 21. B. ~10 nM (X): XL47 • 47\* - 21 • 21 HMT generated three-stranded DNA ICL. Samples were incubated for 1 h at 37°C with 500 nM of protein. For positive control 20 nM of bacterial Nei was used and 500 nM hNEIL1. (Lanes 1-7) Reactions without Piperidine treatment. (Lanes 7-12) Reactions with light piperidine treatment (Lane 7) 21\* mer ds-MA substrate digested with Nei cleavage, product control. (Lane 8) 47\* mer ds-MA substrate digested with Nei, cleavage product control. (Lane 6) A. 21 C21\* MA B.47 • 47\* ss oligonucleotide size marker. (Lane 10) D47, 47 mer ss oligonucleotide size marker. (Lane 12) A. 21\* B. 47\* mer oligonucleotides. (Lane 13-15) A. 21 U • A duplex B. 47 U • A duplex treated with UDG/Hot Piperidine, UDG/Nfo and UDG/Light Piperidine, respectively. Substrate and cleavage products sizes are indicated to the right of the gel. "X" denotes substrate, A. "21-MA" denotes 21 mer fragment containing a psoralen-derived MA, A. "21-mer" B. "47-mer" denote cleavage fragments containing an AP (Lanes 2-4), A. "8<sup>PA</sup>", "8<sup>OH</sup>" and "8<sup>P</sup>" denote 8 mer B. 23<sup>PA</sup>", "23<sup>OH</sup>" and "23<sup>P</sup>" denote 23 mer, fragments containing a 3'-terminal PA, OH and P, respectively.**

Data obtained and displayed in **Figure 4.11** and **Appendix Figure 4** facilitated further mechanistic insight into the biochemical action of hNEIL1/3 recombinant protein resolution of four-stranded psoralen ICL oligonucleotides. This facilitated the schematic representation of the mechanistic action of recombinant Nei, hNEIL1 and hNEIL3 in relation to one another (**Figure 4.12**). Nei and hNEIL1 DNA glycosylases unhook an ICL from both sides of the four-stranded structure, producing a ss-nick through associated  $\beta,\delta$ -elimination by Nei and hNEIL1,

generating a 3'-terminal P. Counter to this hNEIL3 can unhook the psoralen ICL from both sides of the ICL structure, but with a monofunctional profile and subsequently results in the generation of an AP site rather than a ss-nick after unhooking of the covalently linked thymidine. In addition, it is proposed that the ds-MA generated as a product of the initial cleavage by hNEIL1/hNEIL3, may be processed downstream by the previously characterised activity of hNEIL1 (**Figure 4.12**; Couvé-Privat *et al.*, 2007).

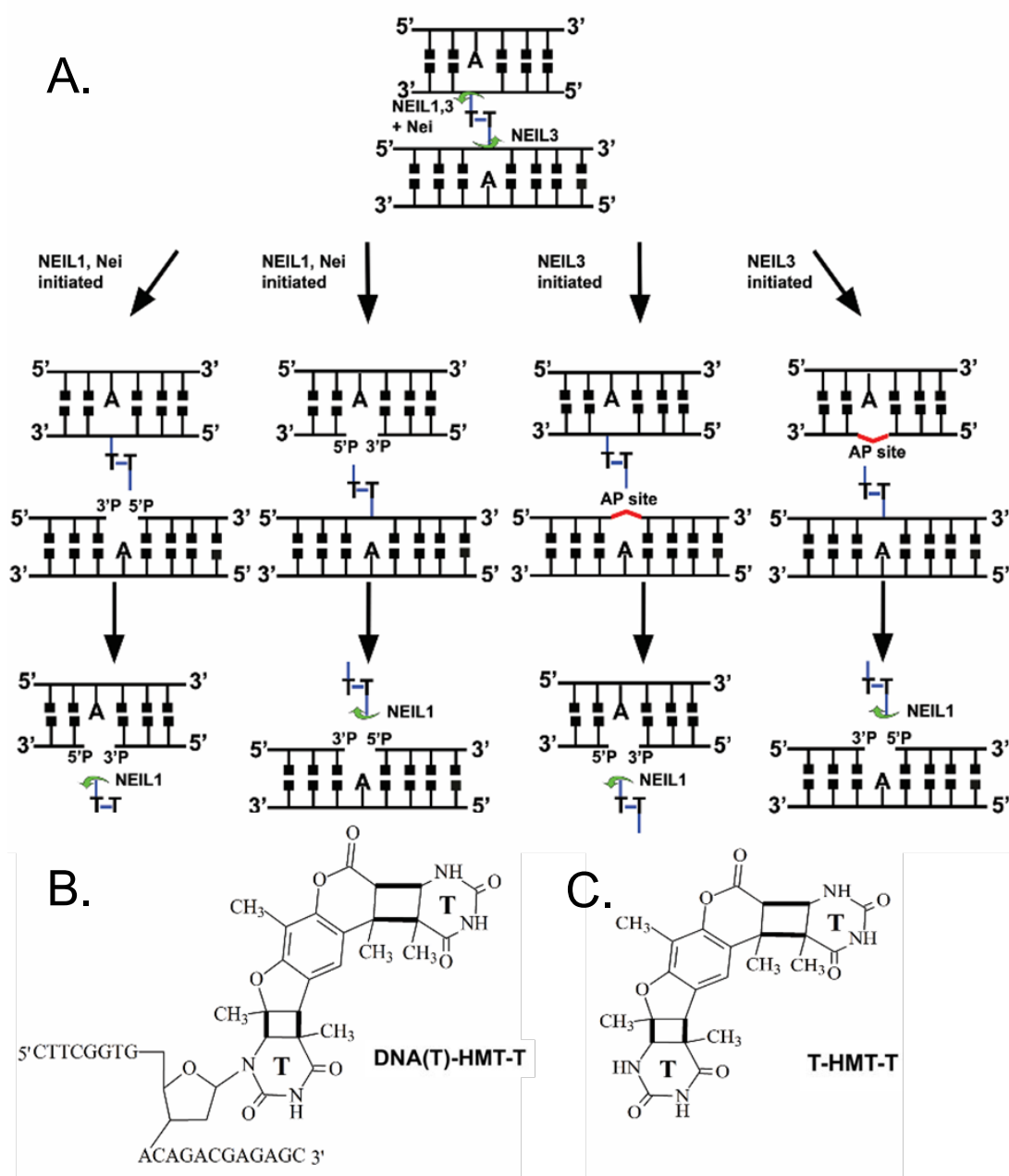


**Figure 4.12: Schematic representation of the mechanistic biochemical action of Nei, hNEIL1 and hNEIL3 DNA glycosylases on four-stranded psoralen ICL oligonucleotide substrates.** A. Mechanism of action of the Nei, hNEIL1 and hNEIL3 recombinant DNA glycosylases on three-stranded psoralen ICL oligonucleotides. B. Skeletal formula of an unhooked ss-21\* mer HMT MA with thymine from opposite complementary DNA strand, produced by Nei, hNEIL1 and hNEIL3 facilitated DNA glycosylases excision. C. Skeletal formula of proposed thymine-HMT-thymine excision product generated post hNEIL3 facilitated unhooking and subsequent downstream processing of ds-MA product by hNEIL1.

#### 4.1.7. hNEIL1, hNEIL3 and Nei unhooking activity of a long three-stranded HMT generated ICL oligonucleotide substrate.

To examine if the length of the psoralen ICL structure was crucial for recognition by the Nei, hNEIL1 and hNEIL3 DNA glycosylases, further enzymatic activity analysis was carried out on a XL101 • 101 – 47\* labelled long three-stranded ICL DNA substrate, generated as described in 3.16. This was to determine if hNEIL1 and hNEIL3 can resolve an ICL adduct larger in size, closer in representation to DNA *in vivo* in replication fork bypass context than as a product of MUS81-EME1 and ERCC1-XPF incision of 47 mer followed by TLS.

**Figure 4.13** demonstrates cleavage by hNEIL3 of the XL101 • 101 – 47\* substrate, with increased efficiency by hNEIL3<sup>Cat</sup> compared to hNEIL3<sup>Trun</sup> and hNEIL3<sup>FL</sup>. A small cleavage product was observed at ~23 mer as a smear without light piperidine, which became defined after light piperidine treatment as a 23<sup>PA</sup>mer. This is representative of the unhooking on the 47\*mer strand side of the ICL, producing an AP site which degrades under normal reaction conditions generating a smear. The light piperidine treatment subsequently facilitates cleavage of the AP site to generate a 23 mer containing a 3'-terminal PA. Additionally, despite a mainly monofunctional profile presented by hNEIL3 recombinant proteins, the definition of a 23<sup>PA</sup>mer product without addition of piperidine is more apparent, indicative of a weak associated  $\beta$ -elimination activity. A doublet of cleavage products was observed in the centre of the gel, the upper of which is proposed to be the 47\* mer strand with the ICL attached unhooked at the 101 mer strand side of the ICL, which migrated in line with the 47\*-MA substrate band. The lower being the 47\*mer strand with an AP site which migrated in line with the C47 size reference. Nei and hNEIL1 however resulted in the formation of the upper band representing the 47\* mer strand with the ICL attached, unhooked at the 101 mer strand, generating a ss-nick through associated  $\beta,\delta$ -elimination.

In reference to C47 size marker, these results suggest that hNEIL3 can unhook the same thymine from the 101 mer side of the structure as Nei and hNEIL1. Additionally, hNEIL3 can unhook an ICL from the 47\* mer strand side of the structure. However, hNEIL3 proteins display a mainly monofunctional profile, generating an AP site independent of ss-nicks. This said, compared to previous observations hNEIL3 recombinant proteins display a weak  $\beta$ -

elimination with the observation of a more defined 23<sup>PA</sup>mer cleavage product, which may indicate a preference for the processing of long three-stranded ICL structures.

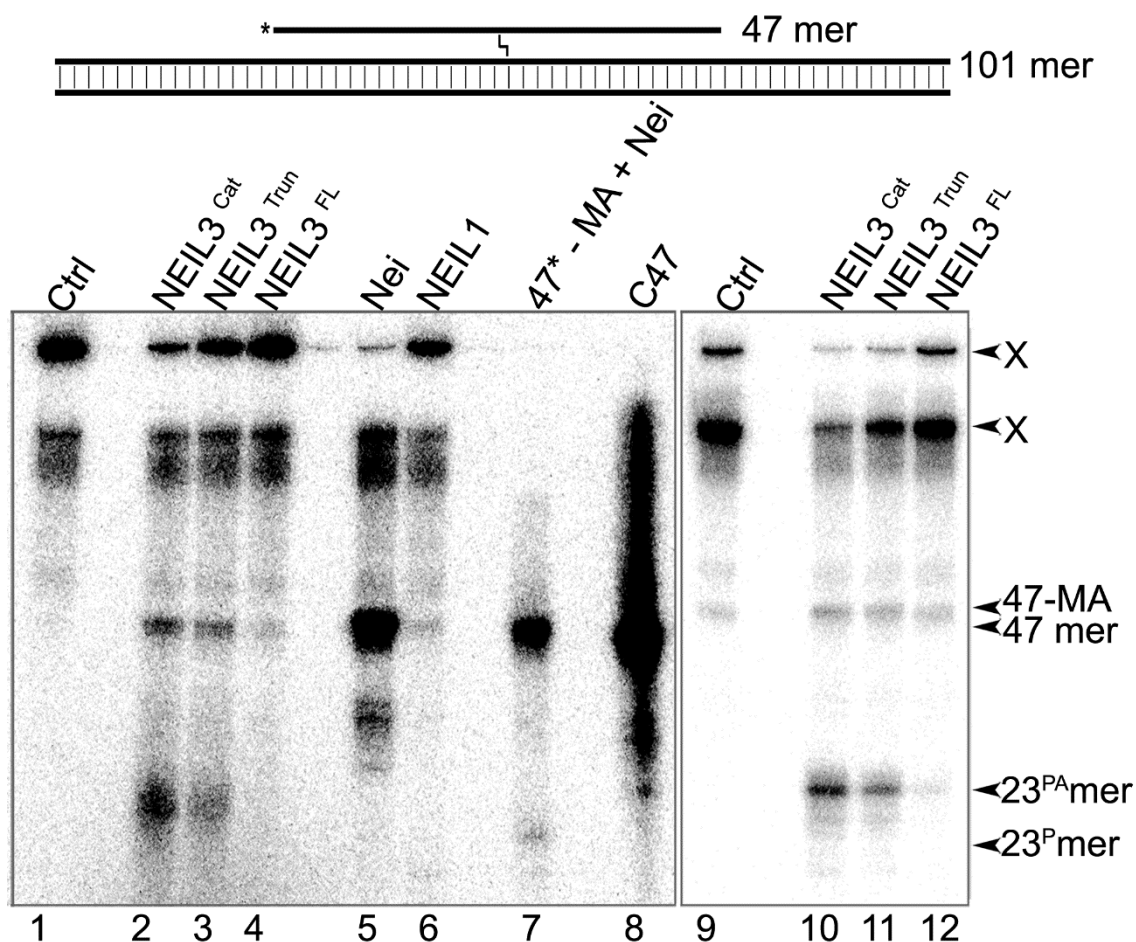


**Figure 4.13: Denaturing PAGE analysis hNEIL3<sup>Cat</sup>, hNEIL3<sup>Trun</sup>, hNEIL3<sup>FL</sup>, hNEIL1 and Nei proteins on ~10 nM (X): XL101 • 101 – 47\* HMT generated three-stranded DNA ICL.** Samples were incubated for 1 h at 37°C with 500 nM of protein. For positive control 20 nM of bacterial Nei was used and 500 nM hNEIL1. (Lanes 1-10) Reactions without piperidine treatment. (Lanes 11-14) Reactions with light piperidine treatment (Lane 7) 21\* mer ds-MA substrate digested with Nei cleavage, product control. (Lane 8) 47\* mer ds-MA substrate digested with Nei, cleavage product control. (Lane 9) C21, 21 mer ss oligonucleotide size marker. (Lane 10) D47, 47 mer ss oligonucleotide size marker. "X" denotes substrate, A. "47-MA" denotes 47 mer fragment containing a psoralen-derived MA, "47-mer" denote cleavage fragments containing an AP (Lanes 2-4). "23<sup>PA</sup>" and "23<sup>P</sup>" denote 23 mer, fragments containing a 3'-terminal PA and P, respectively.

**4.1.8.** hNEIL1, hNEIL3 and Nei protein unhooking activity of an 8-MOP generated three-stranded ICL oligonucleotide substrate.

Further enzymatic activity analysis was carried out on a XL47 • 47 – 21\* labelled three-stranded ICL DNA substrate, generated as described in 3.16. This was to determine if hNEIL3 can resolve an ICL adduct generated by 8-MOP rather than HMT only, to determine if activity was psoralen ICL specific rather than HMT specific.

**Figure 4.14** shows cleavage by hNEIL3 of the XL47 • 47 – 21\* substrate, with increased efficiency by hNEIL3<sup>Cat</sup> compared to hNEIL3<sup>Trun</sup> and <sup>FL</sup>. A small cleavage product was observed at ~8 mer as a smear without piperidine, defined in the presence of piperidine. This is representative of unhooking on the 21\* mer strand side of the ICL, producing an AP site, that degrades under standard reaction conditions to form a smeared pattern. Subsequently, light piperidine treatment cleaves the AP site through  $\beta$ -elimination. A doublet of cleavage products was observed in the centre of the gel, the upper of which migrated in line with 21\*-MA substrate and is proposed to be the 21\* mer strand with the ICL attached, unhooked at the 47 mer strand side of the ICL. The lower band represents the 21\* mer strand with an AP site and the ICL unhooked, migrating in line with D21 size control. Nei and hNEIL1 however resulted in the formation of the upper band of the doublet, representing 21\* mer strand with the ICL attached, unhooked at the 47 mer strand.

In reference to D21 and C47 size markers these results suggest that hNEIL3 can unhook the same thymine as Nei and hNEIL1 on the 47 mer side of the structure. Additionally, hNEIL3 can unhook an ICL from the 21\* mer strand side of the structure. However, hNEIL3 processes the unhooked three-stranded ICL with a monofunctional profile, generating an AP site, while Nei and hNEIL1 generate a ss-nick through associated  $\beta,\delta$ -elimination.

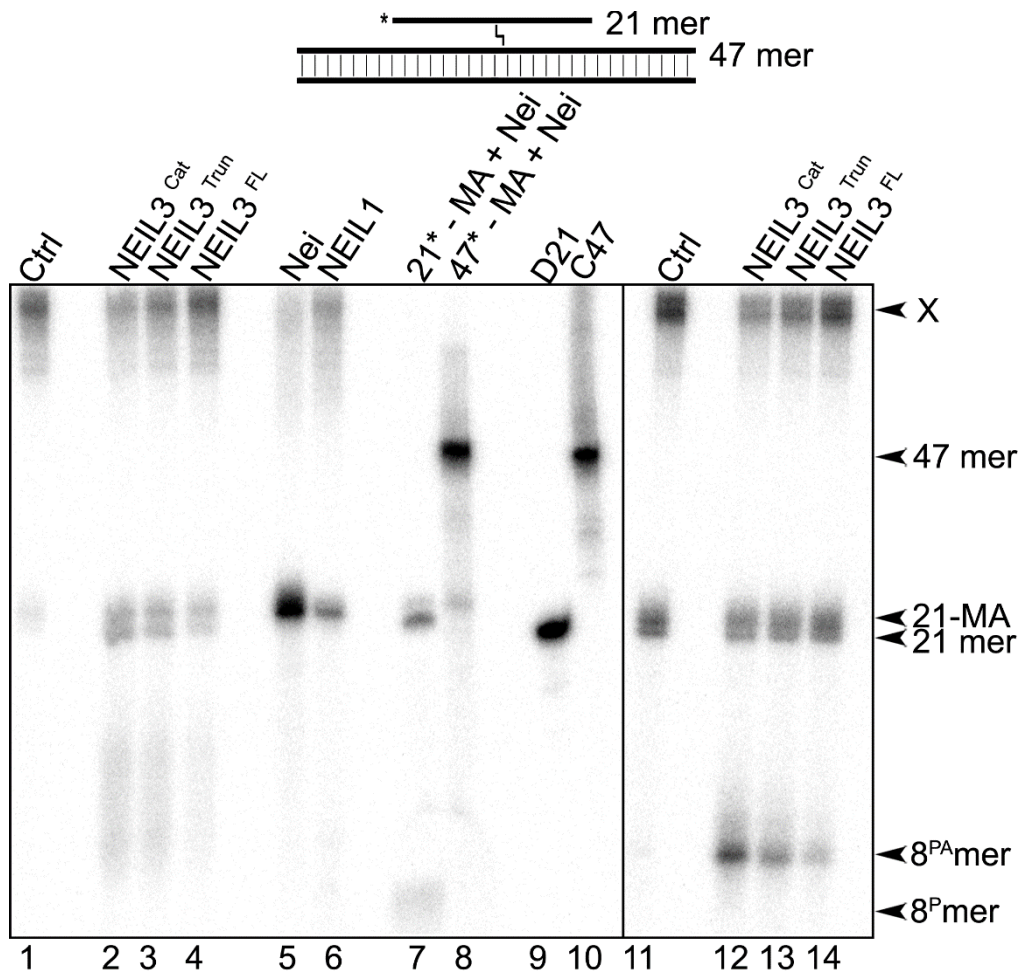


**Figure 4.14: Denaturing PAGE analysis of hNEIL3<sup>Cat</sup>, hNEIL3<sup>Trun</sup>, hNEIL3<sup>FL</sup>, hNEIL1 and Nei protein on ~10 nM (X): XL47 • 47 – 21\* 8-MOP generated three-stranded DNA ICL.** Samples were incubated for 1 h at 37°C with 500 nM of protein. For positive control 20 nM of bacterial Nei was used and 500 nM hNEIL1. (Lanes 1-10) Reactions without piperidine treatment. (Lanes 11-14) Reactions with light piperidine treatment (Lane 7) 21\* mer ds-MA substrate digested with Nei cleavage, product control. (Lane 8) 47\* mer ds-MA substrate digested with Nei, cleavage product control. (Lane 9) C21, 21 mer ss oligonucleotide size marker. (Lane 10) D47, 47 mer ss oligonucleotide size marker. “X” denotes substrate, “21-MA” denotes 21 mer fragment containing a psoralen-derived MA, “21-mer” denote cleavage fragments containing an AP (Lanes 2-4), “8<sup>PA</sup>” and “8<sup>P</sup>” denote 8 mer fragments containing a 3'-terminal PA and P, respectively.

#### 4.1.9. hNEIL1 and hNEIL3 protein kinetics on ss and ds Sp1 substrate.

To establish a protein kinetic reference for recombinant hNEIL3 repair of three-stranded structures and also establish kinetics for uncharacterised hNEIL3<sup>Trun</sup> and hNEIL3<sup>FL</sup> proteins, kinetics analysis through time course experiments was carried out on ss Sp1 DNA oligonucleotide substrate

**Figure 4.15** shows hNEIL3<sup>Cat</sup> cleaved the most substrate up until 20 s. hNEIL3<sup>Trun</sup> cleaved marginally less substrate over the same time, compared to hNEIL3<sup>Cat</sup>. However, hNEIL3<sup>Trun</sup> was observed to cleave ~3% more of the substrate over 60 s. hNEIL3<sup>FL</sup> displayed a far slower kinetic profile, only cleaving ~10% of the substrate over 90 s. These results suggest that recombinant hNEIL3<sup>Cat</sup> and hNEIL3<sup>Trun</sup> are more active than hNEIL3<sup>FL</sup> on a ss-DNA Sp containing oligonucleotide. This is suggested to be due to the inherent instability possessed by hNEIL3<sup>FL</sup> and loss of activity in comparison to the truncated versions. Additionally, the presence of uncharacterised inhibitory domains found in the extended C-terminal of hNEIL3<sup>FL</sup> may limit activity. Finally, the increased size of the hNEIL3<sup>FL</sup> protein could inhibit recognition of the substrate. This said, a maximal cleavage of ~67% and ~71% was observed for hNEIL3<sup>Cat</sup> and hNEIL3<sup>Trun</sup> over the duration of the time course, respectively. Due to the lack of exponential kinetics and a plateau being observed, the reaction became increasingly inhibited. This suggests that *in vivo* hNEIL3 may require co-factors to increase the turnover of enzymatic processing of lesions.

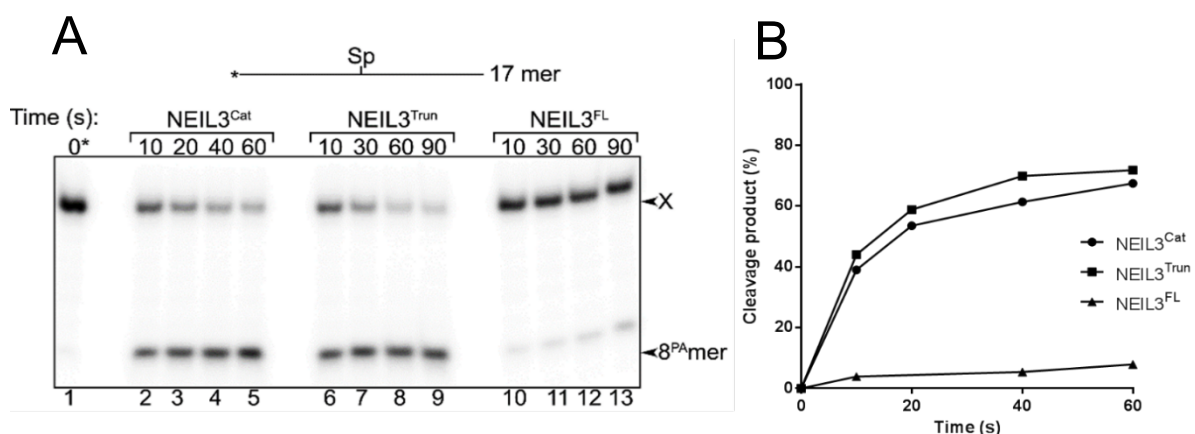


**Figure 4.15: Time dependent cleavage of ss-DNA containing Sp, by hNEIL3<sup>Cat</sup>, hNEIL3<sup>Trun</sup>, hNEIL3<sup>FL</sup>.** A. Denaturing PAGE analysis of 50 nM hNEIL3<sup>Cat</sup>, 50 nM hNEIL3<sup>Trun</sup> and 100 nM hNEIL3<sup>FL</sup> recombinant protein activity on 20 nM of ss Sp1 DNA. Cleavage observed on generation of an 8 mer product. "0\*" Reaction was without recombinant protein. "X" denotes substrate, "8<sup>PA</sup>mer" denotes an 8 mer fragments containing a 3'-terminal PA. B. Quantification of generated cleavage product percentages after enzymatic cleavage assay. Reaction products were treated with light piperidine.

For the comparison of cleavage efficiency of hNEIL3 and hNEIL1, time dependent cleavage of ss and ds Sp1 oligonucleotide substrates were analysed in the presence of hNEIL3<sup>Cat</sup> and hNEIL1 recombinant proteins. hNEIL3<sup>Cat</sup> was used due to observed robust activity when compared to hNEIL3<sup>Trun</sup> and hNEIL3<sup>FL</sup> displayed in **Figure 4.15**, to mitigate the effect of the inactive component of the recombinant protein, due to inherent c-terminal instability.

**Figure 4.16** displays time dependent cleavage of the Sp1 oligonucleotide lesion in either a ss or ds DNA context by hNEIL3<sup>Cat</sup> and hNEIL1. Quantification determined linear kinetics was observed in the first 10 seconds of the reaction by hNEIL3<sup>Cat</sup> in the presence of ss-Sp and by hNEIL1 in the presence of ss and ds-Sp (**Figure 4.16 D; E**). However, in the presence of ds-Sp, hNEIL3<sup>Cat</sup> displays relatively slow kinetics compared to ss and hNEIL1 mediated ds-Sp cleavage. These findings suggest that hNEIL1 processes ss-Sp and ds-Sp with relatively fast kinetics, while hNEIL3<sup>Cat</sup> only processes ss-Sp with relatively fast kinetics. It was observed that hNEIL3<sup>Cat</sup> processed 59% more ss-Sp compared to ds-Sp at 60 s, providing evidence for increased affinity and enzymatic processing of ss-DNA substrates. In comparison hNEIL1 displays similar kinetics for both ss and ds Sp substrates reaching a plateau in cleavage activity relatively quickly, however a preference for ds-DNA substrates is observed cleaving 13% more ds-Sp substrate at 60 s compared to ss-Sp. Both hNEIL1 and hNEIL3<sup>Cat</sup> do not complete the processing of the substrate in either ss or ds-DNA context before reaching a plateau in kinetics (**Figure 4.16 D**). This indicates that hNEIL1 and hNEIL3 DNA glycosylases may require co-factors or protein partners to improve enzymatic turnover for the completion of the reaction, due to inefficient dissociation from the substrates.

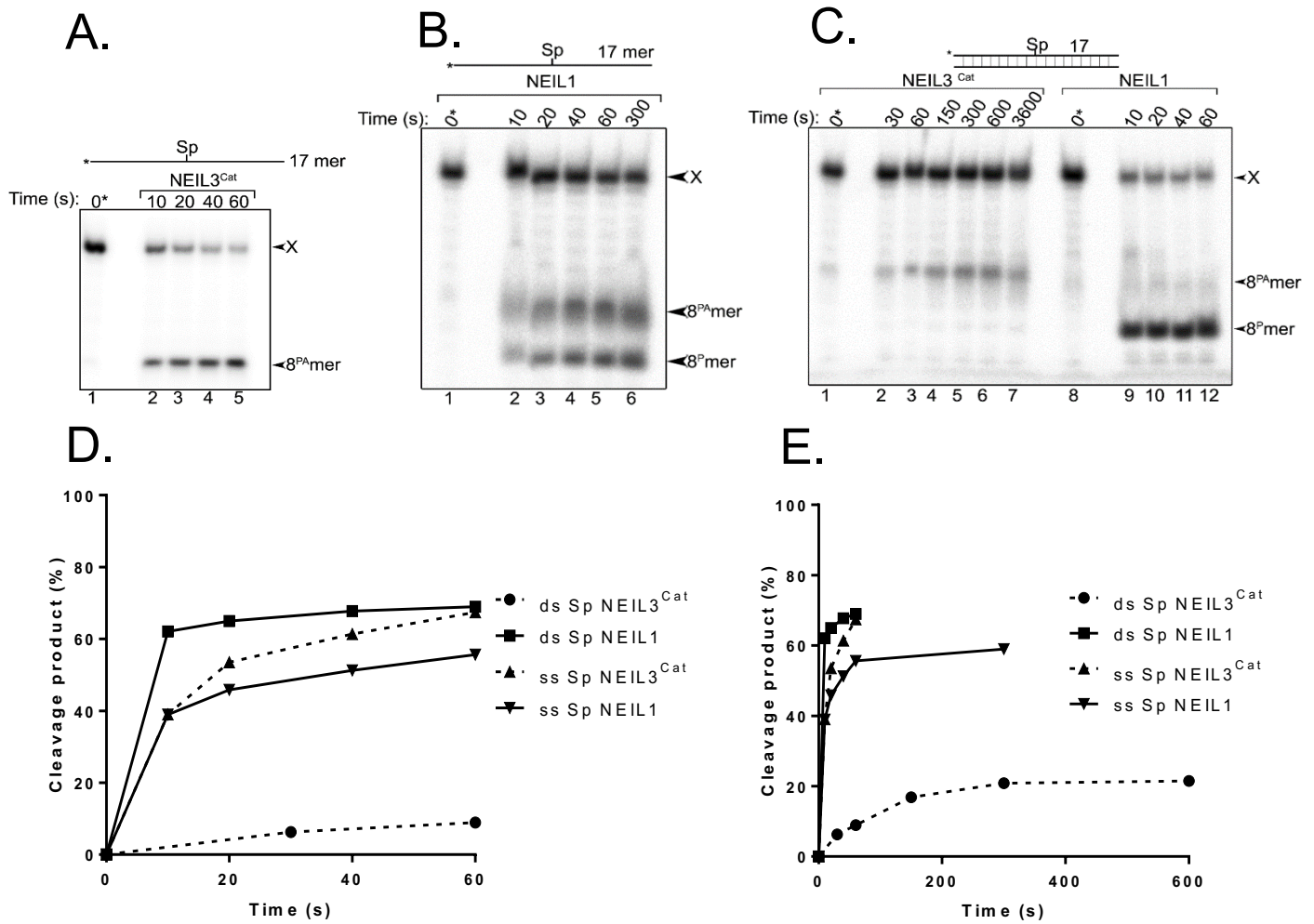


**Figure 4.16: Time dependent cleavage of ss-DNA and ds-DNA containing the Sp lesion by hNEIL1 and hNEIL3<sup>Cat</sup>.** A-B. Denaturing PAGE analysis of 20 nM hNEIL1 and 50 nM recombinant protein activity on 20 nM of ss Sp1 DNA. C. Denaturing PAGE analysis of 20 nM hNEIL1 and 50 nM recombinant protein activity on 20 nM of ds Sp1 DNA. Reactions containing NEIL1 were not treated with piperidine. Reactions containing recombinant hNEIL3<sup>Cat</sup> underwent light piperidine treatment. "0\*" Reactions were without recombinant protein. "X" denotes substrate, "8 PA" 3'-terminal PA. "X" denotes substrate, "8<sup>PA</sup>" and "8<sup>P</sup>" denote 8 mer fragments containing a 3'-terminal PA and P, respectively. D-E. Quantification of generated cleavage product percentages after enzymatic cleavage assay.

#### 4.1.10. hNEIL1 and hNEIL3<sup>Cat</sup> protein kinetics on three-stranded ICL compared to ss and ds Sp substrates.

To establish the kinetic profile of the hNEIL3<sup>Cat</sup> protein and recombinant hNEIL1 protein in the presence of the XL47 • 47 – 21\* three-stranded ICL substrates and compare to Sp lesion processivity displayed in **Figure 4.16**, a time course analysis was undertaken.

**Figure 4.17** shows that hNEIL3<sup>Cat</sup> and hNEIL1 cleave the three-stranded psoralen ICL in a time dependent manner. Over 1 h hNEIL1 cleaves ~75% of the substrate while hNEIL3<sup>Cat</sup> plateaus at ~20%. Due to the lack of exponential kinetics and a plateau being observed, the reaction became increasingly inhibited in the presence of hNEIL3<sup>Cat</sup>. This suggests that *in vivo* hNEIL3 may require co-factors to increase the turnover of enzymatic processing of three-stranded ICL DNA. To understand whether hNEIL3<sup>Cat</sup> and hNEIL1 possess different kinetics on Sp and three-stranded ICL DNA substrates. Results from time course experiments on Sp1 and XL47 • 47 – 21\* three-stranded ICL DNA substrates were compiled and compared, for each enzyme.

**Figure 4.17** shows that hNEIL3<sup>Cat</sup> can process the ss Sp1 lesion more efficiently over a shorter time than the three-stranded substrate. At 60 s ~67% of the ss Sp1 substrate is cleaved whereas only ~10% is resolved in the case of the three-stranded ICL substrate. It can be observed that a maximum of ~67% and ~20% for ss Sp1 and three-stranded ICL substrate processing, respectively, is achieved over the time course. This taken with the gradual plateau reached in both time courses suggests that hNEIL3<sup>Cat</sup> can process ss Sp1 more efficiently than the three-stranded ICL substrate, with the reaction being inhibited to a lesser extent.

These data suggest alternate kinetics by hNEIL3<sup>Cat</sup> in the processing of ss Sp1 and three-stranded ICL substrates and may suggest different mechanisms of lesion resolution by hNEIL3. It is suggested that recognition of the lesion is delayed in the case of the three-stranded ICL substrate in comparison to ss Sp1, due to hNEIL3 possessing strong affinity for ss substrates and Sp lesions. It may also be posited that due to the size difference of ss Sp1 (17 mer) and three-stranded ICL substrate (XL47 • 47 – 21\*), lesion recognition is extended as hNEIL3 takes longer to 'scan' the substrate and recognise the lesion, delaying cleavage.

**Figure 4.17** shows that hNEIL1 can process the ds Sp1 substrate more efficiently over a shorter time than the three-stranded ICL substrate. At 150 s ~79% of the ds Sp1 substrate is cleaved, whereas only ~12% is resolved in the case of the three-stranded ICL substrate. It can be observed that a maximum of ~68% over 60s and ~75% for ds Sp1 and three-stranded ICL substrate over 1 h are cleaved, respectively. This taken with the gradual plateau reached in both reactions suggests that hNEIL1 can process ds Sp1 more efficiently than the three-stranded ICL substrate

These data suggest alternate kinetics by hNEIL1 in the processing of ds Sp1 and three-stranded ICL substrates and may suggest an alternate method of lesion resolution by hNEIL1. It is suggested that recognition of the lesion is delayed in the case of the three-stranded ICL substrate in comparison to ds Sp1, which can be explained by hNEIL1 possessing strong affinity for double stranded substrates and Sp lesions. It may also be proposed that due to the size difference of Sp1 (17 mer) and three-stranded ICL substrate (XL47 • 47 – 21\*), lesion recognition is extended as the hNEIL1 takes longer to 'scan' the substrate and recognise the lesion, delaying cleavage.

**Figure 4.17** provide a general understanding of the processing capacity of hNEIL3 and hNEIL1 of Sp and three-stranded ICL substrates. hNEIL1 can process a far greater proportion of the three-stranded psoralen ICL substrate compared to hNEIL3<sup>Cat</sup>, which is inhibited much earlier in the reaction. This may suggest that hNEIL3<sup>Cat</sup> activity is much more reliant on co-factors or protein partners to increase processivity *in vivo*. Whilst further experiments are required for full characterisation of protein kinetics, they provide initial evidence that Sp lesions are more readily processed than three-stranded ICL lesions by hNEIL1/3 proteins.

As the further oxidation products of 8-OxoG, Sp and Gh, are more common *in vivo* than the generation of ICL lesions, the relatively low processing of three-stranded ICL lesions is expected. Due to gaps within the current understanding of ICL repair, it is difficult to infer why processing of three-stranded ICL lesions differs substantially to Sp lesions. Possible reasons for the differences observed have been discussed, however further experimentation on substrates of different sizes and containing different lesions are required to fully elucidate.

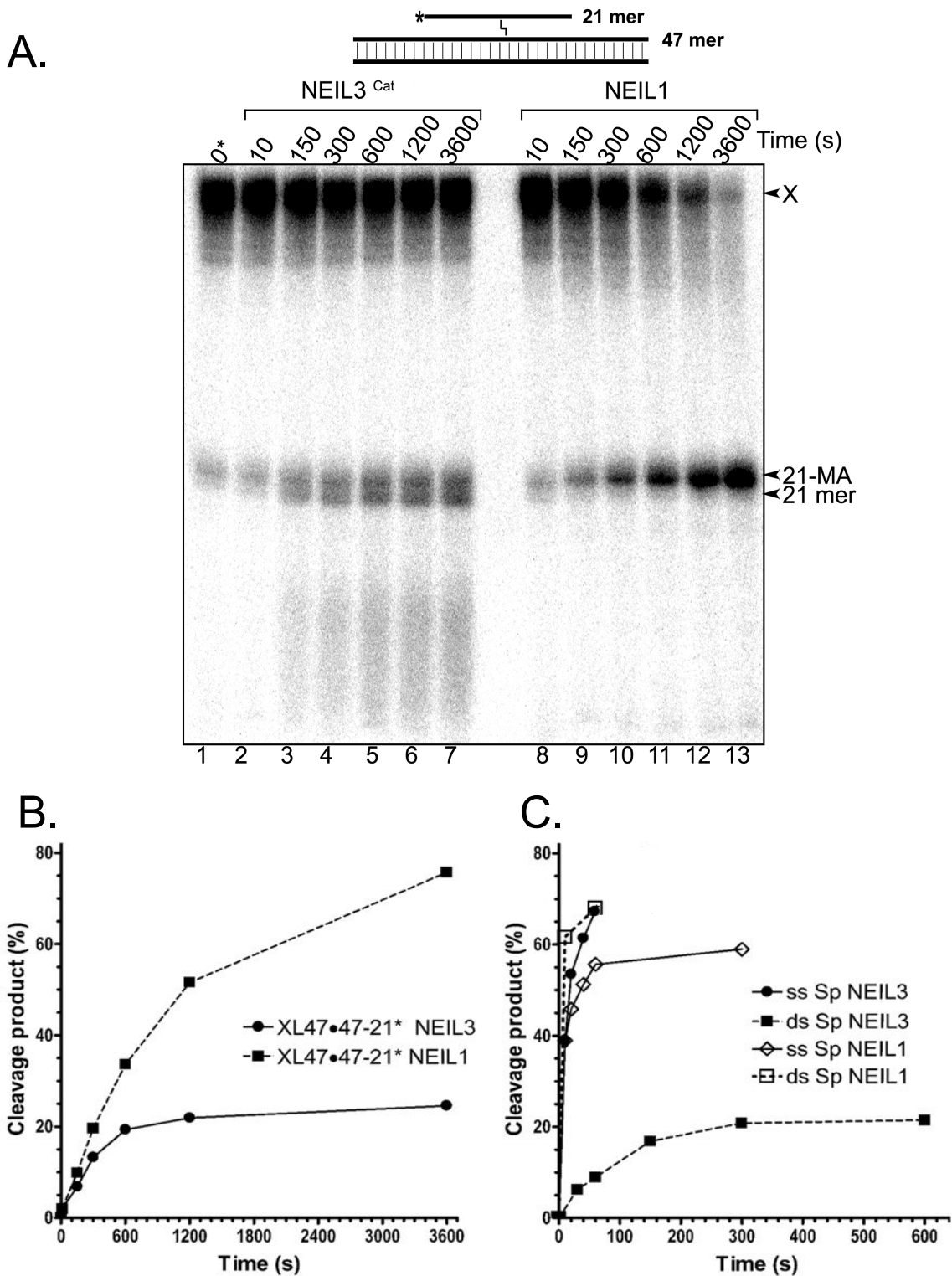


**Figure 4.17: Time dependent cleavage of psoralen (HMT)/ UVA treated XL47 • 47 – 21\* three-stranded ICL DNA substrate by hNEIL1 and hNEIL3<sup>Cat</sup>.** A. Denaturing PAGE analysis of 20 nM hNEIL1 and 50 nM hNEIL3<sup>Cat</sup> recombinant protein activity on ~10 nM (X): XL47 • 47 – 21\* three-stranded DNA ICL substrate. Reaction samples were without Piperidine treatment. “0\*” Reactions without recombinant protein. “21-MA” denotes 21 mer fragment containing a psoralen-derived MA, A. “21-mer” denotes AP-site containing unhooked fragment. B. Quantification of hNEIL3<sup>Cat</sup> and hNEIL1 generated cleavage product percentages after enzymatic cleavage of XL47 • 47 – 21\*. C. Quantification of hNEIL3<sup>Cat</sup> and hNEIL1 generated cleavage product percentages after enzymatic cleavage of ss and ds-Sp1 oligonucleotide substrate.

#### 4.1.11. Generation and confirmation of catalytically inactive mutant hNEIL3<sup>Cat</sup>.

Up to 500 nM of hNEIL3 recombinant protein was required to observe activity on three- and four-stranded substrates. Therefore, minor bacterial contaminant protein may have been responsible for observed activity. To provide evidence to counter this, the generation of catalytically inactive hNEIL3<sup>Cat</sup> recombinant protein was required, to show the abolishment of observed activity and therefore provide evidence that WT hNEIL3 was responsible for the observed activity.

Site-directed mutagenesis was undertaken as described in section 2.20 to convert amino acid residue 81 from lysine to alanine. Purified plasmid DNA was sent for Sanger sequencing analysis. **Figure 4.18** shows the 230-268 region of the nucleotide sequence of the hNEIL3 cDNA, with targeted nucleotides at nucleotide positions 241 and 242. The sequence in black shows the original cDNA sequence and highlighted in red is the targeted nucleotides. The sequencing chromatogram shows the conversion of the nucleotides to G and C, therefore encoding the desired amino acid change of lysine to alanine at aa position 81.

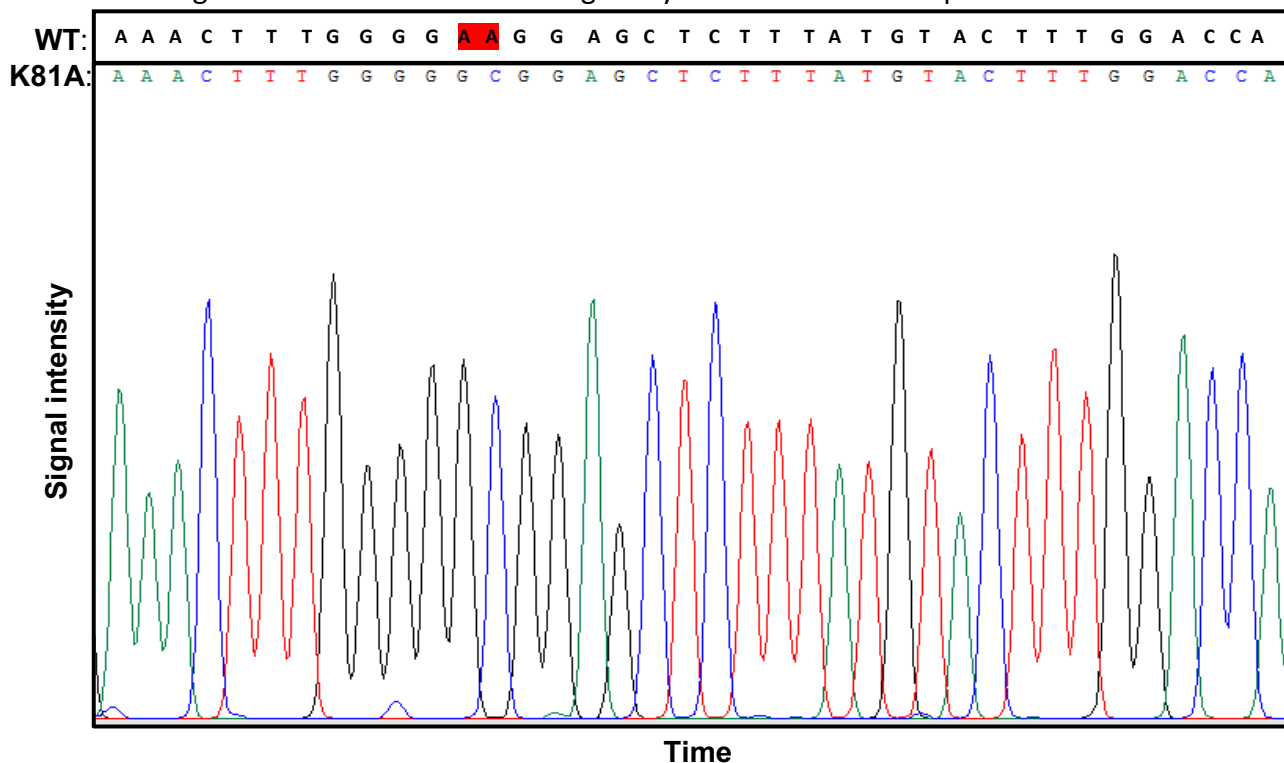


**Figure 4.18: Sanger sequencing chromatogram analysis of pETDUET2-EcoMap-ORF6-hNEIL3<sup>Cat-K81A</sup> and the corresponding wild type hNEIL3<sup>Cat</sup> nucleotide sequence region, 230-268. Targeted nucleotides at position 241 and 242, highlighted in red. Targeted mutations AAG-GCG encode for amino acid residue 81, lysine to alanine mutation, for expression and purification of the catalytically inactive hNEIL3<sup>Cat-K81A</sup> recombinant protein.**

#### 4.1.12. hNEIL3<sup>Cat-K81A</sup> recombinant protein ÄKTA FPLC purification.

After transformation and expression of the hNEIL3<sup>Cat-K81A</sup> recombinant protein, HisTrap HP column FPLC separation of cell lysate was carried out as described in section 3.20 in an attempt to purify hNEIL3<sup>Cat-K81A</sup>.

**Figure 4.19** shows the FPLC chromatogram, 10%SDS and anti-NEIL3 western blot analysis of protein fractions. The chromatogram displays a characteristic trace for recombinant hNEIL3<sup>Cat</sup> elution from *E. coli* lysate using an imidazole gradient, with a peak of ~200 mAU observed between fractions 19 and 24, where hNEIL3<sup>Cat</sup> was previously eluted (**Appendix Figure 1**). The identified peak is in the same position in which WT protein was eluted and therefore was expected to be the K81A mutant hNEIL3<sup>Cat</sup> protein.

SDS-PAGE and hNEIL3 western blot analysis, revealed limited separation of contaminant proteins and the target protein expected at ~32 kDa. This said, fractions 20, 21 and 22 were of improved purity, but with low molecular weight bacterial contaminant proteins present. **Figure 4.19** provides evidence for partial purification of a candidate protein and therefore protein fractions between 19 and 24 were pooled and concentrated with a 10k cut off, to reduce low molecular weight bacterial protein contamination.

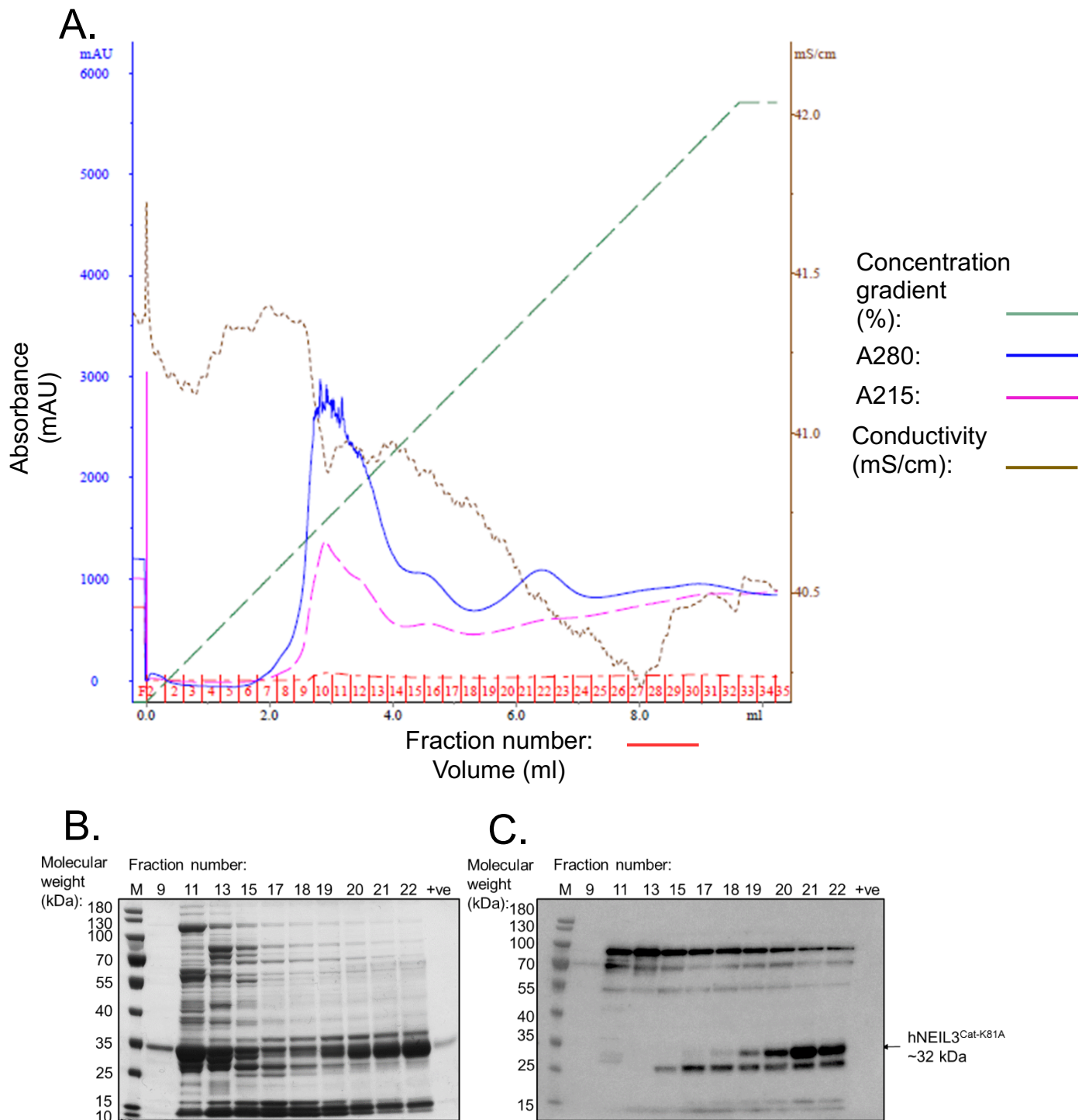


**Figure 4.19: HisTrap HP FPLC Purification of hNEIL3<sup>Cat-K81A</sup> from *E. coli*.** A. Chromatogram analysis of protein fractions generated from *E. coli* lysates overexpressing hNEIL1. B. SDS-PAGE analysis and Instant Blue protein staining. C. Anti-His western blot analysis of hNEIL3<sup>Cat-K81A</sup> FPLC purification fractions. (M) Page ruler prestained protein ladder (ThermoFisher).

The K81A mutant was subsequently analysed by 10% SDS-PAGE. **Figure 4.20 B** displays the fraction purity after Amicon Ultra-15 10 K cut off concentration, which contained the putative K81A mutant purification product. The putative hNEIL3<sup>Cat-K81A</sup> was approximately the same molecular weight as the WT hNEIL3<sup>Cat</sup> protein at ~32 kDa. However, the candidate protein band was close in molecular weight to that expected of bacterial Nei (30 kDa), which is a possible contaminant that would yield ICL repair capabilities. hNEIL3<sup>Cat</sup> and hNEIL3<sup>Cat-K81A</sup> were subsequently sent for LC-MS analysis and detected peptides were aligned with the target K81A mutant protein **Figure 4.20 A**. hNEIL3<sup>Cat-K81A</sup> possessed a sequence match of 49% and was the highest scoring protein match in the generated list of possible proteins with an Ion score of 8345 (**Appendix Table 3**). This said, the peptide containing the K81A mutation was not detected. However, with the confirmation of site-directed mutagenesis at nucleotide level, it is suggested that the purification of recombinant hNEIL3<sup>Cat-K81A</sup> was successful. Additionally, the VEGPGCTLN<sub>1-10</sub>GEK peptide corresponds to the first peptide chain of hNEIL3 and was detected without the initiator methionine, confirming active processing by the co-expressed *EcoMap* (**Appendix Table 3**).

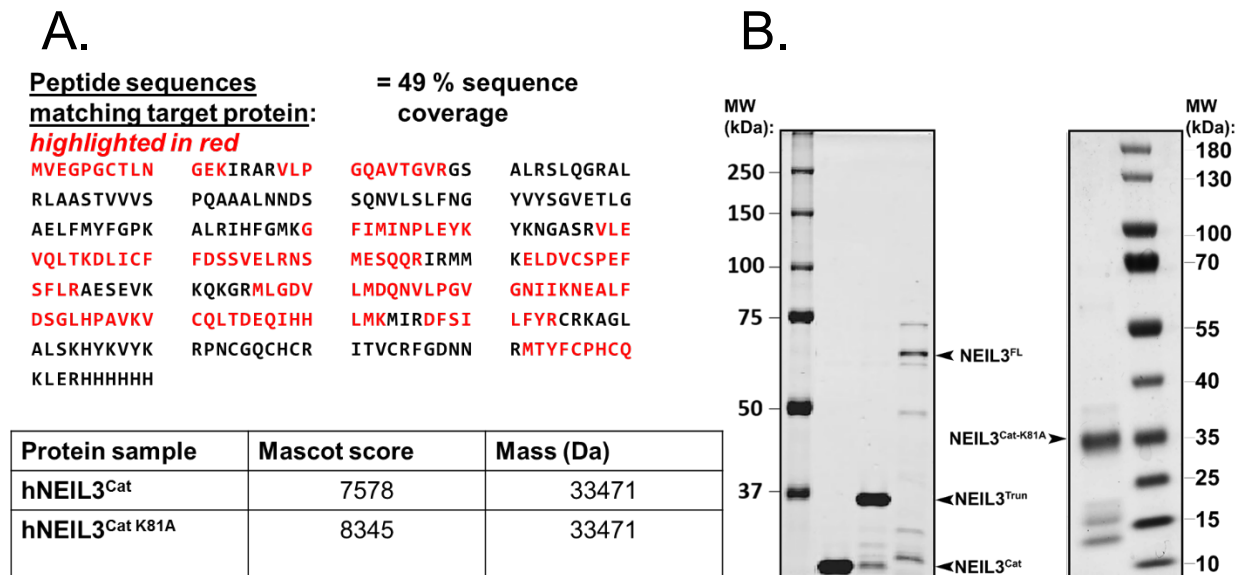


**Figure 4.20: Confirmation of purification of hNEIL3<sup>Cat-K81A</sup> protein.** A. Proteomic analysis by LC-MS, peptide sequences detected in hNEIL3<sup>Cat-K81A</sup> purification product which match target amino acid sequence highlighted in red. MS/MS Ion search of matched proteins detected with highest mascot score hNEIL3<sup>Cat</sup> and hNEIL3 in each sample (full lists displayed in Appendix Table 3). B. SDS-PAGE analysis of final recombinant hNEIL3 protein products stained with instant-blue. “M” Page ruler prestained protein ladder (ThermoFisher).

#### 4.1.13. hNEIL3<sup>Cat-K81A</sup> protein catalytic knockout of DNA glycosylase activity on ss- and ds- Sp1 DNA.

To confirm the successful catalytic inactivation of hNEIL3<sup>Cat</sup> through site-directed mutagenesis, expression and purification of hNEIL3<sup>Cat-K81A</sup>, enzymatic activity analysis on the ss Sp1 substrate was undertaken.

**Figure 4.21** shows hNEIL3, Nei, hNEIL1 and hNEIL3<sup>Cat-K81A</sup> activity on the ss-DNA Sp1 substrate with and without the addition of 10% piperidine. Cleavage of the ss-DNA Sp1 was observed for WT hNEIL3 and hNEIL1 recombinant proteins, which generated an 8 mer product at the site of the Sp lesion. However, hNEIL1 generated a pronounced band below the 8 mer product. This is suggested to be a result of further processing by associated  $\beta,\delta$ -elimination by hNEIL1. hNEIL3<sup>Cat-K81A</sup> generated no cleavage of the ss-DNA Sp1 substrate whereas hNEIL3<sup>Cat</sup>, hNEIL3<sup>Trun</sup> and hNEIL3<sup>FL</sup> did. This suggests successful catalytic inactivation of hNEIL3<sup>Cat</sup> through site-directed mutagenesis, expression and purification. However, the possible bacterial contaminant, Nei, is characterised to lack activity on ss Sp1. Therefore, activity on ds Sp1 was also required for confirmation catalytic knockout through site-directed mutagenesis.

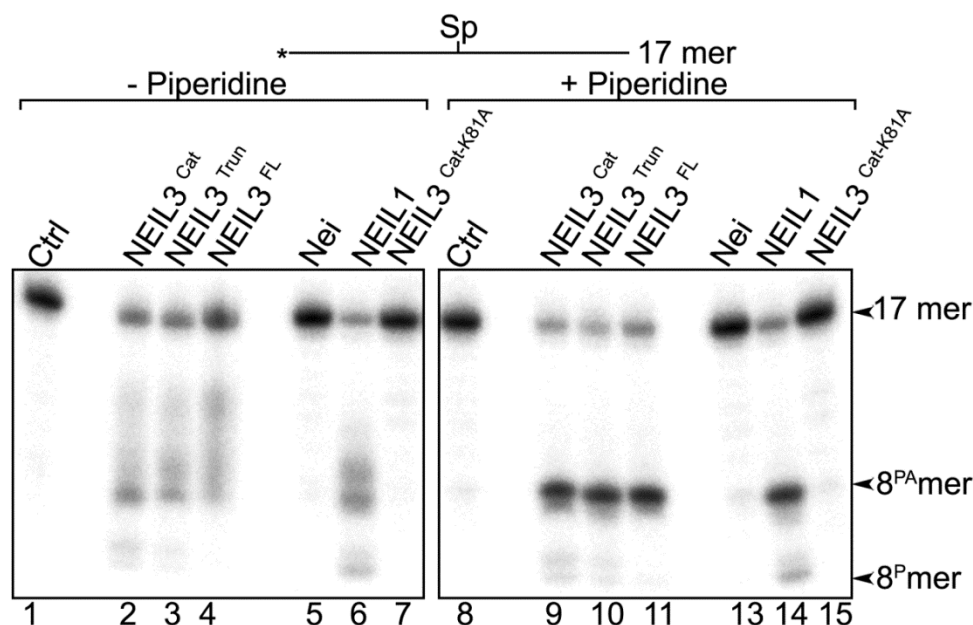


**Figure 4.21: Denaturing PAGE analysis of hNEIL3<sup>Cat</sup>, hNEIL3<sup>Trun</sup>, hNEIL3<sup>FL</sup>, hNEIL1, Nei and hNEIL<sup>Cat-K81A</sup> protein activity on 10 nM ss Sp1 DNA oligonucleotide.** Samples were incubated for 1 h at 37°C with 500 nM of protein. For positive control 20 nM of bacterial Nei was used and 500 nM of hNEIL1 was used. (Lanes 1-7) Reactions were without piperidine treatment. (Lanes 8-15) Reactions were with light piperidine treatment. "Ctrl" samples in the absence of recombinant protein. "8<sup>PA</sup>" and "8<sup>P</sup>" denote 8 mer fragments containing 3'-terminal PA and P, respectively.

**Figure 4.22** shows hNEIL3, Nei, hNEIL1 and hNEIL3<sup>Cat-K81A</sup> activity on the ds-DNA Sp1 substrate with and without the addition of 10% piperidine. Cleavage of the ds-DNA Sp1 substrate was observed for the WT hNEIL3 recombinant proteins, which generated an 8 mer product at the site of the Sp lesion. Nei and hNEIL1 show cleavage of the ds-DNA Sp1 substrate and generated a pronounced band below the identified 8 mer product. This is suggested to be a result of further processing by associated  $\beta,\delta$ -elimination by Nei and hNEIL1. hNEIL3<sup>Cat-K81A</sup> generated no cleavage of the ds-DNA Sp1 substrate whereas hNEIL3<sup>Cat</sup>, hNEIL3<sup>Trun</sup> and hNEIL3<sup>FL</sup> did. This suggests successful catalytic inactivation of hNEIL3<sup>Cat</sup> through site-directed mutagenesis. The lack of activity on ds-DNA Sp1 confirmed the absence of active Nei contamination which possesses ICL repair capabilities.

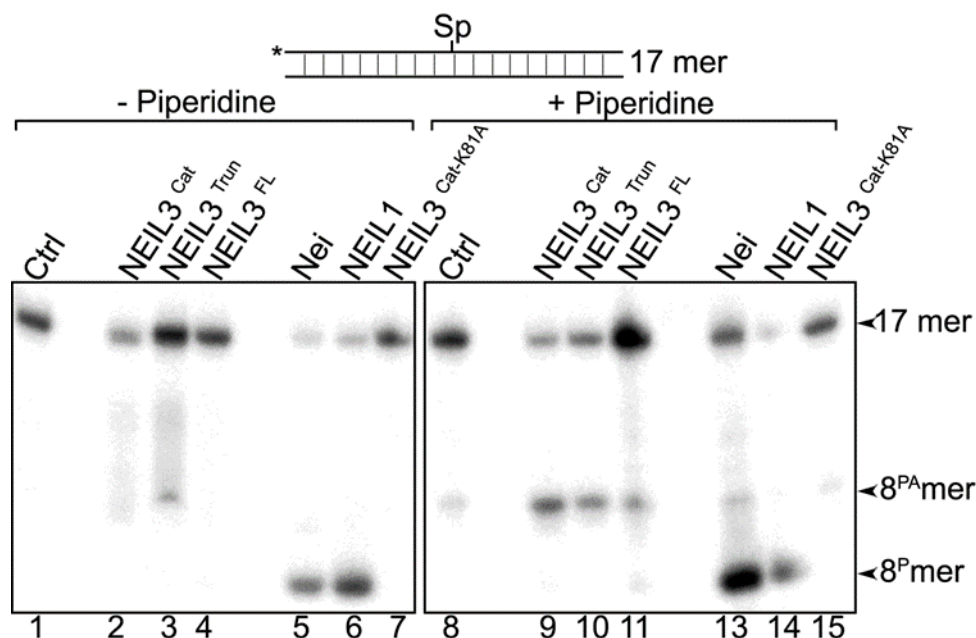


**Figure 4.22: Denaturing PAGE analysis of hNEIL3<sup>Cat</sup>, hNEIL3<sup>Trun</sup>, hNEIL3<sup>FL</sup>, hNEIL1, Nei and hNEIL3<sup>Cat-K81A</sup> protein activity on 10 nM (X): ds Sp1 substrate.** Samples were incubated for 1 h at 37°C with 500 nM of protein. For positive control 20 nM of bacterial Nei was used and 500 nM of hNEIL1 was used. (Lanes 1-7). Reactions without piperidine treatment. (Lanes 8-15) Reactions were with light piperidine treatment. "Ctrl" samples in the absence of recombinant protein. "17 mer" denotes substrate, "8<sup>PA</sup>" and "8<sup>P</sup>" denote 8 mer fragments containing a 3'-terminal PA and P, respectively.

**4.1.14.** hNEIL3<sup>Cat-K81A</sup> catalytic knockout of unhooking activity on HMT generated three-stranded ICL DNA oligonucleotide.

To provide further evidence for hNEIL3 possessing ICL repair capabilities and the generation of hNEIL3<sup>Cat-K81A</sup> catalytically inactive mutant, an enzymatic assay was undertaken on the XL47 • 47 – 21\* three-stranded ICL DNA substrate.

**Figure 4.23** shows hNEIL3, NEIL3<sup>Cat-K81A</sup> and Nei activity on the XL47 • 47 – 21\* three-stranded ICL substrate with and without the addition of 10% piperidine. Cleavage of the three-stranded ICL substrate was observed for the WT hNEIL3<sup>Cat</sup> recombinant protein, which generated an ~8 mer smear, indicating the presence of a 21 mer AP site which degrades under standard reaction conditions. After light piperidine treatment this AP site is cleaved by  $\beta$ -elimination to yield an 8<sup>PA</sup>mer. The generation of a cleavage product doublet in the centre of the gel was also observed. The lower band of the doublet represents the 21\* mer strand with an AP site unhooked at the 21\* mer strand side of the ICL. The upper band of the doublet represents the 21\* mer strand with the ICL adduct attached after unhooking at the 47 mer strand side of the ICL, representing a 21 mer ss-MA. Nei resulted in unhooking of the 21\* mer labelled strand with the addition of the ICL adduct, unhooked at the 47 mer strand side of the ICL to produce a 21 mer ss-MA, consistent with previous observations. hNEIL3<sup>Cat-K81A</sup> was not observed to facilitate cleavage of the three-stranded ICL substrate, with concentrations up to 1  $\mu$ M. These observations display successful catalytic inactivation of hNEIL3<sup>Cat</sup> through site-directed mutagenesis, expression and purification. It also provided evidence that WT hNEIL3 was responsible for the observed unhooking and cleavage of three-stranded ICL substrates previously demonstrated (**Figure 4.9**).

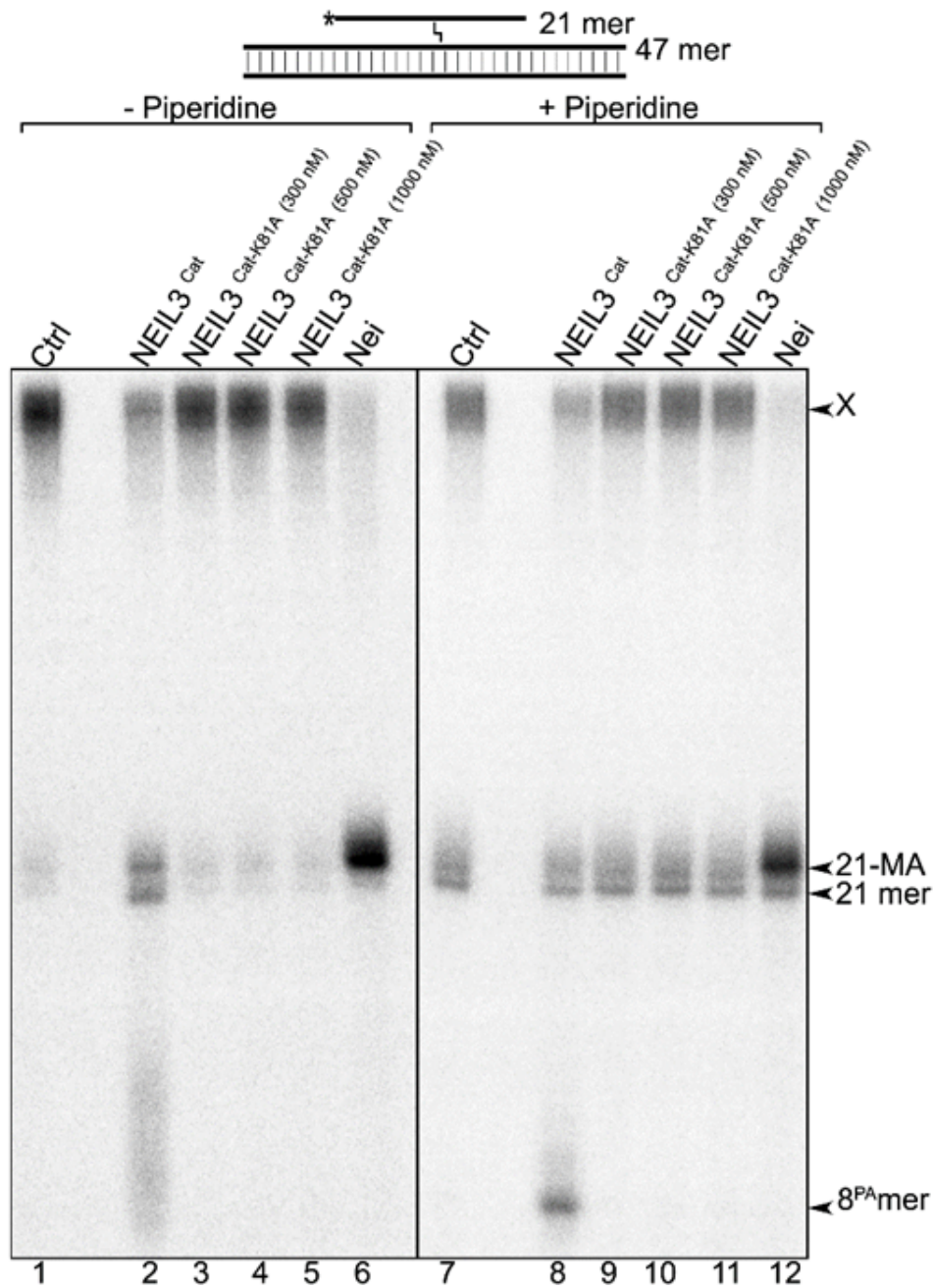


**Figure 4.23: Denaturing PAGE analysis of hNEIL3<sup>Cat</sup> and hNEIL3<sup>Cat-K81A</sup> protein activity on ~10 nM (X): XL47 • 47 – 21\* HMT generated three-stranded DNA ICL.** Samples were incubated for 1 h at 37°C. For hNEIL3<sup>Cat</sup>, 500 nM of protein was used. For the hNEIL3<sup>Cat-K81A</sup>, 300 nM, 500 nM or 1000 nM of protein was used. For positive control 20 nM of bacterial Nei was used. (Lanes 1-6) Reactions were without piperidine treatment. (Lanes 7-12) Reactions were with light piperidine treatment. “Ctrl” samples in the absence of recombinant protein. “X” denotes substrate, “21-MA” denotes 21 mer fragment containing psoralen-derived MA, “21-mer” denote cleavage fragments containing an AP site (Lane 2), “8<sup>PA</sup>mer” denote 8 mer fragments containing a 3'-terminal PA.

**4.1.15.** hNEIL3<sup>Cat-K81A</sup> catalytic knockout of unhooking activity on HMT generated four-stranded ICL DNA oligonucleotide.

To provide further evidence for hNEIL3 possessing ICL repair capabilities and the generation of the hNEIL3<sup>Cat-K81A</sup> catalytically inactive mutant, an enzymatic assay was undertaken on the XL47 • 47 - 21\* • 21 four-stranded ICL DNA substrate.

**Figure 4.24** shows hNEIL3<sup>Cat</sup>, NEIL3<sup>Cat-K81A</sup> and Nei activity on the XL47 • 47 - 21\* • 21 four-stranded ICL substrate with and without the addition of 10% piperidine. Cleavage of the four-stranded ICL substrate was observed for the WT hNEIL3<sup>Cat</sup> recombinant protein, which generated an ~8 mer smear, indicating the presence of a 21 mer AP site which degrades under standard reaction conditions. After light piperidine treatment this AP site is cleaved by  $\beta$ -elimination to yield an 8<sup>PA</sup>mer. The generation of a cleavage product doublet in the centre of the gel was also observed. The lower band of the doublet represents the 21\* mer strand with an AP site unhooked at the 21\* mer strand side of the ICL. The upper band of the doublet represents the 21\* mer strand with the ICL adduct attached after unhooking at the 47 mer strand side of the ICL, representing a 21 mer ds-MA. Nei resulted in unhooking of the 21\* mer labelled strand with the addition of the ICL adduct, unhooked at the 47 mer strand side of the ICL to produce a 21 mer ds-MA which was processed as a secondary substrate for Nei to yield an 8<sup>P</sup>mer cleavage product. hNEIL3<sup>Cat-K81A</sup> was not observed to facilitate cleavage of the four-stranded ICL substrate, at concentrations up to 1  $\mu$ M. These observations display successful catalytic inactivation of hNEIL3<sup>Cat</sup> through site-directed mutagenesis, expression and purification. It also provided evidence that WT hNEIL3 was responsible for observed unhooking and cleavage of four-stranded ICL substrates as previously demonstrated (**Figure 4.11**).

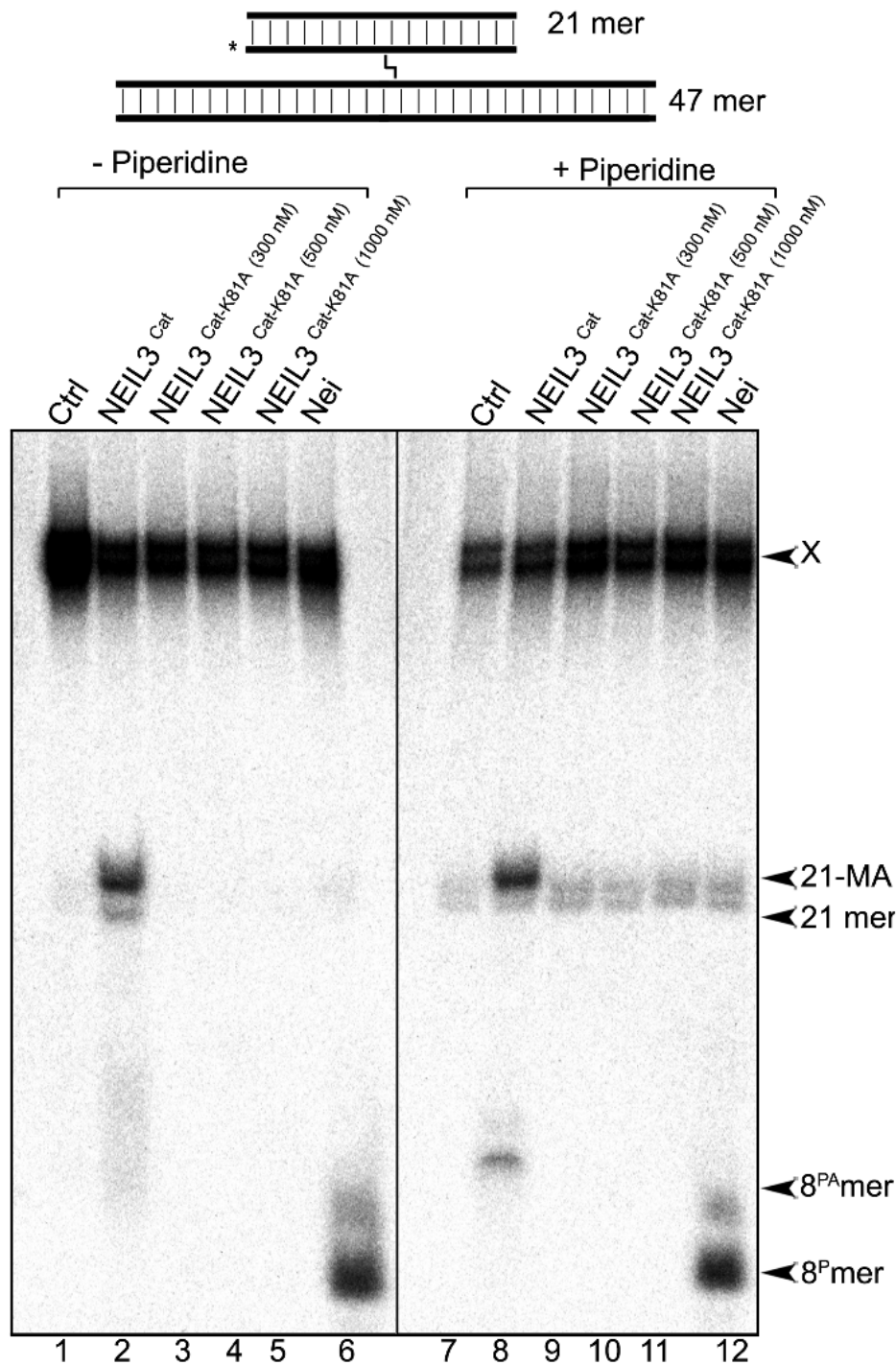


**Figure 4.24: Denaturing PAGE analysis of hNEIL3<sup>Cat</sup> and hNEIL3<sup>Cat-K81A</sup> protein activity on ~10 nM (X): XL47 • 47 – 21\* • 21 HMT generated three-stranded DNA ICL.** Samples were incubated for 1 h at 37°C. For hNEIL3<sup>Cat</sup>, 500 nM of protein was used. For the hNEIL3<sup>Cat-K81A</sup>, 300 nM, 500 nM or 1000 nM of protein was used. For positive control 20 nM of bacterial Nei was used. (Lanes 1-6) Reactions were without piperidine treatment. (Lanes 7-12) Reactions were with light piperidine treatment. “Ctrl” samples in the absence of recombinant protein. “X” denotes substrate, “21-MA” denotes 21 mer fragment containing psoralen-derived MA, “21-mer” denote cleavage fragments containing an AP site (Lane 2), “8<sup>PA</sup>mer” denote 8 mer fragments containing a 3'-terminal PA.

**4.1.16.** hNEIL3<sup>Cat</sup> and hNEIL1 recombinant protein, protein-DNA substrate covalent complex generation with ss and ds Sp1.

To provide further evidence for the observed activity of hNEIL3 and hNEIL1 on ss and ds Sp1 DNA substrates, protein-DNA affinity assays were conducted by NaBH<sub>4</sub> trapping assay, as previously described in section 2.22. A covalent complex between labelled DNA and enzyme should form upon generation of a 'Schiff' base intermediate when DNA glycosylase cleavage had taken place followed by NaBH<sub>4</sub> facilitated reduction and covalent binding of the DNA substrate to the amino acid residue of the protein. Relative band migration based on the total molecular weight of the complex, separated by 10% SDS-PAGE, provides evidence for cleavage by recombinant proteins. Contaminant interacting proteins would result in the generation of complexes with an unexpected migration pattern and presence of additional bands.

**Figure 4.25** shows that covalent enzyme-substrate DNA complexes are formed by hNEIL3<sup>Cat</sup> and hNEIL1 in the presence of ss and ds Sp1 DNA substrates. At the bottom of the gel free substrate DNA was observed. hNEIL3<sup>Cat</sup> is ~32 kDa and hNEIL1 is ~42 kDa, therefore the covalent complex of hNEIL3<sup>Cat</sup> and substrate was expected to migrate below the complex generated by hNEIL1. **Figure 4.25** indicates that recombinant hNEIL3<sup>Cat</sup> mediated cleavage was responsible for the observed activity in previous enzymatic assays. Furthermore, as hNEIL3 is suggested to have increased affinity for ss substrates and hNEIL1 is suggested to have increased affinity for ds substrates, a band of increased intensity should be observed for the favoured substrate. This comparison was clearly observed in **Figure 4.25** and provided further evidence for the activity of these recombinant proteins.

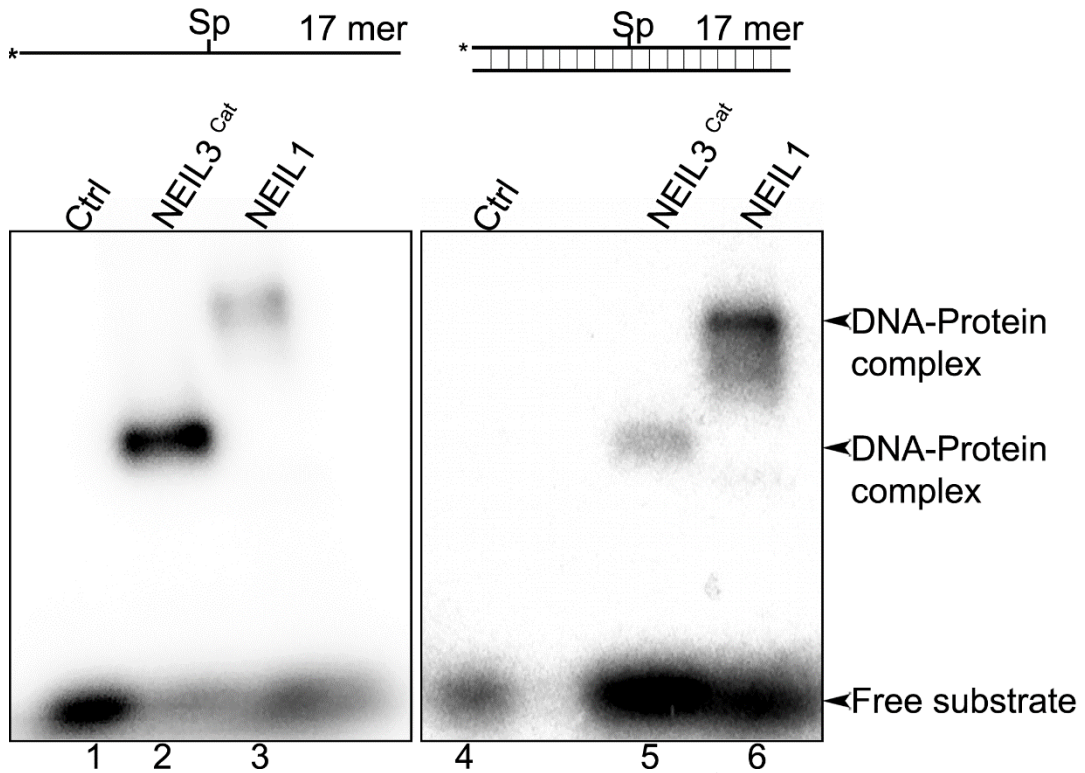


**Figure 4.25: SDS-PAGE analysis of NaBH<sub>4</sub> trapping complexes of hNEIL3<sup>Cat</sup> and hNEIL1 protein formation with 10 nM ss and ds Sp1 DNA lesions.** Reactions were without Piperidine treatment. "Ctrl" samples were without recombinant protein. "DNA-Protein complex" denotes recombinant protein bound by NaBH<sub>4</sub> facilitated reduction of protein amino acid residue to cleavage site on the DNA substrate. "Free substrate" denotes unbound DNA.

**4.1.17.** hNEIL3<sup>Cat</sup>, hNEIL3<sup>Trun</sup>, hNEIL3<sup>FL</sup>, Nei, hNEIL1 and hNEIL3<sup>Cat-K81A</sup> protein-DNA substrate covalent complex generation with a three stranded HMT ICL.

To provide further evidence for the observed activity of hNEIL3<sup>Cat</sup>, hNEIL3<sup>Trun</sup>, hNEIL3<sup>FL</sup>, hNEIL1, Nei and hNEIL3<sup>Cat-K81A</sup> on three-stranded ICL substrates, protein-DNA affinity assays were conducted, as previously described in 2.22.

**Figure 4.26** shows that covalent protein-DNA complexes are formed between hNEIL3<sup>Cat</sup>, hNEIL3<sup>Trun</sup>, hNEIL3<sup>FL</sup> and hNEIL1 in the presence of the XL47 • 47 - 21\* three-stranded ICL DNA substrate. At the bottom of the gel free oligonucleotide substrate was observed. hNEIL3<sup>Cat</sup> is ~32 kDa, hNEIL3<sup>Trun</sup> ~42 kDa, hNEIL3<sup>FL</sup> ~68 kDa. Nei ~30 kDa and hNEIL3<sup>Cat-K81A</sup> ~32 kDa. Therefore, the covalent complex of hNEIL3<sup>Cat</sup> was expected to migrate below the complex generated by hNEIL1, the hNEIL3<sup>Trun</sup> complex in line with hNEIL1 and hNEIL3<sup>FL</sup> above. Nei was expected to generate a band migrating below the hNEIL1 complex and hNEIL3<sup>Cat-K81A</sup> was expected to generate no complex, due to catalytic inactivation.

**Figure 4.26** suggests recombinant hNEIL3 proteins facilitated cleavage of the three-stranded ICL DNA substrate in previous assays. Furthermore, the generation of no complex with hNEIL3<sup>Cat-K81A</sup> provided further indication of the successful inactivation and responsibility of WT hNEIL3 for observed activity. It is suggested that Nei did not generate a complex, due to the complete resolution of substrate before successful reduction of the Schiff base intermediate. The signal intensity of DNA-protein complexes analysed **Figure 4.26** is significantly reduced in comparison to that observed in **Figure 4.25**. This is suggested to be a result of the characterised differences in Sp and three-stranded psoralen ICL processivity displayed by NEIL1 and NEIL3 proteins. This data provided further evidence for the responsibility of hNEIL3 and hNEIL1 proteins in three-stranded ICL resolution.

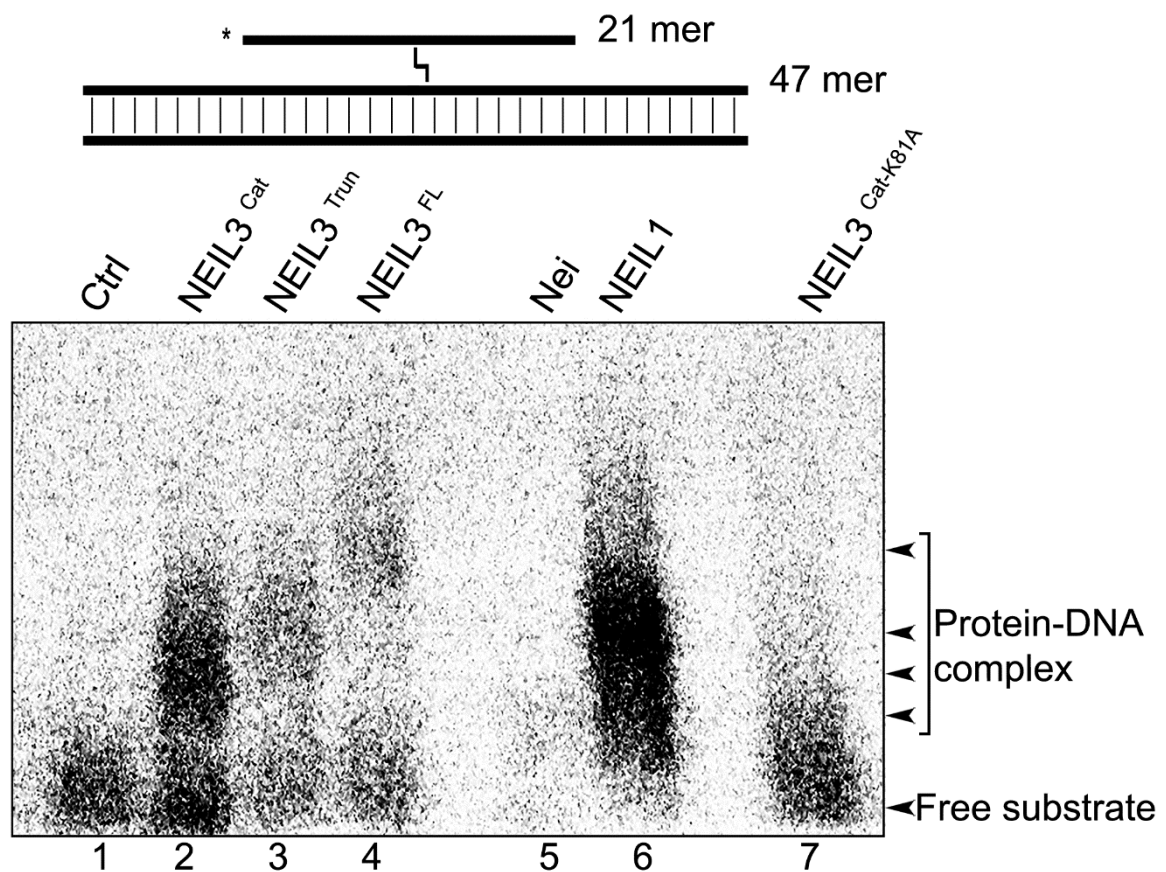


**Figure 4.26: SDS-PAGE analysis of NaBH<sub>4</sub> of hNEIL3<sup>Cat</sup>, hNEIL3<sup>Trun</sup>, hNEIL3<sup>FL</sup>, Nei, hNEIL1 and hNEIL3<sup>Cat-K81A</sup> formation with ~10 nM 21\*<sup>x</sup>47-47 HMT generated three-stranded ICL DNA substrate. 500 nM of recombinant hNEIL1, hNEIL3 and 20 nM of Nei recombinant protein was used. "Ctrl" samples were without recombinant protein. "DNA-Protein complex" denotes recombinant protein bound by NaBH<sub>4</sub> facilitated reduction of protein amino acid residue to cleavage site on the DNA substrate. "Free substrate" denotes unbound DNA.**

#### 4.2. Discussion: Characterisation of the hNEIL1 and hNEIL3 DNA glycosylases in the repair of psoralen interstrand DNA crosslinks.

Previous analysis of the biochemical activity of hNEIL1 and hNEIL3<sup>FL</sup> in the presence of model DNA replication fork DNA structured oligonucleotides containing an oxidative lesion (5-OHU, 8-OxoG and Tg) demonstrated differential roles in the presence of alternative oxidative lesions. It was observed that NEIL3 could excise Tg with robust activity regardless of the DNA replication fork position in which the lesion was placed whereas within a conventional ds-DNA oligonucleotide it could not. This subsequently eluded to a preference of hNEIL3 for the replication blocking lesion Tg within a DNA replication fork structure.

Interstrand DNA crosslinks block DNA replication and transcription and must be removed to avoid the loss of genomic stability (Muniandy *et al.*, 2010; Deans and West, 2011). Subsequently, mammalian cells have evolved repair mechanisms that remove ICLs in quiescent cells through NER and replication dependent ICL repair pathways which conventionally remove ICLs in a DNA replication stress response and FA pathway initiated manner (**Figure 1.10**; Wang *et al.*, 2007; Clauson *et al.*, 2013; Ceccaldi *et al.*, 2016). However, NEIL1 has previously been shown to unhook psoralen MAs in ds-DNA context and ICLs in a three-stranded DNA structure, that mimic the repair intermediates generated through FA pathway-initiated repair. Recently, with the use of an *X. laevis* NEIL3<sup>-/-</sup> egg extract model system, NEIL3 was shown to be the primary repair pathway for the resolution of AP site ICLs and psoralen ICLs in a plasmid-based X shaped DNA structure, representative of a convergent DNA replication fork event (Semlow *et al.*, 2016). It was proposed that FA pathway-initiated repair could not be activated when a single DNA replication fork collided with an ICL and repair required the convergence of two replication forks (Zhou *et al.*, 2015; Semlow *et al.*, 2017).

Subsequently it was hypothesised due to the observations of overlapping complementarity of hNEIL1 and hNEIL3 processing of oxidised pyrimidines, that hNEIL3 would also share three-stranded psoralen ICL crosslink unhooking activity while also possessing the ability to excise psoralen monoadducts. A panel of psoralen ICL substrates were generated (**Figure 4.1**; **Figure 4.2**; **Figure 4.3**; **Figure 4.4**) and used as substrates for biochemical analysis of hNEIL1,

hNEIL3<sup>Cat</sup>, hNEIL3<sup>Trun</sup>, hNEIL3<sup>FL</sup> and Nei recombinant proteins (**Figure 4.5; Figure 4.8; Figure 4.9; Figure 4.11; Figure 4.13; Figure 4.14**).

Denaturing PAGE analysis demonstrated the ability of Nei and hNEIL1 recombinant proteins to unhook three-stranded ICL structures, which mimic DNA repair intermediates generated by the FA pathway, with a bifunctional activity profile conducting associated  $\beta,\delta$ -elimination of the phosphodiester backbone. All three versions of recombinant hNEIL3 protein also displayed the ability to unhook the same structure but with a monofunctional activity profile. Uniquely, the hNEIL3 recombinant proteins could unhook the psoralen ICL not only from the duplex portion of the three-stranded structure but also the ss-ICL/oligomer portion of the structure, subsequently producing a ds-MA as a repair product. It is hypothesised based on previous characterisation, that hNEIL1 may further process the ds-DNA monoadduct repair product (Couvé-Privat *et al.*, 2007). It was also observed that hNEIL3 proteins displayed robust activity in the presence of a long three-stranded psoralen ICL structure consisting of an 101 mer duplex covalently linked to a ss-47 mer oligonucleotide by a single HMT molecule. These observations provided the foundation for a putative FA independent pathway for the resolution of ICLs by NEIL proteins as a large three-stranded structure may not be generated through conventional FA initiated unhooking and associated TLS by polymerases characterised to fill a gap of only a small number of nucleotides (Wang, 2007; Sale *et al.*, 2012; Clauson *et al.*, 2013).

Therefore, an additional oligonucleotide was annealed to generate a four-stranded ICL structure, with two duplex DNA covalently bound by a single HMT molecule. This structure may represent the crosslinking of independent chromosomes after ICL bypass by TLS or translocase activity by FANCM, preventing the separation of DNA during the metaphase of the cell cycle due to the covalently bound intact daughter chromatin (Shen *et al.*, 2006; Minko *et al.*, 2008; Huang *et al.*, 2013; Budzowska, *et al.*, 2015; Xu *et al.*, 2015; Roy *et al.*, 2016; Zhou *et al.*, 2017). hNEIL3, NEIL1 and Nei proteins displayed a conserved unhooking activity in the presence of the alternatively <sup>32</sup>P labelled four-stranded ICL DNA oligonucleotide substrate, with Nei and NEIL1 proteins displaying a bifunctional profile through  $\beta,\delta$ -elimination of the phosphodiester backbone and the generation of a ss-nick (**Figure 4.11; Figure 4.27; Appendix Table 4**). hNEIL3 proteins however, displayed consistent monofunctional DNA glycosylase activity generating an AP site. Interestingly all recombinant

proteins analysed were able to indiscriminately unhook from both sides of the HMT molecule. Additionally, Nei demonstrated the ability to unhook the four-stranded ICL structure and then unhook the ds-MA product as a secondary substrate. As a result, it was proposed that *in vivo* hNEIL1 and hNEIL3 proteins may independently initiate BER for the resolution of a four-stranded ICL structure, with hNEIL1 unhooking ds-MA cleavage products as a secondary substrate. This model would suggest complementarity and redundancy shared between hNEIL1 and hNEIL3 DNA glycosylases. To provide control for these observations, a catalytically null mutant hNEIL3<sup>Cat</sup> protein was generated and was confirmed to be void of ICL unhooking capabilities (Figure 4.18; Figure 4.19; Figure 4.20; Figure 4.21; Figure 4.22; Figure 4.23; Figure 4.24).

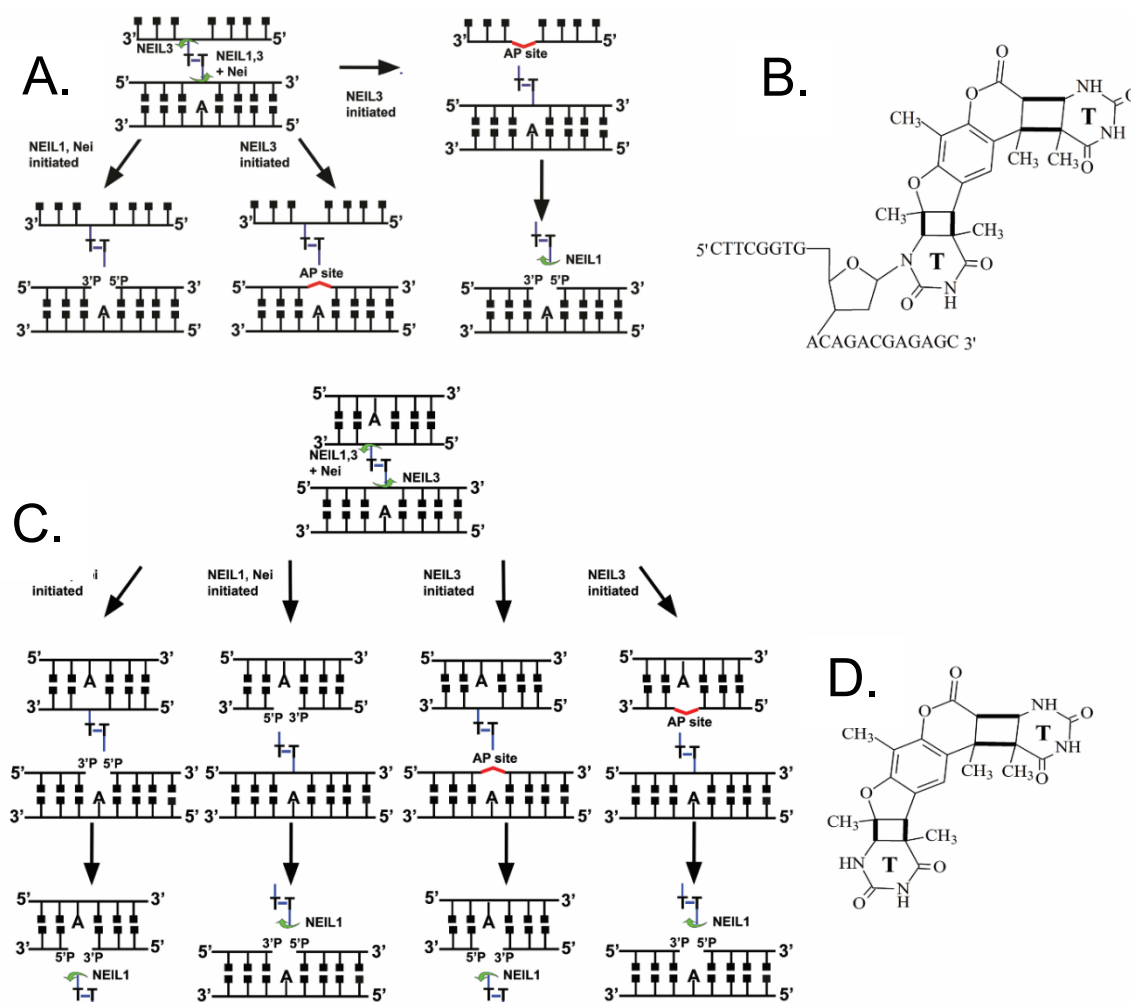


**Figure 4.27: Schematic representation of the mechanisms of action of Nei-like DNA glycosylases on ICLs.** A. Mechanisms of action of Nei-like DNA glycosylases on three-stranded DNA structure containing single psoralen-derived ICL. B. Mechanisms of action of Nei-like DNA glycosylases on four-stranded DNA structure containing single psoralen-derived ICL. C. Skeletal formula of 21 mer fragment containing single thymidine crosslinked to free thymine base by HMT (DNA(T)-HMT-T), an excision product generated by Nei-like DNA glycosylases catalysed repair of ICL in three-stranded DNA structure. D. Skeletal formula of thymine-HMT-thymine cross-link (T-HMT-T), an excision product generated by Nei-like DNA glycosylases catalysed repair of ICL in three- and four-stranded DNA structure.

The formation of a four-stranded structure *in vivo* may have important implications for genomic stability and chromosomal rearrangement events, due to FA initiated incision-dependent repair and subsequent repair of DSBs by HR (Bishop and Schiestl, 2002; Semlow *et al.*, 2016). Cross-linked chromosomes, in tri-radial and quad-radial structure have been described after an anthramycin-crosslinker treatment of cells (Matsumoto *et al.*, 1999). G-quadruplex structures also exist in human DNA and interact with cisplatin, forming quadruplexes with increased stability (Ju *et al.*, 2016). It has also been shown that crosslinking agents can form stable quadruplex ICL structures *in vitro* and have been shown to exert strong cytotoxicity in human tumour cell lines with a mode of action which generates two cross-linked DNA duplex (Ourliac-Garnier *et al.*, 2005; Nováková *et al.*, 2009). As cisplatin has been shown to generate ICLs at parallel G-G sites, it may be proposed that four-stranded ICLs may form in G-quadruplex structures. It has been shown that NEIL1 and NEIL3 can remove oxidative damage from a G-Quadruplex DNA in a telomeric context (Zhou *et al.*, 2013). This said, the role of ICL repair and NEIL proteins is not understood in the context of a G-quadruplex.

Interstrand crosslinks are considered to be absolute blocks to DNA replication and transcription processes (Deans and West, 2011; Clauson *et al.*, 2013). Subsequently the generation of long and three- and four-stranded DNA structures *in vivo* would require specialised bypass or traverse DNA damage tolerance pathways. Indeed, TLS past a duplex ICL by Pol $\kappa$ , Pol $\eta$  and Pol $\nu$  with subsequent primer extension facilitated by the REV1/Pol $\zeta$  complex has been shown (Shen *et al.*, 2006; Minko *et al.*, 2008; Budzowska, *et al.*, 2015; Xu *et al.*, 2015; Roy *et al.*, 2016). It was previously shown that movement past an ICL in an intact duplex is facilitated by the translocase activity of prokaryotic DnaB replication helicase (Bastia *et al.*, 2008). Subsequently, traverse of an ICL in a similar manner was shown by eukaryotic FANCM and was proposed to allow the continuation of replication past an ICL, stimulated by PCNA interaction with the PIP-box domain of the protein (Huang *et al.*, 2013). Additionally, it was proposed that signal transduction mediated by FANCM translocase activity, would signal replication restart at the distal side of the ICL (**Figure 4.28** ; Huang *et al.*, 2013; Rohleder *et al.*, 2016). The FANCM/MHF complex was demonstrated to promote replication traverse across an ICL in DNA, with DNA combing analysis revealing that ~85% of MA and HMT ICLs

that were encountered did not block DNA replication after a 60 min period. Traverse of an ICL was subsequently inhibited in FANCM<sup>-/-</sup> DT40 cells. Importantly deficiency in downstream FA pathway components FANCA, FANCE, FANCF or FANCG did not influence the frequency of replication traverse (Huang *et al.*, 2013). It was then shown that FANCM displayed transient interaction with PCNA, which was stimulated 10-fold under replicative stress induced by HU in HeLa cells (Rohleder *et al.*, 2016). hNEIL1 also interacts with PCNA and its associated RFC loading protein is coimmunoprecipitated in a multiprotein complex proficient in complete BER activity from HEK293 cells (Hegde *et al.*, 2015). This may provide a link between NEIL proteins and the FA pathway in support of previous findings which demonstrated that FA deficient cell lines display depleted hNEIL1 protein levels (Macé-Aimé *et al.*, 2010).

The continuation of DNA replication past an ICL, by a translocase such as FANCM, would facilitate the continuation of strand synthesis on both sides of the parental duplex. Thus, providing a suitable context for the generation of the three- and four-stranded ICL structures described here (**Figure 4.28**). Data presented here indicates a specific affinity for the repair of long three-stranded and four-stranded ICL structures by hNEIL1 and hNEIL3 (**Figure 4.9; Figure 4.11; Figure 4.13; Figure 4.14**). As the three-stranded ICL remnants shown here are relatively large, TLS activity is unlikely to fill the incised gap generated in a FA pathway context, additionally current models of replication associated ICL repair do not facilitate the generation of four-stranded ICL DNA structures (Sale *et al.*, 2012; Yang *et al.*, 2017). Taken together the data provides evidence for a possible hNEIL1 and hNEIL3 initiated ICL repair mechanism that may take place after DNA replication fork bypass or traverse (Huang *et al.*, 2013; Rolseth *et al.*, 2013).

Therefore, it is proposed that the CMG complex encounters an ICL, recruiting the FANCM/MHF complex. FANCM may then promote conventional FA pathway-initiated repair or replication machinery traverse. In the latter, replication machinery on the leading strand may traverse an ICL, generating a second replication fork after the ICL, generating an X-shaped structure, continuing replication and producing a long three-stranded structure (Huang *et al.*, 2013; Rohleder *et al.*, 2016). In the newly generated replication fork, replication machinery from the lagging strand may traverse the ICL after FANCM recruitment, generating a long four-stranded structure. Subsequently, hNEIL1 and hNEIL3 are recruited for the repair of the

ICL bypass products in a post-replicative manner (**Figure 4.27; Figure 4.28**). Downstream BER may then be initiated, avoiding generation of the major toxic DSBs associated with fork collapse and structure specific endonuclease cleavage as consequence of FA pathway repair (**Figure 4.28**; Hanada *et al.*, 2006; Zeman and Cimprich, 2014; Cortez, 2015). It is suggested that when hNEIL1 and hNEIL3 initiated BER proteins become exhausted, the more toxic FA pathway repair is initiated (Semlow *et al.*, 2016). Evidence for this may be provided by the protein kinetics data that demonstrate hNEIL1 and hNEIL3 display relatively slow three- and four-stranded ICL unhooking activity compared to the excision of the oxidative lesion Sp in ss-DNA and ds-DNA (**Figure 4.15; Figure 4.16; Figure 4.17**). Furthermore, the resolution of AP-site and psoralen ICLs in NEIL3 deficient *X. laevis* egg extracts has been shown to be undertaken by the FA pathway in a redundant manner (Semlow *et al.*, 2016).

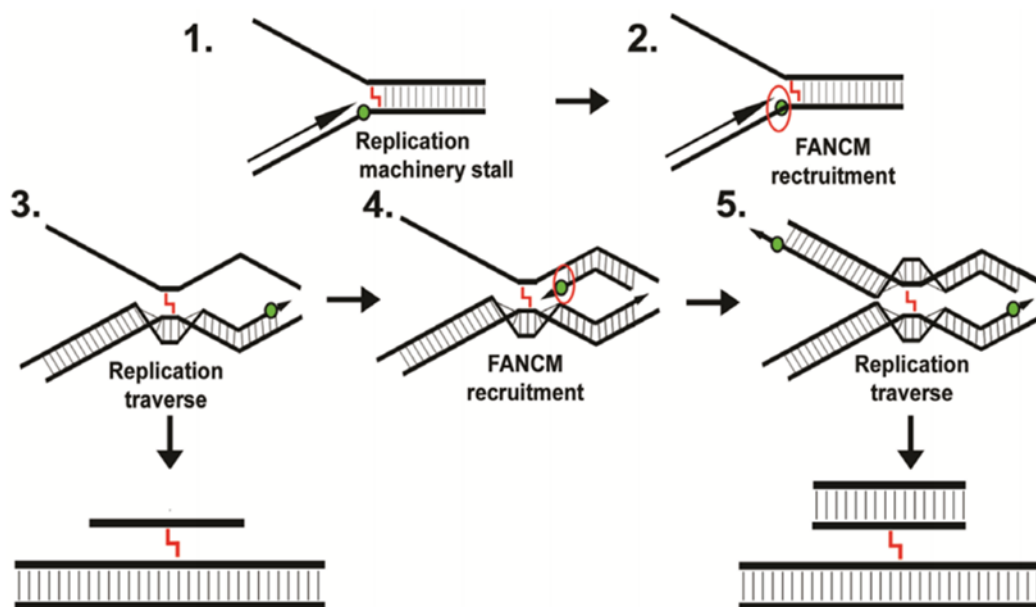


**Figure 4.28: Schematic representation of the proposed model of three- and four-stranded ICL DNA generation and subsequent resolution by hNEIL1 and hNEIL3 proteins.** 1. Leading strand replication machinery stall, 2. Recruitment of FANCM translocase, 3. Continuation of replication fork and strand synthesis, 4. Lagging strand replication machinery stall and recruitment of FANCM translocase, 5. Continuation of replication fork and strand synthesis.

In support of this hypothesis a recent study by Wallace's group determined that depletion of hNEIL3 in HCT116 cells by RNAi lead to an increase in metaphase arrest and chromosome bridging (Zhao *et al.*, 2017). Chromosome bridging has been demonstrated in CHO cells treated with HMT/UVA (Rizzoni *et al.*, 1993). It has also been shown that dysfunction in the FA pathway leads to an increase in the formation of chromatin bridges. Furthermore, FANCM has also been found to localise at DNA bridges (Chan and Hickson, 2011).

Therefore, it is postulated that FANCM may dictate the mode of resolution of an ICL at a stalled DNA replication fork. Conventionally FANCM may recruit the FA pathway in response to exogenously or endogenously generated ICLs but may also promote replication machinery traverse which may then require NEIL1/3 dependent initiation of repair of ICLs (Deans and West, 2011; Clauson *et al.*, 2013; Huang *et al.*, 2013). In addition, FANCM is stimulated through interaction with PCNA, that has been previously identified to interact with the hNEIL1 DNA glycosylase (Theriot *et al.*, 2010; Huang *et al.*, 2013). It may be tempting to speculate that transient interaction between FANCM and PCNA under replicative stress conditions, may lead to the association of the hNEIL1 multiprotein 'BERosome' complex to facilitate the repair of an ICL (Hegde *et al.*, 2015; Rohleder *et al.*, 2016; Martin *et al.*, 2017). Consequently, it would be important to establish if any interaction is observed between the FANCM protein and the hNEIL1 DNA glycosylases. Similarly, it would be important to establish if hNEIL3 displays a similar mode of interaction with PCNA and FANCM to establish the dynamic cellular response to the resolution of ICLs during DNA replication.

hNEIL3 expression has been shown to be restricted to highly proliferating cells such as testes, thyroid, neuronal progenitor cells and in cancers, while being specifically expressed through the S-phase of the cell cycle (Morland *et al.*, 2002; Torisu *et al.*, 2005; Hildrestrand *et al.*, 2009; Neurauter *et al.*, 2012; Zhou *et al.*, 2015). Subsequently, in the context of cancer, upregulation of hNEIL1 and hNEIL3 DNA glycosylases would in turn promote the proposed NEIL1/3 dependent repair of ICLs, avoiding toxic DSB repair intermediates (**Figure 4.27; Figure 4.28**). The FA pathway however, induces multiple DSBs leaving the cell vulnerable to replication fork collapse, chromosomal rearrangement and apoptosis (Clauson *et al.*, 2013; Ceccaldi *et al.*, 2016). It is therefore suggested that certain cancer cells upregulate hNEIL3 to provide a relatively elegant solution to bypass DNA replication blocks, enhance proliferation and minimise the consequences of the significant initiation of the DDR through induction of multiple DSBs typically associated with FA initiated repair (Shinmura *et al.*, 2013; Martin *et al.*, 2017). Indeed, it has been shown that depletion of NEIL3 in glioblastoma cells enhances the sensitivity to ATR and ATR/PARP inhibition, suggesting that in the absence of hNEIL3 the dependence on ATR signalling increases (Klattenhoff *et al.*, 2017).

Psoralen treatment of oligonucleotides may be used to generate model DNA substrates for the study of ICL repair, due to the relatively high percentage of induction of ICLs and relatively low induction of other types of DNA damage when compared to cisplatin (Dronkert and Kanaar, 2001; Couvé-Privat *et al.*, 2007; Couvé *et al.*, 2009; Deans and West, 2011). Sensitisation to cisplatin being observed in mNEIL3<sup>-/-</sup> MEFs may indicate that hNEIL3 can also resolve cisplatin adducts in complex with other proteins *in vivo* or has an associated non-canonical function that facilitates cisplatin induced DNA damage repair (Rolseth *et al.*, 2013). hNEIL3 was shown to co-localise with RPA, a protein involved in ATR mediated DDR, RSR, HR, and NER repair in complex with other DNA replication associated proteins (Patrick and Turchi, 1998; 1999, Morland *et al.*, 2002). Furthermore, it has since been shown that mutation of the Zf-GRF domain of APE2 prevents efficient APE2 dependent RPA recruitment to chromatin in *X. laevis* egg extracts (Wallace *et al.*, 2016). hNEIL3 possesses a Zf-GRF domain, in the extended C-terminal, that has strong homology with the Zf-GRF domain of APE2. This could indicate a similar interaction between RPA and hNEIL3 (Wallace *et al.*, 2016). Given the ability of RPA to denature duplex cisplatin ICLs *in vitro*, in turn generating a cisplatin adducted ss-DNA substrate, it is posited that hNEIL3 may proceed to preferentially initiate repair of single-stranded cisplatin MA lesions through BER (Patrick and Turchi, 1999). To gain a greater insight into the role the NEIL1 and NEIL3 DNA glycosylases play in cisplatin repair, coimmunoprecipitation of hNEIL1 and hNEIL3 protein complexes from untreated and cisplatin treated cells, followed by the identification of protein partners by immunoblot or LC-MS is necessary. Reconstitution of identified protein partners may begin to provide novel insights into the role in which the BER pathway may contribute to the acquired resistance of cancer cells to cisplatin (Rolseth *et al.*, 2013; Taylor *et al.*, 2015).

The data presented here provides a biochemical mechanistic rationale for the findings that hNEIL3 is over expressed in highly proliferating and cancerous cells (Shinmura *et al.*, 2016; de Sousa *et al.*, 2016; Kim *et al.*, 2016). Where the avoidance of persistent replication arrest and generation of DSBs is of benefit to cell survival and thus, NEIL upregulation would fundamentally unlock low toxicity proliferative capacity in cells. Indeed, depletion of hNEIL3 has been shown to increase the formation of spontaneous replication associated DSBs (Klattenhoff *et al.*, 2017). Therefore, hNEIL1 and hNEIL3 expression levels are highlighted as putative biomarkers of resistance to chemotherapeutic crosslinking agents (Macé-Aimé *et al.*,

2010; Rolseth *et al.*, 2013; Taylor *et al.*, 2015; Martin *et al.*, 2017). Strict cellular control of expression, lack of a mutagenic phenotype on deficiency of the NEIL DNA glycosylases under normal physiological conditions, while sensitising cancer cells to ICL inducing and DDR inhibitor therapy, provides a promising rationale for therapeutic targeting of the NEIL DNA glycosylases, for the treatment of cancers displaying abnormal NEIL expression levels and resistance to DNA crosslinking agents (Morland *et al.*, 2002; Torisu *et al.*, 2005; Hildrestrand *et al.*, 2009; Rolseth *et al.*, 2013; Taylor *et al.*, 2015; Klattenhoff *et al.*, 2017; Rolseth *et al.*, 2017; Zhou *et al.*, 2017).

## 5. Characterisation of post-translational modification of hNEIL3 by the ubiquitin proteasome system.

For the investigation of post translational modification and modulation of hNEIL3 by the ubiquitin proteasome, HeLa cell pellets were previously fractionated by Ion exchange and size exclusion chromatography using the ÄKTA Prime FPLC system (Williams and Parsons, 2017). Cell fractions were then analysed by anti-NEIL3 western blot after *in vitro* ubiquitination assays, facilitating the reconstitution of the ubiquitin conjugating cascade.

To investigate the post-translational regulation of hNEIL3<sup>FL</sup> by the UPS, recombinant hNEIL3<sup>FL</sup> was purified and confirmed by SDS-PAGE and anti-NEIL3 immunoblot analysis. HeLa cells were previously sequentially fractionated by Phosphocellulose ion exchange, HiLoad MonoQ sepharose ion exchange, Superdex 200 HR 10/30 gel filtration, CHT ceramic hydroxyapatite and Mono Q 5/50 GL ion exchange chromatography. Laboratory stocks of previously generated fractions were subsequently used for *in vitro* reconstitution with recombinant ubiquitin E1 ubiquitin-activating and recombinant E2 conjugating enzymes from laboratory stocks, for analysis by immunoblot, for the identification of a hNEIL3<sup>FL</sup> interacting E3 ubiquitin ligase. A novel interaction between hNEIL3<sup>FL</sup> and the TRIM26 was elucidated as result. To determine the putative functional role the interaction between endogenous hNEIL3 and TRIM26 plays, immunoblot analysis of previously prepared U2OS WCE treated with TRIM26 siRNA and H<sub>2</sub>O<sub>2</sub> was conducted. This revealed that TRIM26 modulates hNEIL1 and hNEIL3 steady state levels, but they are not induced over time after H<sub>2</sub>O<sub>2</sub> treatment. Previously generated data describing the novel ICL repair capabilities of hNEIL1 and hNEIL3 led to the investigation of the cellular response of U2OS cells to cisplatin. The effect of TRIM26 RNAi on hNEIL3 steady state levels was confirmed and putative evidence of hNEIL3 being inducible in response to cisplatin was determined through immunoblot. TRIM26 RNAi and transient overexpression of hNEIL1 and 3 was undertaken to assess U2OS cell survival after cisplatin treatment by clonogenic survival assays. Complementation is observed between TRIM26 RNAi induced cisplatin resistance and hNEIL1/3 overexpression, highlighting a resistant phenotype to cisplatin, modulated through TRIM26. Finally, a putative CRISPR/Cas9 hNEIL3 U2OS knockout cell line was generated for use as a model for the further investigation of the role of hNEIL3 in TRIM26 modulated cisplatin resistance and genomic stability in U2OS cells.

## 5.1. Results: Characterisation of post-translational modification of hNEIL3 by the ubiquitin proteasome system.

### 5.1.1. Recombinant hNEIL3<sup>FL</sup> purification from *E. coli* for *in vitro* ubiquitination assays.

To investigate *in vitro* post-translational modification of recombinant hNEIL3<sup>FL</sup> by the ubiquitin proteasome, expression and purification of hNEIL3<sup>FL</sup> from *E. coli* was undertaken. The pET-Duet2-*EcoMap*-ORF6-hNEIL3<sup>FL</sup> expression vector was transformed, colonies selected and upscaled before induction. Cultures were then incubated overnight at 16°C, harvested, lysed and purified as described in section 3.4.

As observed in **Figure 5.1 A**, bacterial contaminant proteins were eluted between fractions 5-9, followed by an A280 shoulder suggestive of target protein elution. Further analysis by 10% SDS-PAGE confirmed the co-elution of candidate recombinant hNEIL3<sup>FL</sup> and a hNEIL3<sup>FL</sup> degradation product between fractions 10-19, at the expected molecular weights of ~68 kDa and 52 kDa, respectively. Anti-His and anti-NEIL3 immunoblot analysis confirmed the identity of the candidate recombinant proteins eluted by HisTrap HP column FPLC purification (**Figure 5.1 C;D**). Anti-His immunoblot analysis determined that the recombinant hNEIL3<sup>FL</sup> degradation product was the ~52 kDa C-terminal portion of the recombinant hNEIL3<sup>FL</sup> protein, as the C-terminally fused His Tag was retained (**Figure 5.1 C**).

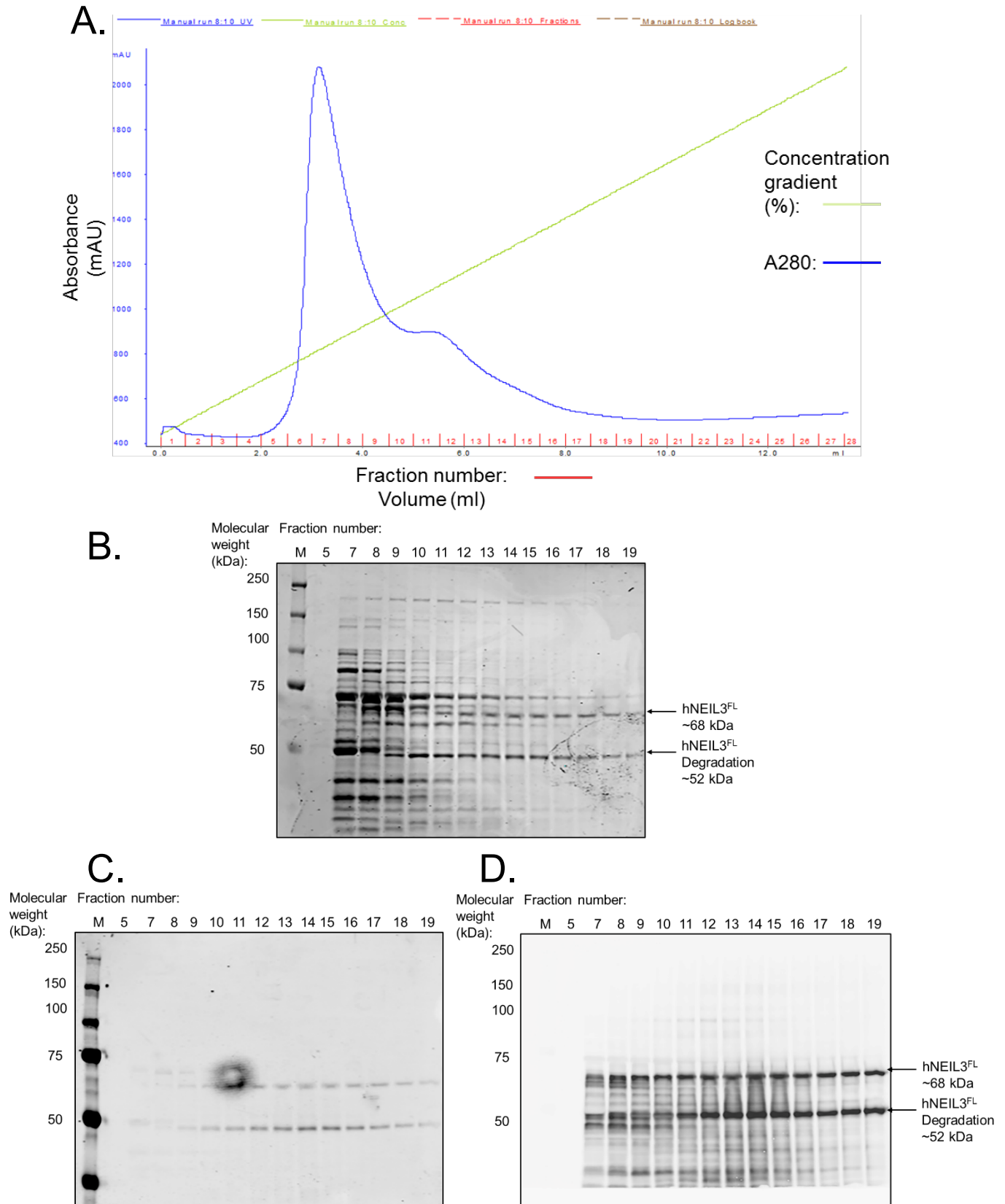


**Figure 5.1: HisTrap-HP FPLC purification of recombinant hNEIL3<sup>FL</sup> from Rosetta 2 (DE3) *E. coli* expression hosts.** A. Chromatogram analysis of protein fractions generated by HisTrap chromatography of lysates from *E. coli* overexpressing hNEIL3<sup>FL</sup>. B. SDS-PAGE and Instant Blue protein staining. C. Anti-His, D. anti-NEIL3 immunoblot analysis. "M" All Blue Prestained Protein Standard (BioRad).

### 5.1.2. Phosphocellulose purified HeLa WCE fraction *in vitro* ubiquitination of recombinant hNEIL3<sup>FL</sup>.

Previous HeLa cell fractionation by phosphocellulose column FPLC elution at 150 mM and 1000 mM KCl facilitated the separation of whole cell extracts based on affinity to DNA (Williams and Parsons, 2018). Reconstitution of ubiquitin, E1 ubiquitin activating and E2 conjugating enzymes in the presence of laboratory stocks of HeLa WCE, PC150 or PC1000 phosphocellulose column elution and recombinant hNEIL3<sup>FL</sup>, were analysed by immunoblot. **Figure 5.2** displays putative ubiquitination of hNEIL3<sup>FL</sup>. **Figure 5.2 A** displays recombinant His tagged E1 and E2 conjugating enzymes, however recombinant His tagged hNEIL3<sup>FL</sup> is probed with weak affinity by the anti-his primary antibody in comparison. **Figure 5.2 B** however displays anti-hNEIL3 probing of recombinant hNEIL3<sup>FL</sup>. Evidence of ubiquitination of hNEIL3<sup>FL</sup> is detected above the band representative of hNEIL3<sup>FL</sup>, in the presence of WCE and PC150 samples. A single band is observed at ~75 kDa and indicative of a mono-ubiquitination activity, highlighted by the red arrow and in agreement with the approximate expected molecular weight of hNEIL3<sup>FL</sup> (~68 kDa) with the addition of ubiquitin (~8 kDa). An increase in a smearing pattern can also be observed in the sample lane containing 10 µg of the PC150 fraction, providing evidence for poly-ubiquitination of recombinant hNEIL3<sup>FL</sup>. Negative controls in the absence of recombinant hNEIL3<sup>FL</sup>, E1, E2, ubiquitin or cellular extract display no observed putative ubiquitination, evidence of ubiquitination is specific to the recombinant hNEIL3<sup>FL</sup> protein (**Figure 5.2 A; B**).

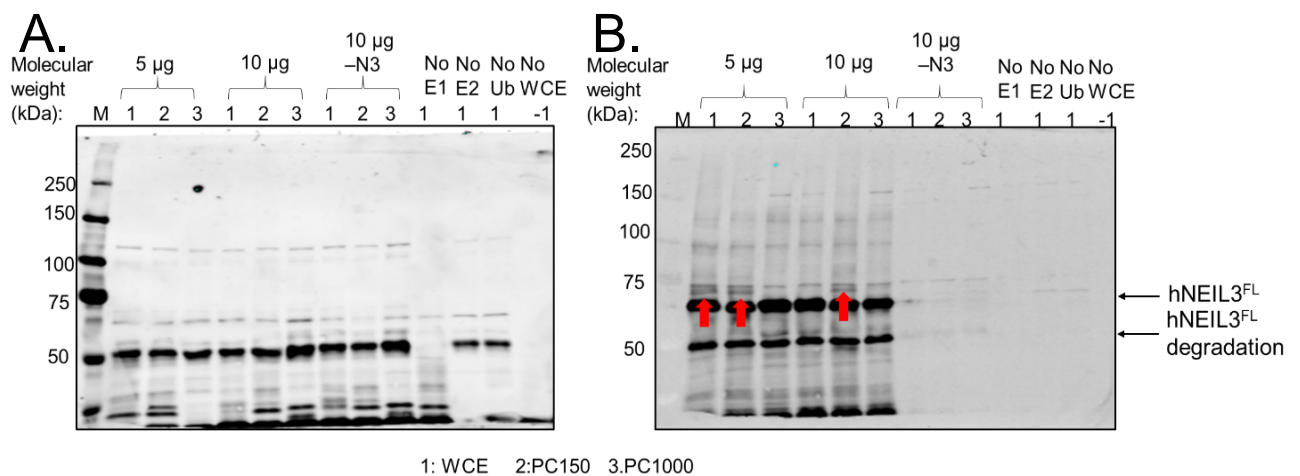


**Figure 5.2: Immunoblot analysis of hNEIL3<sup>FL</sup> incubated with phosphocellulose FPLC purification fractions of HeLa whole cell extracts.** Analysis of reconstituted *in vitro* ubiquitination reactions of PC150 and PC1000 fractions from laboratory stocks in the presence of 600 ng recombinant hNEIL3<sup>FL</sup> (Williams and Parsons, 2017) A. anti-His immunoblot B. anti-NEIL3 immunoblot. “M” All Blue Prestained Protein Standards (BioRad).

### 5.1.3. HiLoad Mono Q Sepharose Ion exchange fraction *in vitro* ubiquitination of recombinant hNEIL3<sup>FL</sup>.

To further purify proteins that were present in the eluted PC150 fraction which facilitated *in vitro* hNEIL3<sup>FL</sup> ubiquitination, the PC150 fraction was previously buffer exchanged and fractionated using a 20 ml HiLoad Mono Q Sepharose ion exchange column. Every second fraction from laboratory stocks was then analysed by *in vitro* ubiquitination reaction in the presence of recombinant hNEIL3<sup>FL</sup> and subsequently analysed by anti-NEIL3 immunoblot (**Figure 5.3 B; C**). Multiple fractions display evidence of hNEIL3<sup>FL</sup> ubiquitination, with reference to section (**Figure 5.2 A; B**). Minor activities are observed between fractions 14-18 and 24-34. However, the fractions displaying the strongest observable putative ubiquitination range from fraction 50 to 62, with the strongest activity observed in fractions 56 and 58. As observed in **Figure 5.3** activity observed in the presence of fractions 56-58 aligned with the largest eluted peak identified by the A280 elution trace during previous FPLC chromatography. Evidence of mono-ubiquitination is observed and highlighted with red arrows at ~ 75 kDa, with consistent increase in the appearance of a smeared pattern within the sample lane, that is indicative of poly-ubiquitination of recombinant hNEIL3<sup>FL</sup> (**Figure 5.3 A; B**). **Figure 5.3** provides evidence for proteins present between fractions 56-58 which facilitated ubiquitination of hNEIL3<sup>FL</sup>, when reconstituted with recombinant Ub, E1 activating and E2 conjugating enzymes.

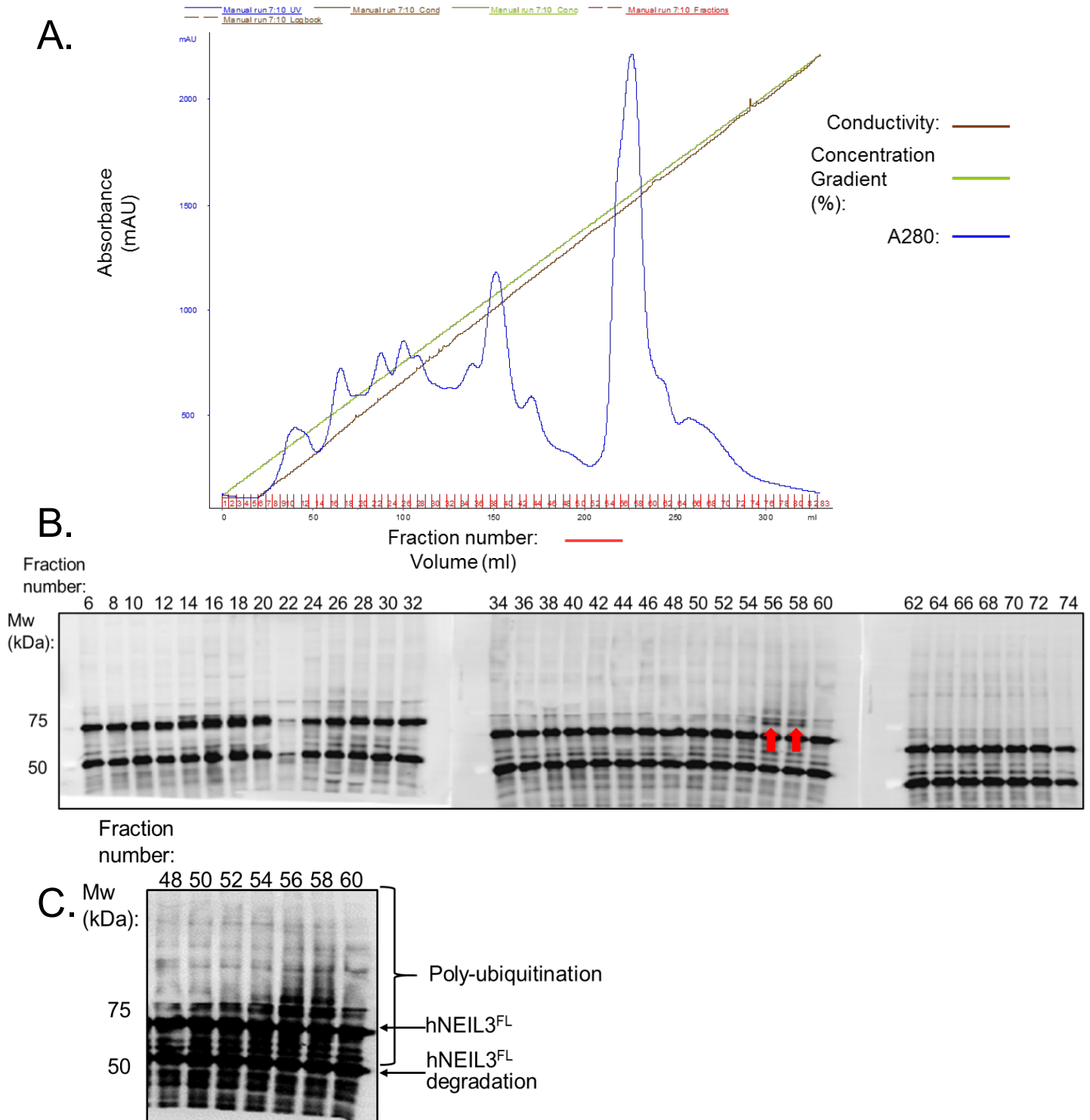


**Figure 5.3: Ubiquitination analysis of HiLoad Mono Q Sepharose column FPLC purification fractions of PC150 elution of HeLa WCE.** A. Chromatogram analysis of previously purified HiLoad Mono Q Sepharose fractions (Williams and Parsons, 2018). *In vitro* ubiquitination reaction of 600 ng recombinant hNEIL3<sup>FL</sup> in the presence of HiLoad Mono Q Sepharose fractionated PC150 laboratory stocks. B. Anti-NEIL3 immunoblot imaged at low scan intensity (5.0), C. anti-NEIL3 immunoblot imaged at high scan intensity (6.5) using the Licor Odyssey InfraRed scanner. “M” All Blue Prestained Protein Standards (BioRad). Arrows identify lanes displaying major ubiquitination activity.

#### 5.1.4. Superdex 200 HR 10/30 gel filtration fraction *in vitro* ubiquitination of recombinant hNEIL3<sup>FL</sup>.

To isolate proteins, present in fractions 51-58 after HiLoad Mono Q Sepharose Ion exchange elution, fractions were previously pooled, and buffer exchanged (Williams *et al.*, 2018). Pooled samples were then fractionated based on protein size, using the Superdex 200 HR 10/30 size exclusion column. Fractions 14-36 from laboratory stocks were analysed based on the FPLC chromatogram A280 elution trace, by *in vitro* ubiquitination and anti-NEIL3 immunoblot analysis.

**Figure 5.4** displays evidence of ubiquitination facilitated by isolated proteins present between fractions 20-24. An increase in the associated band for mono-ubiquitination at ~75 kDa and increased lane smearing indicative of poly-ubiquitination activity were observed (**Figure 5.4 B**). In **Figure 5.4 C**, an increase in the ubiquitination of the hNEIL3<sup>FL</sup> degradation product is also observed. Fractions that display activity align inbetween two observable elution peaks detected by the A280 elution trace as displayed in **Figure 5.4 A**. Observation of ubiquitination of hNEIL3<sup>FL</sup> in the presence of fractions 20, 22 and 24, suggested successful purification and isolation of cellular protein which facilitates ubiquitination of hNEIL3 *in vitro*. Previous anti-His immunoblot of recombinant hNEIL3<sup>FL</sup> displayed probing of the hNEIL3<sup>FL</sup> degradation product and confirmed retention of the C-terminal His tag (**Figure 5.1**; **Appendix Figure 2**; **Appendix Figure 3**). Consequently, ubiquitination of the hNEIL3<sup>FL</sup> degradation product suggested that ubiquitination is dependent on lysine residues present in the ~52 kDa portion of the C-terminal domain.

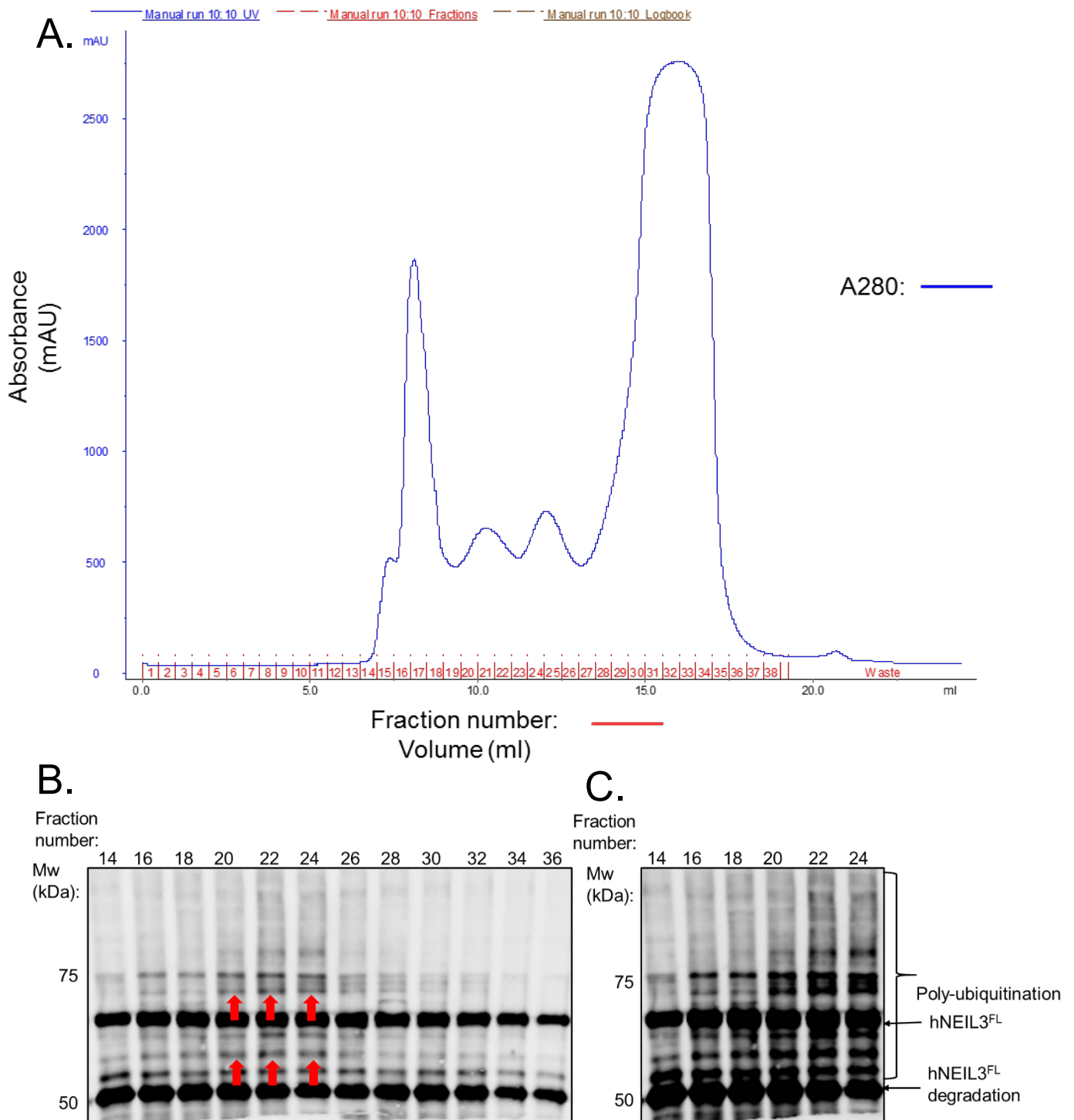


**Figure 5.4: Ubiquitination analysis of Superdex 200 HR 10/30 FPLC purification fractions.** A. Chromatogram analysis of previously purified HiLoad Mono Q Sepharose fractions (Williams and Parsons, 2018). *In vitro* ubiquitination reaction in the presence of 600 ng recombinant hNEIL3<sup>FL</sup> and Superdex 200 HR 10/30 gel filtration fractions from laboratory stocks analysed by B. Anti-NEIL3 immunoblot imaged at low scan intensity (5.0), C. anti-NEIL3 immunoblot image at high scan intensity (6.5), using the Licor Odyssey InfraRed scanner. “M” All Blue Prestained Protein Standards (BioRad).

### 5.1.5. Mono Q 5-50 GL Ion exchange fraction *in vitro* ubiquitination of recombinant hNEIL3<sup>FL</sup>.

Fractions which displayed ubiquitination activity in Section 5.3 were previously pooled buffer exchanged and purified further by a CHT ceramic hydroxyapatite column (Appendix Figure 4; Williams and Parsons, 2018). Subsequently, fractions 18-20 were previously pooled and diluted 10-fold in Mono Q 5/50 GL column buffer A for ion exchange chromatography as a final polishing step (Williams and Parsons, 2018). Based on A280 FPLC chromatogram trace, laboratory stocks of fractions 22-30 were analysed by *in vitro* ubiquitination reaction and anti-NEIL3 western blot analysis. **Figure 5.5 B** displays probing of hNEIL3<sup>FL</sup> with the anti-His antibody however evidence of ubiquitination was difficult to detect. As shown in **Figure 5.5 C**, anti-NEIL3 immunoblot analysis revealed that multiple fractions displayed evidence of ubiquitination activity. All of the analysed fractions displayed differential levels of evidence of ubiquitination *in vitro*. Fraction 25 however, displayed the greatest evidence of mono-ubiquitination activity with a band appearing at ~75 kDa, while maintaining relative poly-ubiquitination activity. Additionally, fraction 25 aligned with the major peak detected by the A280 elution trace and displayed in **Figure 5.5 A**. Fraction 25 was therefore selected for analysis by LC-MS. Results are displayed in **Appendix Table 5** and identify tripartite motif containing 26 (TRIM26), which was the only protein detected that has previously been characterised to possess associated E3 ubiquitin-ligase activity that was present in fraction 25. **Figure 5.5** and **Appendix Table 5** provide putative evidence of the successful identification of TRIM26 as the major hNEIL3<sup>FL</sup> interacting E3 ubiquitin ligase from HeLa cells.

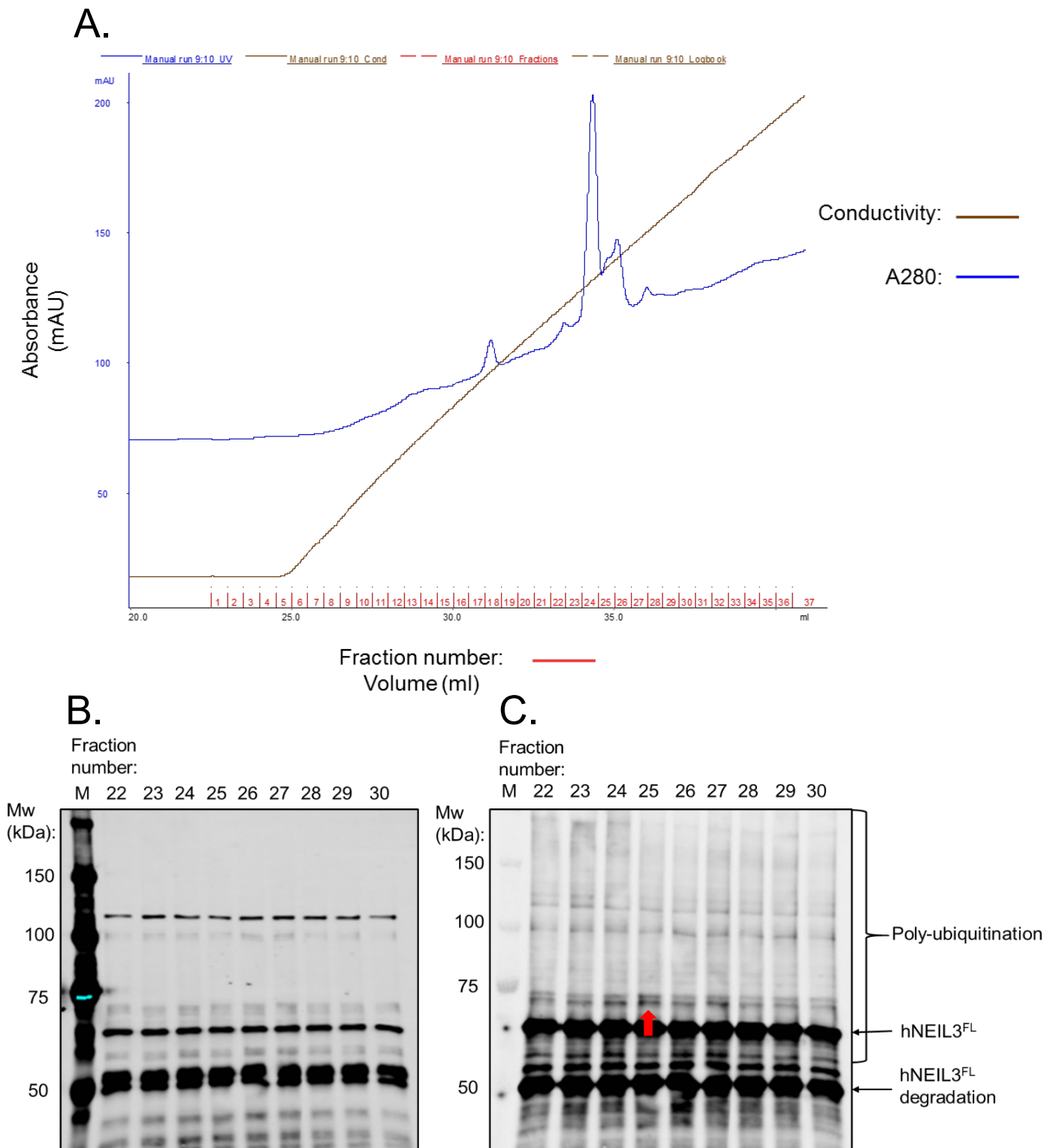


**Figure 5.5: Ubiquitination analysis of Mono Q 5/50 GL purification fractions.** A. Chromatogram analysis of previously purified HiLoad Mono Q 5/50 GL fractions (Williams and Parsons, 2018). *In vitro* ubiquitination reactions in the presence of 600 ng recombinant hNEIL3<sup>FL</sup> and Mono Q 5/50 GL ion exchange fractions from laboratory stocks were analysed by B. Anti-His immunoblot and C. Anti-NEIL3 immunoblot “M” All Blue Prestained Protein Standards (BioRad).

### 5.1.6. Identification and purification of recombinant the TRIM26 E3 ubiquitin ligase.

Mono Q 5/50 GL purified fraction 25 analysis by LC-MS (**Appendix Table 5**) identified TRIM26 as a novel interacting protein with recombinant hNEIL3<sup>FL</sup>. To confirm E3 ubiquitin ligase activity of TRIM26 in the presence of recombinant hNEIL3<sup>FL</sup> the pET28a-TRIM26 bacterial expression plasmid was transformed into Rosetta 2 (DE3) *E. coli* expression hosts and used to express and purify recombinant TRIM26 for *in vitro* ubiquitination assays. Bacterial colonies were selected, scaled and bacterial cultures induced as described in 2.2. HisTrap HP FPLC affinity chromatography was undertaken to isolate recombinant C-terminally His-tagged TRIM26 from bacterial proteins.

**Figure 5.6 A** displays the FPLC chromatogram after gradient elution of *E. coli* protein lysate. A major peak associated with histidine rich bacterial proteins was eluted between fraction 5 and 13. A trace shoulder was identified between fractions 14 and 25. Fractions 5-25 were collected and analysed by 8% SDS-PAGE and anti-His immunoblot analysis (**Figure 5.6 B; C**). SDS-PAGE analysis provided putative evidence for successful separation of extracted proteins, however no candidate band was identified for TRIM26. **Figure 5.6 C** displays, anti-His immunoblot analysis that confirmed the successful isolation of His-tagged TRIM26, at the expected molecular weight of ~63 kDa, with the majority of recombinant TRIM26 eluted between fractions 17 and 25. Fractions 17 to 25 were subsequently pooled and buffer exchanged against (50 mM Tris-HCl pH 8, 50 mM KCl, 1 mM EDTA, 10% glycerol) and the concentration was determined as 0.434 mg/ml.

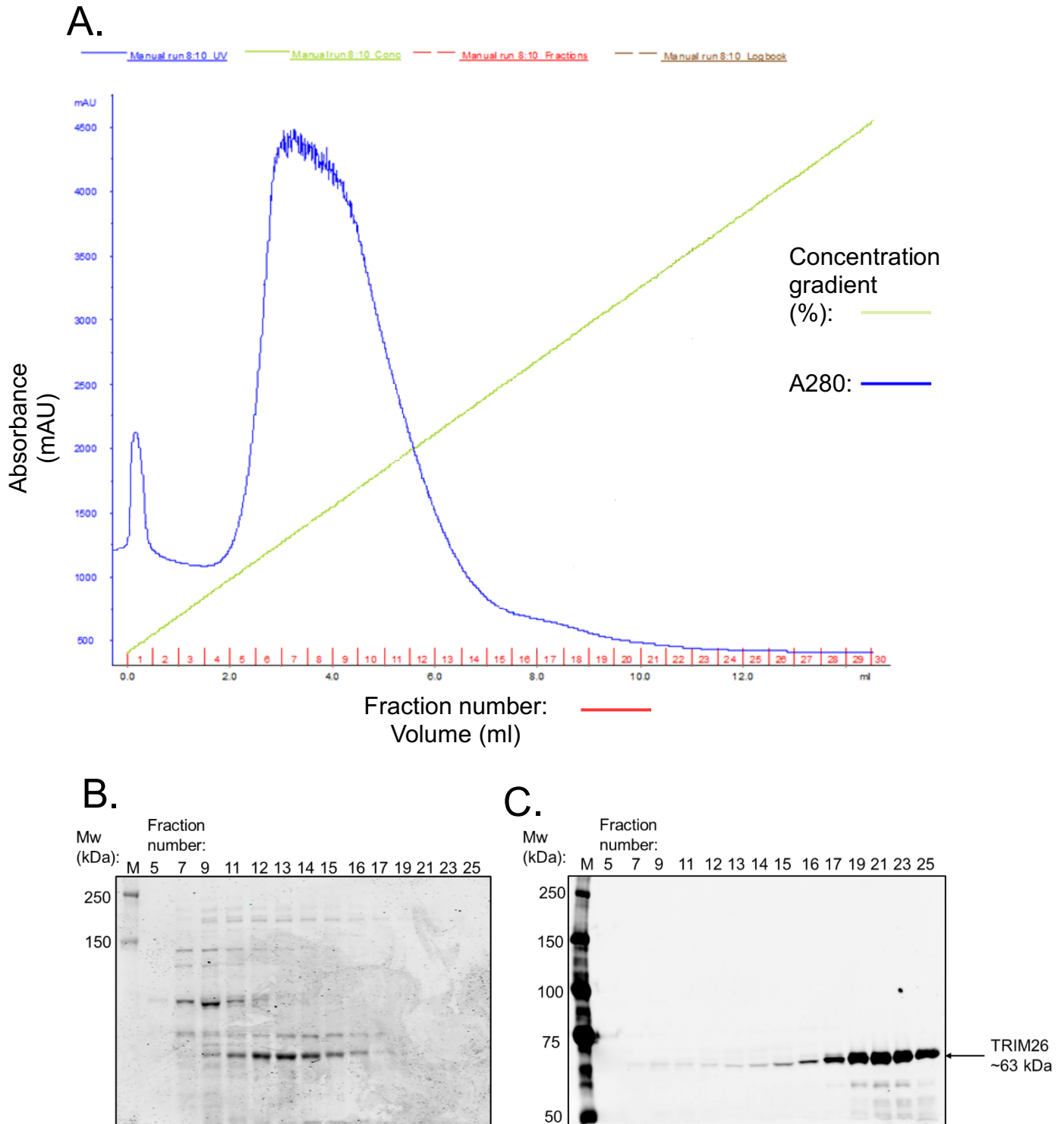


**Figure 5.6: HisTrap-HP FPLC purification of the recombinant TRIM26 from Rosetta 2 (DE3) *E. coli* expression hosts.** A. Chromatogram analysis of protein fractions generated by HisTrap chromatography of lysates from *E. coli* overexpressing TRIM26. B. 8% SDS-PAGE and Instant Blue protein staining. C. Anti-His immunoblot analysis. "M" All Blue Prestained Protein Standards (BioRad).

### 5.1.7. *In vitro* ubiquitination of hNEIL3 by TRIM26 E3 ubiquitin ligase.

To confirm E3 ubiquitin ligase activity of recombinant His-tagged TRIM26 in the presence of hNEIL3<sup>FL</sup> an *in vitro* ubiquitination reaction was conducted and subsequently analysed by anti-NEIL3 western blot analysis. In **Figure 5.7 A**, it can be observed that increasing the concentration of TRIM26 increased the observable evidence of mono-ubiquitination with an increase in the signal intensity of the single band shown at ~75 kDa. Additionally, **Figure 5.7 B** displays a gradual increase in the intensity of a smearing pattern in each lane, in the presence of increasing amounts of recombinant TRIM26, indicative of poly-ubiquitination activity. However, minor mono-ubiquitination and poly-ubiquitination activity was observed in the absence of the TRIM26 sample lane, suggested to be due to sample contamination during loading of the SDS gel. Despite this an observable titration of ubiquitination activity was demonstrated, with an increase in the concentration of recombinant TRIM26. This subsequently provides evidence of E3 ubiquitin-ligase activity in the presence of hNEIL3<sup>FL</sup> by TRIM26 that is above background control levels. In addition, this data provides evidence for the successful isolation, identification and recombinant protein purification from *E. coli*, of an interacting protein that facilitates the post-translational modification of recombinant hNEIL3<sup>FL</sup>.

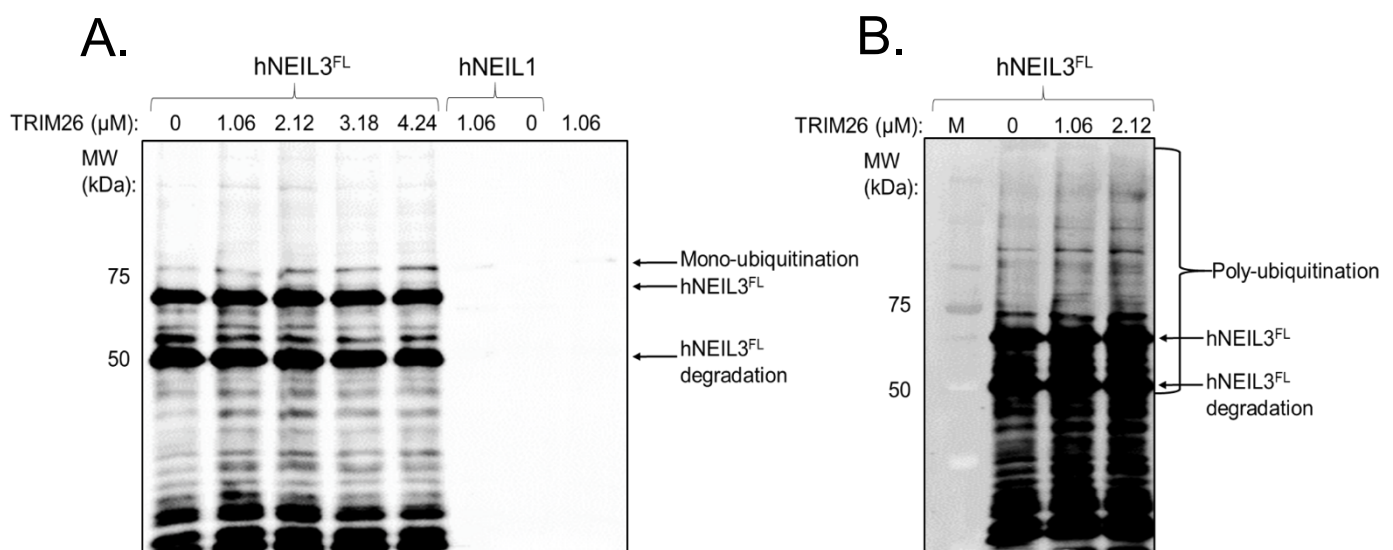


**Figure 5.7: Immunoblot analysis of ubiquitination of hNEIL3<sup>FL</sup> in the presence of recombinant TRIM26.** Anti-NEIL3 immunoblot analysis of *in vitro* ubiquitination reactions with increasing concentrations of recombinant TRIM26 in the presence of 600 ng recombinant hNEIL3<sup>FL</sup>. A. anti-NEIL3 immunoblot imaged at low scan intensity (5.0), B. anti-NEIL3 imaged at high scan intensity (6.5) using the Licor Odyssey InfraRed scanner.

### 5.1.8. Analysis of hNEIL1 and hNEIL3 protein levels post H<sub>2</sub>O<sub>2</sub> and TRIM26 siRNA

To investigate the functional role of TRIM26 in the PTM and modulation of hNEIL3 in a cellular context, laboratory stocks of WCE from U2OS cells treated with either a NT or TRIM26 specific siRNA and the oxidising agent H<sub>2</sub>O<sub>2</sub> were analysed by immunoblot.

Initial analysis was conducted on a known substrate of TRIM26, hNEIL1 (**Figure 5.8**). Steady state levels of hNEIL1 were observed to be increased in TRIM26 siRNA treated U2OS WCE, consistent with previous observations, however significant induction of hNEIL1 in response to H<sub>2</sub>O<sub>2</sub> was not observed in TRIM26 siRNA treated cells (Edmonds *et al.*, 2017). However, minor induction of hNEIL1 is observed between 0 and 0.5 h post treatment in NT siRNA treated cells. **Figure 5.8** provides evidence that steady state levels of hNEIL1 protein are partially modulated by TRIM26 in U2OS cells.

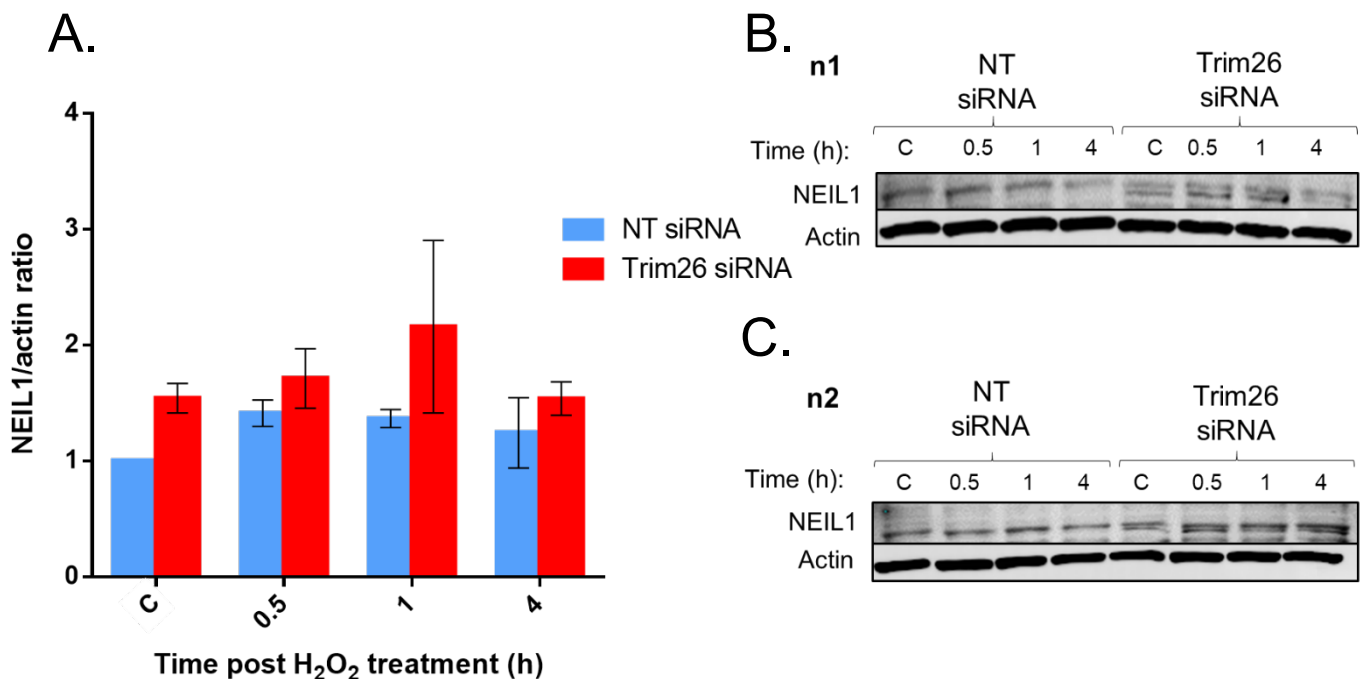


**Figure 5.8: Anti-NEIL1 immunoblot analysis of U2OS cells treated with TRIM26 siRNA and harvested 0-4 h after treatment with 150µM H<sub>2</sub>O<sub>2</sub>.** A. NEIL1/Actin ratios were quantified from results of two independent experiments displayed. B-C Anti-NEIL1 immunoblot of U2OS cell extract lysates treated with 33 pmol NT or TRIM26 siRNA for 48 h and treated with 150 µM H<sub>2</sub>O<sub>2</sub> for 15 min. "C" in the without of H<sub>2</sub>O<sub>2</sub> treatment. Error bars display standard error.

The same U2OS WCEs were then analysed for differences in hNEIL3 protein levels between NT or TRIM26 siRNA treated cells, by anti-NEIL3 immunoblot (**Figure 5.9 B; C**). A significant increase in steady state levels of endogenous hNEIL3 was observed immediately after H<sub>2</sub>O<sub>2</sub> treatment ( $p=0.000149923$ ), 0.5 ( $p=0.0463634$ ) and 1 h post treatment ( $p=0.0213931$ ; **Figure 5.9 A**) but not at 4 h post treatment ( $p=0.412032$ ). Despite steady state levels being significantly elevated immediately post treatment and up to 1 h H<sub>2</sub>O<sub>2</sub> after treatment, induction of hNEIL3 in response to H<sub>2</sub>O<sub>2</sub> was not observed in TRIM26 RNAi cells. This data suggests that TRIM26 regulates steady state levels of hNEIL3. However, only minor induction of hNEIL3 can be observed in NT siRNA treated cells between 0-4 h after H<sub>2</sub>O<sub>2</sub> treatment. Therefore, **Figure 5.9** demonstrates that TRIM26 modulates hNEIL3 protein levels in U2OS cells treated with H<sub>2</sub>O<sub>2</sub>.

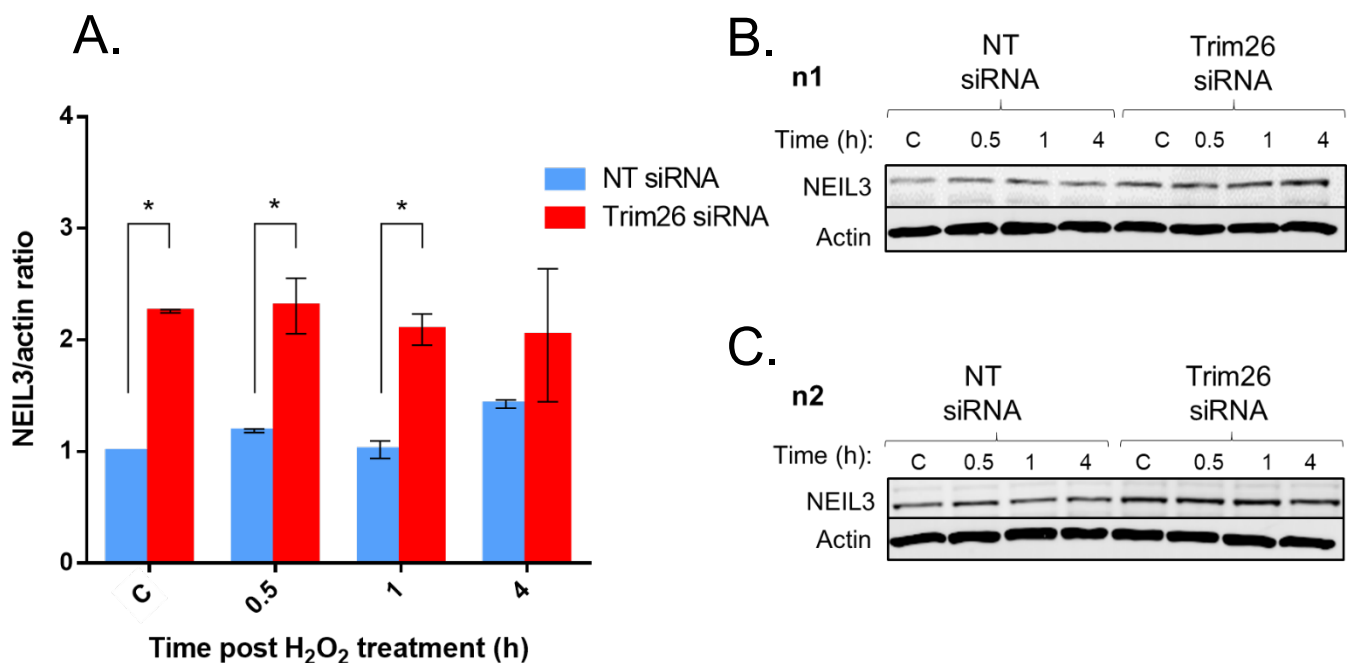


**Figure 5.9: Anti-NEIL3 immunoblot analysis of U2OS cells treated with TRIM26 siRNA and harvested 0-4 h after treatment with 150 $\mu$ M H<sub>2</sub>O<sub>2</sub>** A. Quantification of NEIL3: Actin ratios from results of two independent experiments displayed. B-C Anti-NEIL3 immunoblot of U2OS cell extract lysates treated with 33 pmol NT or TRIM26 siRNA for 48 h and treated with 150  $\mu$ M H<sub>2</sub>O<sub>2</sub> for 15 min. "C" in the without of H<sub>2</sub>O<sub>2</sub> treatment. T-tests between NT and TRIM26 siRNA at: 0 h  $p=0.000149923$ , 0.5 h  $p=0.0463634$ , 1 h  $p=0.0213931$ , 4 h  $p=0.412032$ . Error bars display standard error.

### 5.1.9. Analysis of hNEIL3 protein levels in response to cisplatin and TRIM26 siRNA treatment.

To investigate if TRIM26 modulates the response of hNEIL3 protein levels to the ICL inducing agent cisplatin, U2OS cells were treated with TRIM26 siRNA and increasing concentrations of cisplatin. **Figure 5.10** demonstrates elevated hNEIL3 steady state levels post TRIM26 siRNA treatment, in agreement with previous observations (**Figure 5.9**). **Figure 5.10 A** indicates that hNEIL3 is not induced in response to cisplatin in a dose dependent manner in TRIM26 RNAi U2OS cells. However, in NT RNAi cells minor induction of hNEIL3 was observed between 0 and 7.5  $\mu$ M cisplatin.

**Figure 5.10 B** provides preliminary evidence that hNEIL3 steady state levels are modulated by TRIM26 in U2OS cells treated with cisplatin and hNEIL3 may be recruited in response to cisplatin induced DNA damage in NT siRNA treated U2OS cells. However, no significant differences in hNEIL3/actin ratio protein levels were observed between NT siRNA and TRIM26 siRNA treated cells overall (**Figure 5.10 A**).

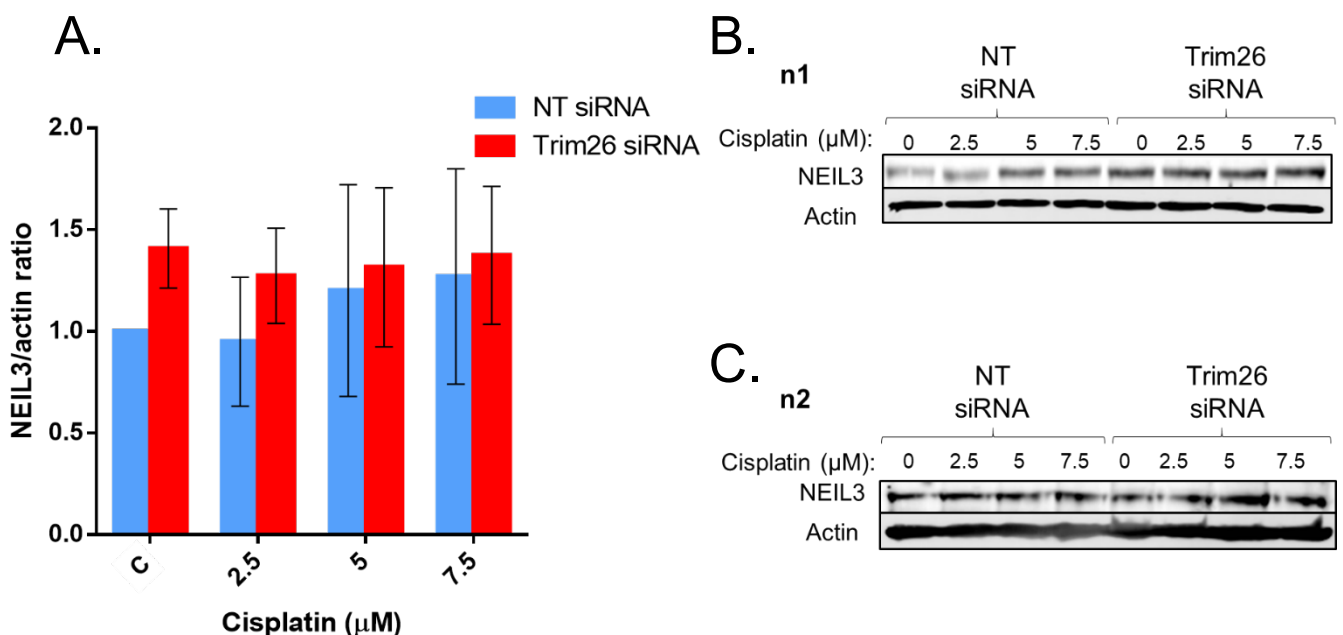


**Figure 5.10: Anti-NEIL3 immunoblot dose response analysis of U2OS whole cell extracts treated with TRIM26 siRNA and cisplatin treatment.** A. Quantification of NEIL3/Actin from results of two independent experiments displayed. B-C Anti-NEIL3 immunoblot of U2OS cell extract lysates treated with 33 pmol NT or TRIM26 siRNA for 48 h and treated with 0-10  $\mu$ M cisplatin for 24 h. "C" without cisplatin treatment.

**5.1.10.** Cisplatin clonogenic analysis of the effect of TRIM26 RNAi or overexpression of hNEIL1/hNEIL3 on U2OS cell survival.

Previously it has been shown that NEIL1 is a substrate for ubiquitination by the E3 ubiquitin ligase TRIM26. A resistant phenotype to X-ray IR of U2OS cells post TRIM26 depletion by siRNA was also observed, however complementation was not observed when transiently overexpressing NEIL1.

To investigate if TRIM26 may modulate hNEIL1 and hNEIL3 protein levels in response to cisplatin as a DNA damage response to cisplatin, clonogenic analysis was undertaken. NT siRNA, TRIM26 siRNA, NEIL1 and NEIL3 transient overexpression were compared in attempt to observe whether a resistant phenotype was observed. NEIL1-3xFLAG overexpression was confirmed by anti-FLAG immunoblot analysis of U2OS WCEs transfected with the pCMV-hNEIL1-Tag3a transient mammalian expression vector (**Figure 5.11 B**). hNEIL3 overexpression was also confirmed by anti-NEIL3 immunoblot analysis of U2OS WCEs transfected with the pCMV-ac-hNEIL3 transient mammalian expression vector (**Figure 5.11 C**). Quantification of colony forming units after treatment revealed a significant resistant phenotype of U2OS cells after TRIM26 siRNA when compared to NT siRNA treated cells ( $p < 2.2 \times 10^{-16}$ ) (**Figure 5.11 F**). U2OS cells treated with overexpression of NEIL1 and NEIL3 also displayed a resistant phenotype when compared to NT siRNA, determined by use of CFAssay package within the R program ( $p < 2.2 \times 10^{-16}$  and  $p < 2.2 \times 10^{-16}$ , respectively; **Figure 5.11 D-E**). **Figure 5.11** provides evidence of a role of NEIL1 and NEIL3 in U2OS cell resistance to cisplatin, presumably through their ICL repair capabilities. In addition, **Figure 5.11** provides evidence for a novel role of the E3 ubiquitin ligase TRIM26 in modulating the response of U2OS cells to the interstrand crosslinking agent cisplatin through its ubiquitination activity.

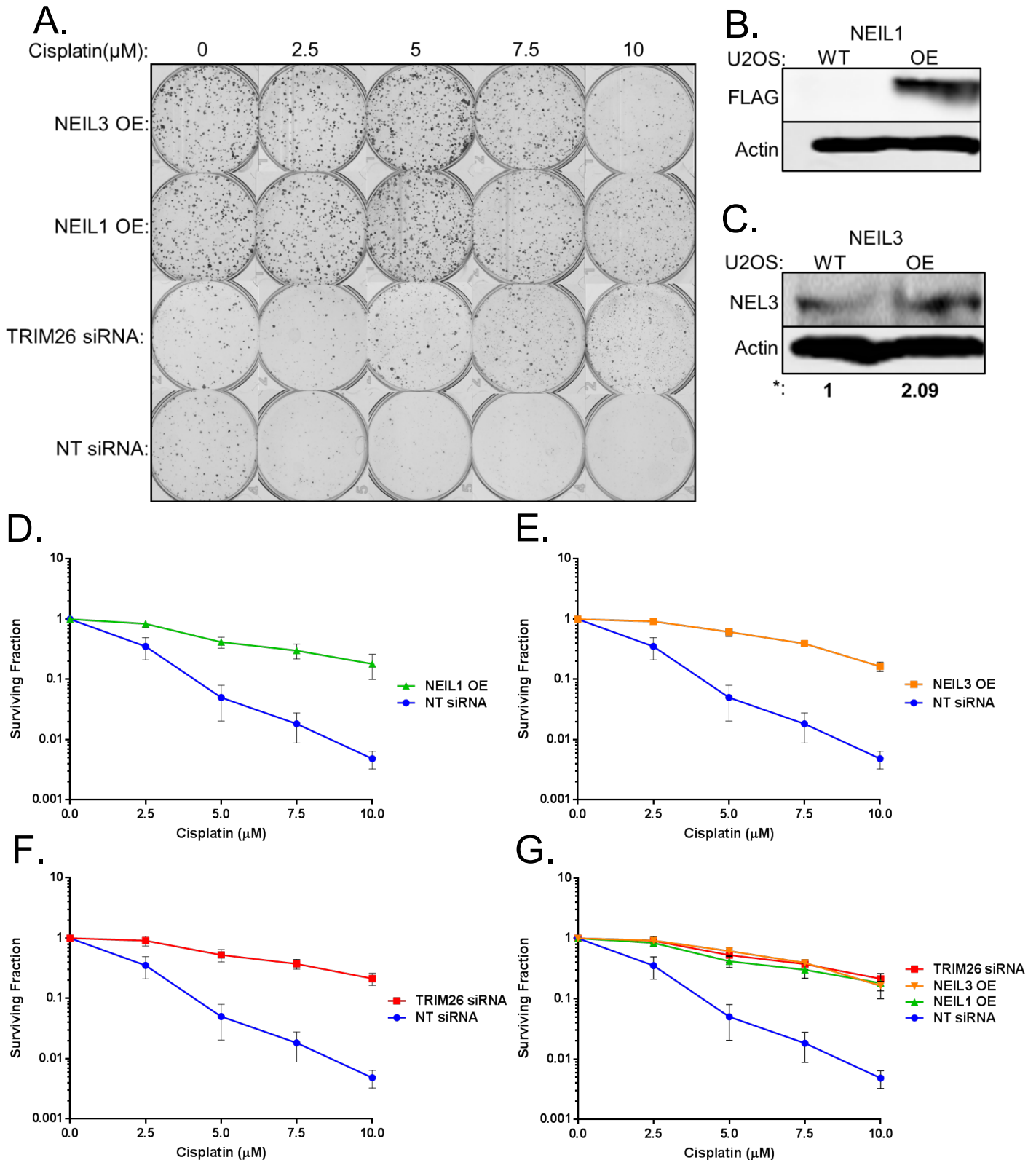


**Figure 5.11: Clonogenic survival assay analysis: cisplatin dose response of U2OS cells pre-treated with NT siRNA, TRIM26 siRNA, NEIL1 or NEIL3.** A. Representative clonogenic plate images. B. Anti-FLAG and anti-actin Immunoblot analysis of overexpression of NEIL1. C. Anti-NEIL3 and anti-actin immunoblot analysis of NEIL3 overexpression, NEIL3/actin ratios displayed below each sample lane. (D-G) Mean surviving fraction is shown with standard errors from the results of three independent experiments.  $P < 2.2 \times 10^{-16}$  (NT siRNA vs TRIM26 siRNA),  $P < 2.2 \times 10^{-16}$  (NT siRNA vs NEIL1 OE) and  $P < 2.2 \times 10^{-16}$  (NT siRNA vs NEIL3 OE) as analysed by the CFAssay for R package.

### 5.1.11. CRISPR/Cas9 mediated knockout of endogenous hNEIL3.

To provide a model to for the investigation of the role of hNEIL3 in U2OS cells, attempts were made to knockout hNEIL3 with CRISPR/Cas9 in U2OS cells. As described in section 2.27, U2OS cells were established for subsequent screening of hNEIL3 protein levels after CRISPR /Cas9 treatment, by SDS-PAGE and anti-NEIL3 immunoblot analysis.

As displayed in **Figure 5.11** variability in hNEIL3 protein levels was observed across single clonal colony U2OS WCEs, providing evidence for CRISPR/Cas9 interaction. In support of this all clonal populations screened were able to continue proliferation in the presence of 1 µg/ml puromycin during antibiotic selection (section 2.27). This indicated puromycin resistance via integration of the donor cassette containing the puromycin resistance gene. However, 84 of the screened WCE displayed presence of hNEIL3 protein indicating low efficiency of Cas9/gRNA interaction, subsequent homology directed repair at the correct locus targeted at exon 1 of the NEIL3 gene sequence. Non-target interaction of the Cas9/gRNA complex is proposed, as cells display puromycin resistance. However, 5 putative knockout clones were identified and highlighted in red in **Figure 5.11**, displaying significant depletion of hNEIL3 protein levels. Subsequently, clones: G1 38, G2 1, G2 12, G2 24 and G2 30 were transferred to 10 cm tissue culture dishes for upscaling for repeated analysis. All but the clonal population G2 30 of putative clones failed to re-establish and continue to proliferate at this stage. This may suggest that the clones that did not continue to proliferate were non-viable due to the successful knockout of hNEIL3, or that a non-target interaction yielded the same phenotype.

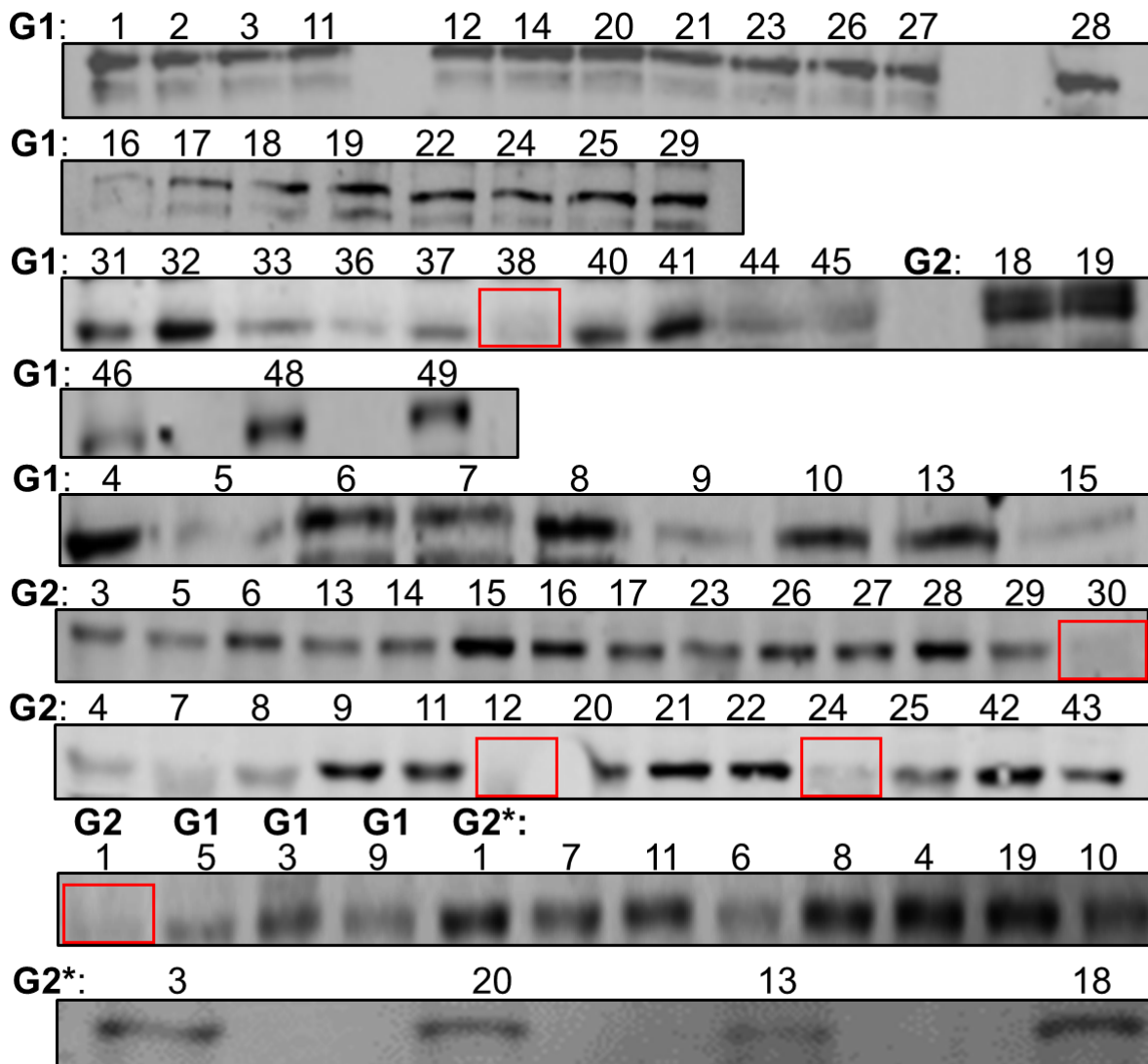


**Figure 5.12: Anti-NEIL3 immunoblot analysis of puromycin resistant U2OS cells.** “G1” denotes whole cell extracts from U2OS cells treated with gRNA sequence 1. “G2” denotes whole cell extracts from U2OS cells treated with gRNA sequence 2. “G2\*” Denotes gRNA 2 containing plasmid treated U2OS clonal populations which were upscaled for screening in a second round of screening.

Putative clonal population G2 30 successfully re-established, proliferated and was subsequently split 1: 2 at 70% confluence to a further 10 cm tissue culture dish and a T75 culture flask. At 70% confluency cells were harvested from the 10 cm tissue culture dish and WCE was prepared as described in 2.25 for analysis by western blot comparably to WT U2OS WCE. **Figure 5.13** shows significantly reduced hNEIL3 in 20  $\mu$ g WCE when compared to WT U2OS WCE, providing further evidence for successful Cas9/gRNA knockout and integration of the donor sequence at the site of the hNEIL3 gene sequence. Minor background smearing can be observed in the G2 30 clonal population WCE sample, which may indicate that the clonal population is a partial knockout rather than a complete gene knockout of hNEIL3 or that the NEIL3 antibody has cross reactivity with other proteins at a similar molecular weight. The T75

flask containing G2 C30 clonal cellular population was subsequently upscaled and processed for long term storage in liquid nitrogen, for further characterisation in the future.

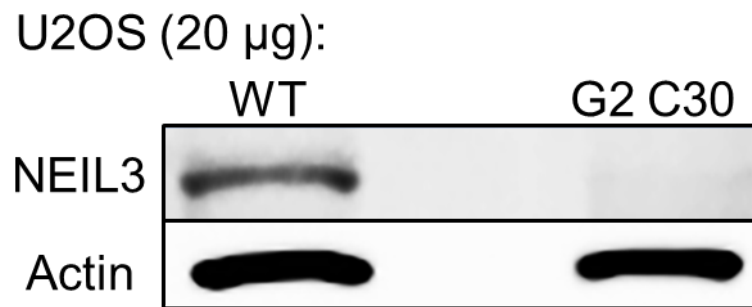


**Figure 5.13: Immunoblot analysis of the U2OS cell G2 30 clone.** “WT” denotes whole cell extracts from wild type and non-treated U2OS cells. “G2” denotes whole cell extracts from U2OS cells treated with gRNA sequence 2.

## 5.2. Discussion: Characterisation of post-translational modification of hNEIL3 by the ubiquitin proteasome system.

In the present study, it was investigated if hNEIL3 was also regulated by the ubiquitin PTM and the possible functional role in which this modification may play in the cellular response to DNA damage in U2OS cells. Previously generated HeLa cell fractions were subsequently analysed and characterised for the possession of E3 ubiquitin ligase activity in the presence of recombinant hNEIL3<sup>FL</sup>, through ubiquitination assays and anti hNEIL3 immunoblot analysis (**Figure 5.2; Figure 5.3; Figure 5.4; Figure 5.5**). Interestingly, the same fractions which facilitated E3 ubiquitin ligase activity and ubiquitination of NEIL1 and NTH1 were also observed to facilitate the ubiquitination of recombinant hNEIL3<sup>FL</sup>. It was identified that TRIM26 was the only candidate E3 ubiquitin ligase present within Mono Q 5/50 GL fraction 25, previously analysed by LC-MS (**Appendix Table 5**). Recombinant TRIM26 was then expressed from a pET28a-TRIM26 expression vector in the expression host Rosetta 2 (DE3) and subsequently purified by HisTrap HP affinity column FPLC. Purification fractions were confirmed for successful purification of TRIM26 by immunoblot analysis, pooled and concentrated for use *in vitro* ubiquitination assays (**Figure 5.6; Figure 5.7**). It was observed that TRIM26 facilitated mono-ubiquitination and polyubiquitination of hNEIL3<sup>FL</sup> (**Figure 5.7**).

TRIM26 RNAi in U2OS cells and analysis of WCE by immunoblot revealed that TRIM26 also regulated the steady state levels of NEIL3 (**Figure 5.9; Figure 5.10**). Furthermore, exposure of cells to H<sub>2</sub>O<sub>2</sub> and cisplatin demonstrated minor induction of NEIL3 in NT RNAi treated control cells, with NEIL3 protein levels remaining high after TRIM26 RNAi treatment (**Figure 5.9; Figure 5.10**).

It has been shown that the end processors, gap fillers and nick sealing enzymes of BER are regulated by the UPS system (Edmonds and Parsons, 2016). More recently it has been shown that the DNA glycosylases which initiate the BER pathway are also regulated by the UPS. NEIL1 was shown by Parsons' group to be ubiquitinated by the E3 ubiquitin ligases MULE and TRIM26. It was shown that both MULE and TRIM26 regulate protein stability in the cell while TRIM26 contributed to cellular resistance to IR in U2OS cells, however transient over expression of NEIL1 in U2OS cells did not compliment the observed phenotype. This said, MULE RNAi in U2OS cells demonstrated that induction of NEIL1 was MULE dependent

(Edmonds *et al.*, 2017). It is suggested that complementation by NEIL1 to TRIM26 RNAi induced IR is attributed to the multiple forms of DNA damage induced on exposure to IR, including SSB, DSBs and oxidative DNA damage and thus the multiple contributory DNA repair pathways that may be activated in the cellular response (Pouget *et al.*, 2002; Yoon *et al.*, 2010; Santivasi and Xia, 2014). It may be possible that other DNA repair proteins from BER and DSB repair pathways are also regulated by TRIM26, accounting for the observed resistance to IR (Edmonds *et al.*, 2017). However, the role of TRIM26 in the cellular response to oxidative DNA damaging agents and ICL inducing agents remained unclear.

Recently, Parsons's group showed that NTH1 was also regulated by TRIM26 *in vitro*. TRIM26 RNAi in HCT116 cells resulted in an increase in steady state protein levels and also an increase in chromatin bound NTH1. Furthermore, clonogenic cell survival assays demonstrated that TRIM26 RNAi resulted in cellular resistance to the oxidising agent H<sub>2</sub>O<sub>2</sub>, with the phenotype complemented by transient overexpression of NTH1. Taken together, it was proposed that TRIM26 is also an important regulator in the response to both oxidative DNA damage and IR (Edmonds *et al.*, 2017; Williams and Parsons, 2018).

As it was previously shown that hNEIL1 was induced in a MULE dependent manner in response to IR but hNEIL1 transient overexpression did not complement TRIM26 RNAi mediated cellular resistance to IR, the role of TRIM26 ubiquitination of hNEIL1 in response to cellular stress remained uncharacterised. Previous investigation revealed that hNEIL1 and hNEIL3 DNA glycosylases possess an innate ability to unhook psoralen MAs and ICLs in a three- and four-stranded DNA structure (Couvé-Privat *et al.*, 2007; Couvé *et al.*, 2009; Semlow *et al.*, 2016; Martin *et al.*, 2017). Furthermore, it has been shown that NEIL1 overexpression provides partial resistance in FA pathway deficient cell lines, to the ICL agents MMC and 8-MOP, while FA deficient cells display a reduction in hNEIL1 protein levels (Macé-Aimé *et al.*, 2010). In addition, MEFs from NEIL3<sup>-/-</sup> mice displayed increased sensitivity to the ICL agent cisplatin (Rolseth *et al.*, 2013). Taken together it was hypothesised that hNEIL1 and hNEIL3 regulation by TRIM26 may also modulate the cellular response to ICL inducing agent DNA damage. Subsequently, U2OS cisplatin clonogenic survival assays were undertaken and revealed that TRIM26 RNAi resulted in significant resistance to cisplatin ( $p = <2.2 \times 10^{-16}$ ), with significant resistance to cisplatin also observed after NEIL1 overexpression ( $p = <2.2 \times 10^{-16}$ ) and NEIL3 overexpression ( $p = <2.2 \times 10^{-16}$ ; **Figure 5.11**).

The findings presented here demonstrate the cellular role in which hNEIL1 and hNEIL3 play in cellular resistance to cisplatin. Taken together with previous biochemical findings that hNEIL1 and hNEIL3 may unhook psoralen ICLs it may be suggested they also play a role in cisplatin DNA damage repair, despite being suggested to be refractory to repair by *X. laevis* NEIL3 (Semlow *et al.*, 2017). Furthermore, it has been demonstrated that TRIM26 plays a role in the regulation of the cellular resistance to cisplatin in U2OS cancer cells. It is characterised that cancer cells display UPS dysfunction (Mansour, 2018). Thus, it is proposed that TRIM26 dysfunction in cancer cells may prove to be an important biomarker for the resistance of cancer cells to multiple types of therapeutic strategy including IR, ROS and ICL inducing agents (Yang *et al.*, 2009; Edmonds *et al.*, 2017; Williams and Parsons, 2018). This taken together with the previous observation that NEIL3 depletion sensitises glioblastoma cells to ATR and PARP inhibition, may indicate that TRIM26 status may provide insight into the resistance or sensitivity of cells to DDR inhibition (Klattenhoff *et al.*, 2017). MYC has been identified as one of the most frequently amplified oncogenes which may negatively regulate genes which promote proliferative arrest and upregulate those which promote cellular proliferation (Beroukhim *et al.*, 2010; Tusell *et al.*, 2010; Dang, 2012; Kress *et al.*, 2015). Furthermore, it has been shown that TRIM26 expression is induced by TGF- $\beta$  and negatively regulates cellular proliferation and TRIM26 transcription may be inhibited by MYC when cells experience persistent TGF- $\beta$  exposure (Nakagawa *et al.*, 2017). Indirect increase in steady state levels of NEIL1, NTH1 and NEIL3 as result of MYC dependent TRIM26 downregulation would facilitate significant cellular resistance to IR, H<sub>2</sub>O<sub>2</sub> and cisplatin (Edmonds *et al.*, 2017; Williams and Parsons, 2018). It would be interesting to determine the relationship between MYC protein levels and hNEIL1, hNEIL3 and NTH1 protein levels in dysfunctional cells, to elaborate on this dynamic association between MYC, TRIM26 and the BER pathway. Furthermore, TRIM26 has been highlighted as a tumour suppressor in hepatocellular carcinomas and cholangiocellular carcinomas, highly radio- and chemo-resistant cancer types (Wang *et al.*, 2015a). As previously discussed it has been shown in cancer cells that hNEIL3 depletion results in mitotic defects, with U2OS cells demonstrating increased recruitment to telomeric DNA sequences in response to oxidative DNA damage (Zhou *et al.*, 2017). Telomeric maintenance is an important mechanism within the cell as dysfunction may lead to the formation of telomere-dependent anaphase bridges which are a hallmark of genomic instability, promoting oncogenesis (Tusell *et al.*, 2010; Bizard and Hickson, 2018). Thus, it would be interesting to

observe the effect of TRIM26 upregulation on spontaneous genomic instability, through the formation of anaphase bridges and mitotic dysfunction complementing observations made on hNEIL3 RNAi (Zhou *et al.*, 2017). Together, these findings provide novel insight into possible mechanisms of oncogenesis and acquired therapeutic resistance in cancer cells displaying MYC overexpression. In addition, this may indicate that hNEIL1, hNEIL3 and NTH1 are biomarkers of therapeutic resistance in cancer cells displaying MYC overexpression.

## 6. Discussion.

In this study the role of the human endonuclease VIII like 1 and 3 (hNEIL1 and hNEIL3) DNA glycosylases in the removal of replication blocking lesions was explored. Previous studies have determined that hNEIL1 and hNEIL3 display increased expression levels in the S/G2M phases of the cell cycle, indicating a primary role in DNA replication (Hazra and Mitra, 2006; Neurauter *et al.*, 2012; Zhou *et al.*, 2015; Zhou *et al.*, 2017). Furthermore, the literature has revealed that hNEIL1 and hNEIL3 are immunoprecipitated on newly synthesised DNA, with hNEIL3 enriched with the replisome and hNEIL1 shown to interact with the DNA replication machinery components RPA, RFC and PCNA in a multiprotein complex, while hNEIL3 was also shown to co-localise with RPA (Moorland *et al.*, 2002; Theriot *et al.*, 2010; Hegde *et al.*, 2015; Bjørås *et al.*, 2017). RPA is recruited to DNA replication forks experiencing replication stress due to the stalling of the replicative machinery at replication blocking DNA lesions, subsequently inducing the DNA damage response sub-pathway the RSR, through ATR signalling (Nam and Cortez, 2011).

This evidence points to a possible role for these proteins within the replication stress response and DNA replication maintenance. Thus, providing rationale for the hypothesis that hNEIL1 and hNEIL3 may demonstrate distinct biochemical roles at a DNA replication fork, working in concert to maintain genomic stability prior to completion of mitosis and indeed, depletion of hNEIL3 in cancer cells has been shown to perpetuate mitotic defects including a significant increase in metaphase arrest (Zhou *et al.*, 2017). Therefore, the biochemical activity of recombinant hNEIL1 and hNEIL3 was characterised in the presence of a model DNA replication fork structure containing a 5-OHU, 8- OxoG and Tg. It was determined that 5-OHU and Tg are likely to be the most biologically relevant oxidative lesions processed by hNEIL1 and hNEIL3 (**Figure 3.3; Figure 3.4**). Furthermore, distinct differences for lesion processing was dependent on the location of the oxidative lesion at the DNA replication fork structure by hNEIL1 and hNEIL3. Interestingly, hNEIL1 and hNEIL3 display discriminatory associated AP-lyase activity based on the lesion type and lesion position within the DNA molecule. Furthermore, hNEIL3 displays robust cleavage of the Tg lesion within a DNA replication fork structure at all DNA lesion positions tested. In contrast, virtually no incision of Tg was

observed in linear ds-DNA, thus implying preference for the removal of the replication blocking lesion Tg in a DNA replication fork structure context.

The involvement of hNEIL1 in the maintenance of cellular resistance to DNA interstrand crosslinking agents was previously demonstrated (Couvé-Privat *et al.*, 2007; Couvé *et al.*, 2009; Macé-Aimé *et al.*, 2010; Martin *et al.*, 2017). Saparbaev's group provided initial biochemical evidence that hNEIL1 could process 8-MOP induced ds-DNA monoadducts providing the first evidence of BER proteins removing lesions generated by ICL agents (Couvé-Privat *et al.*, 2007). However, hNEIL1 did not remove ICLs in a conventional duplex structure (Couvé-Privat *et al.*, 2007). Subsequently, AAG was shown to provide a protective role against the ICL agents 8-MOP, BCNU and MMC demonstrated through the sensitivity of AAG<sup>-/-</sup> mouse embryonic stem cells to these agents (Maor-Shoshani *et al.*, 2008). However, analysis *in vitro* could not establish a direct biochemical role for AAG in the repair of ICLs (Maor-Shoshani *et al.*, 2008). hNEIL1 was then shown to unhook three-stranded oligonucleotide DNA structures containing an 8-MOP ICL, that mimicked the three-stranded intermediate generated through conventional FA replication associated or NER dependent ICL repair. Subsequently, overexpression of hNEIL1 in FA deficient cells was found to complement MMC and 8-MOP sensitivity (Couvé *et al.*, 2009; Macé-Aimé *et al.*, 2010). This demonstrated the cross-talk between BER and FA pathways for the first time. Rolseth *et al.* (2013) successfully generated NEIL3<sup>-/-</sup> mice and showed that their MEF cells displayed sensitivity to the ICL agent cisplatin. With the use of a *X. laevis* NEIL3 knockout egg extract model Semlow *et al.* (2016) revealed that *X. laevis* NEIL3 repaired psoralen induced ICL crosslinks and AP site ICLs in an X-shaped DNA structure, which represented convergent DNA replication forks. Furthermore, it was demonstrated that this repair was backed up by the FA pathway on the deficiency of NEIL3, thus indicating that NEIL3 dependent ICL resolution was the primary cellular response in *X. laevis* egg extracts, in this system. However, direct biochemical evidence for hNEIL3 ICL resolution was not addressed and the question remained whether hNEIL3 possessed overlapping structural affinity for psoralen ICLs with hNEIL1 in unhooking psoralen monoadducts and ICLs (Couvé-Privat *et al.*, 2007; Couvé *et al.*, 2009). Due to overlapping lesion preference and complementary structural affinity displayed in the presence of oxidative lesions within a DNA replication fork structure, it was hypothesised that hNEIL3 may play a complementary biochemical role to hNEIL1 in the presence of psoralen induced

monoadducts and ICLs. Thus, a panel of DNA substrates containing a site-specific psoralen induced ICL were generated and used as substrates for biochemical characterisation of hNEIL3 activity in the repair of ICLs.

Thus, it is reported here that hNEIL3 demonstrated unhooking activity on ss-DNA monoadducts, with hNEIL1 and hNEIL3 displaying complementary unhooking of three-stranded psoralen interstrand crosslinks, typical of the repair intermediates generated by the FA pathway and in agreement with Couvé *et al.* (2009). Interestingly, hNEIL1 demonstrated a bifunctional activity profile, conducting  $\beta,\delta$ -elimination of the phosphodiester backbone, while hNEIL3 proteins maintained a monofunctional profile and as result did not generate DNA breaks (Martin *et al.*, 2017). However, hNEIL3 displayed preference for long three-stranded psoralen ICL structures, unlikely to be produced through TLS and the conventional FA pathway of ICL repair (Sale *et al.*, 2012; Clauson *et al.*, 2013). This then raised the possibility that hNEIL1 and hNEIL3 activity was independent and distinct from the downstream processing and generation of repair intermediates by FA ICL repair and in agreement with the suggestions of pathway independent processing of ICLs by Semlow *et al.* (2016). Therefore, a four-stranded DNA oligonucleotide was constructed, containing a site-specific psoralen ICL and used as a substrate in these assays. Analysis revealed the ability of hNEIL1 and hNEIL3 proteins to unhook four-stranded ICL structures. Again, hNEIL1 displayed a bifunctional activity profile conducting  $\beta,\delta$ -elimination, while hNEIL3 displayed a monofunctional profile and again did not generate DNA breaks. A catalytically inactive recombinant mutant of hNEIL3<sup>Cat</sup> was generated and lacked unhooking activity on three- and four-stranded psoralen ICL substrates, indicating the genuine unhooking activity of hNEIL3. This provided further evidence for a NEIL-dependent psoralen ICL processing pathway, independent of the FA pathway and complementing previous findings (Semlow *et al.*, 2016).

Based on the work of Seidman's laboratory, a model was proposed which suggests that FANCM mediated replication traverse and the continuation of DNA replication would generate the model three- and four-stranded ICL oligonucleotide structures analysed here (Huang *et al.*, 2013). Interestingly, depletion of NEIL3 in cancer cells has been showed to promote genetic instability through mitotic dysfunction and chromosomal aberration (Zhou *et al.*, 2017). The model proposed here would suggest that hNEIL1 and hNEIL3 post-replicative repair of four-stranded DNA structures proceeds after FANCM facilitated ICL traverse, to

facilitate the separation of daughter chromatids during the metaphase stage of the cell cycle (Huang *et al.*, 2013; Rohleder *et al.*, 2016). In agreement with this depletion of hNEIL3 was shown to result in a significant increase in chromatin bridges and an increase in metaphase arrest, suggested to be the result of the failure to resolve chromosomal linkages (Zhou *et al.*, 2017). In addition, FANCM was shown to colocalise at chromatin bridges and deficiency in FA pathway proteins is characterised to promote genetic instability with increased observations of chromatin bridging (Chan and Hickson, 2011; Tusell *et al.*, 2010; Bizard and Hickson, 2018). Therefore, it is proposed that hNEIL1 and hNEIL3 DNA glycosylases play fundamental roles in the maintenance of genomic stability in association with DNA replication. These roles may be exploited in cancer cells to maintain proliferative capacity, in turn evading significant activation through the generation of DNA breaks associated with the FA pathway and thus possible cell cycle arrest and apoptosis on DNA replication fork collapse. In addition, the finding that *X. laevis* NEIL3 may resolve AP site ICLs and observations of the activation of the FA pathway in the presence of endogenous aldehydes, provides rationale for the evolution of distinct ICL repair mechanisms (Sczepanski *et al.*, 2008; Macé-Aimé *et al.*, 2010; Garaycochea *et al.*, 2012; Pontel *et al.*, 2015; Semlow *et al.*, 2016). Furthermore, it appears that the observed ds-DNA-MA and three-stranded psoralen ICL unhooking activity is an evolutionary conserved activity within the Fpg/Nei family of DNA glycosylases. This indicates that the resolution of endogenous ICLs in both prokaryotes and higher eukaryotic organisms is required for genomic stability (Couvé-Privat *et al.*, 2007; Couvé *et al.*, 2009).

Previous investigation by the Parsons' group determined PTM regulation of hNEIL1 by the E3 ubiquitin ligases MULE and TRIM26 (Edmonds *et al.*, 2017). MULE has previously been shown to interact and ubiquitinate the tumour suppressor p53 and is involved in ATR signalling modulation (Chen *et al.*, 2005). This link to ATR signalling through MULE may further implicate hNEIL1 in the RSR. In addition, TRIM26 is suggested to promote proliferative arrest within the cell and has been identified as a possible tumour suppressor in some forms of cancer (Nakagawa *et al.*, 2017). It was shown that the oncogene MYC inhibits the transcription of TRIM26 and was suggested to be a mechanism of the evasion of proliferative arrest, a Hallmark of Cancer (Wang *et al.*, 2015; Nakagawa *et al.*, 2017). In addition, TRIM26 down regulation was observed to induce resistance to IR and oxidative DNA damage by H<sub>2</sub>O<sub>2</sub>, with the latter being complemented by NTH1 overexpression (Edmonds *et al.*, 2017; Williams and

Parsons, 2018). The present investigation revealed that hNEIL3 steady state levels are also regulated by the E3 ubiquitin ligase TRIM26 in U2OS cells. It was then hypothesised that hNEIL1 and hNEIL3 were ubiquitinated by TRIM26 to modulate the cellular response to ICL agents based on the previously observed complementary ICL unhooking activity (Martin *et al.*, 2017). Subsequently, it was observed that hNEIL1 and hNEIL3 over expression complemented the cisplatin resistance observed after TRIM26 RNAi in U2OS cells thus providing further cellular evidence that hNEIL1 and hNEIL3 play a role in the resistance to ICL agents *in vivo* and are modulated by TRIM26 through the UPS. However, the biochemical mechanism of hNEIL1 and hNEIL3 DNA glycosylases in the presence of cisplatin ICLs has yet to be established. Semlow *et al.* (2016) demonstrated that the cisplatin ICL was refractory to repair by the NEIL3 DNA glycosylase in an *X. laevis* egg extract cell free system. This may indicate that the involvement of hNEIL1 and hNEIL3 in the cellular resistance to cisplatin ICLs may be due to an associated secondary function or recruitment of interacting proteins. To elucidate these functions would require the identification of protein partners coimmunoprecipitated from cisplatin treated cells which demonstrate both the upregulation of the NEIL DNA glycosylases and resistance to cisplatin. The sequential reconstitution of proteins in these complexes, in the presence of a cisplatin treated oligonucleotide substrate, may enable the identification of the distinct roles of hNEIL1, hNEIL3 and identified protein partners in the biochemical mechanisms behind cellular resistance to cisplatin treatment in this context.

However, it is tempting to propose a model which links the MYC transcription factor with regulation of the NTH1, hNEIL1 and hNEIL3 DNA glycosylases through TRIM26. In healthy cells TGF- $\beta$  may stimulate the transcription of TRIM26, inducing proliferative arrest and upregulating UPS mediated degradation of the NTH1, hNEIL1 and hNEIL3 DNA glycosylases (Edmonds *et al.*, 2017; Nakagawa *et al.*, 2017; Williams and Parsons, 2018). In dysfunctional cells, overexpression of MYC may inhibit TRIM26 transcription facilitating the continuation of proliferation and increase in the steady state levels of the NTH1, hNEIL1 and hNEIL3 DNA glycosylases (Nakagawa *et al.*, 2017). The latter example is mimicked by TRIM26 RNAi and is presented here (**Figure 5.8; Figure 5.9; Figure 5.10; Figure 5.11**). As a result, TRIM26 downregulation may lead to the acquisition of cellular resistance in cancer cells to IR, H<sub>2</sub>O<sub>2</sub> and cisplatin, in part due to the increase in steady state levels of the NTH1, NEIL1 and NEIL3

DNA glycosylases (Edmonds *et al.*, 2017; Williams and Parsons, 2018). This is in agreement with a previous study that showed that MYC transgenic mice displayed increased cDNA expression levels of NTH1, OGG1, as well as proteins involved in NER and DSB repair, with the observation of a reduction in oxidative DNA damage (Hironaka *et al.*, 2003). Interestingly, MYC has also been shown to regulate the Ras dependent ERK-MAP kinase signalling pathway which can promote oncogenesis if dysregulated (Gramling and Eischen, 2012). In agreement with this, hNEIL3 DNA glycosylase expression has been shown to be induced by the Ras dependent ERK-MAP kinase pathway (Neurauter *et al.*, 2012). This putative link between MYC and the BER pathway in cellular resistance within dysfunctional cells, requires further investigation, but may provide insight into the dysregulation of DNA glycosylases and resistance to therapeutic intervention within cancer (Shinmura *et al.*, 2016).

However, as hNEIL1 induction was shown to be dependent on the MULE E3 ubiquitin ligase in response to IR, it is essential to elucidate the mechanism in which hNEIL1 and hNEIL3 are induced in response to cisplatin (Edmonds *et al.*, 2017). This may help establish the distinct signalling pathways that regulate the induction of DNA glycosylases in response to specific types of DNA damage. Furthermore, an important line of enquiry, is the identification of the distinct structural similarities shared between the DNA glycosylases hNEIL1, hNEIL3 and NTH1 which enable them to be recognised by TRIM26. This in turn may aid in the development of novel biological agents such as proteolysis targeting chimeras (PROTACs) for the targeted ubiquitination of hNEIL1, hNEIL3 and NTH1, thus reducing cellular resistance in UPS dysfunctional cells (Bondeson and Crews, 2017; Cromm and Crews, 2017).

## 7. Conclusion and Future Perspectives.

The findings of this study underline hNEIL1, hNEIL3 and TRIM26 as markers of cellular resistance to ICL inducing agent therapeutics. Initially, the biochemical role of hNEIL1 and hNEIL3 in the repair of oxidative DNA lesions was explored and confirmed a preference for the DNA replication blocking lesion Tg in a model DNA replication fork structure by hNEIL3<sup>FL</sup>. Furthermore, the biochemical activity of hNEIL1 and hNEIL3 DNA glycosylases in the unhooking of an ICL from three- and four-stranded structures was revealed (Martin *et al.*, 2017). Additionally, TRIM26 was shown to ubiquitinate recombinant hNEIL3<sup>FL</sup> *in vitro*, with confirmation that steady state levels of hNEIL1 and hNEIL3 are modulated by TRIM26 in U2OS cells. Furthermore, TRIM26, hNEIL1 and hNEIL3 were implicated in the cellular response to the ICL inducing agent cisplatin. Taken together, the replication associated functions of hNEIL1 and hNEIL3 were confirmed, in agreement with the literature. It is suggested that hNEIL1 and hNEIL3 in collaboration with NTH1 provide a robust and complementary mechanisms for the removal of oxidative damage. In addition, hNEIL1 and hNEIL3 display distinct structural preferences, which may indicate non-canonical roles within the maintenance of genomic stability in association with DNA replication, akin to structure specific endonucleases (Martin *et al.*, 2017).

Depletion of hNEIL3 in cancer cells results in a significant increase in anaphase bridges, instability and also a significant increase in metaphase arrest (Zhou *et al.*, 2017). Taken together with biochemical data, a model is proposed in which long three- and four-stranded DNA ICL structures may be produced *in vivo*, involving the DNA translocase activity of FANCM (Huang *et al.*, 2013, Rohleder *et al.*, 2016). On persistence of these four stranded structures, representing crosslinked daughter chromatids, metaphase is likely to arrest due to the inability to separate the two DNA duplex, in agreement with Zhou *et al.* (2017). It is proposed that this mechanism may be modulated by MYC overexpression and TRIM26 dysfunction within cells, promoting cellular resistance to ICL inducing agents and increased proliferative capacity (Nakagawa *et al.*, 2017). Therefore, this study may provide insights into the mechanisms of acquired cellular resistance in cancer cells through TRIM26, hNEIL1 and hNEIL3. It will be important to establish the relationship between MYC expression levels and the hNEIL1, hNEIL3 and NTH1 DNA glycosylase expression levels in human malignant tumours

to elaborate on this proposed mechanism of acquired resistance through TRIM26 transcription inhibition.

The findings of this study provide motive for the therapeutic targeting of this mechanism in dysfunctional cancer cells, displaying upregulation of hNEIL1 or hNEIL3 and downregulation of TRIM26. Indeed, depletion of hNEIL3 has been shown to significantly improve the efficacy of ATR and PARP inhibitors in highly resistant glioblastoma cells, indicating a protective role within the response to replication stress and prevention of DNA strand breaks (Klattenhoff *et al.*, 2017). hNEIL3 depletion also sensitises HCT116 cells to oxaliplatin and NEIL3 knockout sensitises MEFs to cisplatin, while the findings of this study provide biochemical mechanistic rationale and indicate significant resistance of cancer cells to cisplatin in a hNEIL1 and hNEIL3 dependent manner (Rolseth *et al.*, 2013; Taylor *et al.*, 2015). The establishment of a CRISPR/Cas9 hNEIL3 knockout in the U2OS cancer cell line, will provides a model system for the further study of sensitisation to crosslinking agents through ICL inducing agent treatment and cell viability assays. In addition, providing a model in which the contribution of hNEIL3 to cisplatin resistance in TRIM26 siRNA treated U2OS cells may be confirmed.

The lack of a mutagenic phenotype in NEIL DNA glycosylase deficient mice and the restricted expression of hNEIL3 in normal cells, provides strong motivation for the therapeutic targeting of the NEIL DNA glycosylases in the treatment of cancer, while minimising the detrimental impact on healthy cells (Morland *et al.*, 2002; Torisu *et al.*, 2005; Hildrestrand *et al.*, 2009; Rolseth *et al.*, 2013; Taylor *et al.*, 2015; Klattenhoff *et al.*, 2017; Rolseth *et al.*, 2017; Zhou *et al.*, 2017). Therefore, the data presented here provides further evidence for the clinical relevance of the hNEIL1 and hNEIL3 DNA glycosylases as important biomarkers of resistance and therapeutic targets for the treatment of cancer.

**References.**

- Aizawa, K., Liu, C., Tang, S. *et al.* (2016) Tobacco carcinogen induces both lung cancer and non-alcoholic steatohepatitis and hepatocellular carcinomas in ferrets which can be attenuated by lycopene supplementation. *International Journal of Cancer*, **139**, 1171-1181.
- Aller, P., Rould, M. A., Hogg, M., Wallace, S. S. & Doubl  . (2007) A structural rationale for stralling of a replicative DNA DNA polymerase at the most common oxidative thymine lesion thymine glycol. *Proceedings of the National Academy for Sciences of the U.S.A.*, **104**, 814-818.
- Allton, K., Jain, A. K., Herz, H.M. *et al.* (2009) Trim24 targets endogenous p53 for degradation. *Proceedings of the National Academy for Sciences of the U.S.A.*, **106**, 11612–11616.
- Almeida, K.H. & Sobol, R.W. (2007) A unified view of BER: lesion dependent protein complexes regulated by post-translational modification, *DNA Repair (Amst.)*, **6**, 695–711
- Ameziane, N., May, P., Haitjema, A. *et al.* (2015) A novel Fanconi anaemia subtype associated with a dominant-negative mutation in RAD51. *Nature Communications*. **6**, 8829.
- Anderson, D. & Krummen, L. (2002) Recombinant protein expression for therapeutic applications. *Current Opinion in Biotechnology*, **13**,117-123.
- Andreassen, P. R., D’Andre, A. D. & Taniguchi, T. (2004) ATR couples FANCD2 monoubiquitination to the DNA-damage response. *Genes & Development*, **18**, 1958–1963.
- Angers, S., Li, T., Yi, X., MacCoss, M.J., Moon, R.T., & Zheng, N. (2006) Molecular architecture and assembly of the DDB1–CUL4A ubiquitin ligase machinery. *Nature*. **443**, 590–593.
- Ayala, A., Mu  oz, M. & Arg  elles, S. (2014) Lipid peroxidation: Production, Metabolism, and Signalling Mechanisms of Malondialdehyde and 4-Hydroxy-2-Nonenal. *Oxidative Medicine and Cellular Longevity*, **2014**, 1-31.
- Balakrishnan, L. & Bambara, R. (2013) Flap endonuclease 1. *Annual Review of Biochemistry*, **82**, 119-138.
- Bandaru, V., Sunkara, S., Wallace, S. & Bond, J.P. (2002) A novel human DNA glycosylase that removes oxidative damage and is homologous to *Escherichia coli* endonuclease VIII. *DNA Repair*, **1**, 517-529.
- Barzilai, A., Rotman, G., & Shiloh, Y. (2002) ATM deficiency and oxidative stress: a new dimension of defective response to DNA damage. *DNA Repair (Amst.)*, **1**, 3–25.
- Bastia, D., Zzaman, S., Krings, G., Saxena, M., Peng, X. *et al.* (2008) Replication termination mechanism as revealed y Tus-mediated polar arrest of a sliding helicase. *Proceeding of the National Academy of Sciences of the United States of America*, **105**, 12831-12836.

- Bell, J., Malyukova, A., Holien, J. K. *et al.* (2012) TRIM16 acts as an E3 ubiquitin ligase and can heterodimerize with other TRIM family members. *PLoS One*, **7**, e37470.
- Beltran, H., Prandi, D. Mosquera, J.M. *et al.* (2016) devertgent clonal evolution of castration-resistant neuroendocrine prostate cancer. *Nature Medicine*, **22**, 298-305.
- Beroukhim, R., Mermel, C, H. Porter, D. *et al.* (2010) The landscape of somatic copy-number alteration across human cancers. *Nature*, **463**, 899-905.
- Bessho, T., Roy, R., Yamamoto, K. *et al.* (1993) Repair of 8-hydroxyguanine in DNA by mammalian N-methylpurine-DNA-glycosylase. *Proceedings of the National Academy of Sciences of the U.S.A*, **90**, 8901-8904.
- Bhagwat, M. & Gerlt, J. A. (1996) 3'- and 5'-strand cleavage reactions catalyzed by the Fpg protein from *Escherichia coli* occur via successive beta- and delta-elimination mechanisms, respectively. *Biochemistry*, **35**, 659-665.
- Bhakat, K. K., Hazra, T. K. & Mitra, S. (2004) Acetylation of the human DNA glycosylase NEIL2 and inhibition of its activity. *Nucleic Acids Research*, **32**, 3033-3039.
- Bhattacharjee, S. & Nandi, S. (2017) DNA damage response and cancer therapeutics through the lens of the Fanconi Anemia DNA repair pathway. *Cell. Commun. Signal*, **15**, 41.
- Bishop, A. J. R. & Schiestl, R. H. (2002) Homologous Recombination and Its Role in Carcinogenesis. *Journal of Biomedicine and Biotechnology*, **2**, 75-85.
- Bizard, A. H. & Hickson, I. D. (2018) Anaphase: a fortune-teller of genomic instability. *Current Opinion in Cell Biology*, **52**, 112-119.
- Bjørås, K. A., Sousa, M. M. L., Sharma, A. *et al.* (2017) Monitoring of the spatial and temporal dynamics of BER/SSBR pathway proteins, including MYG, UNG2, MPG, NTH1 and NEIL1-3, during DNA replication. *Nucleic Acids Research*, **45**, 8291-8301.
- Blaisdell, J. O., Hatahet, Z. & Wallace, S. S. (1999) A novel role for *Escherichia coli* endonuclease VIII in the prevention of spontaneous G-T transversions. *Journal of Bacteriology*, **181**, 6396-6402.
- Boiteux, S. & Radicella, J. (2000) The Human *OGG1* Gene: Structure, Functions, and Its Implication in the Process of Carcinogenesis. *Archives of Biochemistry and Biophysics*, **377**, 1-8.
- Boiteux, S., Gajewski, E., Laval, J., Dizdaroglu, M. (1992) Substrate specificity of the *Escherichia coli* Fpg protein (formamidopyrimidine-DNA glycosylase): excision of purine lesions in DNA produced by ionizing radiation or photosensitization. *Biochemistry*, **31**, 106-110.
- Bondeson, D. P. & Crews, C. M. (2017) Targeted Protein Degradation by Small Molecules. *Annual Review of Pharmacology and Toxicology*, **57**, 107-123.
- Boos, D., Frigola, J. & Diffley, J. F. (2012) Activation of the replicative DNA helicase: breaking up is hard to Do. *Current Opinions in Cell Biology*, **24**, 423-430.

- Borlepawar, A., Rangrez, A. Y., Bernt, A. *et al.* (2017) TRIM24 protein promotes and TRIM32 protein inhibits cardiomyocyte hypertrophy via regulation of dysbindin protein levels. *Journal of Biological Chemistry*, **292**, 10180–10196.
- Braselmann, H., Michna, A., Heb, & Unger, K. (2015) CFAssay: statistical analysis of the colony formation assay. *Radiation Oncology*, **10**, 223.
- Brookes, P. & Lawley, P. D. (1960) The reaction of mustard gas with nucleic acids *in vitro* and *in vivo*. *Biochemical Journal*, **77**, 478-484.
- Brookes, P. & Lawley, P. D. (1964) Evidence for the Binding of Polynuclear Aromatic Hydrocarbons to the Nucleic Acids of Mouse Skin: Relation Between Carcinogenic Power of Hydrocarbons and their Binding to Deoxyribonucleic Acid. *Nature*, **202**, 781-784.
- Brooks, P. J. & Zahkari, S. (2003) Acetaldehyde and the genome: Beyond nuclear DNA adducts and carcinogenesis. *Journal of the American Chemical Society*, **125**, 50-61.
- Brown, T. (2010) *Gene Cloning & DNA Analysis: An Introduction*. Wiley-Blackwell, Oxford.
- Budzowska, M., Graham, T. G., Sobeck, A., Waga, S. & Walter, J. C. Regulation of the Rev<sup>1</sup>-pol zeta complex during bypass of a DNA interstrand cross-link. *The EMBO Journal*, **34**, 1971-1985.
- Busso, C.S., Iwakuma, T. & Izumi, T. (2009) Ubiquitination of mammalian AP endonuclease (APE1) regulated by the p53-MDM2 signalling pathway. *Oncogene*, **28**, 1616–1625.
- Byun, T. S., Pacek, M., Yee, M., Walter, J. C. & Cimprich, K. A. (2005) Functional uncoupling of MCM helicase and DNA DNA polymerase activities activates the ATR-dependent checkpoint. *Genes & Development*, **19**, 1040-1052.
- Cadet, J. & Wagner, J. R. (2013) DNA Base Damage by Reactive Oxygen Species, Oxidizing Agents, and UV Radiation. *Cold Spring Harbour Perspectives in Biology*, **5**, a012559.
- Cancer Research UK. (2015) Cancer statistics for the UK, <https://www.cancerresearchuk.org/health-professional/cancer-statistics-for-the-uk> [Accessed 25 August, 2018].
- Cancer Research UK. (2016) Cancer statistics for the UK, <https://www.cancerresearchuk.org/health-professional/cancer-statistics-for-the-uk> [Accessed 25 August, 2018].
- Cantoni, O., Murray, D., Meyn, R.E. (1987) Induction and repair of DNA single-strand breaks in EM9 mutant CHO cells treated with hydrogen-peroxide. *Chem.-Biol. Interact*, **63**, 29–38.
- Carter, R. J. & Parsons, J. L. (2016) Base Excision Repair, a Pathway Regulated by Posttranslational Modifications. *Mol. Cell. Biol*, **36**, 1426-1437.
- Chakraborty, A., Wakamiya, M., Venkoca-Canova, T. *et al.* (2015) *Neil2*-null Mice Accumulate Oxidized DNA Bases in the Transcriptionally Active Sequences of the Genome and are Susceptible to Innate Inflammation. *Journal of Biological Chemistry*, **250**, 24636-24648.

- Chan, K. L. & Hickson, I. D. (2011) New insights into the formation and resolution of ultra-fine anaphase bridges. *Seminars in cell & Developmental Biology*, **22**, 906-912.
- Chanoux, R. A., Yin, B., Urtishak, K. A., Asare, A., Bassing, C. H. *et al.* (2009) ATR and H2AX cooperate in maintaining genome stability under replication stress. *J. Biol. Chem.* **284**, 5994–6003.
- Cheadle, J. & Sampson, J. (2007) MUTYH- associated polyposis- From defect in BER to clinical genetic testing. *DNA Repair*, **6**, 274-279.
- Chen, D., Kon, N., Li, M., Zhang, W., Qin, J., & Gu, W. (2005) ARF-BP1/Mule is a critical mediator of the ARF tumour suppressor. *Cell*, **121**, 1071–1083.
- Chen, J. & Chen, Z. J. (2013) Regulation of NF-KappaB by ubiquitination. *Current opinions in immunology*, **25**, 4-12.
- Chen, X. B., Melchionna, R. Denis, C. M. *et al.* (2001) Human Mus81- associated endonuclease cleaves Holliday junctions *in vitro*. *Mol. Cell*, **8**, 1117-1127.
- Chen, Z. J., & Sun, L. J. (2009) Nonproteolytic functions of ubiquitin in cell signalling. *Mol. Cell*, **33**, 275–286
- Chetsanga, C.J. & Lindahl, T. (1979) Release of 7-methylguanine residues whose imidazole rings have been opened from damaged DNA by a DNA glycosylase from *Escherichia coli*. *Nucleic Acids Res*, **6**, 3673–3684.
- Cheung, R. S. & Taniguchi, T. (2017) recent insight into the molecular basis of Fanconi anemia: genes, modifiers, and drivers. *International Journal of Haematology*, **106**, 335-344.
- Cho, Y. J., Wang, H., Kozekov, I. D. *et al.* (2006) Stereospecific formation of interstrand carbinolamine DNA cross-links by crotonaldehyde and acetaldehyde-derived alpha-CH3-gamma-OH-1,N2,propano2'-deoxyguanosine adducts in the 5 'CpG-3' sequence. *Chemical Research in Toxicology*, **19**, 195-208.
- Chou, W., Wang, H., Wong, F. *et al.* (2008) Chk2-depenent phosphorylation of XRCC1 in the DNA damage reponse promotes BER. *The EMBO Journal*, **27**, 3140-3150.
- Christensen, D. E., Brzovic, P. S. & Klevit, R. E. (2007) E2-BRCA1 RING interactions dictate synthesis of mono- or specific polyubiquitin chain linkages. *Nat. Struct. Mol. Biol*, **14**, 941-948.
- Christie, N.T., Cantoni, O., Evans R.M., Meyn, R.E. & Costa, M. (1984) Use of mammalian DNA repair-deficient mutants to assess the effects of toxic metal compounds on DNA, *Biochem. Pharmacol*, **33**, 1661–1670.
- Christmann, M., Verbeek, B., Roos, W. P. & Kaina, B. (2011) O(6)-Methylguanine-DNA methyltransferase (MGMT) in normal tissues and tumours: enzyme activity, promoter methylation and immunohistochemistry. *Biochimica et biophysica acta*, **1816**, 179-190.
- Churchill, M.E., Peak, J.G. & Peak, M.J. (1991) Correlation between cell-survival and DNA single-strand break repair proficiency in the Chinese hamster ovary cell-lines aa8 and EM9 irradiated with 365-nm ultraviolet—a radiation. *Photochem. Photobiol*, **53**, 229–236.

- Ciccia, A. & Elledge, S. (2010) The DNA Damage Response: Making It Safe to Play with Knives. *Molecular Cell*, **40**, 179-204.
- Cipak, L., Watanabe, N. & Bessho, T. (2006) The role of BRCA2 in replication-coupled DNA interstrand cross-link repair *in vitro*. *Nature structural & molecular biology*, **18**, 729-733.
- Clauson, C., Schärer, O. D. & Niedernhofer, L. (2013) Advances in Understanding the Complex Mechanisms of DNA Interstrand Cross-Link Repair. *Cold Spring Harbour Perspectives in Biology*, **5**, 1-25.
- Cohen, P., & Tcherpakov, M. (2010) Will the Ubiquitin System Furnish as Many Drug Targets as Protein Kinases? *Cell*, **143**, 686–693.
- Collins, G. A. & Goldberg, A. K. (2017) The Logic of the 26S Proteasome. *Cell*, **169**, 792-806.
- Compe, E. & Egly, J. M. (2012) TFIIH: When transcription met DNA repair. *Nature Reviews*, **13**, 343-354.
- Compe, E. & Egly, J. M. (2012) TFIIH: when transcription met DNA repair. *Nature Reviews Molecular Cell Biology*, **13**, 343-345.
- Cortez, D. (2015) Preventing Replication Fork Collapse to Maintain Genome Integrity. *DNA Repair*, **32**, 149-157.
- Couvé, S., Macé-Aimé, G., Rosselli, F. & Sapparbaev, M. (2009) The Human Oxidative DNA Glycosylase NEIL1 Excises Psoralen-induced Interstrand DNA Cross-links in a Three-stranded DNA Structure. *The Journal of Biological Chemistry*, **284**, 11963-11970.
- Couvé-Privat, S., Gaëtane, M., Rosselli, F. & Sapparbaev, M. (2007) Psoralen-induced DNA adducts are substrates for the BER pathway in human cells. *Nucleic Acids Research*, **17**, 5672-5682.
- Cromm, P. M. & Crews, C. M. (2017) Targeted Protein Degradation: from Chemical Biology to Drug Discovery. *Cell Chemical Biology*, **24**, 1181-1190.
- Dang, C. V. (2012) MYC on the path to cancer. *Cell*, **149**, 22-35.
- Danielsen, J.M., Sylvestersen, K.B., Bekker-Jensen, S. *et al.* (2011) Mass spectrometric analysis of lysine ubiquitylation reveals promiscuity at site level. *Mol. Cell. Proteomics*, **10**, M110.003590.
- Das, A., Boldogh, I., Lee, J. W. *et al.* (2007) The Human Werner Syndrome Protein Stimulates Repair of Oxidative DNA Base Damage by the DNA Glycosylase NEIL1. *The Journal of Biological Chemistry*, **282**, 26591-26602.
- Das, A., Rajagopalan, L. Mathura, V. S., Rigby, S. J., Mitra, S. & Hazra, T. K. (2004) Identification of a Zinc Finger Domain in the Human NEIL2 (Nei-like-2) Protein. *The Journal of Biological Chemistry*, **279**, 47132-47138.
- de Silva, I. U., McHugh, P. J., Clingen, P. H. & Hartley, J. A. (2000) Defining the roles of nucleotide excision repair and recombination in repair of DNA interstrand cross-links in mammalian cell. *Molecular Cell Biology*, **20**, 7980-7990.

- de Sousa, J. F., Torrieri, R., Serafim, R. B. *et al.* (2017) Expression signature of DNA repair genes correlate with survival prognosis of astrocytoma patients. *Tumour Biology*, **39**, 1-11.
- de Waard, H, de Wit, J., Andressoo, J. *et al.* (2004) Different Effects of CSA and CSB deficiency on Sensitivity to oxidative DNA Damage. *Molecular and Cellular Biology*, **24**, 7941-7948.
- Deans, J. & West, S. (2011) DNA interstrand crosslink repair and cancer. *Nature Reviews*, **11**, 467-480.
- Desai, N.A. & Shankar, V. (2003) Single-strand-specific nucleases. *FEMS Microbiology Reviews*, **26**, 457-491.
- Dianov, G., Bischoff, C., Sunesen, M & Bohr, V. A. (1999) Repair of 8-oxoguanine in DNA is deficient in Cockayne syndrome group B cells. *Nucleic Acids Research*, **27**, 1365-1368.
- Dorn, J., Ferrari, E., Imhof, R., Ziegler, N., & Hubscher, U. (2014) Regulation of human MutYH DNA glycosylase by the E3 ubiquitin ligase Mule. *J. Biol. Chem*, **289**, 7049–7058.
- Dou, H., Mitra, S. & Hazra, T. K. (2003) Repair of Oxidized Bases in DNA Bubble Structures by Human DNA glycosylases NEIL1 and NEIL2. *Journal of Biological Chemistry*, **278**, 49679-49684.
- Douwel, K., Boonen, R. A. C. M, Long, D. T. *et al.* (2014) ERCC1-XPF acts in unhooking DNA interstrand crosslinks in cooperation with FANCD2 and FANCP/SLX4. *Mol. Cell*, **54**, 460-471.
- Douwel, K., Hoogenboom, W. S., Boonen, R. A. C. M. & Knipscheer, P. (2017) Recruitment and positioning determine the specific role of the ERCC1-XPF endonuclease in interstrand crosslink repair. *The EMBO Journal*, **36**, 2034-2046.
- Dronkert, M. & Kanaar, R. (2001) Repair of DNA interstrand cross-links. *DNA Repair*, **486**, 217-247.
- Duncan, T., Trewick, S. C., Koivisto, P., Bates, P. A., Lindahl, T. & Sedgwick. (2002) Reversal of DNA alkylation damage by two human dioxygenases. *Proceedings of the National Academy of Sciences of the U.S.A*, **99**, 16660-16665.
- Dutta, S., Chowdhury, G. & Gates, K. S. (2006) Interstrand Cross-Links Generated by Abasic Sites in Duplex DNA. *Journal of The American Chemical Society*, **129**, 1852-1853.
- Duxin, J. P. & Walter, J. C. (2015) What is the DNA repair defect underlying Fanconi anemia? *Current Opinion in Cell Biology*, **37**, 49-60.
- Edmonds, M. J. & Parsons, J. L. (2016) Regulation of BER proteins by ubiquitylation. *Experimental Cell Research*, **329**, 132-138.
- Edmonds, M. J., Carter, R.J., Nickson, C.M., Williams, S.C., Parsons, J.L., (2017) Ubiquitylation-dependent regulation of NEIL1 by Mule and TRIM26 is required for the cellular DNA damage response. *Nucleic Acids Res*, **45**, 726-738.

- Elder, R. H., Jansen, J. G., Weeks, R. J. *et al.* (1998) Alkylpurine-DNA-N- Glycosylase Knockout Mice Show Increased Susceptibility to Induction of Mutations by Methyl Methanesulfonate. *Molecular and Cellular Biology*, **18**, 5828-5837.
- Elledge, S. (2015) The DNA Damage response- self-awareness for DNA. *American Medical Association*, **314**, 1111-1112.
- Engelward, B. P., Dreslin, A., Christensen, J., Huszar, D. & Samson, L. D. (1996) Repair-deficient 3-methyladenine DNA glycosylase homozygous mutant mouse cells have increased sensitivity to alkylation-induced chromosome damage and cell killing. *The EMBO Journal*, **15**, 945-952.
- Engelward, B. P., Weeda, G., Wyatt, M. D. *et al.* (1997) Base excision repair deficient mice lacking the Aag alkylation DNA glycosylase. *Proceeding of the National Academy of Sciences of the U.S.A*, **94**, 13087-13092.
- Enoiu, M., Jiricny, J. & Schärer, O. D. (2012) Repair of cisplatin-induced DNA interstrand crosslinks by a replication-independent pathway involving transcription-coupled repair and translesion synthesis. *Nucleic Acids Research*, **40**, 8953-8964.
- Esposito, D., Kolipoulos, M. G. & Rittinger, K. (2017) Structural determinants of TRIM protein function. *Biochemical Society Transactions*, **45**, 183-191.
- Esteller, M., Garcia-Foncillas, J., Andion, E. *et al.* (2000) Inactivation of the DNA-repair gene MGMT and the clinical response of gliomas to alkylating agents. *New England Journal of Medicine*, **343**, 1350-1354.
- Fagbemi, A. F., Orelli, B., Scharer, O. D. (2011) Regulation of endonuclease activity in human nucleotide excision repair. *DNA Repair*, **10**, 722-729.
- Fagerlie, S. R. & Bagby, G. C. (2006) Immune defects in Fanconi anemia. *Critical Reviews in Immunology*, **26**, 81-96.
- Fantini, D., Moritz, E., Auvre, F. *et al.* (2013) Rapid inactivation and proteasome mediated degradation of OGG1 contribute to the synergistic effect of hyperthermia on genotoxic treatments. *DNA Repair*, **12**, 227-237.
- Fekairi, S., Scaglione, S., Chahwan, C. *et al.* (2009) Human SLX4 is a Holliday junction resolvase subunit that binds multiple DNA repair/recombination endonucleases. *Cell*, **138**, 78-89.
- Fernandez-Capetillo, O. & Nussenzweig, A. (2013) Naked replication forks break apRPA. *Cell*, **155**, 979-980.
- Foo, J. & Michor, F. (2014) Evolution of acquired resistance to anti-cancer therapy. *Journal of Theoretical Biology*, **0**, 10-20.
- Fousteri, M., Vermeulen, W., van Zeeland, A. A. & Mullenders, L. H. (2006) Cockayne syndrome A and B proteins differentially regulate recruitment of chromatin remodelling and repair factors to stalled RNA DNA polymerase II *in vivo*. *Molecular Cell*, **23**, 471-482.

- Fu, D., Calvo, J. A. & Samson, L. D. (2012) Genomic instability in cancer Balancing repair and tolerance of DNA damage caused by alkylating agents. *Nature Reviews Cancer*, **12**, 104-120.
- Fuchs, R. P. & Fujii, S. (2013) Translesion DNA synthesis and Mutagenesis in Prokaryotes. *Cold Spring Harbor Perspectives in Biology*, **5**, a012682.
- Fujita, T., Ikeda, H., Kawasaki, K., *et al.* (2009) Clinicopathological relevance of Ubch10 in breast cancer. *Cancer Science*, **100**, 238-248.
- Gack, M. U., Albrecht, R. A., Urano, T. *et al.* (2007) TRIM25 RING-Finger E3 ubiquitin ligase is essential for RIG-I-mediated antiviral activity. *Nature*, **446**, 916-920.
- Galick, H. A., Kathe, S., Liu, M. *et al.* (2013) Germ-line variant of human NTH1 DNA glycosylase induces genomic instability and cellular transformation. *Proceedings of the National Academy of Sciences of the U. S. A*, **110**, 14314–14319.
- Gambus A., Khoudoli, G. A., Jones, R. C. & Blow, J. J. (2011) MCM2-7 form double hexamers at licensed origins in *Xenopus* egg extract. *Journal of Biological Chemistry*, **286**, 11855-11864.
- Garaycochea, J. L., Crossan, G. P., Langevin, F., Daly, M., Arends, M. J. *et al.* (2012) Genotoxic consequences of endogenous aldehydes on mouse haematopoietic stem cell function. *Nature*, **489**, 571-575.
- Garcia, C. C., Angeli, J. P., Freitas, F. *et al.* (2011) [<sup>13</sup>C<sub>2</sub>]-Acetaldehyde promotes unequivocal formation of 1, N<sup>2</sup>-propano, 2'-deoxyguanosine in human cells. *Journal of the American Chemical Society*, **133**, 9140-9143.
- Gari, K., Décaillet, C., Delannoy, M., Wu, L. & Constantinou, A. (2008) Remodelling of DNA replication structures by the branch point translocase FANCM. *Proceeding of the National Academy of Sciences of the United States of America*, **42**, 16107-16112.
- Ghosal, G. & Chen, J. (2013) DNA damage tolerance: a double-edged sword guarding the genome. *Translational Cancer Research*, **2**, 107-129.
- Giri, N., Batista, D. L., Alter, B. P. & Stratakis, C. A. (2007) endocrine abnormalities in patients with Fanconi anemia. *Journal of Clinical Endocrinology and Metabolism*, **92**, 2624-2631.
- Glickman, M. H., and Ciechanover, A. (2002) The ubiquitin-proteasome proteolytic pathway: destruction for the sake of construction. *Nat. Rev.* **82**, 373–428
- Glover, T. (2017) Fragile Sites in Cancer: More Than Meets the Eye. *Nature reviews cancer*, **17**, 489-501.
- Grabbe, C., Husnjak, K., and Dikic, I. (2011) The spatial and temporal organization of ubiquitin networks. *Nat. Rev. Mol. Cell. Biol.* **12**, 295–307
- Gramling, M. W. & Eischen, C. M. (2012) Suppression of Ras/Mapk pathway signalling inhibits Myc- induced lymphomagenesis. *Cell Death & Differentiation*, **19**, 1220-1227.

- Groisman, R., Polanowska, J., Kuraoka, I. *et al.* (2003) The ubiquitin ligase activity in the DDB2 and CSA complexes is differentially regulated by the COP9 signalosome in response to DNA damage. *Cell*, **113**, 357-367.
- Guo, Y., Wallace, S. & Bandaru, V. (2009) A novel bicistronic vector for overexpressing *Mycobacterium tuberculosis* proteins in *Escherichia coli*. *Protein Expression and Purification*, **65**, 230-237.
- Guo, Y., Bandaru, V., Jaruga, P., Zhao, X., Burrows, C.J., Iwai, S. *et al.* (2010) The oxidative DNA glycosylases of *Mycobacterium tuberculosis* exhibit different substrate preferences from their *Escherichia coli* counterparts. *DNA Repair (Amst)*, **9**, 177–190.
- Hanada, K., Budzowska, M., Davies, S. L. *et al.* (2007) The structure-specific endonuclease Mus81 contributes to replication restart by generating double-strand DNA breaks. *Nature Structural and Molecular Biology*, **14**, 1096-1104.
- Hanada, K., Budzowska, M., Modesti, M. *et al.* (2006) The structure-specific endonuclease MUS81-EME1 promotes conversion of interstrand DNA crosslinks into double-strand breaks. *The EMBO Journal*, **14**, 1096-1104.
- Hanahan, D. & Weinberg R, A. (2011) Hallmarks of cancer : the next generation. *Cell*, **144**, 646-674.
- Hang, B., Singer, B., Margison, G. P. & Elder, R. H. (1997) Targeted deletion of alkylpurine-DNA-N-glycosylase in mice eliminates repair of 1,N6-ethenoadenine and hypoxanthine but not of 3,N4-ethenocytosine or 8-oxoguanine. *Proceedings of the National Academy of Sciences of the U.S.A*, **94**, 12869-12874.
- Hao, Z., Duncan, G. S., Su, Y. W. *et al.* (2012) The E3 ubiquitin ligase Mule acts through the ATM-p53 axis to maintain Lymphocyte homeostasis
- Haracska, L., Prakash, S. & Prakash, L. (2002) Yeast Rev1 Protein Is a G Template-specific DNA Polymerase. *J Biol Chem*, **277**, 15546–15551.
- Hassanpour, S. H. & Dehghani, M. (2017) Review of cancer from perspective of molecular. *Journal of Cancer Research and Practice*, **4**, 127-129.
- Hatakeyama, S. (2011) TRIM proteins and cancer. *Nature Reviews Cancer*, **11**, 792-804.
- Hatakeyama, S. (2017) TRIM Family Proteins: Roles in Autophagy, immunity and carcinogenesis. *Trends in Biochemical Science*, **42**, 297-311.
- Haupt, Y., Maya, R., Kazaz, A. & Oren, M. (1997) Mdm2 promotes the rapid degradation of p53. *Nature* **387**, 296–299.
- Hay, N. & Sonenberg, N. (2004) Upstream and downstream of mTOR. *Genes & Development*, **18**, 1926-1945.
- Hazra, T. & Mitra, S. (2006) Purification and Characterization of NEIL1 and NEIL2, Members of a Distinct Family of Mammalian DNA glycosylases for Repair of Oxidized Bases. *Methods In Enzymology*, **408**, 33-48.
- Hazra, T. K., Izumi, R., Venkataraman, R., Kow, Y. W., Dizdaroglu, M. & Mitra, S. (2000) Characterization of a novel 8-oxoguanine-DNA glycosylase activity in *Escherichia coli* and

identification of the enzyme as endonuclease VIII. *Journal of Biological Chemistry*, **275**, 27762-27767.

Hazra, T. K., Izumi, T., Boldogh, I. *et al.* (2002a) Identification and characterization of a human DNA glycosylase for repair of modified bases in oxidatively damaged DNA. *Proceeding of the National Academy of Sciences of the U.S.A*, **99**, 3523-3528.

Hazra, T., Kow, Hatahet, Z. *et al.* (2002b) Identification and Characterization of a Novel Human DNA glycosylase for the repair of Cytosine-derived Lesions. *The Journal of Biological Chemistry*, **277**, 30417-30420.

He, Y.J., McCall, C.M., Hu, J., Zeng, Y. & Xiong, Y. (2006) DDB1 functions as a linker to recruit receptor WD40 proteins to CUL4-ROC1 ubiquitin ligases. *Genes Dev*, **20**, 2949–2954.

Hegde, M. L., Hegde, P. M., Bellot, L. J. *et al.*, (2013) Prereplicative repair of oxidized bases in the human genome is mediated by NEIL1 DNA glycosylase together with replication proteins. *Proceedings of the National Academy for Sciences of the U. S. A.*, **110**, 3090-3099.

Hegde, M. L., Izumi, T. & Mitra, S. (2012) Oxidized Base Damage and Single-Strand Break Repair in Mammalian Genomes: Role of Disordered Regions and Posttranslational Modifications in Early Enzymes. *Progress in molecular biology and translational science*, **110**, 1236-153.

Hegde, M., Hazra, T. & Mitra, S. (2008) Early steps in the DNA base excision/single-strand interruption repair pathway in mammalian cells. *Cell Research*, **18**, 27-47.

Hegde, P. M., Dutta, A., Sengupta, S. *et al.* (2015) The C-terminal Domain (CTD) of Human DNA Glycosylase NEIL1 is Required for Forming BERosome Repair Complex with DNA replication Proteins at the Replicating Genome. *The Journal of Biological Chemistry*, **290**, 20919-20933.

Hegi, M. E., Diserens, A. C., Gorja, T. *et al.* (2005) MGMT gene silencing benefit from temozolomide in glioblastoma. *New England Journal of Medicine*, **352**, 997-1003.

Herold, S., Hock, A., Herkert, B. *et al.*, (2008) Miz1 and HectH9 regulate the stability of the checkpoint protein TopBP1. *The EMBO Journal*, **27**, 2851-2861.

Hicks, J. K., Chute, L. C., Paulsen, M. *et al.* (2010) Differential Roles for DNA Polymerases Eta, Zeta, and REV1 in Lesion Bypass of Intrastrand versus Interstrand DNA Cross-links. *Molecular and Cellular Biology*, **30**, 1217-1230.

Hildrestrand, G., Neurauter, C., Diep, D. *et al.* (2009) Expression patterns of NEIL3 during embryonic brain development and neoplasia. *BMC Neuroscience*, **10**, 1-8.

Hillier, L., Graves, T., Fulton, F. *et al.* (2005) Generation and annotation of the DNA sequences on chromosomes 2 and 4. *Nature*, **434**, 724-731.

Hinz, J. M. (2010) Role of Homologous Recombination in DNA Interstrand Crosslink Repair. (2010) Role of Homologous Recombination in DNA Interstrand Crosslink Repair. *Environment and Molecular Mutagenesis*, **51**, 582-603.

- Hironak, K., Factor, V. M., Calvisi, D. F., Conner, E. A. & Thorgeirsson, S. S. (2003) Dysregulation of DNA repair Pathways in Transforming Growth Factor  $\alpha$ /c-myc Transgenic Mouse Model of Accelerated Hepatocarcinogenesis. *Laboratory Investigation*, **83**, 643-645.
- Ho, T. V. & Schärer, O. D. (2010) Translesion DNA Synthesis Polymerases in DNA Interstrand Crosslink Repair. *Environment and Molecular Mutagenesis*, **51**, 552-566.
- Ho, T.V., Guainazzi, A., Derkunt, S.B. *et al.* (2011) Structure-dependent bypass of DNA interstrand crosslinks by translesion synthesis DNA polymerases. *Nucleic Acids Research*, **39**, 7455-7464.
- Hoffmann, S., Smedegaard, S., Nakamura, K., *et al.* (2016) TRAP1 is a PCNA-binding ubiquitin ligase that protects genome stability after replication stress. *Journal of Cell Biology*, **2**, 63-75.
- Hornbeck, P.V., Zhang, B., Murray, B., Kornhauser, J.M, Latham, V., & Skrzypek, E. (2015) PhosphoSitePlus, 2014: mutations, PTMs and recalibrations. *Nucleic Acids Res*, **43**, D512-20.
- Huang, H. & Hopkins, P. B. (1993) DNA interstrand cross-linking by formaldehyde: nucleotide sequence preference and covalent structure of the predominant cross-link formed in synthetic oligonucleotides. *Journal of the American Chemistry Society*, **115**, 9402-9408.
- Huang, H., Regan, K. M., Wang, F., *et al.* (2005) Skp2 inhibits FOXO1 in tumour suppression through ubiquitin-mediated degradation. *Proceedings of the National Academy of Sciences of the U.S.A*, **102**, 1649-1654.
- Huang, J., Liu, S., Bellani, M. *et al.* (2013) The DNA Translocase FANCM/MHF Promotes Replication Traverse of DNA interstrand Crosslinks. *Molecular Cell*, **52**,
- Huang, Y. & Li, L. (2013) DNA crosslinking damage and cancer – a tale of friend and foe. *Translational Cancer Research*, **2**, 144-154.
- Huen, M. & Chen, J. (2008) The DNA damage response pathways: at the crossroad of protein modifications. *Cell Research*, **18**, 8-16.
- Husnjak, K. & Dikic, I. (2012) Ubiquitin-binding proteins: decoders of ubiquitin-mediated cellular functions. *Annual Review of Biochemistry*, **8**, 291-322.
- Hwang, B. J., Shi, G. & Lu, A. L. (2014) Mammalian MutY homolog (MYH or MUTYH) protects cells from oxidative DNA damage. *DNA Repair (Amst)*, **13**, 10-21.
- Ibusuki, M., Yamamoto, Y., Shinriki S, Ando, Y. & Iwase, H. (2011) Reduced expression of ubiquitin ligase FBXW7 mRNA is associated with poor prognosis in breast cancer patients. *Cancer Science*, **102**, 439-445.
- Ikeda, F. & Dikic, I. (2008). Atypical ubiquitin chains: new molecular signals. 'Protein modifications: beyond the usual suspects' review series. *EMBO Rep*, **9**, 536–542.

- Ikeda, S., Biswas, T., Roy, R. *et al.* (1998) Purification and Characterization of Human NTH1, a Homolog of *Escherichia coli* Endonuclease III: Direct Identification of Lys-212 as the active nucleophilic residue. *The Journal of Biological Chemistry*, **273**, 21585-21593.
- Ilves, I., Petojevic, T., Pesavento, J. J. & Botchan M. R. (2010) Activation of the MCM2-7 helicase by association with Cdc45 and GINS proteins. *Mol. Cell*, **37**, 247-258.
- International Agency for Research on Cancer (2018) IARC Monographs on the Evaluation of Carcinogenic Risks to Humans <https://monographs.iarc.fr/agents-classified-by-the-iarc/> [Accessed 03 August 2018].
- Izumi, T., Brown, D. B., Naidu, C. V. *et al.* (2005). Two essential but distinct function of the mammalian abasic endonuclease. *Proceedings of the National Academy of Sciences of the U.S.A*, **102**, 5739-5743.
- Jackson, S. P. & Durocher, D. (2013) Regulation of DNA Damage Responses by Ubiquitin and SUMO, *Mol. Cell*, **49**, 795-807.
- Jalland, C., Scheffler, K., Benestad, S. *et al.* (2016) NEIL3 induced neurogenesis protects against prion disease during the clinical phase. *Scientific Reports*, **6**, 37844.
- Javanbakht, H., Yuan W, Yeung. D. F. *et al.* (2006) Characterisation of the TRIM5alpha trimerization and its contribution to human immunodeficiency virus capsid binding. *Virology*, **353**, 234-2346.
- Jena, N. & Mishra, P. C. (2012) Formation of ring-opened and rearranged products of guanine: Mechanisms and biological significance. *Free Radical Biology and Medicine*, **53**, 81-94.
- Jena, N. & Mishra, P. C. (2013) Is FapyG Mutagenic?: Evidence from the FT Study. *ChemPhysChem*, **14**, 3236-3270.
- Jena, N. (2012) DNA damage by reactive species: Mechanisms, mutation and repair. *Journal of Bioscience*, **37**, 503-517.
- Jevsevar, S., Gaberc-Porekar, V., Fonda, I. *et al.* (2005) Production of Nonclassical Inclusion Bodies from Folded Protein Can Be Extracted. *Biotechnology Progress*, **21**, 632-639.
- Jiang, D., Hatahet, Z., Blaisdell, J. O., Melamede, R. J. & Eallace, S. S. (1997a) *Escherichia coli* endonuclease VIII: cloning, sequencing, and overexpression of the Nei structural gene and characterization of nei and nei nth mutants. *Journal of Bacteriology*, **179**, 3773-3782.
- Jiang, D., Hatahet, Z., Melamede, R., Kow, Y. & Wallace, S. (1997b) Characterisation of *Escherichia coli* Endonuclease VIII. *The Journal of Biological Chemistry*, **272**, 32230-32239.
- Jiang, Y., Hong, H., Cao, H. & Wang, Y. (2007) In vivo formation and invitro replication of a guanine-thymine intrastrand cross-link lesion. *Biochemistry*, **46**, 12757-12763.
- Johnson, R.E., Yu, S.L., Prakash, S. & Prakash, L. (2003) Yeast DNA DNA polymerase zeta ( $\alpha$ ) is essential for error-free replication past thymine glycol. *Genes & Development*, **17**, 77-87.
- Ju, H. P., Wang, Y., You, J. *et al.* (2016) Folding Kinetics of Single Human Telomeric G-Quadruplex Affected by Cisplatin. *American Chemical Society Omega*, **1**, 244-250.

- Jung, C., R. Hwang, K. S., Yoo, J. (2006) E2-EPF UCP targets pVHL for degradation and associates with tumour growth and metastasis. *Nature Methods*, **12**, 809-816.
- Kamura, T., Hara, T., Kotoshiba, S., Yada, M., Ishida, N., Imaki, H. (2003) Degradation of p57<sup>kip2</sup> mediated by SCF<sup>Skip2</sup>-dependent ubiquitylation. *Proceedings of the National Academy of Sciences of the U.S.A*, **100**, 10231-10236.
- Kamura, T., Koepp, D. M., Conrad, M. N., *et al.* (1999) Rbx1, a component of the VHL tumour suppressor complex and SCF ubiquitin ligase. *Science*, **284**, 657-661.
- Kang, H.C., Lee, Y.I., Shin, J.H., *et al.* (2011) Iduna is a poly(ADP-ribose) (PAR)-dependent E3 ubiquitin ligase that regulates DNA damage, *Proc. Natl. Acad. Sci. USA*, **108**, 14103–14108.
- Kanno, Y., Watanabe, M., Kimura, T., Nonomura, K., Tanaka, S. & Hatakeyama, S. (2014) TRIM29 as a novel prostate basal cell marker for diagnosis of prostate cancer. *Acta Histochem* **116**, 708–712.
- Kannouche, P. L., Wing, J. & Lehmann, A.R. (2004) Interaction of Human DNA DNA polymerase  $\eta$  with Monoubiquitinated PCNA: A possible Mechanism for the Polymerase Switch in Response to DNA Damage. *Mol. Cell*, **14**, 491-500.
- Karakaya, A., Jaruga, P., Bohr, V.A., Grollman, A.P. & M. Dizdaroglu. (1997) Kinetics of excision of purine lesions from DNA by *Escherichia coli* Fpg protein. *Nucleic Acids Research*, **25**, 474–479.
- Kattah, M.G., Malynn, B.A., Ma, A. (2017) Ubiquitin-modifying enzymes and regulation of the inflammasome. *J. Mol. Biol*, **429**, 3471–3485.
- Kauffmann, A., Rosselli, F., Lazar, V. *et al.* (2008) High expression of DNA repair pathways is associated with metastasis in melanoma patients. *Oncogene*, **27**, 565-573.
- Kee, Y. & D’Andrea, A. D. (2012) Molecular pathogenesis and clinical management of Fanconi anemia. *Journal of Clinical Investigation*, **122**, 3799-3806.
- Kelley, R., Logsdon, D. & Fishel, M. (2014) Targeting DNA repair pathways for cancer treatment: what’s new? *Future Oncology*, **10**, 1215-1237.
- Kesik-Brodacka, M., Romanik, A., Mikiewicz-Sygula, D. *et al.* (2012) A novel system for stable, high-level expression from the T7 promotor. *Microbial Cell Factories*, **11**, 1-7.
- Kino, K., Hirao-Suzuki, M., Morikawa, M., Sakaga, A. & Miyazawa. (2017) Generation, repair and replication of guanine oxidation. *Genes and Environment*, **39**, 1-8.
- Kim, J. M, Kee, Y., Gurtan, A. & D’Andrea, A. D. (2008) Cell cycle-dependent chromatin loading of the Fanconi anemia core complex by FANCM/FAAP24. *Blood*, **10**, 5215-5222.
- Kim, W., Bennet, E.J, Huttlin, E.L., *et al.* (2011a) Systematic and quantitative assessment of the ubiquitin-modified proteome. *Mol Cell*, **44**, 325-340.
- Kim, Y. & Wilson, D. (2012) Overview of Base Excision Repair Biochemistry. *Current Molecular Pharmacology*, **5**, 3-13.

- Kim, Y., Lach, F. P., Desetty, R. *et al.* (2011b) Mutations of the SLX4 gene in Fanconi anemia. *Nature Genetics*, **43**, 142-146.
- Kim, Y., Spitz, G. S., Veturi, U., Lach, F. P., Auerbach, A. D. & Smogorzewska, A. (2013) Regulation of multiple DNA repair pathways by the Fanconi anemia protein SLX4. *Blood*, **121**, 54-63.
- Kim, Y.S., Kim, Y, Choi, J., Oh, H. & Lee, J. (2016) Genetic variants and risk of prostate cancer using pathway analysis of a genome-wide association study. *Neoplasia*, **63**, 629-634.
- Klattenhoff, A. W., Thakur, M., Chu, C. S., Ray, D., Habib, S. L. & Kidane, D. (2017) Loss of NEIL3 DNA glycosylase markedly increases replication associated double strand breaks and enhances sensitivity to ATR inhibitor in glioblastoma cells. *Oncotarget*, **8**, 112942-112958.
- Klaunig, J., Xu, Y., Isenberg, J. *et al.* (1998) The Role of Oxidative Stress in chemical Carcinogenesis. *Environmental Health Perspectives*, **106**, 289-295.
- Klaunig, J.E., Wang, Z., Pu, X. *et al.* (2011) Oxidative stress and oxidative damage in chemical carcinogenesis. *Toxicology and Applied Pharmacology*, **254**, 86-99.
- Komander, D., Clague, M. J., and Urbé, S. (2009) Breaking the chains: structure and function of the deubiquitinases. *Nat. Rev. Mol. Cell Biol.* **10**, 550–563
- Kottemann, M. C. & Smogorzewska, A. (2013) Fanconi anaemia and the repair of Watson and Crick DNA crosslinks. *Nature*, **493**, 356-363.
- Kraemer, K. H., Patronas, N. J., Schiffmann, R. *et al.* (2007) Xeroderma pigmentosum, Trichothiodystrophy and Cockayne syndrome: A complex genotype-phenotype relationship. *Neuroscience*, **145**, 1388-1396.
- Kress, T. R., Sabo, A. & Amanti, B. (2015) MYC: connecting selective transcriptional control to global RNA production. *Nature Reviews Cancer*, **15**, 593-607.
- Krishnamurthy, N., Zhao, X., Burrows, C. & David, S. (2008) Superior Removal of Hydantoin Lesions Relative to Other Oxidized Bases by the Human DNA glycosylase hNEIL1. *Biochemistry*, **47**, 7137-7146.
- Krokan, H., E. & Bjørås, M. (2013) Base Excision Repair. *Cold Spring Harbor Perspectives in Biology*, **5**, a012583.
- Krokeide, S.Z., Bolstad, N., Laerdahl, J.K., Bjørås, M. & Luna, L. (2009) Expression and purification of NEIL3, a human DNA glycosylase homolog, *Protein Expression and Purification*, **65**, 160-164.
- Krokeide, S.Z., Laerdahl, J.K., Salah, M. *et al.* (2013) Human NEIL3 is mainly a monofunctional DNA glycosylase removing spiroiminodihydantoin and guanidinohydantoin. *DNA Repair*, **12**, 1160- 1164.
- Kuiper, R. & Hoogerbrugge, N. (2015) NTH1 defines novel cancer syndrome. *Oncotarget*, **6**, 34069-34070.

- Kulak, N.A., Pichler, G., Paron, I., Nagaraj, N. & Mann, M. (2014) Minimal, encapsulated proteomic-sample processing applied to copy-number estimation in eukaryotic cells. *Nat. Methods*, **11**, 319–324
- Kuraoka, I., Kobertz, W. R., Ariza, R. R., Biggerstaff, M., Essigmann, J. M. & Wood, R. D. (2000) Repair of an interstrand DNA cross-link initiated by ERCC1-XPF repair/recombination nuclease. *Journal of Biological Chemistry*, **275**, 26632–26636.
- Kuzminov, A. (2001) Single-strand interruptions in replicating chromosomes cause double-strand breaks. *Proceedings of the National Academy of Sciences of the U.S.A*, **98**, 8241–8246.
- Langevin, F., Crossan, G., Rosado, I., Arends, M. & Patel, K. (2011) Fancd2 counteracts the toxic effects of naturally produced aldehydes in mice. *Nature*, **475**, 53–58.
- Laursen, B., Sørensen, H., Mortensen, K. & Sperlin-Petersen, H. (2005) Initiation of Protein Synthesis in Bacteria. *Microbiology and Molecular Biology Reviews*, **69**, 101–123.
- Lawley, P. & Phillips, D. (1996) DNA adducts from chemotherapeutic agents. *Mutation Research*, **355**, 13–40.
- Lee, J. T. & Gu, W. (2010) The multiple levels of regulation by p53 ubiquitination. *Cell Death Differ.* **17**, 86–92.
- Li, Y., Park, J., Piao, L. (2013) PHB-mediated PHF20 phosphorylation on Ser291 is required for p53 function in DNA damage. *Cell Signalling*, **25**, 74–84.
- Liang, C., Li, Z., Lopez-Martinez. *et al.* (2016) The FANCD2-FANCI complex is recruited to DNA interstrand crosslinks before monoubiquitination of FANCD2. *Nature Communications*, **7**, 1–10.
- Liang, Y., Lin, S. & Brunnicardi, C. (2009) DNA Damage Response Pathways in Tumour Suppression and Cancer Treatment. *World Journal of Surgery*, **33**, 661–666.
- Lindahl, T. (1990) Repair of intrinsic DNA lesions. *Mutation Research*, **223**, 305–311.
- Lindahl, T. (1993) Instability and decay of the primary structure of DNA. *Nature*, **362**, 709–715.
- Lindahl, T. (1974) An *N-Glycosidase* from *Escherichia coli* That Releases Free Uracil from DNA Containing Deaminated Cytosine Residues. *Proceedings of the National Academy of Sciences of the United States of America*, **9**, 3649–3653.
- Lipton, J. O. & Sahin, M. (2014) The neurology of mTOR. *Neuron*, **84**, 275–291.
- Liu, M., Bandaru, V., Bond, J. P. *et al.* (2010) The mouse ortholog of NEIL3 is a functional DNA glycosylase *in vitro* and *in vivo*. *Proceedings of the National Academy of Sciences of the United States of America*, **107**, 4925–4930.
- Liu, M., Bandaru, V., Holmes, A. *et al.* (2012) Expression and purification of active mouse and human NEIL3 proteins. *Protein Expression and Purification*, **84**, 130–139.
- Liu, M., Doublé, S. & Wallace, S. (2013a) NEIL3, the final frontier for the DNA glycosylases that recognize oxidative damage. *Mutation Research*, **743**, 4–11.

- Liu, M., Imamura, K., Averill, A. M., Wallace, S. S. & Doubl  , S. (2013b) Structural characterization of a mouse ortholog of human NEIL3 with a marked preference for single-stranded DNA. *Structure*, **5**, 247-256.
- Liu, W. M. & Zhang, X, A. (2006) KAI1/CD82, a tumour metastasis suppressor. *Cancer Letters*, **240**, 183-194.
- Ljungman, M. & Zhang, F. (1996) Blockage of RNA DNA polymerase as possible trigger for U. V. light induced apoptosis. *Oncogene*, **13**, 823-831.
- Lobitz, S. & Velleuer, E. (2006) Guido Fanconi (1892–1979): a jack of all trades. *Nature Reviews Cancer*, **6**, 893–898.
- Lopez-Contreras, A. J. & Fernandez-Capetillom A. (2010) The ATR barrier to replication-born DNA damage. *DNA repair*, **9**, 1249-1255.
- Love, L. M., Shi, D. & Grossman, S. R. (2013) p53 Ubiquitination and proteasomal degradation. *Methods Mol. Biol*, **962**, 63-73.
- Lu, R., Nash, H. M. & Verdine, G. L. (1997) A mammalian DNA repair enzyme that excises oxidatively damaged guanines maps to a locus frequently lost in lung cancer. *Current Biology*, **7**, 397-407.
- Lu, W., Ogasawara, M. & Huang, P. (2007) Models of reactive oxygen species in cancer. *Drug Discovery Today: Disease Models*, **4**, 67-73.
- Luo, W., Muller, J.G., Rachlin, E.M. & Burrows, C.J. (2000) Characterization of spiroiminodihydantoin as a product of one-electron oxidation of 8-Oxo-7,8-dihydroguanosine. *Org Lett*, **2**, 613–616.
- Lyu, X. M., Zhu, X. W., Zhao, X. B. *et al.* (2018) A regulatory mutant on TRIM26 conferring risk of nasopharyngeal carcinoma by inducing low Immune response. *Cancer Medicine*, **7**, 3848-3861.
- Mac  -Aim  , G., Couv  , S., Khassenov, B., Rosselli, F. & Sapparbaev, M. K. (2010) The Fanconi Anemia Pathway Promotes DNA Glycosylase-Dependent Excision of Interstrand DNA Crosslinks. *Environmental and Molecular Mutagenesis*, **51**, 508-519.
- Maki, H. & Sekiguchi, M. (1992) MutT protein specifically hydrolyses a potent mutagenic substrate for DNA synthesis. *Nature*, **355**, 273–275.
- Mandal, S., Hegde, Chatterjee, A. *et al.* (2011) Role of Human DNA Glycosylase Neilike2 (NEIL2) and Single Strand Break Repair Protein Polynucleotide Kinase 3'-Phosphatase in Maintenance of Mitochondrial Genome. *The Journal of Biological Chemistry*, **287**, 2819-2829.
- Mansour, M. A. (2018) Ubiquitination: Friend and foe in cancer. *International Journal of Biochemistry and Cell Biology*, **101**, 80-93.
- Maor-Shoshani, A., Meira, L. B., Yang, X. & Samson, L. (2008) 3-Methyladenine DAN glycosylase is important for cellular resistance to psoralen interstrand cross-links. *DNA repair (Amst)*, **7**, 1399-1406.

- Margulies, C. M., Chaim, I. A., Mazumder, A., Criscione, J. & Samson, L. D. (2017) Alkylation induced cerebellar degeneration dependent on Aag and Parp! Does not occur via previously established cell death mechanisms. *PLoS One*, **12**, e0184619.
- Marietta, C. Thompson, L. H., Lamerdin, J. E. & Brooks, P. J. (2009) Acetaldehyde stimulates FANCD2 monoubiquitination, H2AX phosphorylation, and BRCA1 phosphorylation in human cells *in vitro*: implications for alcohol-related carcinogenesis. *Mutation Research*, **664**, 77-83.
- Markkanen, E., Dorn, J. & Hübscher, U. (2013) MUTYH DNA glycosylase: the rationale for removing undamaged bases from the DNA. *Frontiers in Genetics*, **4**, 1-20.
- Marteijn, J. A., Lans, H., Vermeulen, W., Hoeijmakers, J. H. (2014) Understanding nucleotide excision repair and its roles in cancer and ageing. *Nature Reviews Molecular Cell Biology*, **15**, 465-481.
- Martin, P. R., Couvé, S., Zutterling, C., *et al.* (2017) The Human DNA glycosylase NEIL1 and NEIL3 Excise Psoralen-Induced-DNA-DNA Cross-Links in a Four-Stranded DNA Structure. *Scientific Reports*, **7**, 17438.
- Massaad, M., Zhou, J., Tsuchimoto, D. *et al.* (2016) Deficiency of BER enzyme NEIL3 drives increased predisposition to autoimmunity. *Journal of clinical investigation*, **126**, 4219-4236.
- Masuda, Y., Takahashi, H., Sato, S. *et al.* (2015) TRIM29 regulates the assembly of DNA repair proteins into damaged chromatin. *Nature Communications*, **6**, 1-13.
- Masutani, C., Sugasawa, K., Yanagisawa, J. *et al.* (1994) Purification and cloning of a nucleotide excision repair complex involving the xeroderma pigmentosum group C protein and a human homologue of yeast RAD23 *EMBO Journal*, **13**, 1813-1843.
- Mathieu, N., Kaczmarek, N., Rüthermann, P., Luch, A. & Naegeli, H. (2013) DNA quality control by a lesion sensor pocked of the xeroderma pigmentosum group D helicase subunit of TFIIH. *Current Biology*, **23**, 204-212.
- Maynard, S., Schurman, S., Harboe, C. *et al.* (2009). Base excision repair of oxidative DNA damage and association with cancer and aging. *Carcinogenesis*, **30**, 2-10.
- Mazouzi, A., Velimezi, G. & Loizou, J. I. (2014) DNA replication stress: Causes, resolution and disease. *Experimental Cell Research*, **329**, 85-93.
- McCabe, K. M., Olson, S. B. & Moses, R. E. (2009) DNA Interstrand Crosslink Repair in Mammalian Cells. *Journal of Cellular Physiology*, **220**, 569-573.
- Mccann, A. H., Kirley, A., Garney, Corbally, N., Magee, H. M. *et al.* (1995) Amplification of the MDM2 gene in human breast cancer and its association with MDM2 and p53 protein status. *British Journal of Cancer*, **71**, 981-985.
- Meira, L.B., Moroski-Erkul, C. A., Green, S. L. *et al.* (2009) Aag-initiated BER drives alkylation-induced retinal degeneration in mice. *Proceeding of the National Academy of Sciences of the U.S.A*, **106**, 888-893.

- Meisenberg, C., Tait, P.S., Dianova, I.I. *et al.* (2012) Ubiquitin ligase UBR3 regulates cellular levels of the essential DNA repair protein APE1 and is required for genome stability, *Nucleic Acids Res*, **40**, 701–711.
- Melamede, R. J., Hatachat, Z., Kow, Y. W., Ide, H. & Wallace, S. S. (1994) Isolation and characterization of endonuclease VIII from *Escherichia coli*. *Biochemistry*, **33**, 1255-1264.
- Mertins, P., Qiao, J. M., Patel, J., *et al.* (2013) Integrated proteomic analysis of post-translational modifications by serial enrichment. *Nat Methods*. **10**, 634-637.
- Metzger, M. B., Pruneda, J. N., Klevit, R. E. & Weissman, A. M. (2014) RING-type E3 ligases: Master manipulators of E2 ubiquitin-conjugating enzymes and ubiquitination. *Biochimica et Biophysica Acta*, **1843**, 47-60.
- Michaels, M.L. & Miller, J.H. (1992) The GO system protects organisms from the mutagenic effect of the spontaneous lesion 8-hydroxyguanine (7,8-dihydro-8-oxoguanine). *J Bacteriol*, **174**, 6321– 6325.
- Michaels, M.L., Cruz, C., Grollman, A.P. & Miller, J.H. (1992) Evidence that MutY and MutM combine to prevent mutations by an oxidatively damaged form of guanine in DNA. *Proc Natl Acad Sci USA*. **89**, 7022–7025.
- Michl, J., Zimmer, J. & Tarsounas, M. (2016) Interplay between Fanconi anemia and homologous recombination pathways in genome integrity. *EMBO Journal*, **35**, 909-923.
- Mijic, S., Zellweger, R., Chappidi, N., *et al.* (2017) Replication fork reversal triggers fork degradation in BRCA2-defective cells. *Nature Communications*, **8**, 859.
- Min, J., & Pavletich, N. P. (2007) Recognition of DNA damage by the Rad4 nucleotide excision repair protein. *Nature*, **449**, 570-575.
- Minko, I. G., Harbut, M. B. Kozekov, ID. *et al.* (2008) Role for DNA polymerase kappa in the processing of N2-N2-guanine interstrand cross-links. *Journal of Biological Chemistry*, **283**, 17075-17082.
- Mojas, N., Lopes, M. & Jiricny, J. (2007) Mismatch repair-dependent processing of methylation damage gives rise to persistent single-stranded gaps in newly replicated DNA.
- Momand, J., Zambetti, G. P., Olson, D. C., George, D. & Levine, A. J. (1992) The mdm-2 oncogene product forms a complex with the p53 protein and inhibits p53-mediated transactivation. *Cell*, **69**, 1237-1245.
- Monia, B.P. *et al.* (1989) Gene synthesis, expression, and processing of human ubiquitin carboxyl extension proteins. *J. Biol. Chem.* **264**,4093–4103
- Morland, I., Rolseth, V., Luna, L. *et al.* (2002) Human DNA glycosylases of the bacterial Fpg/MutM superfamily: an alternative pathway for the repair of 8-oxoguanine and other oxidation products in DNA. *Nucleic Acids Research*, **30**, 4926-4936.
- Mortusewicz, O., Herr, P. & Helleday, T. (2013) Early replication fragile sites: where replication-transcription collisions cause genetic instability. *EMBO Journal*, **32**, 493-495.

- Mosammaparast, N. & Shi, Y. (2010) Reversal of histone methylation: biochemical and molecular mechanisms of histone demethylases. *Annual Review of Biochemistry*, **79**, 155-179.
- Moser, J., Kool, H., Giakzidis, I. *et al.* (2007) Sealing of chromosomal DNA nicks during nucleotide excision repair requires XRCC1 and DNA ligase III alpha in a cell-cycle-specific manner. *Molecular Cell*, **27**, 311-323.
- Mukhopadhyay, D., and Riezman, H. (2007) Proteasome-independent functions of ubiquitin in endocytosis and signalling. *Science*, **315**, 201–205
- Muniandy, P., Liu, J., Majumdar, A., Liu, S. & Seidman, M. (2010) DNA Interstrand Crosslink Repair in Mammalian cells: Step by Step. *Critical Reviews in Biochemistry and Molecular Biology*, **45**, 23-48.
- Myung, J., Kim, K. B. & Crews, C. M (2001) The Ubiquitin-Proteasome Pathway and Proteasome Inhibitors. *Medicinal Research Reviews*, **21**, 245-273.
- Naim, V., Wilhelm, T., Debatisse, M. & Roselli, F. (2013) ERCC1 and MUS81-EME1 promote sister chromatid separation by processing late replication intermediates at common fragile sites during mitosis. *Nature Cell Biology*, **15**, 1008-1015.
- Nakagawa, T., Hosogane, M., Nakagaw, M. *et al.* (2017) TGF- $\beta$ -Induced proliferative arrest mediated by TRIM26-Dependent TAF7 degradation and Its antagonism by MYC. *Mol. Cell. Biol.* **38**, e00449-17
- Nakamura, J. & Swenberg, J. A. (1999) Endogenous Apurinic/Apyrimidinic Sites in Genomic DNA of Mammalian Tissues. *Cancer Research*, **59**, 2522-2526.
- Nalepa, G. & Clapp, D. W. (2018) Fanconi anaemia and cancer: an intricate relationship. *Nature Reviews Cancer*, **18**, 168-185.
- Nam, E. & Cortez, D. (2011) ATR signalling: more than meeting at the fork. *Biochemical Journal*, **436**, 527-536.
- Napolitano, L.M. and Meroni, G. (2012) TRIM family: pleiotropy and diversification through homomultimer and heteromultimer formation. *IUBMB Life*, **64**, 64–71.
- Narayan, G., Bourden, V., Chaganti, S., *et al.* (2007) gene dosage alterations revealed by cDNA microarray analysis in cervical cancer: identification of candidate amplified overexpressed genes. *Genes Chromosomes Cancer*, **46**, 373 -384.
- Neurauter, C., Luna, L. & Bjørås, M. (2012) Release from quiescence stimulates the expression of human NEIL3 under the control of the Ras dependent ERK-MAP kinase pathway. *DNA Repair*, **11**, 401-409.
- Neveling, K., Endt, D., Hoehn, H. & Schindler, D. (2009) Genotype-phenotype correlations in Fanconi anemia. *Mutation Research*, **668**, 73-91.
- Naim, V., Wilhelm, T., Debatisse, M. & Roselli, F. (2013) ERCC1 and MUS81-EME1 promote sister chromatid separation by processing late replication intermediates at common fragile sites during mitosis. *Nature Cell Biology*, **15**, 1008-1015.

- Niedzwiedz, W., Mosedale, G., Johnson, M., Ong, C. Y., Pace, P. & Patel, K. J. (2004) The Fanconi Anaemia gene FANCC Promotes Homologous Recombination and Error-Prone DNA repair. *Mol. Cell*, **15**, 607-620.
- Nijman, S. M., Huang, T. T., Dirac, A. M. *et al.* (2005) The deubiquitinating enzyme USP1 regulates the Fanconi anemia pathway. *Mol. Cell*, **17**, 331–339.
- Niles, J. C., Wishnok, J.S. & Tannenbaum, S.R. (2004) Spiroiminodihydantoin and Guanidinohydantoin are the dominant products of 8-oxoguanosine oxidation at low fluxes of peroxynitrite: mechanistic studies with  $^{18}\text{O}$ . *Chemical research in toxicology*, **17**, 1510-1519.
- Novagen. (2004) *Competent Cells: User Protocol*. EMD Biosciences, Darmstadt, Germany.
- Novagen. (2005) *pET system manual*. EMD Biosciences, Darmstadt, Germany.
- Nováková, O., Nazarov, A. A., Hartinger, C. G., Keppler, B. H., Brabec, V. (2009) DNA interactions of a dinuclear  $\text{Ru}^{\text{II}}$  arene antitumor complexes in cell-free medium. *Biochemical Pharmacology*, **77**, 364-374.
- O'Connor, M. (2015) Targeting the DNA Damage Response in Cancer. *Molecular Cell*, **60**, 547-560.
- Ogi, T., Limsirichaikul, S., Overmeer, R. M. *et al.* (2010) Three DNA polymerases, recruited by different mechanisms, carry out NER repair synthesis in human cells. *Nature Cell Biology*, **8**, 714-727.
- Ohta, T. Michel, J. J., Schottelius, A. J. & Xiong, Y. (1999) ROC1, a homolog of APC11, represents a family of cullin partners with an associated ubiquitin ligase activity. *Mol. Cell*, **3**, 535-541.
- Olsson, M. & Lindahl, T. (1980) Repair of alkylated DNA in *Escherichia coli*. Methyl group transfer from  $\text{O}^6$ -methylguanine to a protein cysteine residue. *The Journal of Biological Chemistry*, **255**, 10569-10571.
- Oshikawa, K., Matsumoto, M., Oyamada, K., & Nakayama, K.I. (2012) Proteome-wide identification of ubiquitylation sites by conjugation of engineered lysine-less ubiquitin. *J. Proteome Res*, **11**, 796–807.
- Ourliac-Garnier, I., Elizondo-Riojas, M., Redon, S., Farrell, N. P. & Bombard, S. (2005) Cross-Links of Quadruplex Structures from Human Telomeric DNA by Dinuclear Platinum Complexes Show the Flexibility of Both Structures. *Biochemistry*, **44**, 10620-10634.
- Palles, C., Cazier, J., Howarth, K. *et al.* (2013) Germline mutations in the proof-reading domains of *POLE* and *POLD1* predispose to colorectal adenomas and carcinomas. *Nature Genetics*, **45**, 136-144.
- Palovcak, A., Liu, W., Yuan, F. & Zhang, Y. (2017) Maintenance of genome stability by Fanconi anemia proteins. *Cell Bioscience*, **7**, 8.
- Parsons, J. L, Tait, P. S, Finch, D., Dianova, I. I, Allinson, S. L, Dianov, G. L. (2008) CHIP-mediated degradation and DNA damage-dependent stabilization regulate BER proteins. *Mol. Cell*, **4**, 477-487.

- Parsons, J. L. & Elder, R. H. (2003) DNA N-glycosylase deficient mice: a tale of redundancy. *Mutation Research*, **531**, 165-175.
- Parsons, J. L., Dianova, I. I., Khoronenkova, S. V. *et al.* (2011) USP47 Is a Deubiquitylating Enzyme that Regulates Base Excision Repair by Controlling Steady-State Levels of DNA Polymerase  $\beta$ . *Mol. Cell*, **41**, 609-615.
- Parsons, J.L., Khoronenkova, S.V., Dianova, I.I., *et al.* (2012) Phosphorylation of PNKPP by ATM prevents its proteasomal degradation and enhances resistance to oxidative stress. *Nucleic Acids Res* **40**, 11404–11415.
- Parsons, J.L., Tait, P.S., Finch, D., Dianova, I.I., Allinson, S.L., & Dianov, G.L. (2008) CHIP-mediated degradation and DNA damaged dependent stabilization regulate BER proteins. *Mol. Cell*, **29**, 477–487.
- Parsons, J.L., Tait, P.S., Finch, D., *et al.* (2009) Ubiquitin ligase ARF-BP1/Mule modulates BER. *EMBO J.* **28**, 3207–3215.
- Pascucci, B., Russo, M. T., Crescenzi, M., Bignami, M. & Dogliotti, E. (2005) The accumulation of MMS-induced single strand breaks in G1 phase is recombinogenic in DNA polymerase beta defective mammalian cells. *Nucleic Acids Research*, **33**, 280-288.
- Patrick, S. & Turchi, J. (1998) Human replication protein A preferentially binds cisplatin-damaged duplex DNA *in vitro*. *Biochemistry*, **37**, 8808-8815.
- Patrick, S. & Turchi, J. (1999) Replication Protein A (RPA) Binding To Duplex Cisplatin-damaged DNA is Mediated through the Generation of Single-stranded DNA. *The Journal of Biological Chemistry*, **274**, 14972-14978.
- Pesola, F., Ferlay, J. & Sasieni, P. (2017) Cancer incidence in English children, adolescents and young people: past trends and projections to 2030. *British Journal of Cancer*, **117**, 1865-1873.
- Petermann, E. & Helleday, T. (2010) Pathways of mammalian replication fork restart. *Nature Reviews Molecular Cell Biology*, **11**, 683–687.
- Pierce, N. W., Kleiger, G., Shan, S. O. & Deshaies, R. J. (2009) Detection of sequential polyubiquitylation on a millisecond timescale. *Nature*, **462**, 615-619.
- Pizzolato, J., Mukherjee, S., Shärer, O. D. & Jiricny, J. (2015) FANCD2-associated Nuclease 1, but Not Exonuclease 1 or Flap Endonuclease 1, Is Able to Unhook DNA Interstrand Cross-links *In Vito*. *The Journal of Biological Chemistry*, **290**, 22602-22611.
- Pontel. L. B., Rosado, I. V., Burgos-Barragan, G. *et al.* (2015) Endogenous Formaldehyde is a Hematopoietic Stem Cell Genotoxin and Metabolic Carcinogen. *Mol. Cell*, **60**, 177-188.
- Poon, S. L., McPherson, J. R., Tan, P., Teh, B. T. & Rozen, S. G. (2014). Mutation signatures of carcinogen exposure: genome-wide detection and new opportunities for cancer prevention. *Genome Medicine*, **6**, 1-14.
- Popuri, V., Croteau, D. L. & Bohr, V. A. (2010) Substrate specific stimulation of NEIL1 by WRN but not the other human RecQ helicases. *DNA Repair (Amst)*, **9**, 636-642.

- Pouget, J. O., Frelon, S., Ravanat, J. L., Testard, I., Odin, F. *et al.* (2002) Formation of modified DNA bases in cells exposed either to gamma radiation or to high-LET particles. *Radiation Research*, **157**, 589-595.
- Poulogiannis, G., McIntyre, R., Dimitriadi, M., *et al.* (2010) *PARK2* deletions occur frequently in sporadic colorectal cancer and accelerate adenoma development in *Apc* mutant micr. *Proceedings of the National Academy of Sciences of the U.S.A.*, **107**, 15145-15150.
- Prakash, A. & Doublié, S. (2015) Base Excision Repair in the Mitochondria. *Journal of Cellular Biochemistry*, **116**, 1490-1499.
- Prakash, A., Doublié, S. & Wallace, S. S. (2012) The Fpg/Nei Family of DNA glycosylases: Substrates, Structures and Search for Damage. *Progress in molecular biology and translational science*, **110**, 71-91.
- Price, N. E., Catalano, M. J., Liu, S., Wang, Y. & Gates, K. S. (2015) Chemical and structural characterization of interstrand cross-links formed between abasic sites and adenine residues in duplex DNA. *Nucleic Acids Research*, **13**, 3434-3441.
- Purmal, A. A., Lampman, G. W., Bond, J. P., Hatahet, Z. & Wallace, S. S. (1998) Enzymatic processing of uracil glycol, a major oxidative product of DNA cytosine. *Journal of Biological Chemistry*, **273**, 10026-10035.
- Quaresma, M., Coleman, M. P. & Rachet, B. (2015) 40-year trends in an index of survival for all cancers combined and survival adjusted for age and sex for each cancer in England and Wales, 1971-2011: a population-based study. *Lancet*, **385**, 1206-1218.
- Quintet, A., Lemacon, D. & Vindigni, A. (2017) Replication Fork Reversal: Players and Guardians. *Mol. Cell*, **68**, 830-833.
- Quiros, S., Roos, W. P. & Kaina, B. (2010) Processing of O6-methylguananine into DNA double-strand breaks requires two rounds of replication whereas apoptosis is also induced in subsequent cell cycles. *Cell Cycle*, **9**, 168-178.
- Ragland, R. L., Patel, S., Rivard, R. S., *et al.* (2013) RNF4 PLK1 are required for replication fork collapse in ATR-deficient cells. *Genes & Development*, **27**, 2259-2273.
- Ran, Y., Zhang, J., Liu, L. *et al.* (2016) Autoubiquitination of TRIM26 links TBK1 to NEMO in RLR-mediated innate antiviral immune response. *Journal of molecular cell biology*, **8**, 31-43.
- Rankin, E. B. & Giaccia, A. J. (2016) Hypoxic control of metastasis. *Science*, **352**, 175-182.
- Regnell, C., Hildrestrand, G., Sejersted, Y. *et al.* (2012) Hippocampal Adult Neurogenesis Is Maintained by NEIL3-Dependent Repair of Oxidative DNA Lesions in Neural Progenitor Cells. *Cell Reports*, **2**, 503-510.
- Reymond, A., Meroni, G., Fantozzi, A. *et al.* (2001) The tripartite motif family identifies cell compartments. *The EMBO Journal*, **20**, 2140-2151.
- Rittié, L. & Perbal, B. (2008) Enzymes used in molecular biology: a useful guide. *Journal of Cell Communication and Signalling*, **2**, 25-45.

- Rizzoni, M., Cundari, E., Perticone, P. & Gustavino, B. (1993) Chromatin Bridges between Sister Chromatids Induced in Late G2 Mitosis in CHO cells by Trimethylpsoralen+ UVA. *Experimental Cell Research*. **209**, 149-155.
- Rodriguez, M.S., Desterro, J.M., Lain, S, Lane, D.P. & Hay, R.T. (2000) Multiple C-terminal lysine residues target p53 for ubiquitin-proteasome-mediated degradation. *Mol Cell Biol*, **20**, 8458–8467.
- Rohleder, F., Huang, J., Xue, Y. *et al.* (2016) FANCM interacts with PCNA to promote replication traverse of DNA interstrand crosslinks. *Nucleic Acids Research*, **44**, 3219-3232.
- Rolseth, V., Krokeide, S., Kunke, D. *et al.* (2013) Loss of NEIL3, the major DNA glycosylase activity for removal of hydantoins in single stranded DNA, reduces cellular proliferation and sensitises cells to genotoxic stress. *Biochimica et biophysica acta*, **1833**, 1157-64.
- Rolseth, V., Luna, L., Olsen, A. K. *et al.* (2017) No cancer predisposition or increased spontaneous mutation frequencies in NEIL DNA glycosylase-deficient mice. *Scientific Reports*, **7**, 4384
- Ronson, G. E., Piber, A. L., Higgs, M. R., *et al.* (2018) PARP1 and PARP2 stabilise replication forks at BER intermediates through Fbh-dependent Rad51 regulation. *Nature Communications*, **9**, 1-12.
- Rosado, I., Langevin, F., Crossan, G., Takata, M. & Patel, K. (2011) Formaldehyde catabolism is essential in cells deficient for the Fanconi anemia DNA-repair pathway. *Nat. Struct. Mol. Biol.* **18**, 1432–1434.
- Rosenberg, P. S., Tamary, H. & Alter, B. P. (2011) How high are carrier frequencies of rare recessive syndromes? Contemporary estimates for Fanconi anemia in the United States and Israel. *Am. J. Med. Genet. A*, **155A**, 1877–1883.
- Rosenquist, T., Zaika, E., Fernandes, A. *et al.* (2003) The novel DNA glycosylase, NEIL1, protects mammalian cells from radiation-mediated cell death. *DNA Repair*, **2**, 581-591.
- Roy, U., Mukherjee, S., Sharma, A., Frank, E. G. & Scharer, O. D. (2016) The structure and duplex context of DNA interstrand crosslinks affects the activity of DNA polymerase  $\epsilon$ . *Nucleic Acids Research*. **44**, 7281-7297.
- Sacco, E., Hasan, M. M., Alberghina, L. & Vanoni, M. (2012) Comparative analysis of the molecular mechanisms controlling the initiation of chromosomal DNA replication in yeast and in mammalian cells. *Biotchnology Advances*, **30**, 73-93.
- Sacco, J. J., Coulson, J. M., Clague, M. J. & Urbé, S. (2010) Emerging roles of deubiquitinases in cancer-associated pathways. *IUBMB Life*, **62**, 140–157
- Sale, J. E., Lehmann, A. R. & Woodgate, R. (2012) Y-family DNA polymerases and their role in tolerance of cellular DNA damage. *Molecular Cell Biology*, **13**, 141-152.
- Santivasi, W. L. & Xia, F. (2014) Ionizing Radiation-Induced DNA Damage, Response, and Repair. *Antioxidants & Redox Signalling*, **21**, 251-259.

- Saparbaev, M., Kleibl, K. & Laval, L. (1995) *Escherichia coli*, *Saccharomyces cerevisiae*, rat and human 3-methyladenine DNA glycosylases repair 1, N6-ethonoadenine when present in DNA. *Nucleic Acids Research*, **23**, 3750-3755.
- Sarkar, S., Davies, A. A., Ulrich, H. D. & McHugh, P. J. (2006) DNA interstrand crosslink repair during G1 involves nucleotide excision repair and DNA polymerase zeta. *The EMBO Journal*, **25**, 1285-1294.
- Sarker, A. H., Chatterjee, A., Williams, M. *et al.* (2014) NEIL2 protects against Oxidative DNA Damage Induced by Sidestream Smoke in Human Cells. *PLoS One*, **9**, e90261.
- Sastry, S.S., Ross, B. & P'arraga, A. (1997) Cross-linking of DNA-binding Proteins to DNA with Psoralen and Psoralen Furan-side Monoadducts. *The Journal of Biological Chemistry*, **272**, 3715-3723.
- Schärer, O. (2003) Chemistry and Biology of DNA Repair. *Angewandte Chemie International Edition*, **42**, 2946-2974.
- Schärer, O. D. (2013) Nucleotide Excision Repair in Eukaryotes. *Cold Spring Perspectives in Biology*, **5**, a012609.
- Scheffner, M., Nuber, U. & Huibregtse, J. M. (1995). Protein ubiquitination involving an E1-E2-E3 enzyme ubiquitin thioester cascade. *Nature*, **373**, 81-83.
- Scrima, A., Koníčková, R., Czyzewski, B. K. *et al.* (2008) Structural basis of UV DNA damage recognition by the DDB1-DDB2 complex. *Cell*, **135**, 1213-1223.
- Sczepanski, J. T., Jacobs, A. C. & Greenberg, M. M. (2008) Self-promoted DNA interstrand cross-link formation by an abasic site. *Journal of American Chemical Society*, **130**, 9646-9647.
- Sczepanski, J. T., Jacobs, A. C., Van Houten, B. & Greenberg, M. M. (2009) Double Strand Break Formation During Nucleotide Excision Repair of a DNA Interstrand Cross-link. *Biochemistry*, **48**, 7565-7567.
- Seetharam, R., Sood, A., Basu-Mallick, A. *et al.* (2010) Oxaliplatin Resistance Induced by *ERCC1* Up-regulation Is Abrogated by siRNA-mediated Gene Silencing in Human Colorectal Cancer Cells. *Anticancer Research*, **30**, 2531-2538.
- Segal-Raz, Mass, G., Baranes-Bachar, K. *et al.* (2011) ATM-mediated phosphorylation of polynucleotide kinase/phosphatase is required for effective DNA double-strand break repair. *EMBO reports*, **12**, 713-719.
- Semlow, D. R., Zhang, J., Budzowska, M., Drohat, A. C. & Walter, J. C. (2016) Replication-Dependent Unhooking of DNA interstrand Cross-Links by the NEIL3 Glycosylase. *Cell*, **167**, 498-511.
- Seol, J. H., Feldman, R. M. R., Zachariae, W., *et al.* (1999). Cdc53/cullin and the essential Hrt1 RING-H2 subunit of SCF define a ubiquitin ligase module that activates the E2 enzyme Cdc34. *Genes & Development*, **13**, 1614-1626.
- Shangary, S. & Wang, S. (2008). Targeting the MDM2-p53 Interaction for Cancer Therapy. *Clin. Cancer Res*, **14**, 5318-5324.

- Shen X., Jun, S., O'Neal, L. E. *et al.* (2006) REV3 and REV1 play major roles in recombination-independent repair of DNA interstrand cross-links mediated by monoubiquitinated proliferating cell nuclear antigen (PCNA). *Journal of Biological Chemistry*, **281**, 13869-13872.
- Shen, D., Pouliot, L. M., Hall, M. D., & Gottesman, M. M. (2012) Cisplatin Resistance: A Cellular Self-Defense Mechanism Resulting from Multiple Epigenetic and Genetic Changes. *Pharmacological Reviews*, **64**, 706-721.
- Shen, L., Song, C. X., He, C. & Zhang, Y. (2014) Mechanism of function of oxidative reversal of DNA and RNA methylation. *Annual Review of Biochemistry*, **83**, 585-614.
- Shi, C., Pan, B. Q., Shi, F. *et al.* (2018). Sequestosome 1 protects oesophageal squamous carcinoma cells from apoptosis via stabilizing SKP2 under serum starvation condition. *Oncogene*, **37**, 3260-3274.
- Shimamura, A. Montes de Oca, R., Svenson, J. L. *et al.* (2002) A novel diagnostic screen for defects in the Fanconi anemia pathway. *Blood*, **100**, 4649-4654.
- Shinmura, K., Kato, H., Kawanishi, Y. *et al.* (2016) Abnormal Expressions of DNA glycosylase Genes NEIL1, NEIL2 and NEIL3 Are Associated with Somatic Mutation Loads in Human Cancer. *Oxidative Medicine and Cellular Longevity*, **2016**, 1-10.
- Shrivastav, N., Li, D. & Essigmann, J. M. (2010) Chemical biology of mutagenesis and DNA repair: cellular responses to DNA alkylation. *Carcinogenesis*, **31**, 59-70.
- Siddik, Z. (2003) Cisplatin: mode of cytotoxic action and molecular basis of resistance. *Oncogene*, **22**, 7265-7279.
- Siegel, R. L., Miller, K. D. & Jemal, A. (2018) Cancer Statistics, 2018. *CA: A cancer journal for clinicians*, **68**, 7-30.
- Singh, T. R., Ali, A. M., Paramasivam, M. *et al.* (2013) ATR-dependent phosphorylation of FANCM at serine 1045 is essential for FANCM functions. *Cancer Res.* **73**, 4300-4310
- Singleton, M. R., Scaife, S. & Wigley, D. B. (2001) Structural analysis of DNA replication fork reversal by RecG. *Cell*, **107**, 79-89.
- Smith, F. W. & Feigon, J. (1992) Quadruplex structure of oxytricha telomeric DNA oligonucleotides. *Nature*, **356**, 164-168.
- Smith, S. A. & Engelward, B. P. (2000) *In vivo* repair of methylation damage in AAG 3-methyladenine DNA glycosylase null mouse cells. *Nucleic Acids Research*, **28**, 3294-3300.
- Soll, J. M., Sobol, R. W. & Masomparast, N. (2017) Regulation of DNA Alkylation Damage Repair: Lessons and Therapeutic Opportunities. *Trends in Biochemical Sciences*, **42**, 206-218.
- Staresinic, L., Fagbemi, A., Enzlin, J. H. *et al.* (2009) Coordination of dual incision and repair synthesis in human nucleotide excision repair. *The EMBO Journal*, **28**, 1111-1120.
- Stelter, P. & Ulrich, H. D. (2003) Control of spontaneous and damage-induced mutagenesis by SUMO and ubiquitin conjugation. *Nature*, **425**, 188-191.

- Stevnsner, T., Muftuoglu, M., Aamann, M. D. & Bohr, V. A. (2008) The role of Cockayne Syndrome Group B (CSB) protein in BER and aging. *Mechanisms of ageing and development*, **129**, 441-448.
- Stevnsner, T., Nyaga, S., de Souza-Pinto, N. C. (2002) Mitochondrial repair of 8-oxoguanine is deficient in Cockayne syndrome group B. *Oncogene*, **21**, 8675-8682.
- Stewart, M. D., Ritterhoff, T., Klevit, R. E. & Brzovic, P. S. (2016) E2 enzymes: more than just middle men. *Cell Res*, **26**, 423-440.
- Summerfield, S. W. & Tappel, A. L. (1984) Detection and measurement by high-performance liquid chromatography of malondialdehyde crosslinks in DNA. *Analytical Biochemistry*, **143**, 1482-1485.
- Suhasini, A. N. & Brosh, R. M. (2010) Mechanistic and Biological Aspects of Helicase Action on Damaged DNA. *Cell Cycle*, **9**, 2317-2329.
- Suhasini, A. N., Sommers, J. A., Mason, A, C. *et al.* (2009) FANCD1 Helicase Uniquely Senses Oxidative Base Damage in Either Strand of Duplex DNA and Is Stimulated by Replication Protein A to Unwind the Damaged DNA substrate in a Strand-specific Manner. *Journal of Biological Chemistry*, **284**, 18458-18470.
- Takahashi, K., & Yamanaka, S. (2006). Induction of pluripotent stem cells from mouse embryonic and adult fibroblast cultures by defined factors. *Cell*, **126**, 663–676.
- Takahashi, K., Tanabe, K., Ohnuki, M. *et al.* (2007). Induction of pluripotent stem cells from adult human fibroblasts by defined factors. *Cell*, **131**, 861–872.
- Takao, M., Oohata, Y., Kitadokoro, K. *et al.* (2009) Human Nei-like protein NEIL3 has AP lyase activity specific for single-stranded DNA and confers oxidative stress resistance in *Escherichia coli* mutant. *Genes to Cells*, **14**, 261-270.
- Tan, P., Fuchs, S. Y., Chen, A., *et al.*, (1999) Recruitment of a ROC1-CUL1 ubiquitin ligase by Skp1 and HOS to catalyse ubiquitination of I kappa B alpha. *Mol. Cell*, **3**, 527-333.
- Tanaka, S., & Araki, H. (2010) Regulation of the initiation step of DNA replication by cyclin dependent kinases. *Chromosoma*, **119**, 565-574.
- Taniguchi, T., Tischkowitz, M., Ameziane, N. *et al.* (2003) Disruption of the Fanconi-anemia-BRCA pathway in cisplatin sensitive ovarian tumours. *Nature Methods*, **9**, 568-74.
- Taylor, J., Ferry, N. & Elder, R. (2015) RNA interference-based target validation of NEIL3 for use in a cancer selective lectin fusion delivery system. *Tomas Lindahl Conference on DNA Repair*, 17-21 June 2015, Oslo.
- Tedesco, D., Lukasm J. & Reed, J. I. (2002) The pRb-related protein p130 is regulated by phosphorylation-dependent proteolysis via the protein-ubiquitin ligase SCF (Skp2). *Genes & Development*, **16**, 1504-1509.
- Tegel, H., Ottoson, J. & Hober, S. (2011) Enhancing the protein production levels in *Escherichia coli* with a strong promoter. *The FEBS Journal*, **278**, 729-739.

- Theriot, C., A, Hegde, M. L., Hazra, T. & Mitra, S. (2010) RPA physically interacts with the human DNA glycosylase NEIL1 to regulate excision of oxidative DNA base damage in primer-template structures. *DNA Repair*, **9**, 643-652.
- Thiviyanathan, V., Somasunderam, A., Volk, D. E. *et al.* (2008) Base-pairing Properties of the Oxidized Cytosine Derivative, 5-Hydroxy Uracil. *Biochemical and Biophysical Research Communications*, **366**, 752-757.
- Thompson, L.H. & West, M.G. (2000) XRCC1 keeps DNA from getting stranded. *Mutation Research*, **459**, 1-18.
- Thompson, L.H., Brookman, K.W., Dillehay, L.E., *et al.* (1982) A CHO-cell strain having hypersensitivity to mutagens, a defect in DNA strand-break repair, and an extraordinary baseline frequency of sister-chromatid exchange, *Mutation Research*, **95**, 427-440.
- Thorslund, T., von Kobbe, C., Harrigan, J. A., Indig, F. E., Christiansen, M. *et al.* (2005) Cooperation of the Cockayne syndrome group B protein and poly (ADP-ribose) DNA polymerase 1 in the response to oxidative stress. *Molecular and Cellular Biology*, **25**, 7625-7636.
- Torisu, K., Tsuchimoto, D., Ohnishi, Y. & Nakabeppu, Y. (2005) Hematopoietic tissue-specific expression of mouse NEIL3 for endonuclease VIII-like protein. *Journal of Biochemistry*, **138**, 763-772.
- Torok, M. & Etkin, L. D. (2001) Two B or not two B? Overview of the rapidly expanding B-box family of proteins. *Differentiation*, **67**, 63-71.
- Torres-Garcia, S. J., Cousineau, L., Caplan, S. & Panasci, L. (1989). Correlation of resistance to nitrogen mustards in chronic lymphocytic leukemia with enhanced removal of melphalan-induced DNA cross-links. *Biochemical Pharmacology*, **38**, 3122-3123.
- Trakselis, M. A., Cranford, M. T. & Chu, A. M. (2017) Coordination and Substitution of DNA polymerases in Response to Genomic Obstacles. *Chemical Research in Toxicology*, **30**, 1956-1971.
- Tusell, L., Pampalona, J., Soler, D., Frias, C. & Genescà, A. (2010) Different outcomes of telomere-dependent anaphase bridges. *Biochemical Society Transactions*, **38**, 1698-1703.
- Tzelepi, V., Zhang, J., Lu, J. F., *et al.* (2012) Modeling a lethal prostate cancer variant with small-cell carcinoma features. *Clinical Cancer Research*, **18**, 666-677.
- Udeshi, N.D., Mani, D.R., Eisenhaure, T., *et al.* (2012) Methods for quantification of in vivo changes in protein ubiquitination following proteasome and deubiquitinase inhibition. *Mol. Cell. Proteomics*, **11**, 148-159.
- Udeshi, N.D., Svinkina, T., Mertens, P., *et al.* (2013) Refined preparation and use of anti-diglycine remnant (K-ε-GG) antibody enables routine quantification of 10,000s of ubiquitination sites in single proteomics experiments. *Mol Cell Proteomics*, **12**, 825-831.
- Uniprot. (2010) UniProtKB - Q8TAT5 (NEIL3\_HUMAN). <http://www.uniprot.org/uniprot/Q8TAT5> [Accessed 20 June 2016].

- van Loon, B., Markkanen, E. & Hübscher, U. (2010) Oxygen as a friend and enemy: How to combat the mutational potential of 8-oxo-guanine. *DNA Repair*, **9**, 604-616.
- van Ree, J.H., Jeganathan, K., Malureanu, L. & van Deursen, J. M. (2010) Overexpression of the E2 ubiquitin-conjugating enzyme UbcH10 causes chromosome missegregation and tumour formation. *Journal of Cell Biology*, **188**, 83-100.
- Vincze, T., Posfai, J. & Roberts, R.J. (2003) NEBcutter: a program to cleave DNA with restriction enzymes. *Nucleic Acids Research*, **31**, 3688-3691.
- Voulgaridou, G., Anastopoulos, I., Franco, R. Panayiotidis, M. J. & Pappa, A. (2011) DNA damage induced by endogenous aldehydes: Current state of knowledge. *Mutation Research*, **711**, 13-17.
- Wagner, S.A., Beli, P., Weinert, B.T., *et al.* (2011) A proteome-wide, quantitative survey of in vivo ubiquitylation sites reveals widespread regulatory roles. *Mol. Cell. Proteomics*, **10**, M111.013284.
- Wakasugi, M., Sasaki, T., Matsumoto, M. *et al.* (2014) Nucleotide Excision Repair-dependent DNA Double-strand Break Formation and ATM Signalling Activation in Mammalian Quiescent Cells. *Journal of Biological Chemistry*, **289**, 28730-28737.
- Wallace, B. D., Berman, Z., Mueller, G. A. *et al.* (2016) Ape2 Zf-GRF facilitates 3'-5' resection of DNA damage following oxidative stress. *Proceedings of the National Academy of Sciences of the United States of America*, **114**, 304-309.
- Wallace, S. (2014). Base excision repair: A critical player in many games. *DNA repair*, **19**, 14-26.
- Wallace, S., Bandaru, V., Kathe, S. & Bond, J. (2003) The enigma of endonuclease VIII. *DNA Repair*, **13**, 441-453.
- Wallace, S., Murphy, D. & Sweasy, J. (2012). Base excision repair and cancer. *Cancer Letters*, **327**, 73-89.
- Wang, A. T., Sengerová, B., Catell, E. *et al.* (2011) Human SNM1A and ERCC1-XPF collaborate to initiate DNA interstrand cross-link repair. *Genes and Development*, **25**, 1859-1870.
- Wang, C., Xu, J., Fu, H. *et al.* (2018) TRIM32 promotes cell proliferation and invasion by activating  $\beta$ -catenin signalling in gastric cancer. *Journal of Cellular and Molecular Medicine*, 1-9.
- Wang, J. C. & Gautier, J. (2010) The Fanconi anemia pathway and ICL repair: implications for cancer therapy. *Critical reviews in biochemistry and molecular biology*, **45**, 424-439.
- Wang, L., Li, S. & Dorf, M. E. (2012) NEMO binds ubiquitinated TANK-binding Kinase 1 (TBK1) to regulate innate immune responses to RNA viruses. *PLoS One*, **7**, e43756.
- Wang, L., Yang, H., Palmbo, P.L. *et al.* (2014) AtDC/TRIM29 phosphorylation by ATM/MAPKAP kinase 2 mediates radioresistance in pancreatic cancer cells. *Cancer Research*, **74**, 1778-1788.

- Wang, Y., He, D., Yang, L. *et al.* (2015a) TRIM26 functions as a novel tumour suppressor of hepatocellular carcinoma and its downregulation contributes to worse prognosis. *Biochemical and biophysical research communications*, **463**, 458-465.
- Wang, P., Zhao, W., Zhao, K., Zhang, L. & Gao, C. (2015b) TRIM26 Negatively Regulates Interferon- $\beta$  Production and Antiviral response through Polyubiquitination and Degradation of Nuclear IRF3. *PLoS Pathogens*, **11**, e1004726
- Wang, W. (2007) Emergence of a DNA-damage response network consisting of Fanconi anemia and BRCA proteins. *Nature reviews genetics*, **8**, 735-748.
- Watanabe, M. & Hatakeyama, S. (2017) TRIM proteins and diseases. *Journal of Biochemistry*, **161**, 135-144.
- Weinfeld, M., Mani, R.S., Abdou, I., Aceytuno, R.D., Glover, J.N. (2011) Tidying up loose ends: the role of polynucleotide kinase/phosphatase in DNA strand break repair, *Trends Biochem. Sci*, **36**, 262–271.
- Weiss, J., Goode, J., Ladiges, W. & Ulrich, C. (2005) Polymorphic variation in hOGG1 and risk of cancer: a review of the functional and epidemiological literature. *Molecular Carcinogenesis*, **42**, 127-141.
- Weissman, A. M. (2001) Themes and variations on ubiquitylation. *Mol. Cell Biol.* **2**, 169–178.
- Weller, M., Stupp, R., Reifenberger, G., Brandes, A. A, van den Bent, M. J. *et al.* (2010) MGMT promoter methylation in malignant gliomas: ready for personalized medicine? *Nature Reviews Neurology*, **6**, 39-51.
- Wenzel, E. S. & Singh, A. T. K. (2018) Cell-cycle Checkpoints and Aneuploidy on the Path to Cancer. *In Vivo*, **32**, 1-5.
- Wilkinson, K. D. (2009). DUBs at a glance. *J. Cell Sci*, **122**, 2325–2329.
- Will, O., Gocke, I., Eckert, I. *et al.*, (1999) Oxidative DNA damage and mutations induced by a polar photosensitizer, Ro19-8022. *Mutation Research*, **435**, 89-101.
- Williams, H. L., Gottesman, M. E. & Gautier, J. (2012) Replication-independent repair of DNA interstrand crosslinks. *Mol Cell*, **47**, 140-147.
- Williams, S. C. & Parsons, J. L. (2018) NTH1 is a new target for ubiquitylation-dependent regulation by TRIM26 required for the cellular response to oxidative stress. *Molecular and Cellular Biology*, **38**, e00616-17.
- Williamson, J. R., Raghuraman, M. K. & Cech, T. R. (1989) Monovalent cation-induced structure of telomeric DNAL The G-quartet model. *Cell*, **59**, 871-880.
- Witkiewicz, A. K., McMillan, E. A., Balaji, U. *et al.* (2015) Whole-exome sequencing of pancreatic cancer defines genetic diversity and therapeutic targets. *Nature Communications*, **6**, 6744.
- Wong, H. K., Muftuoglu, M., Beck, G., Imam, S. Z., Bogr, V, A. *et al.* (2007) Cockayne syndrome B protein stimulates apurinic endonuclease 1 activity and protects against agents that introduce BER intermediates. *Nucleic Acids Research*, **35**, 4103-4113.

- Wood, R. D. (2010) Mammalian nucleotide excision repair proteins and interstrand crosslink repair. *Environmental and Molecular Mutagenesis*, **51**, 520-526.
- Wu, Z., Shen, S., Zhang, Z., Zhang, W. & Xiao, W. (2014). Ubiquitin-conjugating enzyme complex Uev1-Ubc13 promotes breast cancer metastasis through nuclear factor-small ka, CyrillicB mediated matrix metalloproteinase-1gene regulation. *Breast Cancer Research*, **16**, R75.
- Xin, B. (2015) Mechanisms of DNA damage tolerance. *World Journal of Biologocial Chemistry*, **6**, 48-56.
- Xu, W., Ouellette, A., Shosh, S., O'Neil, T. C., Greenberg, M. M. & Zhao, L. (2015) Mutagenic bypass of an Oxidized Abasic lesion induced DNA interstrand cross-link Analogue by Human Translesion Synthesis DNA polymerases. *Biochemistry*, **54**, 7409-7422.
- Yamamoto, K. N., Kobayashi, S., Tsuda, M. *et al.* (2011) Involvement of SLX4 in interstrand cross-link repair is regulated by the Fanconi anemia pathway. *Proceeding of the National Academy of Sciences of the U.S.A*, **108**, 6492-6496.
- Yamamoto, R., Ohshiro, Y., Shimotani, T. *et al.* (2014) Hypersensitivity of mouse NEIL1-knockdown cells to hydrogen peroxide during S phase. *Journal of Radiation Research*, **55**, 707-712.
- Yamazaki, S., Hayano, M. & Masai, H. (2013) Replication timing regulation of eukaryotic replicons: Rif1 as a global regulator of replication timing. *Trends in Genetics*, **29**, 449-460.
- Yang, B., O'Herrin, S.M., Wu, J., *et al.* (2007) MAGE-A, mMage-b, and MAGE-C proteins form complexes with KAP1 and sup- press p53-dependent apoptosis in MAGE-positive cell lines. *Cancer Res*, **67**, 9954–9962.
- Yang, H., Lu, X., Liu, Z. *et al.* (2015) FBXW7 suppresses epithelial-mesenchymal transition, stemness and metastatic potential of cholangiocarcinoma cells. *Oncotarget*, **6**, 6310-6325.
- Yang, Y., Kitagaki, J., Wang, H., Hou, D. & Perantoni, A. O. (2009) Targeting the ubiquitin-proteasome system for cancer therapy. *Cancer Science*, **100**, 24-28.
- Yang, Z., Nejad, M. I., Varela, J. G., Price, N. E., Wang, Y. & Gates, K. S. (2017) A role for the BER enzyme NEIL3 in replication-dependent repair of interstrand DNA cross-links derived from psoralen and abasic sites. *DNA Repair*, **52**, 1-11.
- Yao, Y. & Dai, W. (2014) Genomic Instability and Cancer. *Journal of carcinogenesis & mutagenesis*, **5**, 1-17.
- Ye, Y. & Rape, M. (2009) Building ubiquitin chains: E2 enzymes at work. *Nature Rev. Mol. Cell Biol*, **10**, 755–764.
- Yokoi, M., Masutani, C., Maekawa, T. *et al.* (2000) The xeroderma pigmentosum group C protein complex XPC HR23B plays an important role in the recruitment of transcription factor IIH to damaged DNA. *Journal of Biological Chemistry*, **275**, 9870-9875.

- Yoon, J., Bhatia, G., Prakash, S. & Prakash, L. (2010) Error-free replicative bypass of thymine glycol by the combined action of DNA polymerases  $\kappa$  and  $\zeta$  in human cells. *Proceedings of the National Academy of Sciences of the U.S.A*, **107**, 14116-14121.
- Yoshioka, K., Yoshioka, Y. & Hsieh, P. (2006) ATR kinase activation mediated by MutS $\alpha$  and MutL $\alpha$  in response to cytotoxic O6-methylguanine adducts. *Mol Cell*, **22**, 501-510.
- Yu, J., Vodyanik, M.A., Smuga-Otto, K. *et al.* (2007). Induced pluripotent stem cell lines derived from human somatic cells. *Science*, **318**, 1917–1920.
- Zafar, M. K. & Eoff, R. L. (2017) Translesion DNA synthesis in Cancer: Molecular Mechanisms and Therapeutic Opportunities. *Chemical Research in Toxicology*, **30**, 1942-1955.
- Zeman, M. K. & Cimpirich, K. A. (2014) Causes and consequences of replication stress. *Nature Cell Biology*, **16**, 2-9.
- Zhang, J., Dewar, J. M., Budzowzka, M. *et al.* (2015) DNA interstrand cross-link repair requires replication-fork convergence. *Nature structural and molecular biology*, **22**, 242-247.
- Zhao, W., Li, Q., Ayers, S. *et al.* (2013) Jmjd3 Inhibits Reprogramming by Upregulating expression of Ink4a/Arf and Targeting for Ubiquitination. *Cell*, **152**, 1037-1050.
- Zheng, N. & Shabek, N. (2017) Ubiquitin Ligases: Structure, Function, and Regulation. *Annual Review of Biochemistry*, **86**, 129-157.
- Zhou, H., Xu, M., Huang, Q. *et al.* (2008) Genome-Scale RNAi Screen for Host Factors Required for HIV Replication. *Cell Host & Microbe*, **4**, 495-504.
- Zhou, J., Chan, J., Lambel , M. *et al.* (2017) Neil3 repairs Telomere Damage during SPhase to Secure Chromosome Segregation at Mitosis. *Cell Reports*, **20**, 2044-2056.
- Zhou, J., Liu, M., Fleming, A. M., Burrows, C. J. & Wallace, S. (2013) NEIL3 and NEIL1 DNA Glycosylases Remove Oxidative Damages from Quadruplex DNA and Exhibit Preferences for Lesions in the Telomeric Sequence Context. *Journal of Biological Chemistry*, **288**, 27263–27272.
- Zolner, A. E., Abdou, I., Ye, R. *et al.* (2011) Phosphorylation of polynucleotide kinase/phosphatase by DNA- dependent protein kinase and ataxia-telangiectasia mutated regulates its association with sites of DNA damage. *Nucleic Acids Research*, **39**, 9224-9237.
- Zou, L. & Elledge, S. (2003) Sensing DNA damage through ATRIP recognition of RPA-ss-DNA complexes. *Science*, **300**, 1542-1548.

## Appendices.

**Appendix Table 1: Sequences of oligonucleotides used in the “characterisation of the hNEIL1 and hNEIL3 DNA glycosylases in the repair of psoralen interstrand DNA crosslinks”.**

Oligonucleotide name	Oligonucleotide sequence (5'-3')	TpA site position and possible cleavage product size.
<b>R18</b> , 18 mer	GCUCUCGUCUGTACACCG	TpA position 12-13; excision of T12 generates an 11 mer cleavage product.
<b>D21</b> , 21 mer	CTTCGGTGTACAGACGAGAGC	TpA position 9-10; excision of T9 generates 8 mer cleavage product
<b>C21</b> , 21 mer	GCTCTCGTCTGTACACCGAAG)	TpA position 12-13; excision of T12 generates 11 mer cleavage product
<b>C47</b> , 47 mer	GACGACGACAAGGCTCTCGTCTGTACAC CGAAGAGCTGCTCTGCCTG	TpA position 24-25; excision of T24 generates 23 mer cleavage product
<b>D47</b> , 47 mer	CAGGCAGAGCAGCTCTTCGGTGTACAGACGAGAGCCTTGTCGTCGTC	TpA position 23-24; excision of T23 generates 22 mer cleavage product
<b>C101</b> , 101 mer	GCCGGTAAAAATATACGATGGCTGC AAGACGACGACAAGGCTCTCGTCTGTACACCGAAGAGCTGCTCTGCCTGG AGACAGCACAGCTGCCCAAGGTGTT C	TpA position 51-52; excision of T51 generates 50 mer cleavage product
<b>D101</b> , 101 mer	GAACACCTTGGGCAGCTGTGCTGTC TCCAGGCAGAGCAGCTCTTCGGTGTACAGACGAGAGCCTTGTCGTCGTC TGCAGCCATCGTATATTTTTACCGGC	TpA position 50-51; excision of T50 generates 49 mer cleavage product
<b>Sp1</b> , 17 mer	CCACCAAC[Sp1]CTACCACC	Sp1 position 9; excision of Sp19 generates 8 mer cleavage product

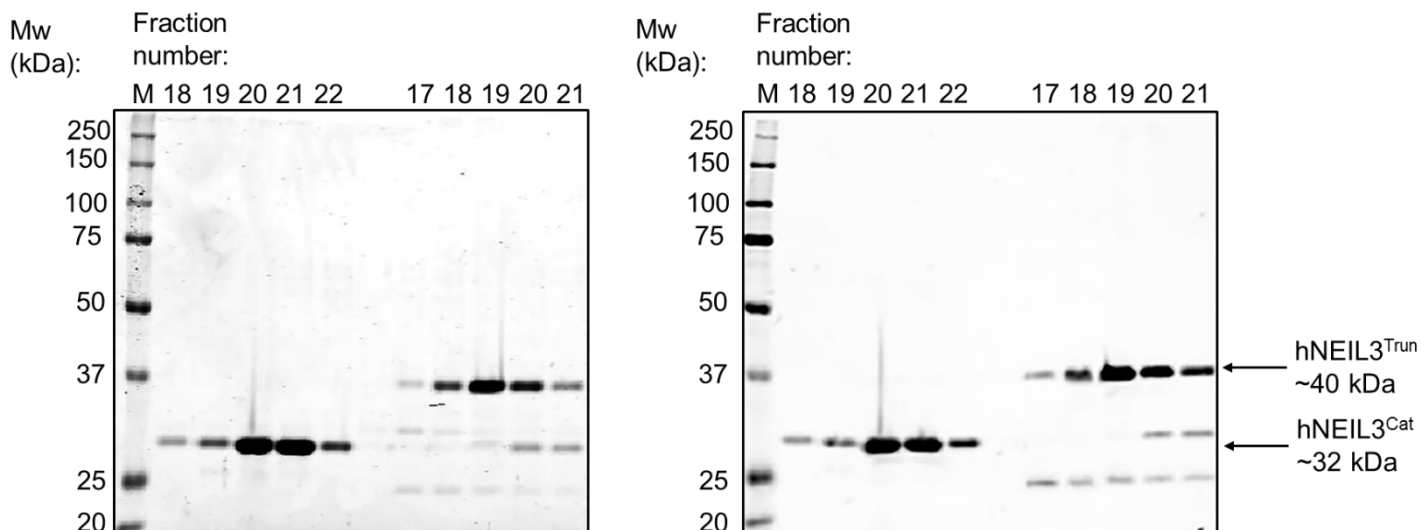
<b>Sp1 complement,</b> 17 mer	GGTGGTAGCGTTGGTGG	Cytosine complementary to Sp1 at position 10
<b>D21-U, 21 mer</b>	CTTCGGTGUACAGACGAGAGC	U position 9; excision of U9 generates 8 mer cleavage product
<b>C47-U, 21 mer</b>	GACGACGACAAGGCTCTCGTCTGUA CACCGAAGAGCTGCTCTGCCTG	U position 24; excision of U24 generates 23 mer cleavage product

**Appendix Table 2: LC-MS proteomic analysis results, showing matched proteins after database alignment with detected peptides.** An ion score cut off of 25 was used. hNEIL3<sup>Cat</sup> is expected to be ~32 kDa, however is detected at ~33 kDa. This is accounted for with the addition of C-terminal polyhistidine tag present in fusion with the recombinant protein. Major protein contaminants include keratin proteins, characteristically detected after handling procedures and in trypsin used in the protein band purification process. The lowest scoring protein detected in this list was the co-expressed *E. coli* MAP1 (*EcoMap*) protein. (Accession) Protein Accession number. (Score) MS/MS Ion score, matched to amino acid sequences, higher score indicates increased confidence.

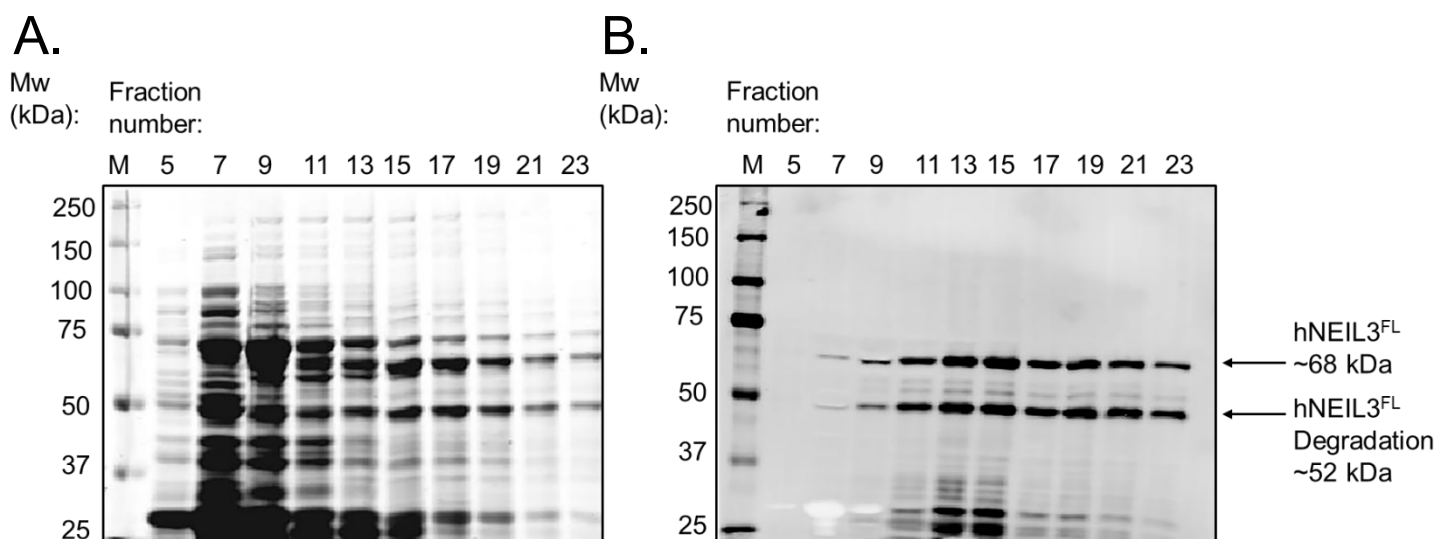
Accession	Score	Mass	Number of sequences	Description
<b>hNEIL3 (843)</b>	<b>7578</b>	<b>33471</b>	<b>15</b>	<b>hNEIL3 (843) provided reference sequence</b>
sp P04264 K2C1_HUMAN	6951	66170	37	sp P04264 K2C1_HUMAN Keratin, type II cytoskeletal 1 OS=Homo sapiens GN=KRT1 PE=1 SV=6
sp P13645 K1C10_HUMAN	4043	59020	28	sp P13645 K1C10_HUMAN Keratin, type I cytoskeletal 10 OS=Homo sapiens GN=KRT10 PE=1 SV=6
sp P35527 K1C9_HUMAN	3688	62255	20	sp P35527 K1C9_HUMAN Keratin, type I cytoskeletal 9 OS=Homo sapiens GN=KRT9 PE=1 SV=3
sp Q6IMF3 K2C1_RAT	2751	65190	9	sp Q6IMF3 K2C1_RAT Keratin, type II cytoskeletal 1 OS=Rattus norvegicus GN=Krt1 PE=2 SV=1
sp P35908 K22E_HUMAN	2701	65678	28	sp P35908 K22E_HUMAN Keratin, type II cytoskeletal 2 epidermal OS=Homo sapiens GN=KRT2 PE=1 SV=2
sp Q3MHN7 NEIL3_BOVIN	1808	69222	6	sp Q3MHN7 NEIL3_BOVIN Endonuclease 8-like 3 OS=Bos taurus GN=NEIL3 PE=2 SV=2
sp P00761 TRYP_PIG	1299	25078	3	sp P00761 TRYP_PIG Trypsin OS=Sus scrofa PE=1 SV=1
sp P04259 K2C6B_HUMAN	896	60315	19	sp P04259 K2C6B_HUMAN Keratin, type II cytoskeletal 6B OS=Homo sapiens GN=KRT6B PE=1 SV=5
sp P02533 K1C14_HUMAN	814	51872	17	sp P02533 K1C14_HUMAN Keratin, type I cytoskeletal 14 OS=Homo sapiens GN=KRT14 PE=1 SV=4
sp P08779 K1C16_HUMAN	702	51578	16	sp P08779 K1C16_HUMAN Keratin, type I cytoskeletal 16 OS=Homo sapiens GN=KRT16 PE=1 SV=4
sp P02538 K2C6A_HUMAN	600	60293	20	sp P02538 K2C6A_HUMAN Keratin, type II cytoskeletal 6A OS=Homo sapiens GN=KRT6A PE=1 SV=3
sp P13647 K2C5_HUMAN	596	62568	24	sp P13647 K2C5_HUMAN Keratin, type II cytoskeletal 5 OS=Homo sapiens GN=KRT5 PE=1 SV=3
sp Q04695 K1C17_HUMAN	380	48361	14	sp Q04695 K1C17_HUMAN Keratin, type I cytoskeletal 17 OS=Homo sapiens GN=KRT17 PE=1 SV=2
sp P0AA43 RSUA_ECOLI	221	25963	3	sp P0AA43 RSUA_ECOLI Ribosomal small subunit pseudouridine synthase A OS=Escherichia coli (strain K12) GN=rsuA PE=1 SV=1
sp P76422 THID_ECOLI	120	28787	2	sp P76422 THID_ECOLI Hydroxymethylpyrimidine/phosphomethylpyrimidine kinase OS=Escherichia coli (strain K12) GN=thid PE=1 SV=1
sp P15924 DESP_HUMAN	95	334021	7	sp P15924 DESP_HUMAN Desmoplakin OS=Homo sapiens GN=DSP PE=1 SV=3
sp P81605 DCD_HUMAN	81	11391	2	sp P81605 DCD_HUMAN Dermcidin OS=Homo sapiens GN=DCD PE=1 SV=2
sp P0AE18 MAP1_ECOLI	55	29711	2	sp P0AE18 MAP1_ECOLI Methionine aminopeptidase OS=Escherichia coli (strain K12) GN=map PE=1 SV=1

**Appendix Table 3: LC-MS proteomic analysis results, showing matched proteins after database alignment with detected peptides.** An ion score cut off of 25 was used. hNEIL3<sup>Cat</sup> is expected to be ~32 kDa, however is detected at ~33 kDa. This is accounted for with the addition of C-terminal polyhistidine tag present in fusion with the recombinant protein. Major protein contaminants include keratin proteins, characteristically detected after handling procedures and in trypsin used in the protein band purification process. The second highest scoring protein detected in this list was the co-expressed *E. coli* MAP1 (*EcoMap*) protein. (Accession) Protein Accession number. (Score) MS/MS Ion score, matched to amino acid sequences, higher score indicates increased confidence.

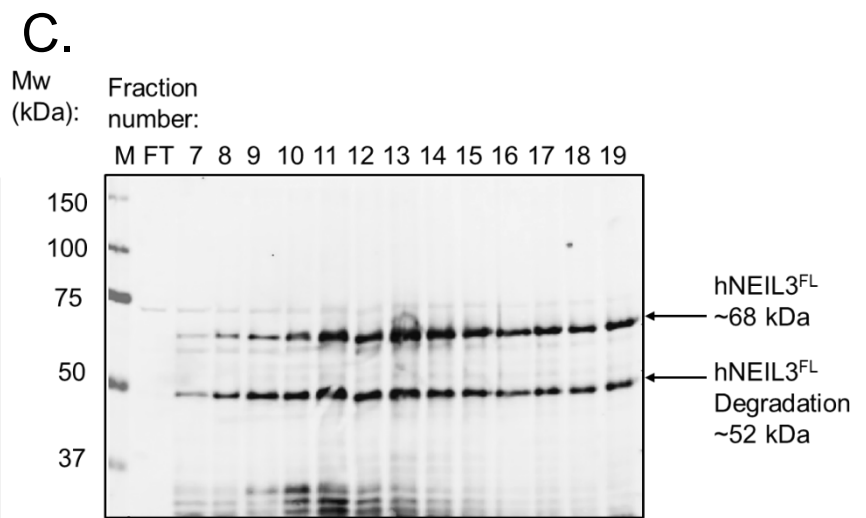
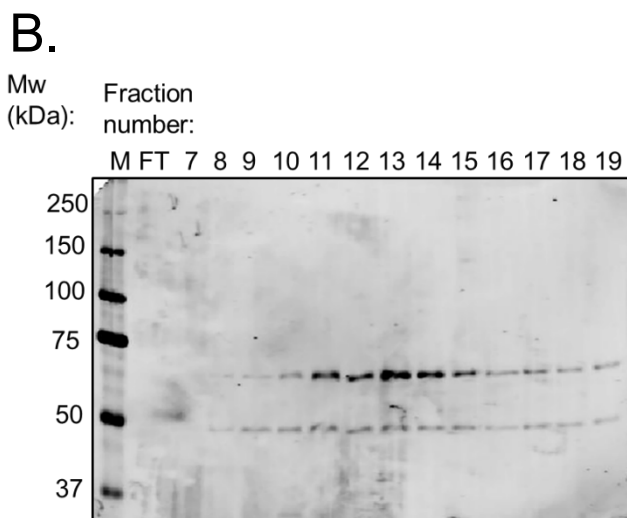
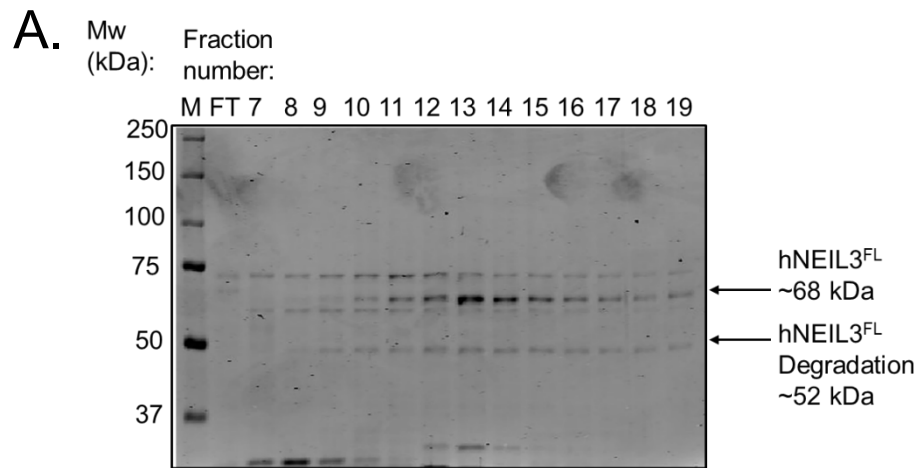
Accession	Score	Mass	Number of sequences	Description
<b>hNEIL3 (843 K81A)</b>	<b>8345</b>	<b>33471</b>	<b>13</b>	<b>hNEIL3 (843 K81A) provided reference sequence</b>
sp P0AE18 MAP1_ECOLI	3941	29711	16	sp P0AE18 MAP1_ECOLI Methionine aminopeptidase OS=Escherichia coli (strain K12) GN=map PE=1 SV=1
sp P04264 K2C1_HUMAN	3609	66170	26	sp P04264 K2C1_HUMAN Keratin, type II cytoskeletal 1 OS=Homo sapiens GN=KRT1 PE=1 SV=6
sp P13645 K1C10_HUMAN	2868	59020	21	sp P13645 K1C10_HUMAN Keratin, type I cytoskeletal 10 OS=Homo sapiens GN=KRT10 PE=1 SV=6
sp Q3MHN7 NEIL3_BOVIN	2166	69222	5	sp Q3MHN7 NEIL3_BOVIN Endonuclease 8-like 3 OS=Bos taurus GN=NEIL3 PE=2 SV=2
sp P35527 K1C9_HUMAN	1826	62255	16	sp P35527 K1C9_HUMAN Keratin, type I cytoskeletal 9 OS=Homo sapiens GN=KRT9 PE=1 SV=3
sp P00761 TRYP_PIG	1807	25078	3	sp P00761 TRYP_PIG Trypsin OS=Sus scrofa PE=1 SV=1
sp P35908 K22E_HUMAN	1719	65678	24	sp P35908 K22E_HUMAN Keratin, type II cytoskeletal 2 epidermal OS=Homo sapiens GN=KRT2 PE=1 SV=2
sp Q6IMF3 K2C1_RAT	1406	65190	9	sp Q6IMF3 K2C1_RAT Keratin, type II cytoskeletal 1 OS=Rattus norvegicus GN=Krt1 PE=2 SV=1
sp P0AA43 RSUA_ECOLI	1104	25963	7	sp P0AA43 RSUA_ECOLI Ribosomal small subunit pseudouridine synthase A OS=Escherichia coli (strain K12) GN=rsuA PE=1 SV=1
sp P0A7V0 RS2_ECOLI	832	26784	7	sp P0A7V0 RS2_ECOLI 30S ribosomal protein S2 OS=Escherichia coli (strain K12) GN=rpsB PE=1 SV=2
sp P02533 K1C14_HUMAN	509	51872	9	sp P02533 K1C14_HUMAN Keratin, type I cytoskeletal 14 OS=Homo sapiens GN=KRT14 PE=1 SV=4
sp P0A9K9 SLYD_ECOLI	298	21182	2	sp P0A9K9 SLYD_ECOLI FKBP-type peptidyl-prolyl cis-trans isomerase SlyD OS=Escherichia coli (strain K12) GN=slyD PE=1 SV=1
sp P0A7V8 RS4_ECOLI	200	23512	4	sp P0A7V8 RS4_ECOLI 30S ribosomal protein S4 OS=Escherichia coli (strain K12) GN=rpsD PE=1 SV=2
sp A5A6M8 K2C5_PANTR	134	62728	15	sp A5A6M8 K2C5_PANTR Keratin, type II cytoskeletal 5 OS=Pan troglodytes GN=KRT5 PE=2 SV=1
sp COQ0B0 RS3_SALPC	112	25967	2	sp COQ0B0 RS3_SALPC 30S ribosomal protein S3 OS=Salmonella paratyphi C (strain RKS4594) GN=rpsC PE=3 SV=1
sp COQ6K4 LPXA_SALPC	106	28357	2	sp COQ6K4 LPXA_SALPC Acyl-[acyl-carrier-protein]--UDP-N-acetylglucosamine O-acyltransferase OS=Salmonella paratyphi C (strain RKS4594) GN=lpxA PE=3 SV=1
sp P81605 DCD_HUMAN	84	11391	2	sp P81605 DCD_HUMAN Dermcidin OS=Homo sapiens GN=DCD PE=1 SV=2
sp AOKRL9 RS12_SHESA	51	13809	2	sp AOKRL9 RS12_SHESA 30S ribosomal protein S12 OS=Shewanella sp. (strain ANA-3) GN=rpsL PE=3 SV=1



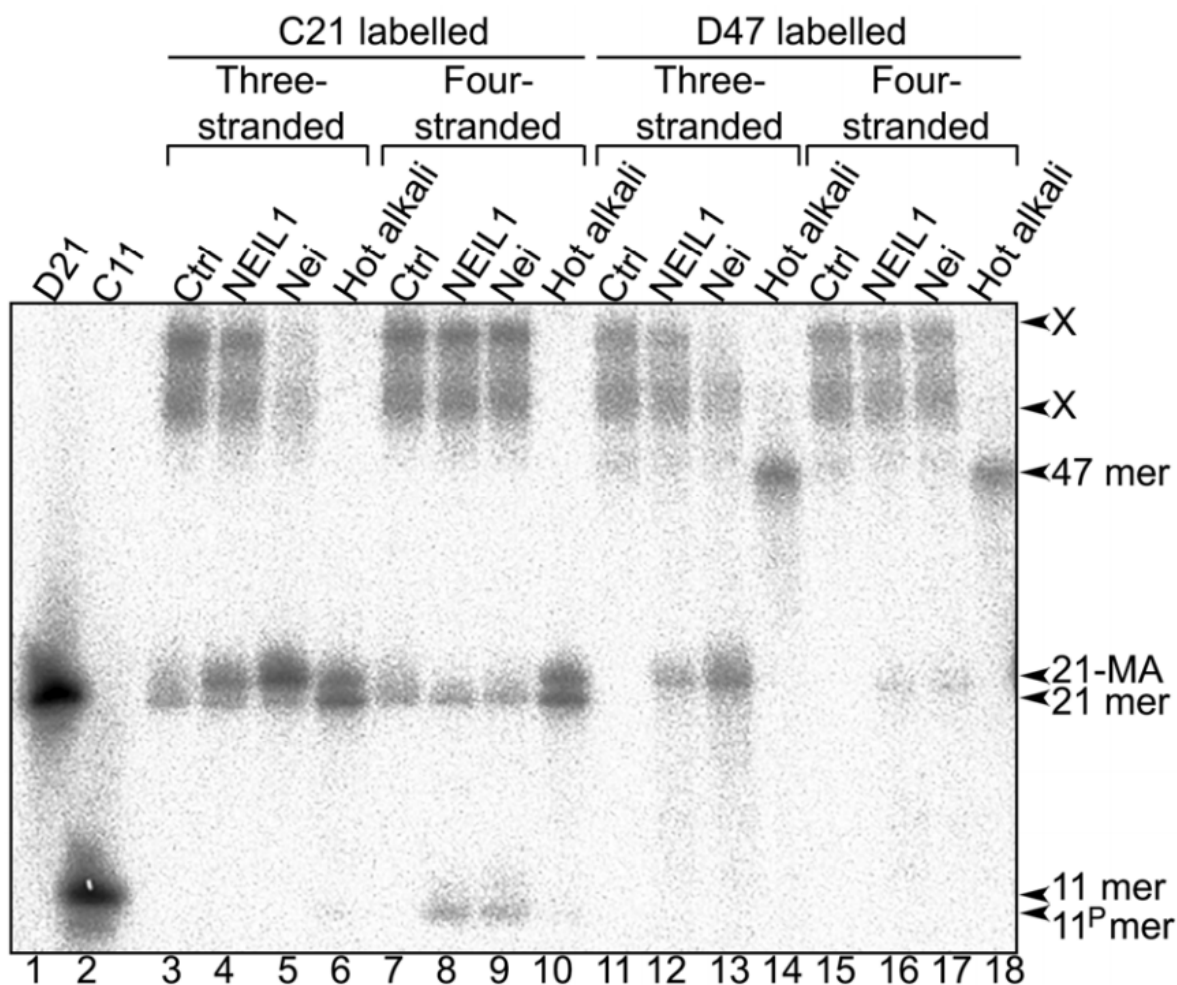
**Appendix Figure 1: ÄKTA FPLC HisTrap HP purification analysis of recombinant hNEIL3<sup>Cat</sup> and hNEIL3<sup>Trun</sup>.** A. 10% SDS-PAGE analysis stained with Instant-blue coomassie blue (Merk). B. Anti-His western blot analysis. Target protein bands annotated. (M) BioRad All Blue Prestained Protein Standard (Mustafa Albelazi).



**Appendix Figure 2: ÄKTA FPLC HisTrap HP purification analysis of recombinant hNEIL3<sup>FL</sup>.** A. 10% SDS-PAGE analysis stained with Instant-blue coomassie blue (Merk). B. Anti-His western blot analysis. Target protein bands annotated. (M) BioRad All Blue Prestained Protein Standard (Mustafa Albelazi).



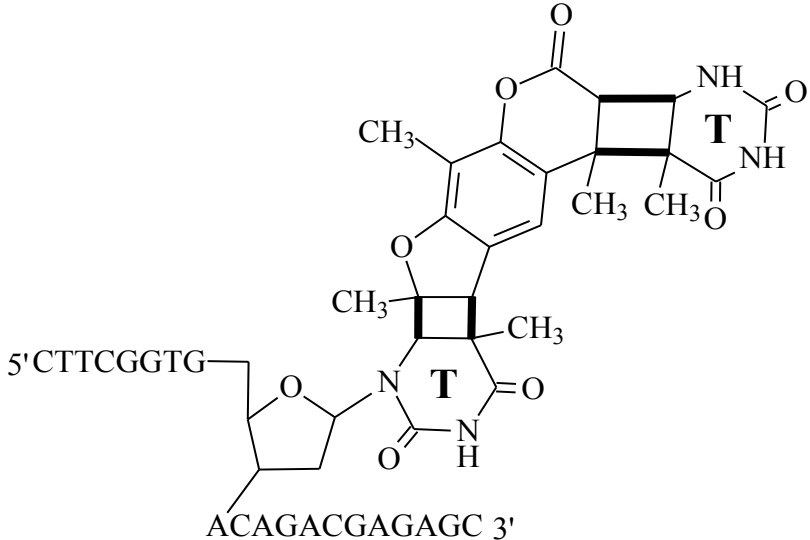
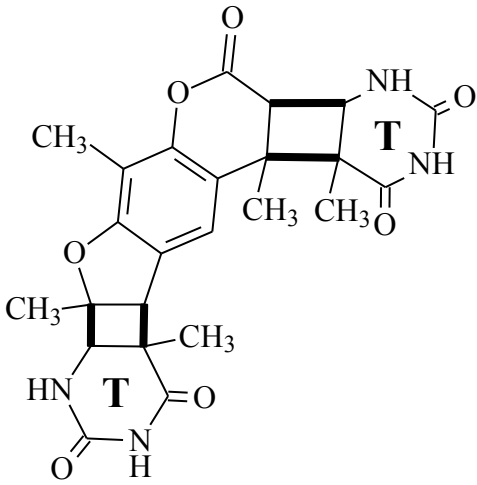
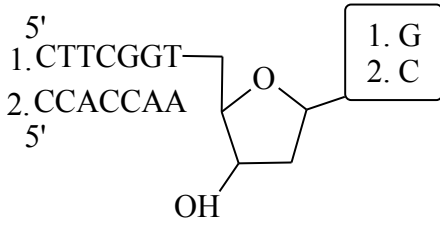
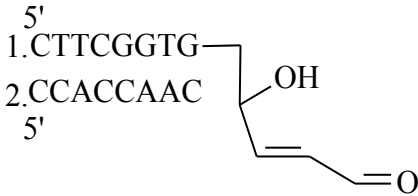
**Appendix Figure 3: ÄKTA FPLC Mono S 5/50 GL purification analysis of recombinant hNEIL3<sup>FL</sup>.** **A.** 10% SDS-PAGE analysis stained with Instant-blue coomassie blue (Merk). **B.** Anti-His western blot analysis. **C.** Anti-NEIL3 western blot analysis. Target protein bands annotated. (M) BioRad All Blue Prestained Protein Standard (Mustafa Albelazi).

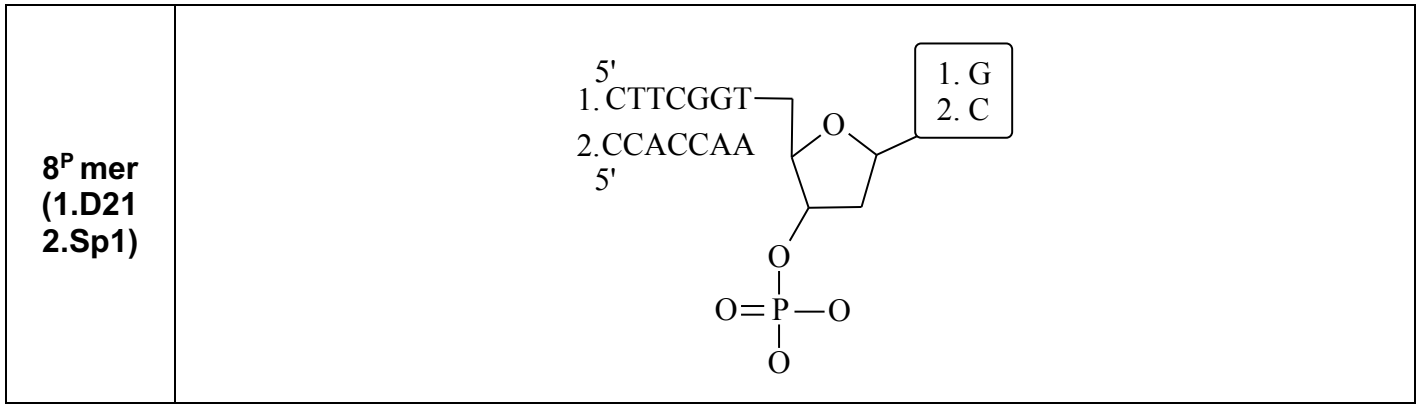


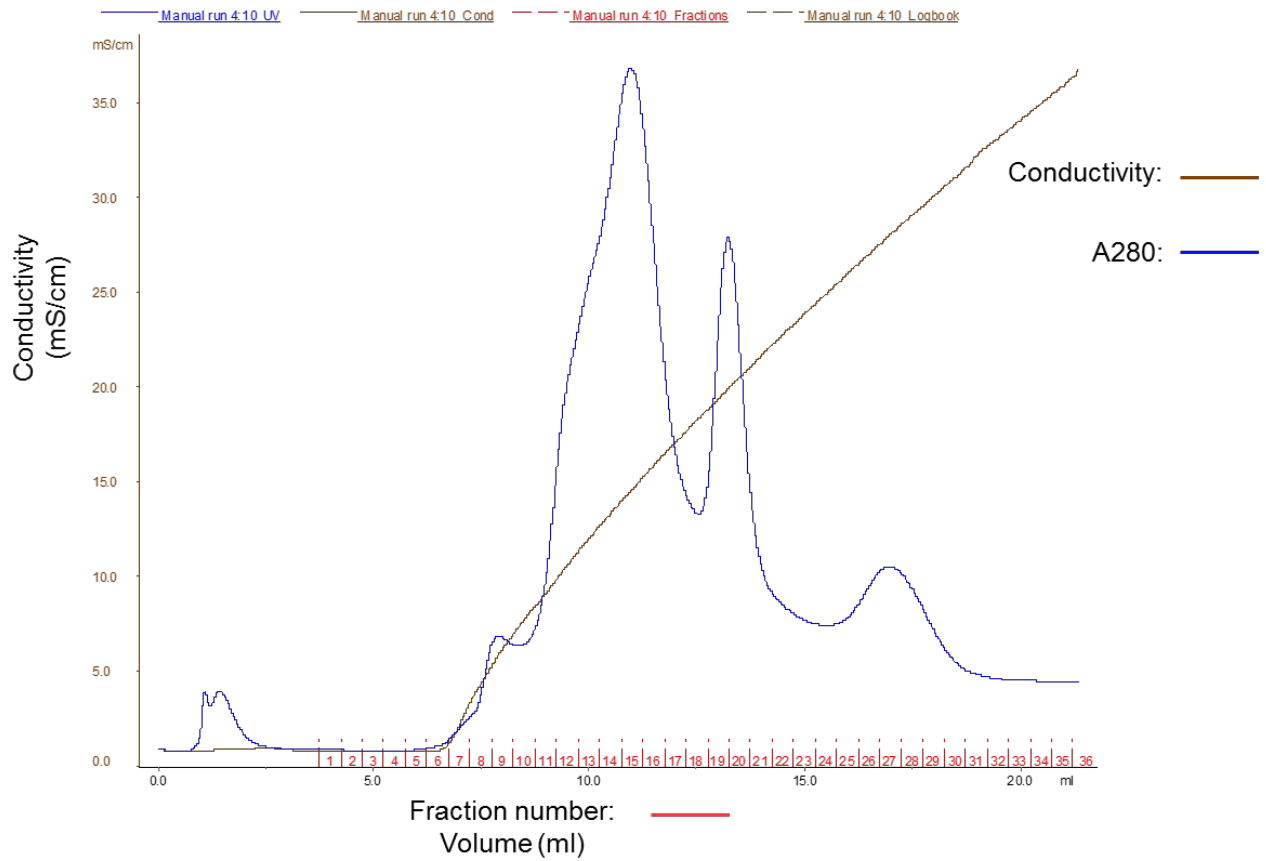
**Appendix Figure 4: Denaturing PAGE analysis of hNEIL1 and Nei protein incubated with XL47 • 47 - 21\*, XL47 • 47\* - 21 • 21, XL47 • 47 - 21\* • 21, or XL47 • 47\* - 21 • 21 (Sophie Couvé, Gustave Roussy Institute).** Samples were incubated for 1 h at 37°C. For positive control 20 nM of bacterial Nei was used and hNEIL1. C21/D47 hot alkali treated duplex ICL MA product control. D21 and C11 3' OH size markers. Substrate and cleavage products sizes are indicated to the right of the gel. Substrate and cleavage products sizes are indicated to the right of the gel. "X" denotes substrate, "47 mer" denotes alkaline cleavage product containing either MA or regular thymine residue, "21-MA" denotes 21 mer fragment containing 8-MOP-derived MA. "21 mer" denotes 21 mer size marker, and "11 mer" denotes 11 mer size marker. "11<sup>P</sup>mer" denotes cleavage fragment of 11 mer with 3' terminal P.

Appendix Table 4: The skeletal formula of HMT generated MAp, MAf, ICLs and DNA products generated by Nei-like DNA glycosylases, UNG, Nfo mediated cleavage and piperidine treatments.

Cleavage product	Chemical structure
<p><b>D21-C47 ICL</b></p>	
<p><b>21 mer-MAf (furan)</b></p>	
<p><b>21 mer-MAp (pyrone)</b></p>	

<p><b>21 mer DNA(T)- HMT-T</b></p>	
<p><b>T-HMT-T</b></p>	
<p><b>8<sup>OH</sup> mer (1.D21 2.Sp1)</b></p>	
<p><b>8<sup>PA</sup> mer (1.D21 2.Sp1)</b></p>	





**Appendix Figure 5: CHT ceramic hydroxyapatite column (Bio-Rad, Hemel Hempstead, United Kingdom) FPLC purification of pooled and buffer exchanged HiLoad Mono Q sepharose fractions 20-24 (Williams and Parsons, 2018).**

**Appendix Table 5: LC-MS tandem mass spectrometry analysis.** Q Exactive instrument operated in data-dependent positive (electrospray ionization<sup>+</sup> [ESI<sup>+</sup>]) mode was used, showing matched proteins after database alignment with detected peptides in final Mono Q (2 mL) fraction 25 (Edmonds *et al.*, 2017; Williams and Parsons, 2018). Tripartite motif-containing protein 26 highlighted in bold and only E3 ubiquitin-ligase detected in fraction. Matched amino acids are highlighted in red (taken from Williams and Parsons, 2018).

Number	Score	Description
Q01105	530	Protein SET
P35527	395	Keratin, type I cytoskeletal 9
P35908	257	Keratin, type I cytoskeletal 2
P13645	220	Keratin, type I cytoskeletal 10
P04264	216	Keratin, type II cytoskeletal 1
P04259	109	Keratin, type II cytoskeletal 6B
P02533	107	Keratin, type I cytoskeletal 14
P08579	101	U2 small nuclear ribonucleoprotein B
P39687	95	Acid leucine-rich nuclear phosphoprotein 32
P13647	93	Keratin, type II cytoskeletal 5
P62318	93	Small nuclear ribonucleoprotein Sm D3
P09661	90	U2 small nuclear ribonucleoprotein A

Number	Score	Description
P62318	84	Small nuclear ribonucleoprotein F
P02538	76	Keratin, type II cytoskeletal 6A
P62316	74	Small nuclear ribonucleoprotein Sm D2
O00629	69	Importin subunit alpha-3
P05455	66	Lupus La protein
P14678	66	Small nuclear ribonucleoprotein-associated proteins B and B'
<b>Q12899</b>	<b>62</b>	<b>Tripartite motif-containing protein 26</b>
Q92688	61	Acid leucine-rich nuclear phosphoprotein 32
P07437	59	Tubulin beta chain
P11142	58	Heat shock cognate 71 kDa protein
P11021	53	78 kDa glucose-related protein

```

1   MATSAPLRSL EEEVTCISL  DYLRDPVTID  CGHVFCRSCT  TDVRPISGSR
51  PVCPLCKKPF KKENIRPVWQ  LASLVENIER  LKVDKGRQPG  EVTREQQDAK
101 LKERHREKLH YCEDDGKLL  CVMCRSREH  RPHTAVLMEK  AAQPHREKIL
151 NHLSTLRRDR DKIQGFQAKG  EADILAALKK  LQDQRQYIVA  EFEQGHQFLR
201 EREEHLLLEQL AKLEQELTEG  REKFKSRGVG  ELARLALVIS  ELEGKAQQPA
251 AELMQDTRDF LNRYPRKKFW VGKPIARVVK  KKTGEFSDKL  LSLQRGLREF
301 QGKLLRDLEY KTVSVTLDPQ  SASGYLQLSE  DWKCVTYTSL  YKSAYLHPQQ
351 FDCEPGVLGS KGFTWGKVYV  EVEVEREGWS  EDEEEGDEEE  EGEEEEEEEE
401 AGYGDGYDDW  ETDEDEESLG  DEEEEEEEEE  EEVLESCMVG  VARDSVKRKG
451 DLSLRPEDGV  WALRLSSSGI  WANTSPEAEL  FPALRPRRVG  IALDYEGGTV
501 TFTNAESQEL  IYFTATFTR  RLVPFLLWLK  W  PGTRLLLRP

```

**Scientific Research Articles.**

Contents of the thesis, in part, have been previously published.

Data presented in chapter 3, describing the differential and distinct excision capabilities of recombinant hNEIL1 and hNEIL3<sup>FL</sup> in the presence of oxidative lesions within a mock DNA replication fork oligonucleotide structure is currently in preparation for submission to the international peer reviewed journal *Genes*.

Data presented in chapter 4, describing the novel ICL unhooking activities possessed by recombinant hNEIL1 and hNEIL3 proteins was published in the international peer reviewed journal *Scientific Reports* on the 12<sup>th</sup> of December 2017.

“Martin, P. R., Couvé, S., Zutterling, C., *et al.* (2017) The Human DNA glycosylase NEIL1 and NEIL3 Excise Psoralen-Induced-DNA-DNA Cross-Links in a Four-Stranded DNA Structure. *Scientific Reports*, **7**, 17438.”